Molecular Recognition and Coordination Chemistry of Mixed Donor Ligands

A Dissertation Submitted to the
Indian Institute of Technology Guwahati
As Partial Fulfillment for the Degree
Doctor of Philosophy

Submitted by

Avijit Pramanik

Roll No 05612201

Department of Chemistry

Indian Institute of Technology Guwahati

Guwahati-781039

Dedicated

to

My Parents

& Best Wishers

INDIAN INSTITUTE OF TECHNOLOGY GUWAHATI

Department of Chemistry

STATEMENT

I do hereby declare that the matter embodied in this thesis is the result of investigations carried out by me in the Department of Chemistry, Indian Institute of Technology Guwahati, India under the guidance of Associate Professor Dr. Gopal Das.

In keeping with the general practice of reporting scientific observations, due acknowledgements have been made wherever the work described is based on the findings of other investigators.

December, 2009. Avijit Pramanik

I.I.T. Guwahati

INDIAN INSTITUTE OF TECHNOLOGY GUWAHATI

Department of Chemistry

CERTIFICATE

This is to certify that Avijit Pramanik has been working under my supervision since July, 2005 as a regular registered Ph. D. student. I am forwarding his thesis entitled "**Molecular Recognition and Coordination Chemistry of Mixed Donor Ligands**" being submitted for the Ph. D. (Science) Degree of this Institute. I certify that he has fulfilled all the requirements according to the rules of this Institute regarding the investigations embodied in his thesis and this work has not been submitted elsewhere for a degree.

December, 2009.
I.I.T. Guwahati

Dr. Gopal Das
Supervisor

INDIAN INSTITUTE OF TECHNOLOGY GUWAHATI

Department of Chemistry

CERTIFICATE OF COURSE WORK

This is to certify that Avijit Pramanik has satisfactorily completed all the courses required for the Ph.D degree program. These courses include

CH 605:	Applied Crystallography
CH 621:	New Reagents in Organic Synthesis
CH 630:	A Fundamental Approach to Physical Chemistry
CH 611:	Bioinorganic Chemistry

Avijit Pramanik has successfully completed his Ph.D qualifying examination in May 2005.

Prof. Arun Chattopadhyay
Head
Department of Chemistry
I. I. T. Guwahati

Prof. T. Punniyamurthy
Secretary
Departmental Post Graduate Committee
I. I. T. Guwahati

Acknowledgements

At the very outset I take opportunity to express my deep sense of gratitude to my Ph.D. supervisor Dr. Gopal Das, Department of Chemistry, IIT Guwahati for his able guidance, tireless efforts, constant encouragements and moral supports at each and every step of my research work, which enabled me to complete my thesis work. I am fortunate enough to have his guidance to cultivate scientific thoughts.

I would like to acknowledge my sincere gratitude to all of my doctoral committee members, Dr. Manabendra Ray (Chairman), Professor Bhisma K. Patel and Dr. Biplab Bose for their insightful advices and valuable suggestions.

I am grateful to Professor Arun Chattopadhyay Head, Department of Chemistry, IIT Guwahati Professor Abu T. Khan, Ex-Head, Department of Chemistry, IIT Guwahati, Professor M. K. Chaudhuri (Ex-chairman, doctoral committee) and Dr Biplab Mondal for their valuable suggestions and providing good research environment.

I would also like to give special thanks to Dr. Pradyot Kumar Bera (Panskura Banamali College), Dr Bidhan Chandra Bag and Dr Pranab Sarkar (Visva-Bharati, Santiniketan) for their constant inspiration and valuable suggestions in my carrier.

I am thankful to Indian Institute of Technology, Guwahati for providing me with the state of the art infrastructure and facilities for advanced research. My sincere thanks are due to all other faculty members in the Department of Chemistry for their help and encouragement and the non-teaching staffs of the Department for their technical support. I would like to take this opportunity to thank Centre for Environment and Centre for Nanotechnology for providing me the necessary instrumental facilities during the entire duration of my research tenure. My sincere thanks to Chandan Borgohain and K. Senapati of Central Instruments facility, IIT Guwahati for their help in all the characterizations required during my research work.

I would like to thanks my current group members Ballav da, Harajyoti, Bedabrata, Bimlesh, Sandeep, Arghya, Jiban and all other former group members Hema Laksmi, Mouchumi, Srinivas, Mrinmoy, Nikhil, Suvojeet, Madhubrata, Soma, Sourav, Rajib, Dipankar, Priyotosh, Pallab, Dimpy for their constant help, support and the wonderful time we have shared during this period. I am also thankful to Dr. P. K. Iyer and his group members, Bolin da and Pranjal da for their help and pleasant association with whom we shared the lab in the initial stage of my research.

I extend the sincerest thanks to my seniors and friends Abhilasha di, Babulal da, Babu da, Biplab da, Gunin da, Raju da, Rik di, Sahid da, Santanu da, Sarala di, Shampa di , Sonit da, Aali, Amardip, Anirban, Aditi, Atreyi, Avishek, Faizi, Hari, Jashmini, Krishna, Mrigendra, Pallab, Prasanta, Pramod, Saitanya, Shyam, Siva, Suri, Subash, for their constant help, motivation, enthusiastic company and all the wonderful time we spent in various events.

I would like to offer special thanks to my Visva-Bharati, Santiniketan M.Sc. batch mates Anirban Avishek, Rupam, Susanta, Srijit, Sandip, Tanmoy, Tarak and Madhuparna, Samarpita for their constant unfailing support, encouragement and the help they extended from time to time whenever required. I would also like to extend my gratitude to my old friends Amalesh, Biman, Shelly, Bidus, Dipendu, Santanu, Subrata, Dinesh, Subhojit, Arunda, Tapasda and others.

The financial support from Council of Scientific and Industrial Research (CSIR), New Delhi in the form of JRF and SRF is duly acknowledged.

Finally, my Ph. D. endeavor could not be completed without the endless love, unending support, tolerance and blessings from my family. I wish to express my sincere gratitude to my parents and my sister. They are the main soul and inspiration for each and every step I achieved in my life.

Avijit Pramanik

Contents

Contents

SYNOPSIS

The thesis entitled, "**Molecular Recognition and Coordination Chemistry of Mixed Donor Ligands**" is divided into five chapters.

Chapter-1 gives a brief introduction as well as literature survey of molecular recognition and coordination chemistry of various mixed donor ligand systems. It describes various aspects of supramolecular self-assembly processes, molecular recognition, supramolecular photochemistry. It also describes the literature regarding the coordination chemistry of aryl azo dyes containing mixed donor sites.

Host-Guest chemistry of molecular recognition is a highly expanding area of supramolecular chemistry. The term molecular recognition refers to the specific interaction between two or more molecules through noncovalent bonding such as hydrogen bonding, metal coordination, hydrophobic forces, van der Waals forces, π-π interactions, electrostatic and/or electromagnetic effects. The host and guest involved in molecular recognition exhibit molecular complementarities. Chemists have demonstrated that artificial supramolecular systems can be designed that exhibit molecular recognition. Molecular recognition can be subdivided into static molecular recognition and dynamic molecular recognition. Static molecular recognition is likened to the interaction between a key and a key hole; it is a 1:1 type complexation reaction between a host molecule and a guest molecule to form a host-guest complex. To achieve advanced static molecular recognition, it is necessary to make recognition sites that are specific for guest molecules. In the case of dynamic molecular recognition the binding of the first guest to the first binding site of a host affects the overall association.

Syntheses of organic dyes are important in the field of molecular sensor technologies, particularly; their use in biological applications has gained considerable interest in the last few years. Azo-dyes are widely used in analytical chemistry and dyestuff industry, while textile mills predominantly use them. Recently they have received much attention in the field of nonlinear optics, optical storage and other photoelectric applications. Derivatives of azo-chromophore with pyrazole or imidazole as the heterocyclic component belong to class of organic ligand that contain four nitrogen atoms coupled in conjugated system of π-bonds. Azo function is photochromic, redox active, pH responsive and their complexes act as a molecular switch.

Various fluorescent hosts have been developed for sensitive and simple detections of various guest molecules. However, these approaches have often involved the synthesis of structurally complicated hosts. Therefore, it is of high importance in the filed of photochemistry to discover and/or develop new simple and sensitive host molecule with fluorophore attached to it. Due to the many possible applications in analytical chemistry and biomedical research, considerable

attention has been focused on the design of receptors that have the ability to selectively bind and sense anions through an optical response.

Chapter-2 discusses the sources of chemicals and solvents, method for preparing some starting materials, determination of elements and particulars of all equipment used for characterization, physico-chemical, photo-physical studies.

Chapter-3 discusses molecular recognition of anion, cation and aromatic guest and solvent encapsulation by various ligands in solution and solid state. This chapter is sub-divided into three parts based on the type of ligands.

In 1st part, we have reported a simple and novel tripodal fluorescent sensor, Tris-[2-(naphthalen-1-yloxy)-ethyl]-amine (**L_1**). The binding of the hosts to a series of anions was investigated by fluorescence, NMR and single crystal X-ray crystallography. In solution the anion binding property was investigated by monitoring the changes in the fluorescence intensity of dry THF solution of **L_1** at 298 K upon addition of F^-, Cl^-, Br^-, NO_3^-, ClO_4^-, CF_3COO^- and Pyromellitate as their tetrabutylammonium (TBA) salt. The ligand **L_1** shows a drastic change in the fluorescence intensity after anion binding and more effective towards nitrate anions (Figure 1).

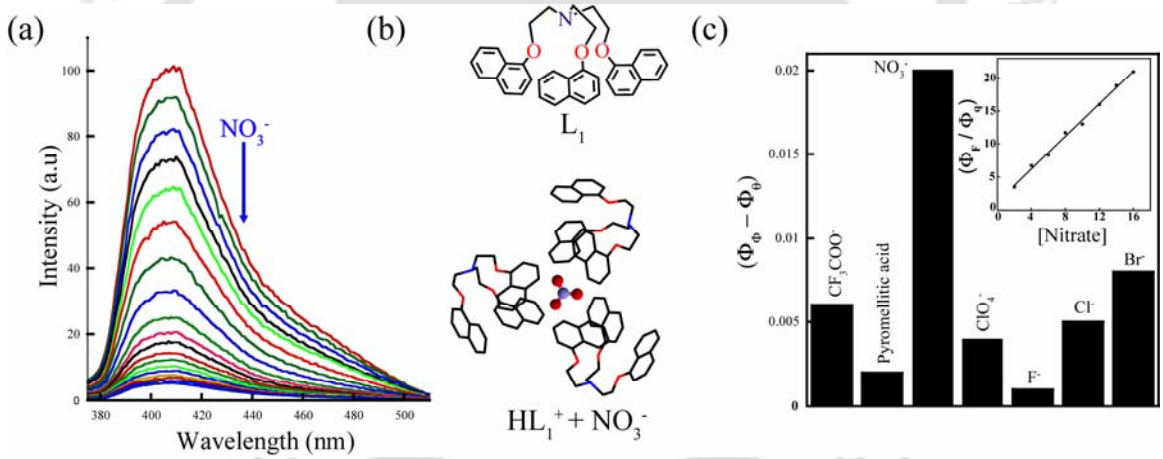

Figure 1. (a) Anion recognization in solution phase, (b) anion recognization in solid phase and (c) Schematic representation showing the change of fluorescence quantum yield. Inset: Stern-Volmer plot for fluorescence quenching of tripodal ligand ($1x10^{-6}$ M) on gradual addition of nitrate ($1x10^{-6}$ M) in dry THF.

We have also described the molecular recognition properties of another tripodal napthyl ether ligand Tris-[2-(naphthalen-2-yloxy)-ethyl]-amine (**L_2**). Electron rich **L_2** shows dramatic color change and a concomitant quenching of fluorescence in solution as well as solid phase when titrated with electron deficient aromatic guest molecules (Figure 2).

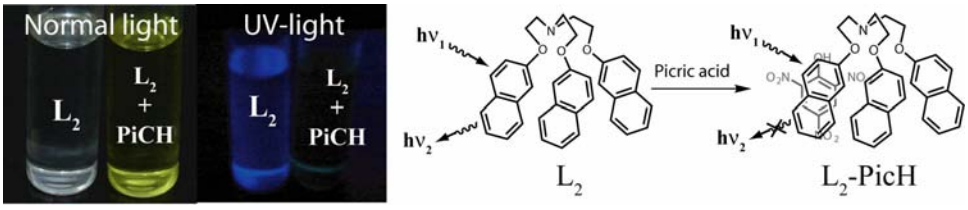

Figure 2. Pictorial representation of fluorescence quenching of $\mathbf{L_2}$ and formation of inclusion complex in presence of picric acid.

Electron rich $\mathbf{L_2}$ also bind with various metal ions (*viz.* Na^+, K^+, Cs^+, Ca^{2+}, Mg^{2+}, Co^{2+}, Ni^{2+}, Cu^{2+}, Zn^{2+}, Ag^+, Pb^{2+} and Hg^{2+}). Ag^+ shows marked enhancement in fluorescence intensity in contrast to the other cations (Figure 3).

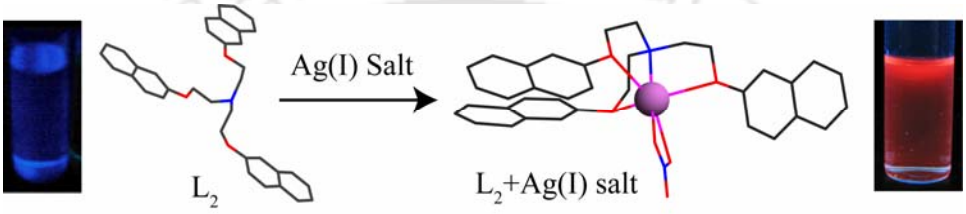

Figure 3. Schematic representations of fluorescence enhancement of $\mathbf{L_2}$ in addition of Ag(I) salt.

In 2nd part of the chapter 3, we have discussed about tripodal aminoquinoline based ligand, tris-(N-ethyl-8-aminequinoline) amine ($\mathbf{L_3}$), which have three chemically different types of nitrogen donating sites. This ligand is an example of selective phosphate ion sensor. Here we have reported two types of supramolecular interactions are possible for the selectivity towards phosphate salt and their corresponding acid. (i) Hydrogen bonding interactions between amine hydrogen and phosphate anion and (ii) electrostatic interaction of cationic protonated amine or quinoline group with anions which is responsible for monomer as well as excimer transduction process (Figure 4).

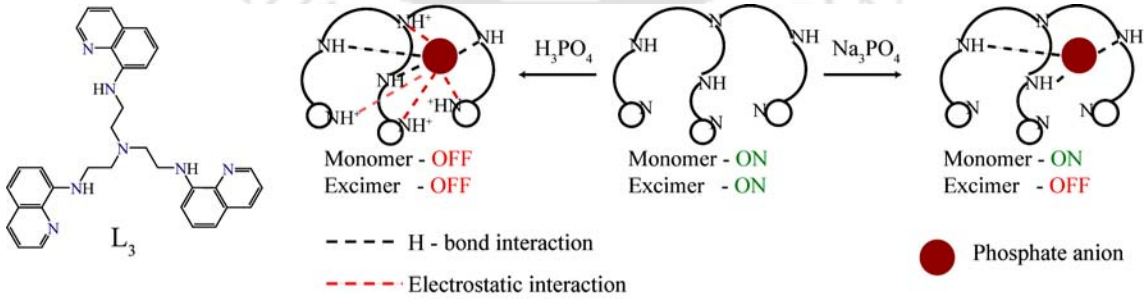

Figure 4. Schematic representation of supramolecular non covalent interaction through host–guest complexes of $\mathbf{L_3}$ in presence of phosphoric acid and its salt.

3rd part of the chapter 2, discussed about chiral *trans*-1,2-*bis*-(3-(naphthalen-1-yl)-thioureido cyclohexane ($\mathbf{L_4}$) compound as a new host material with considerable structural adaptability

over range of solvent. It has found that solvents have a significant role in governing the solid state conformation of **L_4**. The solid state structural similarities and disimilarities and 3D packing can be rationalized through multipoint solute-solvent non-covalent interactions. In addition to the strong hydrogen bonds, different types of non-covalent intermolecular C-H····O, C-H····S, N-H····S C-H····π, π····π and lone pair (lp)····π interactions were found to stabilize the crystal structures. Powder X-ray diffraction, thermal analysis and optical microscopic studies were also performed to support the crystallographic studies. Solution phase photo-physical (steady state and time resolved fluorescence) studies also carried out to emphasize the role of solvent polarity in non-covalent interactions (Figure 5).

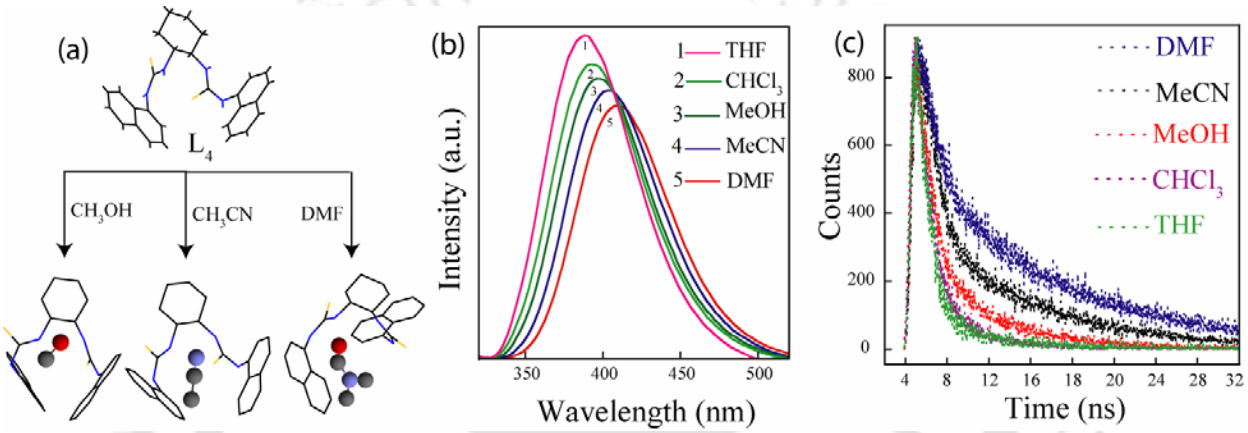

Figure 5. (a) Schematic representation of solvated **L_4**; (b) Emission spectra of **L_4** in different solvents (λ_{ex} = 320 nm, 1.0 x 10^{-5} M, 298 K) and (c) Time-resolved fluorescence decay of **L_4** at room temperature in different solvents.

Next we have synthesized a series of substituted 2-Aryl azo dyes containing imidazole group (Scheme 1). We have studied there molecular recognition property and their coordination chemistry.

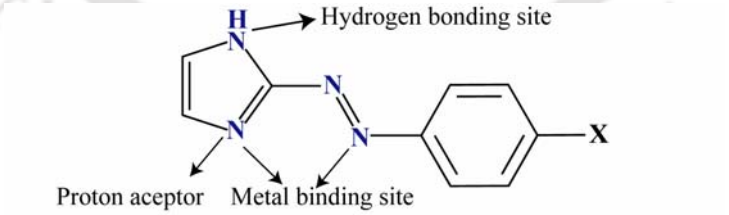

X = H (L_5), Me (L_6), OMe (L_7), Cl (L_8), Br (L_9), I (L_{10}) and Ar-Nap (L_{11})

Scheme 1

In chapter 4, we have discussed the Aryl azo imidazoles assisted assembly of anion/anion-water through salt formation. Aryl azo dyes containing imidazole group can act as an acid or base. They are also potential hydrogen bond donor and acceptor. Imidazolium form of these dyes can form salt with various inorganic anions. Effect of shape of the anions (linear, planner, spherical) on higher dimensional supramolecular assembles of these salts have been analyzed and

rationalized. Ligand assisted anion or anion-water assembly formation has been discussed. Presence of water in the crystal structure also plays a vital role in controlling the higher dimensional networks. All supramolecular self-assembled networks of salts (Figure 6) are guided by various non-covalent interactions, *viz.* directional hydrogen bonds, halogen bonds and π-stacking. Interaction of anions with the ligands in the solution phase was also investigated by absorption and fluorescence spectroscopy.

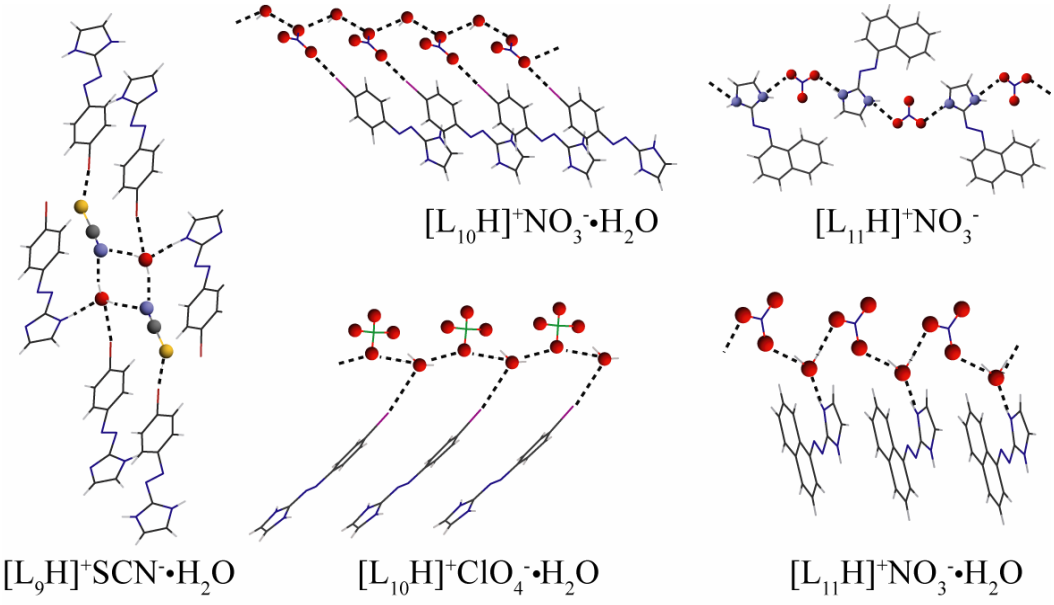

Figure 6. Schematic representation of 2-aryl azo imidazole assisted assembly of anion/anion-water through salt formation.

In chapter 5, we have discussed of the coordination chemistry of mixed-donor 2-aryl azo imidazole dyes. We have sub-divided this chapter into three parts based on the substitution of the aryl part of the ligand.

In the 1st part, we have discussed the coordination chemistry of un-substituted ligand **L_5** (Figure 7). Simultaneous presence of hydrogen bonding site and metal coordination site of different chemical nature helps to form metal complexes with different metal ions and also helps them to self-assemble in the solid-state with different higher dimensional architectures. Aryl azo imidazole ligand can act as unidentate or bidentate ligand, in which one of the azo N atoms is the second coordinating atom. We have also shown that, coordination of the azo N decrease the electron density from N=N, which in turn decrease the azo bond strength. In this part we have shown how to molecular level structure (coordination chemistry) changes the formation of higher dimensional architectures. Finally various physicochemical studies *viz.* thermal behaviors, absorption spectra, electrochemistry and EPR studies have been conducted to rationalize their coordination chemistry in solution phase.

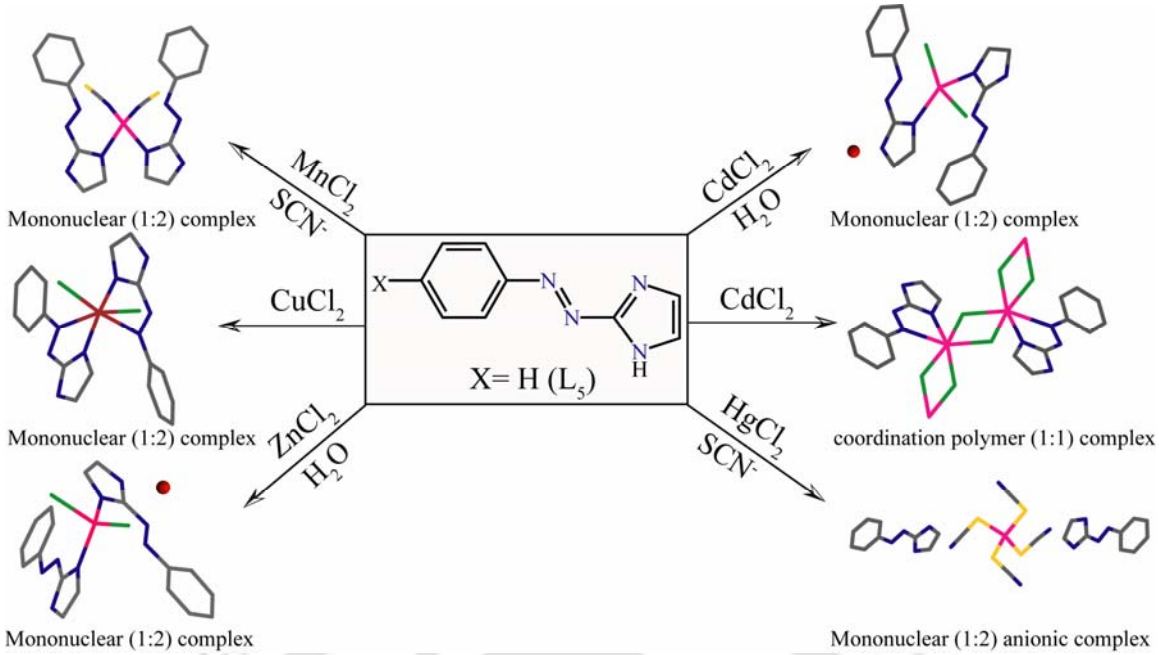

Figure 7**.** Schematic representation of various coordination environments in the solid state.

The 2nd part of this chapter focused on the formation of a series of metal complexes using electron donating *p*-substituted aryl azo system with Cu^{II}, Zn^{II} and Cd^{II} salts (Figure 8). Presence of –Me, -OMe, in the phenyl azo fragment shows some unusual coordination behaviors in presence of Cu^{II}. Varying coordination environment as well as electron donating effect, the Cu-**L_6** complex is showing unusual Cu-S bond and Cu-**L_7** complex is showing square pyramidal geometry where H_2O is in equatorial position. Counter anions and metal ions tune the coordination environment of complexes. Finally, thermal behaviors, absorption spectra, electrochemistry and EPR studies have been conducted to support their structure in solution phase.

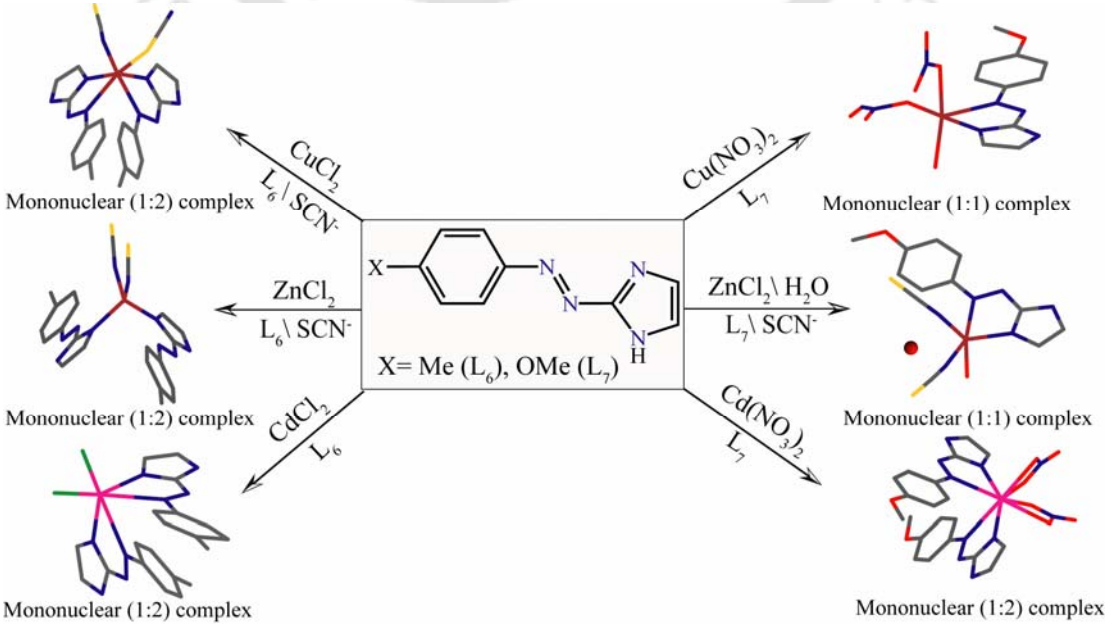

Figure 8. Influences of electron donating substituents in coordination chemistry of aryl azo systems.

Last part of this chapter describe the coordination chemistry with electron deficient 2-aryl azo ligands with d^{10} metal *i.e.* Zn(II), Cd(II), Hg(II). It also describes the effect of counter anion (Cl^-, NO_3^-, SCN^-) in controlling the solid state structures (Figure 9). We have rationalize the effect of coordination behavior of the metal ion, the size of the anions and the substitution effects of ligands upon the structure adopted by these metal complexes. Upon closer inspection, we have seen that variation in the coordination sphere environment is the key for the construction of supramolecular architectures in solid-state *via* higher dimensional self-assembly. Influences of halogen (Cl^-, Br^-, I^-) substitutions are reflected in the precise molecular level architecture in the individual complexes. The parameters related to the coordination sphere depend on the metal-to-ligand ratios and are also influenced by the solvent of crystallization. A competition between the coordinating capabilities of the counter anion with ligands and its shape led to neutral and anionic metal complexes. Furthermore, we have also investigated the thermal behaviors; absorption spectra which have been conducted to rationalize their structure in solution phase.

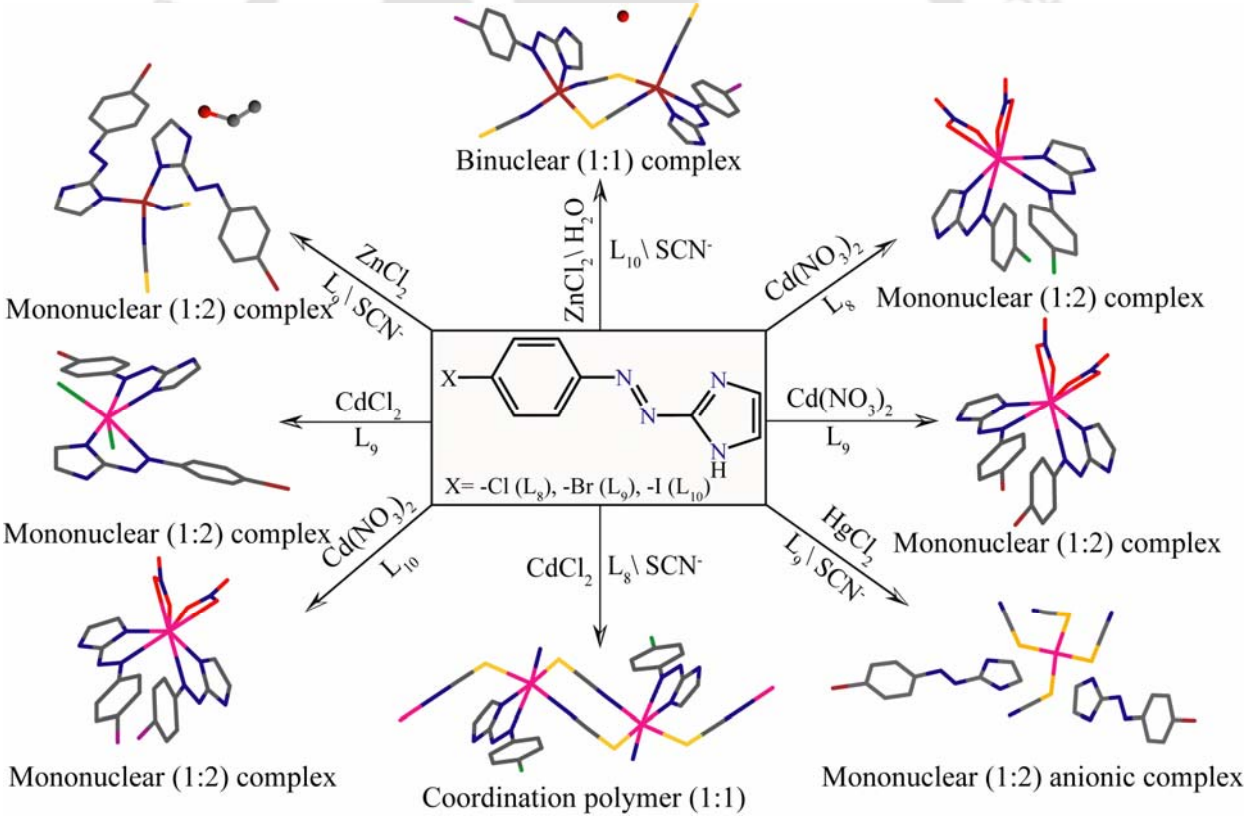

Figure 9. Schematic representation of effect of substituents and counter ions of self assembly d^{10} metal complexes assisted by aryl azo system.

Chapter 1

INTRODUCTION

1.1 Supramolecular chemistry

Supramolecular chemistry refers to the area of chemistry beyond the molecules and focuses on the chemical systems made up of a discrete number of assembled molecular subunits or components (Figure 1.1). The forces responsible for the spatial organization may vary from weak (intermolecular forces,[1.1] electrostatic[1.2] or electromagnetic and hydrogen bonding) to strong (covalent bonding), provided that the degree of electronic coupling between the molecular component remains small with respect to relevant energy parameters of the component.[1.3] While traditional chemistry focuses on the covalent bond, supramolecular chemistry examines the weaker and reversible noncovalent interactions between molecules. These forces include hydrogen bonding, metal coordination, hydrophobic forces, van der Waals forces, pi-pi interactions and electrostatic effects. Important concepts that have been demonstrated by supramolecular chemistry include molecular self-assembly, folding, molecular recognition, host-guest chemistry, mechanically-interlocked molecular architectures, and dynamic covalent chemistry.[1.4] The study of non-covalent interactions is crucial to understanding many biological processes. Biological systems are often the inspiration for supramolecular research.

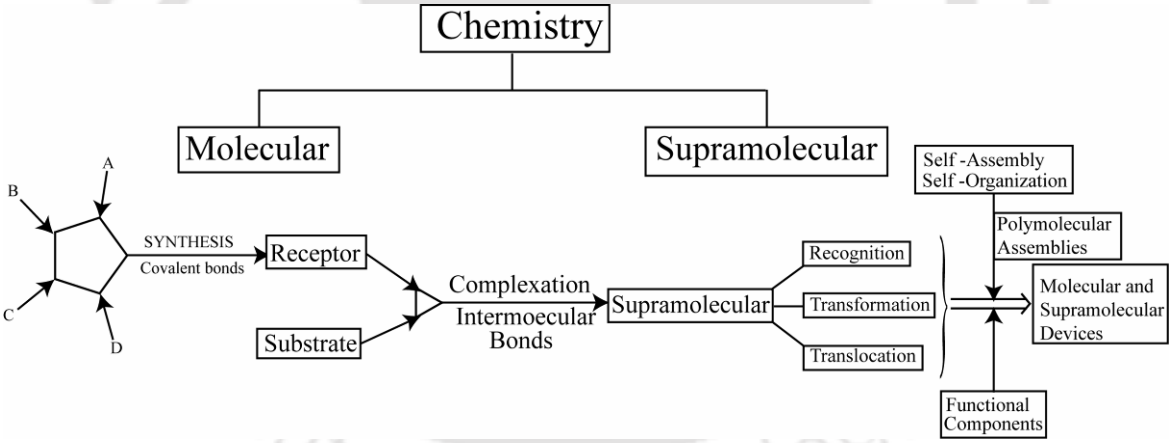

Figure 1.1. (a) From molecular to supramolecular chemistry.

The field of supramolecular chemistry involves taking control of the assembly of matter to a stage beyond covalent molecules, allowing the preparation of elaborate species in which components with useful functions may be assembled in spatially well-defined arrays using kinetically labile interactions.[1.5] In parallel with the developments in synthesis, the fields of photophysics and photochemistry—and their associated spectroscopic methodology—have never been more topical. The efficient use of light in emission-based sensors for analytical and diagnostic applications, and as a means for information processing,[1.6]

transfer and data storage,[1.7] and in LED[1.8] type display devices, are all areas where real-world applications either already exist or are close to development.

1.2 Supramolecular photochemistry

Photochemistry[1.9] is a natural phenomenon as old as the world and a modern branch of science, at the interface between light and matter and at the crossroads of chemistry, physics, and biology. Photochemistry is of paramount importance to life (photosynthesis,[1.10] vision,[1.11] phototaxis,[1.12] *etc*.) as well as to technology (image reproduction,[1.13] photocatalysis,[1.14] photodegradation,[1.15] *etc*. In the last two decades photochemistry has reached a remarkable level of experimental and theoretical efficacy. The photochemical and photophysical processes of thousands of organic molecules, coordination compounds, and organometallic complexes have been elucidated, and suitable theoretical treatments are now available to rationalize the structural, energetic, and dynamic properties of the most important excited states of several families of molecules. Up until now most of the fundamental photochemical investigations have dealt with molecular species *(molecular photochemistry)*. In the same way as combination of atoms leads to molecules, combination of molecular components leads to *supramolecular species*. Current literature clearly shows that chemical research is rapidly moving from molecular to supramolecular species. There are at least four reasons for this trend: (1) the high degree of knowledge reached on molecular species; (2) the extraordinary progress made by synthetic methods: (3) the continuous search for new materials (e.g., for a "small-upward" approach to nanostructures); (4) the need to fill the gap which separates chemistry from biology. One of the most interesting aspects of the chemistry of supramolecular species is their interaction with light and the great variety of processes that may ensue. This is the realm of *supramolecular photochemistry.'* In the last few years supramolecular photochemistry has grown very rapidly along several directions. Photochemistry and supramolecular chemistry are, by their own nature, interdisciplinary areas, and this is even truer for supramolecular photochemistry.

'Supramolecular photochemistry' encompasses both of these themes, spanning many orders of magnitude in both size of assembly involved and the timescales of the events arising from their excited states. It is one of the most vibrant and exciting areas of modern chemical research, lying at the interface of chemistry, physics, biology and materials science, combining elegant synthesis with detailed studies of excited state processes. This breadth of scope is amply illustrated by many contributors to this issue which includes accounts of work as diverse as photocatalysis; sensitization of near-infrared luminescence

for biological imaging purposes; energy migration in polymeric assemblies; photoinduced energy and electron transfer in supramolecular assemblies; and photophysical properties of new sensors and singlet oxygen sensitisers.

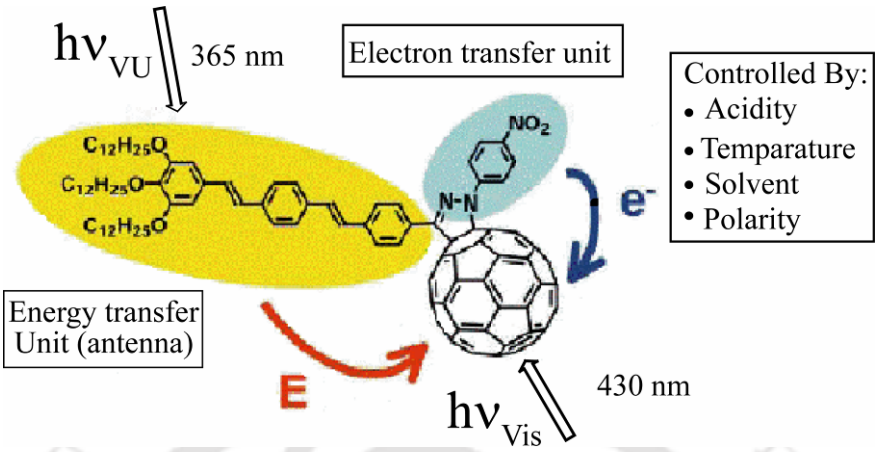

Figure 1.2. Oligophenylenevinylene–fullerene–pyrazoline triad where the fullerene unit acts as energy or electron acceptor for the OPV and the pyrazoline moiety, respectively. Switching of photoinduced processes can be obtained by operating on different parameters, namely excitation wavelength, proton concentration, solvent polarity, and temperature.

Figure 1.2 shows the supramolecular photochemistry aspect of an azo dye containing *β*-napthol system, in which a strongly fluorescent moiety (oligophenylenevinylene, OPV), is attached to an anisylphenanthroline unit (Phen).[1.16] The results obtained with OPV–Phen upon reversible additions of acid and base are illustrated in figure 1.3. The direction of photoinduced energy transfer is addressed at wish by means of the reversible protonation–deprotonation reaction of the Phen receptor, because the fluorescent energy levels of Phen and Phen•H^+ are put below/above the luminescent level of OPV, which acts act as an energy acceptor (in OPV–Phen) or donor (in OPV–Phen•H^+). The process is conveniently signalled by the on/off switching of the very intense OPV fluorescence. Thus a simple method of controlling the widely exploited luminescence of OPV's is also suggested. Many examples of molecular switches and sensors that take advantage of changes in proton concentration can be found in current literature.[1.17]

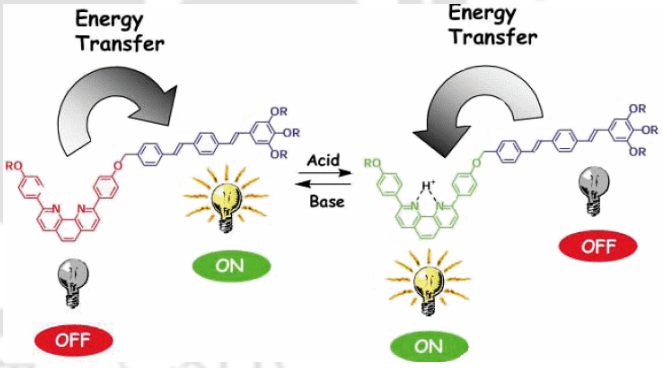

Figure 1.3. On/off switching of the luminescence in OPV–Phen as a consequence of the inversion of photoinduced energy transfer direction.

1.3 Molecular recognition

The term molecular recognition refers to the specific interaction between two or more molecules through noncovalent bonding such as hydrogen bonding, metal coordination, hydrophobic forces, and other non covalent interactions.[1.18] The host and guest involved in molecular recognition exhibit molecular complementarity.[1.19] Chemists have demonstrated that artificial supramolecular systems can be designed that exhibit molecular recognition. One of the earliest examples of such a system is crown ethers which are capable of selectively binding specific cations. However, a number of artificial systems have since been established. Molecular recognition can be subdivided into static molecular recognition and dynamic molecular recognition. Static molecular recognition is likened to the interaction between a key and a key hole; it is a 1:1 type complexation reaction between a host molecule and a guest molecule to form a host-guest complex. To achieve advanced static molecular recognition, it is necessary to make recognition sites that are specific for guest molecules (Figure 1.4.a). In the case of dynamic molecular recognition the binding of the first guest to the first binding site of a host affects the association constant of a second guest with a second binding site.[1.20]

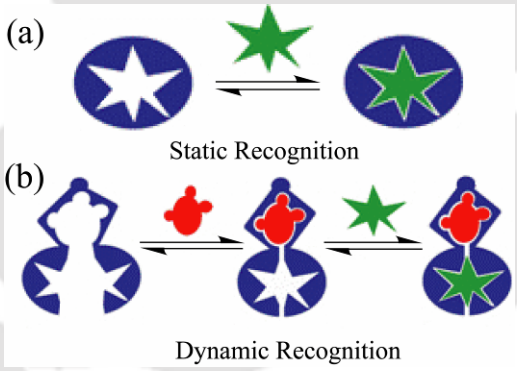

Figure 1.4. (a) Static recognition between a single guest and a single host; (b) Dynamic molecular recognition of host and guests.

In the case of positive allosteric systems the binding of the first guest increases the association constant of the second guest. While for negative allosteric systems the binding of the first guest decreases the association constant with the second (Figure 1.4.b). The dynamic nature of this type of molecular recognition is particularly important since it provides a mechanism to regulate binding in biological systems. Dynamic molecular recognition is also being studied for application in highly functional chemical sensors and molecular devices

1.4 General feature of molecular recognition

"Molecular recognition", which became a popular phrase in the early decays, covers a set of phenomena that may be more precisely but less economically described as being controlled by specific noncovalent interactions. Such phenomena are crucial in biological systems, and much modern chemical research is motivated by the prospect that molecular recognition by design could lead to new technologies. In earlier we have reported the processes of molecular recognition and self-assembly/self-organization is of fundamental importance for the formations of higher organized chemical systems that result from the association of two or more chemical species through various noncovalent interactions. Furthermore, coordinative metal-ligand bonds are today frequently used for the programmed synthesis of supermolecules.[1.21] The solvent often plays an active role in these processes by solvating or desolvating the interacting molecules during the receptor-substrate association. In particular, the hydrophobic effect in aqueous media can be very strong and can determine the stability of the associates to a substantial extent.[1.22] Multiple weak bonds are necessary to form supermolecules which are, on one hand, sufficiently stable under normal conditions (e.g., room temperature in aqueous solution) and, on the other hand, sufficiently flexible to undergo conformational changes and partial or complete dissociation without changing these conditions dramatically. Besides the well-preorganized macrocycles, such as cyclodextrins,[1.23] cyclophanes,[1.24] carcerands,[1.25] cryptophanes,[1.26] cucurbit[*n*]urils (CB[*n*]),[1.27] and supramolecular capsules[1.28] (formed by self-assembly of suitable molecular building blocks), no cyclic compounds with cavities of flexible size, which are frequently termed as molecular tweezers[1.29] and clips,[1.30] proved to be effective as synthetic receptors.

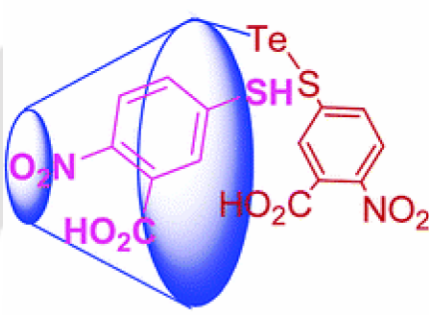

Figure 1.5. (a) Molcular recognition of 3-carboxy-4-nitrobenzenethiol (ArSH) in β-cyclodextrin cavity.

We have focused on multiple noncovalent interactions of arene units in the receptor with neutral or ionic aromatic substrates (π-π, CH-π, and cation-π interactions). Classical examples of aromatic interactions are the base stacking in DNA and the protein folding caused by phenylalanine and other aromatic amino acid side chain interactions.[1.31] The preference of the edge-to-face over the face-to-face orientation of two benzene rings, as found in the crystal structure of benzene[1.32] or in the protein structures, can be explained with a simple electrostatic model for benzene consisting of a positively charged σ

framework sandwiched between two clouds of π electron density. Figure 1.5 says that, the artificial glutathione peroxidase (GPx) model 2, 2′-ditellurobis (2-deoxy-β-cyclodextrin) (2-TeCD) which has the desirable properties exhibited high substrate specificity and remarkably catalytic efficiency when 3-carboxy-4-nitrobenzenethiol (ArSH) was used as a preferential thiol substrate. In this artificial enzyme model 2-TeCD the active site designed had been placed on the secondary side of cyclodextrin since it was established that a bound substrate would have its prosthetic groups at the secondary side of cyclodextrin.[1.33] Another example of molecular recognition through inclusion phenomena where sulfate and nitrate anions are encapsulated in asymmetric aza cryptands system.[1.34] Sulfate and nitrate anions are bound with laterally asymmetric aza cryptands. Cryptand **Lm** having a larger cavity than that of **Lo**, prefers to encapsulate a planar nitrate (Figure 1.6.c.) over T_d sulfate (Figure 1.6.d.) in its cavity when both anions are available for complexation.

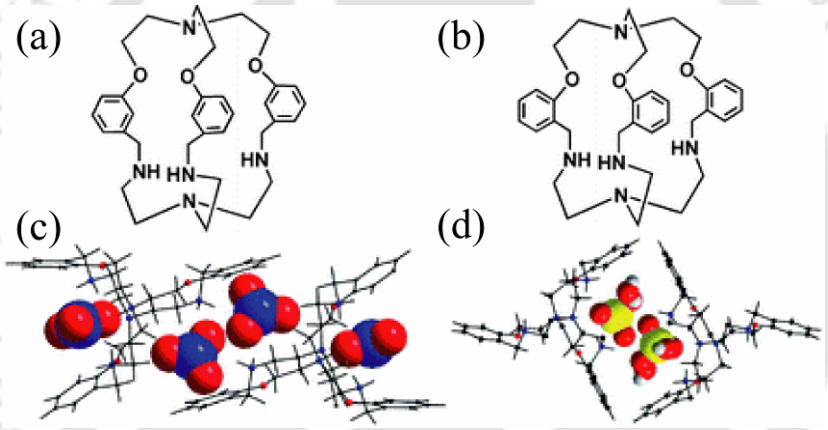

Figure 1.6. (a) Meta substituted aza cryptant ligand (**Lo**); (b) Ortho substituted aza cryptant ligand (**Lm**); (c) Nitrate recognition of meta substituted aza cryptant ligand; (d) Sulphate recognition of meta substituted aza cryptant ligand.

1.5 Anion recognition

Anion sensing has been of great interest in biological and environmental sciences for several decades. Various fluorescent sensors have been developed for sensitive and simple detections of anions.[1.35] The rapid detection of anionic species is of great significance in the environment and in physiological systems. [1.36] As signaling mechanisms, photoinduced electron transfer (PET), [1.37] intramolecular charge transfer (ICT),[1.38] excited-state proton transfer,[1.39] metal to ligand charge transfer,[1.40] excimer/exciplex formation[1.41] and competitive binding[1.42] have been reported. Currently, molecular recognition of anions by synthetic receptors is an expanding field of research. [1.43] Typically, synthetic anions receptors consist of various combinations of macrocyclic polyammonium

/guanidiniums,[1.44] pyrrols,[1.45] Lewis acids,[1.46] calix[n]arenes,[1.47] amides, [1.48] and urea/thiourea moieties.[1.49] For the design of a selective anion receptor the geometry and the basicity of the anion and the nature of the solvent have to be considered. The main features for the design of tripodal anion receptors are: (i) there are a sufficient number of positively charged or neutral electron-deficient groups in the ligand to serve as interaction sites. (ii) Receptors with a flexible tripodal structure have a strong affinity for trigonal oxoanions, such as carbonate, phosphate and chlorate, because the geometry and the orientation of the host molecules favour the formation of a stable host-guest complex.[1.50] (iii) the classical complexation mechanism can also be applied. Here, the interactions occur based on non-covalent interactions. The non-covalent interactions include electrostatic interactions, hydrogen bonding, hydrophobicity, coordination to a metal ion, and a combination of these interactions. On the other hand, for the anions it selves, the size, shape, H bonding capability, acid/base properties and the number of interaction sites should also be considered. The tripodal tris-urea ligand xhibited recognition of sulfate in solution and the crystalline state.[1.50] Notably, the m-CN-Ph substituted triourea ligand encapsulated sulfate in a 2:1 complex when incorporated into a silver coordination polymer, with the resulting formation of 12 hydrogen bonds representing the highest coordination number reported for SO_4^{2-} ions in a synthetic receptor[1.51] (Figure 1.7). However, selective and efficient separation of sulfate from aqueous solutions with this or other analogous crystalline frameworks proved elusive so far owing to the low stability and relatively high solubility of the frameworks in water.

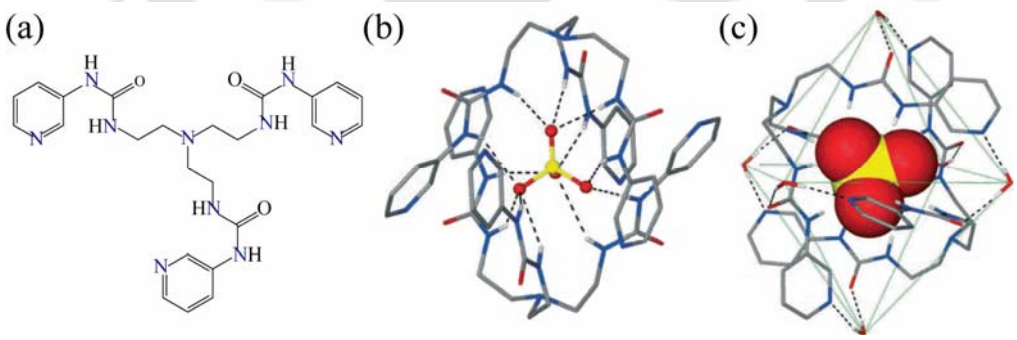

Figure 1.7. (a) tripodal tris-urea ligand; (b) Sulfate encapsulation by12 hydrogen bonds (dashed lines) from six urea groups; (c) Hydrogen-bonded capsule assembled from two ligand (stick model), one SO_4^{2-} ion (space filling model), and six bridging water molecules (stick model).

As a typical example of halide Recognition by heteroatom-bridged heteroaromatic calixarenes, tetraoxacalix [2] arene [2] triazine 1 (Figure 1.8.a) has been reported to adopt a pre-organized 1,3-alternate conformation,yielding a cleft formed by two π-electron deficient triazine rings.[1.52] This π electron-deficient cavity would act as a receptor to

interact with anions through π–anion interactions. Herein, we have seen halide recognition by tetraoxacalix [2] arene [2] triazine host molecules, and considerable substituent effects of the triazine on the halide–p interaction. Most astonishingly-ray crystallography revealed the concurrent formation of noncovalent π–halide and π–lone-pair electron interactions between water (Figure 1.8.b), chloride, or bromide, and the dichlorosubstituted tetraoxacalix [2] arene [2] triazine host.

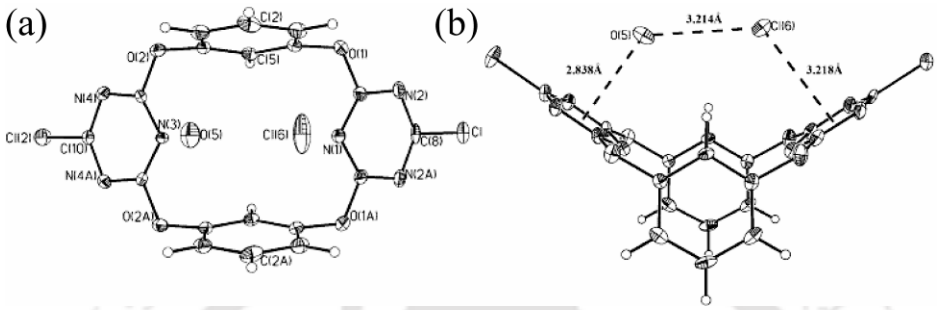

Figure 1.8. (a) Molecular structure of the ternary complex, chloride and water. (b) Concurrent Noncovalent Halide–π and Lone-pair–π Interactions in Host–Halide–Water Ternary Complexes.

The *cis*-poly (phenylacetylene) polymer with the urea as a pendant (PPA-Urea) shows the anion responsive property. The anion-urea host-guest interaction triggered a drastic color change of the polymer solution from pale yellow to red in response to guest anions such as CH_3COO^-, Cl^-, and Br^-.[1.53] The polyacetylene backbone served as not only a signaling component but also the structural scaffold for the anion recognition unit. Therefore, installation of a sulfonamide group onto the surface of the synthetic helical constructs would act as a facile anion sensing systems with unique guest selectivity (Figure 1.9). More recently, cispoly (phenylacetylene) with the amide anion receptors as a pendant (PPA-Amide) showed high sensitivity toward anionic guests.[1.54]

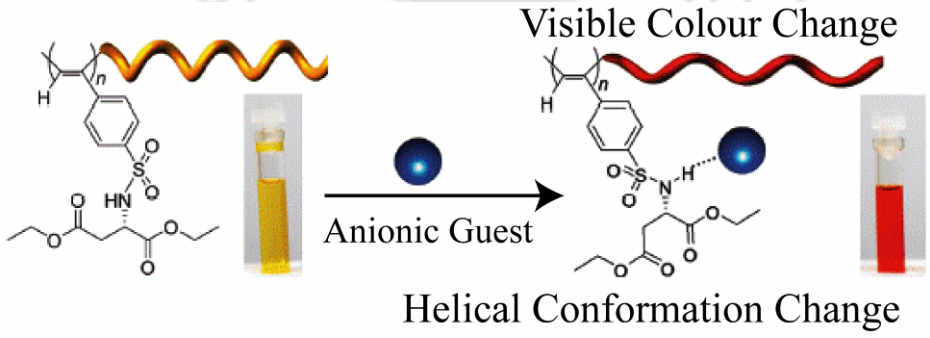

Figure 1.9. Pictorial representation of the anion reception triggered helical conformation change of polyacetylene helicity at a molecular level.

Figure 1.10.a says anion binding of non fluorescents bipyridine bearing amino groups at the 6-position show emission properties with a large quantum yield (up to ca. 0.3). Bipyridine receptor **1** showed response for diphenyl phosphate but not for carboxylic acids.[1.55] Upon addition of phosphate to aqueous solutions of receptor **2** at pH 6, a remarkable emission intensity enhancement was observed. At this pH, both the polyamine and the phosphate are partially protonated and the fluorescence enhancement could be attributed to a favorable intra-complex proton transfer that leads to the benzilic amine protonation (Figure 1.10.b). The polyamine binding site originates some selectivity due to the formation of a suitable cavity for phosphate. Other anionic species such as ATP, citrate, sulfate, acetate, and dimethyl phosphate gave smaller fluorescence enhancements upon binding with receptor **2**. The chemosensor consists of a guanidinium group as the cationic receptor for carboxylates and monoaza-18-crown-6 ether for coordination with the ammonium terminus (Figure 1.10.c). A family of amino acids was tested, and the fluorescence enhancement interestingly depended on the alkylic chain length between the acid and the ammonium group. The largest fluorescence enhancement factor was found for γ-amino butyric acid, which is a principal neurotransmitter in the brain. γ-Amino butyric acid also displays the larger binding constant with anthracene based receptor.[1.56] Similarly, receptor **4** illustrates how without changing the signaling subunit (anthracene), the selectivity against anions is controlled by the topology of the binding site. Thus, receptor **4** was able to discriminate between phosphate and pyrophosphate.[1.57] The two polyammonium arms of the receptor are geometrically disposed for binding the six external oxygen atoms of the pyrophosphate anion (Figure 1.10.d). Studies were carried out in water at pH 7. The larger stability constant found for pyrophosphate *vs.* phosphate was in line with the larger fluorescence enhancement in the presence of the former. The recognition mechanism was similar to that described above (PET chemosensor). The use of receptor **5** to sense ATP and CTP over other nucleotides tested (AMP, ADP and GTP) in water at pH 7.6 through an enhancement of the fluorescence emission of the appended acridine fluorophore was reported.[1.58] This fluorescence enhancement was attributed to π-stacking interactions between the acridine fluorophore and the aromatic part of the nucleotides in the 1:1 complex formed (Figure 1.10.e). The new upcoming advances, innovative points of view, and original ideas will seed the imagination of future research in order to meet the challenge of developing highly selective and specific sensing receptors for a number of target anions.

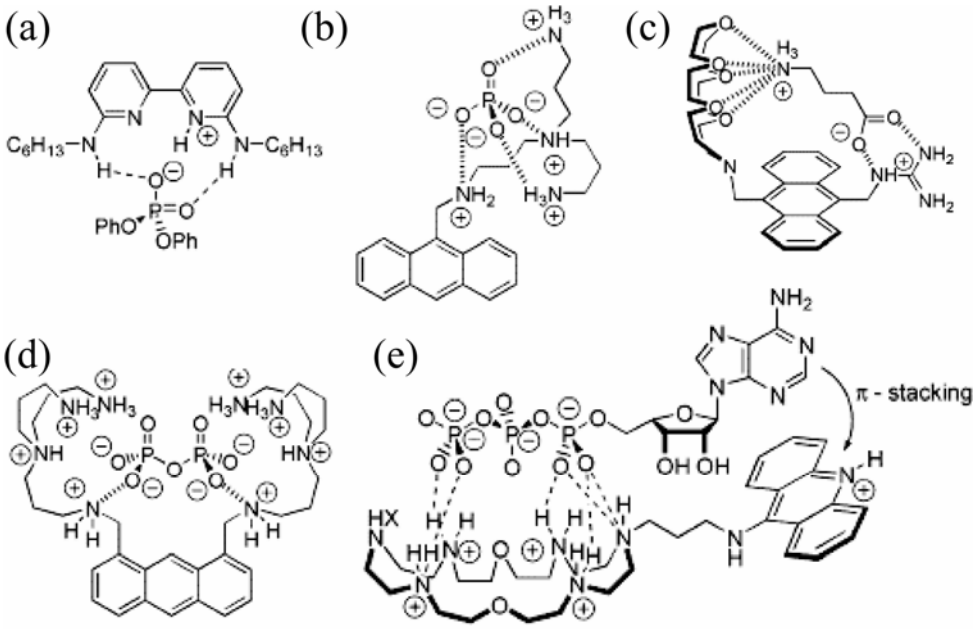

Figure 1.10. (a) Proposed structure of the complex formed between receptor **1** and diphenyl phosphate anion through hydrogen-bonding interactions; (b) Host-guest binding interaction between receptor **2** and phosphate anion through the formation of hydrogen bonds; (c) Proposed structure for the adduct formed between receptor **3** and γ-aminobutirate; (d) Binding pattern of receptor **4** with pyrophosphate anion by means of hydrogen-bonding interactions; (e) Schematic representation of the complex formed between receptor **5** and ATP by means of hydrogen bonding, electrostatic, and π-stacking interactions.

1.6 Application of molecular recognition

A known host-guest assembly, organized only by means of relatively weak dispersive forces, exhibits hitherto unappreciated thermal stability. The calixarenes comprise an extensively studied class of macrocyclic, polyphenolic compounds that are usually strongly associated with host-guest inclusion chemistry. The simplest representative of this family of compounds is calyx [4] arene, a bowl-shaped molecule with a shallow cleft. Its rigid cone conformation is stabilized by a cyclic array of hydrogen bonds between adjacent phenolic OH groups at the lower rim. The hexagonal close-packed arrangement of calyx [4] arene contains lattice voids that can conclude small, highly volatile molecules. This host-guest system can be exploited to retain a range of freons, (Figure 1.11) as well as methane, not only well above their normal boiling points, but also at relatively high temperatures and low pressures. The usually overlooked van der Waals interactions in organic crystals can indeed be used in a highly stable supramolecular system for gas storage. [1.59] Figure 1.12 shows the hemiaminal intermediate of triphenylene derivative which is kinetically trapped at low temperatures, but simply warming the crystal facilitated its further conversion to an imine. The structure obtained after warming the crystal to 270K and keeping it at that temperature for 30 min showed complete conversion of the

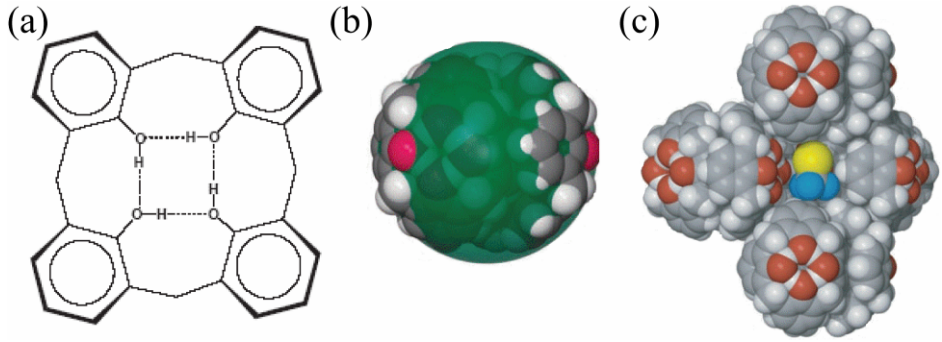

Figure 1.11. (a) calyx [4] arene ligand; (b) Space-filling representation viewed perpendicular to the threefold axis; (c) Space-filling representation of calyx [4] arene -CF_3Br viewed perpendicular to the crystallographic *c* axis. The interstitial void of the host lattice is occupied by one molecule of CF_3Br, which is surrounded by five units of calyx [4] arene ligand.

hemiaminal to the final imine product. At the hemiaminal stage, the triphenylene core is not completely planar, owing to steric repulsions between the pendant N–H bond and the adjacent C–H bond. Steric repulsion is reduced in the final imine structure, however, where the triphenylene core is no longer distorted and adopts a planar conformation. Here we have seen that *in situ* observation by X-ray crystallography of a hemiaminal intermediate transiently produced during Schiff-base formation illustrates that reactions can occur smoothly within the pores of a coordination network, and that the network's robust crystalline enables direct reaction monitoring through the collection of sequential X-ray 'snapshots'. Here we have seen that such systems even enable X-ray observations of reaction intermediates that are usually transient and non-isolable and the simple and ubiquitous reaction between an amine and an aldehyde, which normally form a very short-lived hemiaminal that yields the Schiff-base product.[1.60]

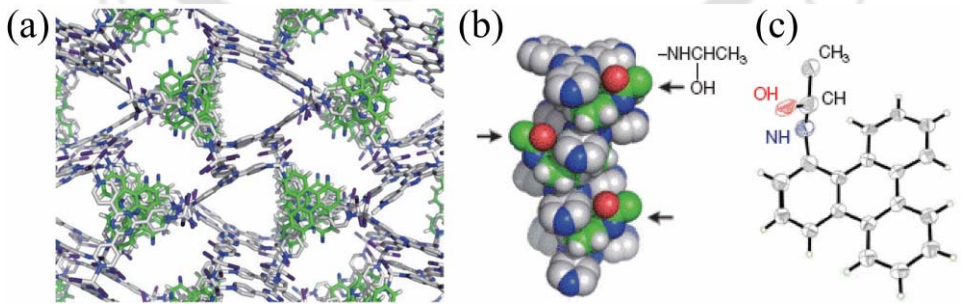

Figure 1.12. (a) Network structure of (In the boxed region) aromatic amine in an alternating donor–acceptor fashion with triazine ligand. The pore is filled with solvent molecules (ethyl acetate), which are omitted for clarity; (b) view of the recognition of columnar stack of hemiaminal and the triazine ligand; (c) Crystal structure of embedded hemiaminal system.

The air-sensitive nature of white phosphorus underlies its destructive effect as a munition. Tetrahedral P_4 molecules readily react with atmospheric dioxygen, leading this form of the

element to spontaneously combust upon exposure to air. The hydrophobic P_4 molecules are rendered air-stable and water-soluble within the hydrophobic hollows of self-assembled tetrahedral container molecules, which form in water from simple organic subcomponents and iron(II) ions (Figure 1.13). This stabilization is not achieved through hermetic exclusion of O_2 but rather by constriction of individual P4 molecules; the addition of oxygen atoms to P_4 would result in the formation of oxidized species too large for their containers. The phosphorus can be released in controlled fashion without disrupting the cage by adding the competing guest benzene. [1.61]

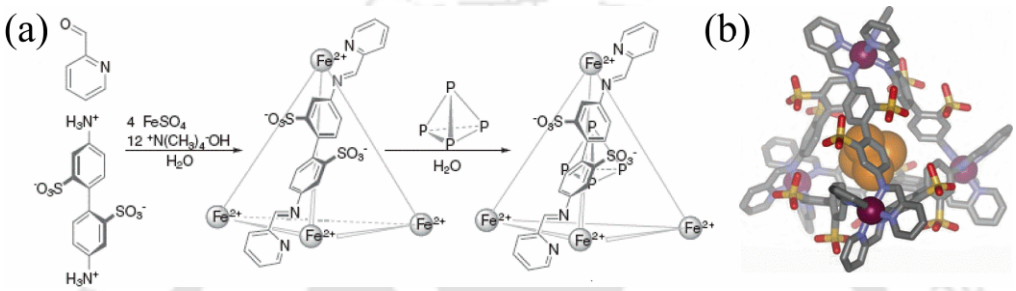

Figure 1.13. (a) Air-stable white Phosphorus within a self-assembled tetrahedral capsule; (b) Crystal structure Crystal structure of $P_4 \subset$1igand.

1.7 Chemistry of aryl azo dyes: Coordination and self assembly

Molecules that change color reversibly due to exposure to radiation of various wave lengths are defined as photochromic compounds. Recently, photochromic compounds have attracted remarkable attention due to their potential application as photonic switch devices, erasable-memory media, and optical data storage and photodrive actuators, and also in photochromic lenses, filters, smart coatings for windows and sun-blinds, specialist clothing, and jewelry.[1.62] The structural change upon light irradiation may switch on target chemical/biochemical reactions, which have immense importance in chemical research.[1.63] On-off switching of electron and energy transfer processes in response to external stimuli is required to communicate information at the molecular level. Photochromic compounds have been used in photoswitchable electron transfer systems and have been applied in photonic molecular devices. However, the terms photoisomerization, photochromism, and photo switching are synonymous with a slight difference in their explicabilities: photoisomerization refers to complete structural change upon light irradiation, while photochromism is also a light-assisted reversible structural change which returns the compound to its primary structure slowly upon switching off the source or irradiating at another wavelength zone. Photochromic materials based on extended π-electron systems such as spiropyrans, benzochromenes, spiroxazines, and azobenzenes are well-known,[1.64]

but these molecular systems have poor long-term light and heat stability. For the development of efficient, stable photochromic performances, research on the design of organic-inorganic hybrid materials[1.65] is important, particularly research on materials which rise to high color ability, fast thermal or photochemical bleaching, low degradation, and so forth. The combination of a photofunctional molecule and metal ions that exhibit magnetic, optical, and electronic properties are of recent importance toward photochromic complexes.[1.62] Azo-conjugated metal complexes exhibit unique properties upon light irradiation in the area of photon-mode high-density information storage photo switching devices.[1.66] Arylazoimidazoles constitute an interesting class of heterocyclic azo compounds as a potential switching group in biological applications and in coordination chemistry, since imidazole is a ubiquitous and essential group in biology, especially as a metal coordination site. π-Deficient nitrogen donor ligands are excellent non-innocent molecules and their complexes comprise special interest in coordination chemistry. Complexes with N heterocycles exhibit rich electrochemistry and interesting optical properties. Ligands have been modified by substituting electron withdrawing/donating groups or bulky groups to the aromatic backbone, substituting other heterocycles, appending extra donor centers to aromatic and/or heterocyclic rings etc.[1.67] One group of conjugated N-hetereocycles is constructed by combining with arylazo ($Ar-\overset{+}{N}\equiv N$) molecular unit. They are known as arylazoheterocycles.[1.68] Azo conjugated transition metal complexes can provide new opportunity towards redox, magnetic and optical properties originating from the *d* orbitals.[1.69] A characteristic feature of these conjugated complexes that the transition metals can interact with each other through the π-conjugated backbone to permit electronic communication. Bis-/tris–hetero chelated complexes may exhibit inter-ligand charge transferences along with some structural distortion and/or backbone deformation.[1.70] For the last several years there are several complexes with aryl

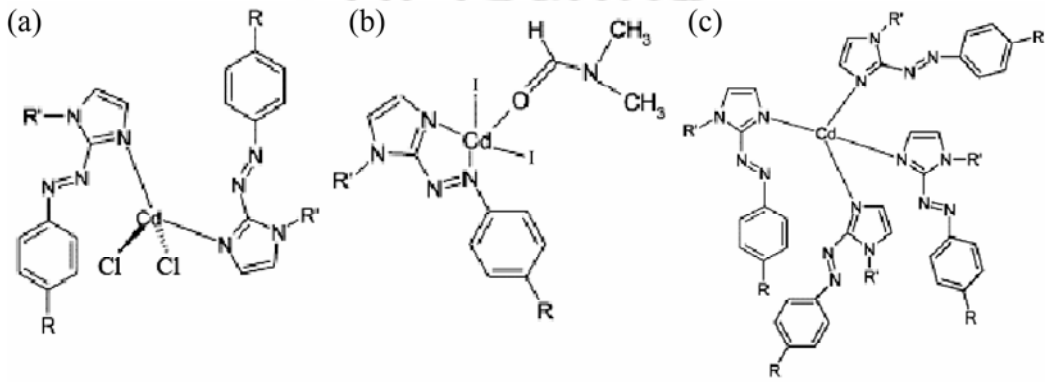

Figure 1.14. Molecular structures of : (a) $[Cd(PaiMe)_2Cl_2]$; (b) $[Cd(PaiEt)(I)_2.DMF]$; (c) $[Cd(PaiMe)_4]^{2+}$.

azo dyes with different metals with alkali metals, alkaline earth metals, transition metals, heavy metals and even lanthanides are known in literature.[1.71] Figure 1.12 shows that, the aryl azo imidazole system containing the metal complexes with salts Cd(II) salts (Figure 1.14.a). The reaction between CdI_2 and the ligand 1-methyl-2-(p-tolylazo) imidazole (PaiMe) gives a neutral mononuclear complex of composition $[Cd(PaiEt)(I)_2.DMF]$ (Figure 1.14.b). Likewise, the reaction between $Cd(ClO_4)_2$ and the ligand 1-methyl-2-(p-tolylazo) imidazole (PaiMe) produces $[Cd(PaiMe)_4][(ClO_4)_2]$ (Figure 1.14.c).[1.71c]

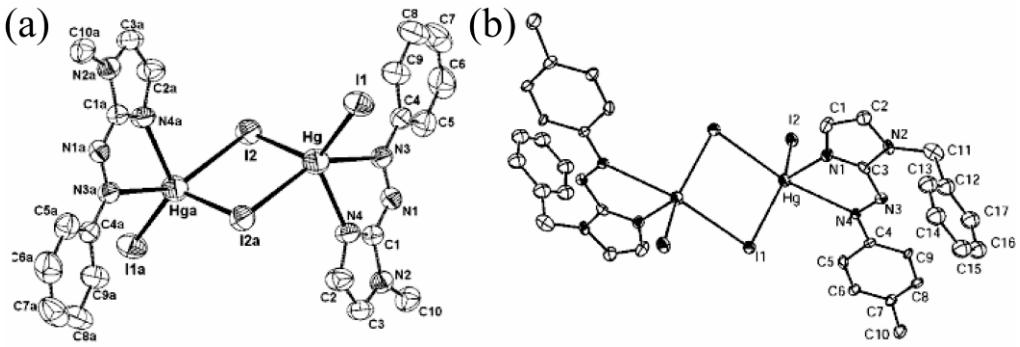

Figure 1.13. Molecular structures of iodo-bridged dimers: (a) $[Hg(Pai\text{-}Me)(\mu\text{-}I)(I)]_2$; (b) $[Hg(Pai\text{-}CH_2Ph)(\mu\text{-}I)(I)]_2$.

Metal center is surrounded by one unidentate ligands and two iodo-bridged dimer groups (Figure 1.13.a). Microwave irradiation of HgI_2 and the ligand 1-benzyl-2-(p-tolylazo) imidazole (PaiMe) form $[Hg(Pai\text{-}CH_2Ph)(\mu\text{-}I)(I)]_2$ (Figure 1.15.b). Single crystal of both the complexes shows intercalated HgI_2 in the layers of Pai-Me and they exist independently in interpenetrated arrays.[1.72]

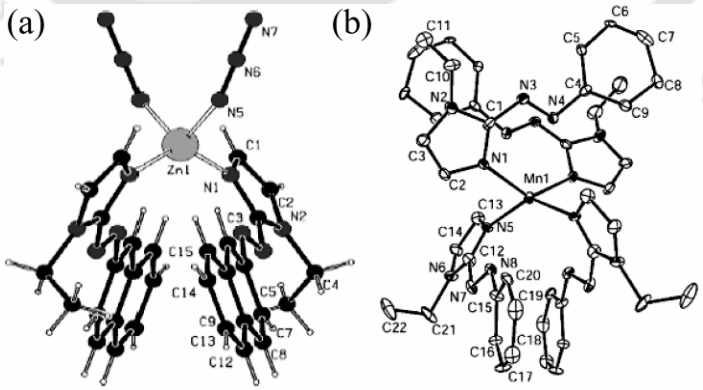

Figure 1.15. (a) Molecular structures mononuclear $[Zn(Napai\text{-}Et)_2\text{-}N_3)_2]$ complex; (b) Molecular structures mononuclear $[Mn(HaaiEt)_4]^{2+}$ complex.

Likewise, aryl azo imidazole system shows the metal complexes with Zn(II) and Mn(II) salts (Figure 1.15 b). Manganese is chosen because of its essential structural and catalytic role in many proteins.[1.73] The active site involves the binding of imidazoles-N from

histidine residues to Mn(II). Besides, the high local spin value of Mn(II) (d^5) enable this metal ion in the exploration of magnetic materials.[1.74] Similarly, Zn(II) containing aryl azo complexes have been considerably investigated as potential luminescent materials.[1.75, 1.76] Figure 1.16.a shows the $CaCl_2$ salts of 4-(4-hydroxyphenylazo) benzene sulfonic acid.[1.77] Each Ca atom bonds to two terminal and mutually *trans* water ligands. The remaining four bonds are to the O atoms of the sulfonate groups of four azo ligands which form bridges of the M–O–S– O–M type to give a one-dimensional chain of eight-membered rings lying parallel to the *b* direction. Figure 1.16.b. shows bimetallic complexes are linked together using diazotization reactions that generate a chromophore at the heart of the assembly, permitting visible light excitation of the bound lanthanide ions. The stability of systems such as these in the forcing conditions inherent to diazotization reactions is further evidence for the kinetic inertness of such complexes. This approach allows not only the preparation of heterometallic systems containing different lanthanide ions but also the simultaneous incorporation of a sensitizing chromophore.

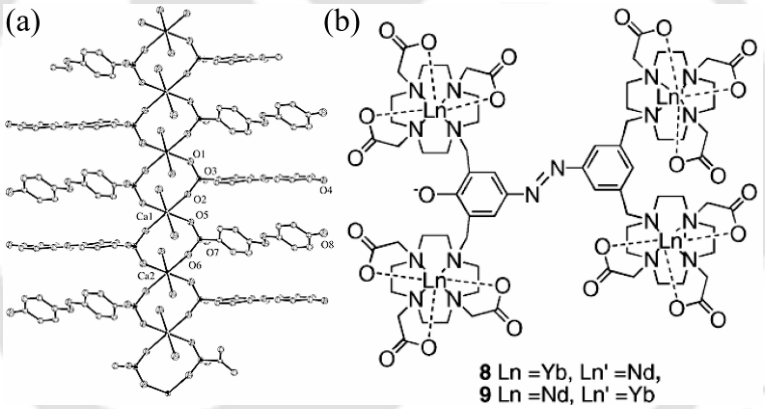

Figure 1.16. (a) Supramolecular motifs in s-block metal bound sulfonated monoazo dyes; (b) Azo-Dye Derivatives of Polymetallic Lanthanide Complexes

References:

1.1 (a) Akin-Ojo, O.; Wang, F. *J. Phys. Chem. B,* **2009**, *113*, 1237; (b) Baek, S. H.; Chang, W-J.; Baek, J-Y.; Yoon, D. S.; Bashir, R.; Lee, S. W. *Anal. Chem.,* **2009**, *81*, 7737; (b) Li, T.; Ayers, P. W.; Liu, S.; Swadley, M. J. Aubrey-Medendorp, C. *Chem. Eur. J.,* **2009**, *15*, 361;

1.2 (a) Matsumoto, Y.; Unal, U.; Kimura, Y.; Ohashi, S.; Izawa, K. *J. Phys. Chem. B,* **2008**, *112*, 7145; (b) Bosshard, H. R. Marti, D. N. Jelesarov , I. *J. Mol. Recognit.,* **2004**, *17*, 1; (c) Fogolari, F.; Brigo, A.; Molinari, H. *J. Mol. Recognit.,* **2002**, *15*, 377.

1.3 (a) Lehn, J. M. *Supramolecular chemistry*, 1**993**, *Science, 260*, 1762; (b) Lehn, J.-M. *Supramolecular Chemistry,* Wiley-VCH, **1995**.

1.4 (a) Oshovsky, G. V.; Reinhoudt, D. N.; Verboom, W. *Angew. Chem. Int. Ed. Engl.,* **2007**, *46*, 2366; (b) Xu, X-N.; Wang, L.; Wang, G-T.; Lin, J-B.; Li, G-Y.; Jiang, X-K.; Li, Z-T. *Chemistry - A European Journal,* **2009***, 15*, 5763; (c) Liu, Y.; Liu, X.; Warmuth, R. *Chem. Eur. J.*, 2007*, 13*, 8953.

1.5 (a) Sato, S.; Ishido, Y.; Fujita, M. *J. Am. Chem. Soc.,* **2009**, *131*, 6064; (b) Melman, G.; Vimal, P.; Melman, A. I*norg. Chem.,* **2009**, *48*, 8662. (c) Hawley, J. C.; Bampos, N.; Sanders J. K. M. *Chem. Eur. J.,* **2003**, *9*, 5211; (d) Chang, S-Y.; Jang, H-Y.; Jeong, K-S.; *Chem. Eur. J.,* **2003**, *9*, 1535.

1.6 (a) Medda, S. K.; De, G. Ind. Eng. Chem. Res., 2009, 48, 6906; (b) Ohtaka, A.; Kuniyasu, H.; Kinomoto, M.; Kurosawa, H. *J. Am. Chem. Soc.,* **2002**, *124*, 14324.

1.7 (a) Adams, R. D. *J. Am. Chem. Soc.,* **2008**, *130,* 14019; (b) Altisent, R.; Graell, J.; Lara, I.; Lopez, L.; Echeverrla, G. *J. Agric. Food Chem.,* **2008**, *56,* 8490; (c) O'Doherty, G. A. *J. Am. Chem. Soc.,* **2008**, *130*, 6651.

1.8 (a) Harke, B.; Ullal, C. K.; Keller, J.; Hell, S. W. *Nano Lett.,* **2008**, *8*, 1309; (b) Lee, S. H.; Nakamura, T.; Tsutsui, T. *Org. Lett.,* **2001**, *3*, 2005; (c) Jiang, H.; Taranekar, P.; Reynolds, J. R.;. Schanze, K. S. *Angew. Chem. Int. Ed. Engl.,* **2009**, *48*, 4300; (d) Zacharias, P.; Gather, M. C.; Kohnen, A.; Rehmann, N.; Meerholz, K.; *Angew. Chem. Int. Ed. Engl.,* **2009**, *48*, 3883.

1.9 (a) Turro, N. J. *Modern Molecular Photochemistry*; University Science Books: Herndon, VA, **1991**; (b) Turro, N. J.; Scaiano, J. C.; Ramamurthy, V. *Principles of Molecular Photochemistry: An Introduction*; University Science Books: Herndon, VA, **2009**. (c) Horspool, W. M.; Lenci, F. *CRC Handbook of Organic Photochemistry and Photobiology*; CRC Press: Boca Raton, FL, **2003.**

1.10 (a) Crofts, A. R. *Book Review of Primary Processes of Photosynthesis: Principles and Apparatus, Parts 1−2.; J. Am. Chem. Soc.,* **2009**, *131*, 1620; (b) Muller, A. M.; Wasmund, N.; *Internat. Rev. Hydrobiol.,* **2003**, *88,* 482; (d) Sage, R. F. *New Phytologist*., **2004**, *161,* 341.

1.11 (a) Zhang, Y.; Yiping R.; Zhang, Y. *Chem. Rev.*, **2009**, *109*, 4375; (b) Diamond, D.; Coyle, S.; Scarmagnani, S.; Hayes, J. *Chem. Rev.*, **2008**, *108*, 652; (c) Waitt, C.; Buchanan-Smith, H. M. *Am. J. Primatol.,* 2006, *68*, 1054; (d) Buchanan-Smith, H. M. *Am. J. Primatol.,* 2005, *67*, 393.

1.12 (a) Shitanda, I.; Tatsuma, T.; *Anal. Chem.*, **2006**, *78*, 349; (b) Ito, M.; Sudo, Y.; Furutani, Y.; Okitsu, T.; Wada, A.; Homma, M.; Spudich, J. L.; Kandori, H.; *Biochemistry*, **2008**, *47*, 6208; (c) Josef, K.; Saranak,

J.; Foster, K. W. *Cell Motility and the Cytoskeleton,* **2005**, *61*, 97; (d) Bhaya, D. *Molecular Microbiology*, **2004**, *53*, 745.

1.13 (a) Roh, J-Y.; Sim, S. J.; Yi, J,; Park, K.; Chung, K. H.; Ryu, D-Y.; Choi, J. *Environ. Sci. Technol.*, **2009**, *43*, 3933; (b) Pieters, B. J.; Liess, M. *Environ. Sci. Technol.*, **2006**, *40*, 6157; (c) Ruegg1, S.; Hunziker, P.; Marsch, S.; Schindler, C. *Epilepsia,* **2007**, *48*, 1; (d) Tsumura, N. *Col Res Appl.,* **2006***, 31,* 270.

1.14 (a) Stock, N. L.; Peller, J.; Vinodgopal, K.; Kamat, P. V. *Environ. Sci. Technol.*, **2000**, *34*, 1747; (b) Bellobonoa, I. R.; Bianchib, R.; Martinic, G. D.; Tozzic, P. M.; Bonardid, M. L.; Groppid, F.; Rossi, M. J. *Chemometrics*, **2008**, *22,* 425; (c) Damszel, J. G.; Morawski, A. W. *Asia-Pac. J. Chem. Eng.* **2009**, *4*, 239; (d) Min, L.; Wu, X-Z.; Tetsuya, S.; Inoue, H. *Luminescence,* **2007**, *22*, 105.

1.15 (a) He, Y.; Lv, Yi.; Hu, J.; Qi1, L.; Hou, X. *Luminescence,* **2007**, *22*, 309; (b) Ferreira, J.; Menezes, P.F.C.; Kurachi, C.; Sibata, C.; Allison, R. R.; Bagnato, V. S. *Laser Phys. Lett.,* **2008**, *5*, 156; (c) Wang, G.; Wu, F.; Zhang, Xu.; Luo, M.; Deng, N. *J Chem Technol Biotechnol.,* **2006**, *81*, 805; (d) Stapleton, H. M.; Davis, E. F. *Environ. Sci. Technol.*, **2009**, *43*, 7994.

1.16 (a) Armaroli, N.; Eckert, J. F.; Nierengarten, J. F. *Chem. Commun.*, **2000**, 2105; (b) Armaroli, N. *Photochem. Photobiol. Sci.*, **2003**, *2*, 73.

1.17 (a) Gunnlaugsson, T.; Mac Donaill, D. A.; Parker, D. *J. Am. Chem. Soc.*, **2001**, *123*, 12866; (b) de Silva, A. P.; Fox, D. B.; Huxley, A. J. M.; Moody, T. S. *Coord. Chem. Rev.*, **2000**, *205*, 41; (c) Fabbrizzi, L.; Licchelli, M.; Rabaioli, G.; Taglietti, A. *Coord. Chem. Rev.*, **2000**, *205*, 85.

1.18 (a) Borzsonyi, G.; Fenniri, H. *J. Am. Chem. Soc.*, **2009**, *131*, 3405; (b) Vasconcelos, A.; Freddi, G.; Cavaco-Paulo, A. *Biomacromolecules*, **2009**, *10* , 1019; (c) Chekmeneva, E.; Hunter, C. A.; Packer, M. J.; Turega, S. M. *J. Am. Chem. Soc.*, **2009**, *131*, 3786.

1.19 (a) Samuel H. Gellman, *Chem. Rev.,* **1997***, 97,* 1231; (b) Berlin, K. D. *J. Am. Chem. Soc.*, **2009**, *131*, 15963; (c) Rich, R. L.; Myszka, D. G. J. Mol. Recognit. **2007**, 20, 300; (d) Kim, S. K.; Lee, D. H.; Hong, J-I.; Yoon, J. *Acc. Chem. Res.*, **2009**, *42*, 23.

1.20 (a) Shinkai, S.; Ikeda, M.; Atsushi, S.; Takeuchi, M.; *Acc. Chem. Res.,* **2001**, *34*, 494; (b) Ma, M.; Gong, Y.; Bong, D. *J. Am. Chem. Soc.*, **2009**, *131*, 16919; (c) Oishi, S.; Yoshimoto, J.; Saito, S. *J. Am. Chem. Soc.*, **2009**, *131*, 8748; (d) Chung, M-K.; White, P. S.; Lee, S. J.; Gagne, M. R. *Angew. Chem. Int. Ed. Engl.,* **2009**, *48*, 8683.

1.31 Lehn, J. M. *Angew. Chem., Int. Ed.* **2002**, *41*, 3738; (b) Seidel, S. R.; Stang, P. J. *Acc. Chem. Res.,* **2002**, *35*, 972-; (c) Lusby, P. J.; Moller, P.; Pike, S. J.; Slawin, A. M. Z. *J. Am. Chem. Soc.*, **2009**, *131*, 16398; (d) Rivera, D.l G.; Wessjohann, L. A. *J. Am. Chem. Soc.*, **2009**, *131*, 3721.

1.22 (a) Meyer, E. A.; Castellano, R. K.; Diederich, F. *Angew. Chem., Int. Ed.,* **2003**, 42, 1210; (b) Gamez, P.; Mooibroek, T. J.; Teat, S. J.; Reedijk, J. *Acc. Chem. Res.*, **2007**, *40*, 435; (c) Gung, B. W.; Wekesa, F.; Barnes, C. L. *J. Org. Chem.*, **2008**, *73*, 1803; (d) Mazik, M.; Konig, A. *J. Org. Chem.*, **2006**, *71*, 7854.

1.23 (a) Rekharsky, M. V.; Inoue, Y. *Chem. Rev.,* **1998**, *98*, 1875; (b) Petrillo, M.; Marinescu, L.; Rousseau, C.; Bols, M. *Org. Lett.*, **2009**, *11*, 1983; (c) Cho, S. Y.; Allcock, H. R. *Macromolecules*, **2009**, *42*, 4484.

1.24 (a) Danjo, H.; Hirata, K.; Yoshigai, S.; Azumaya, I.; Yamaguchi, K. *J. Am. Chem. Soc.*, **2009**, *131*, 1638; (b) Mori, K.; Ohmori, K.; Suzuki, K. *Angew. Chem., Int. Ed.,* **2009**, 48, 5638.

1.25 (a) Wang, B-Y.; Rieth, S.; Badjic, J. D. *J. Am. Chem. Soc.*, **2009**, *131*, 7250; (b) Ihm, C.; Jo, E.; Kim, J.; Paek, K. *Angew. Chem., Int. Ed.,* **2006**, 45, 2056.

1.26 (a) Brotin, T.; Dutasta, J-P. *Chem. Rev.*, **2009**, *109*, 88; (b) Brotin, T.; Barbe, R.; Darzac, M.; Dutasta, J-P. *Chem. Eur. J.*, **2003**, *9*, 5784.

1.27 (a) Hill, P. A.; Wei, Q.; Troxler, T.; Dmochowski, I. J. *J. Am. Chem. Soc.*, **2009**, *131*, 3069; (b) French, D. C.; Lutz, M. R.; Lu, J. C.; Zeller, M.; Becker, D. P. *J. Phys. Chem. A*, **2009**, *113*, 8258.

1.28 (a) Hof, F.; Craig, S. L.; Nuckolls, C.; Rebek, J. *Angew. Chem., Int. Ed.,* **2002**, *41*, 1488; (b) Yamanaka, M.; Toyoda, N.; Kobayashi, K. *J. Am. Chem. Soc.*, **2009**, *131*, 9880; (c) Pluth, M. D.; Bergman, R. G.; Raymond , K. N. *Acc. Chem. Res.*, **2009**, *42*, 1650.

1.29 (a) Han, X.; Zhou, Z.; Yang, F.; Deng, Z. *J. Am. Chem. Soc.*, **2008**, *130*, 14414;(b) Su, X.; Luo, K.; Xiang, Q.; Lan, J.; Xie, R. *Chirality*, **2009**, *21*, 539.

1.30 (a) Kirsch, M.; Talbiersky, P.; Polkowska, J.; Bastkowski, F.; Schaller, T.; Groot, H. D.; Klarner, F-G.; Schrader, T. *Angew. Chem., Int. Ed.,* **2009**, *48*, 2886; (b) Gomes, R.; Parola, A. J.; Bastkowski, F.; Polkowska, J.; Klarner, F-G. *J. Am. Chem. Soc.*, **2009**, *131*, 8922.

1.31 (a) Katagiri, K.; Tohaya, T.; Masu, H.; Tominaga, M.; Azumaya, I. *J. Org. Chem.*, **2009**, *74*, 2804; (b) Wei, W.; Wu, M; Gao, Q.; Zhang, Q.; Huang, Y.; Jiang, F.; Hong, M, *Inorg. Chem.*, **2009**, *48*, 420.

1.32 (a) Podeszwa, R. *J. Phys. Chem. A*, **2008**, *112* , 8884; (b) Kohmoto, S.; Kuroda, Y.; Kishikawa, K.; Masu, H.; Azumaya, I. *Cryst. Growth Des.*, **2009**, *9*, 5017.

1.33 (a) Dong, Z.; Liu, J.; Mao, S.; Huang, X.; Yang, B.; Ren, X.; Luo, G.; Shen J. *J. Am. Chem. Soc.,* **2004**, *126*, 16395; (b) Ren, X.; Jemth P.; Board, P. G.; Luo, G.; Mannervik, B.; Liu, J.; Zhang K.; Shen, *J. Chem. Biol.,* **2002**, *9*, 789; (c) Ren, X.; Gao, S.; You, D.; Huang, H.; Liu, Z.; Mu, Y.; Liu, J.; Zhang, Y.; Yan, G.; Luo, G.; Yang, T.; Shen, J. *Biochem. J.,* **2001**, *359*, 369; (d) Ding, L.; Liu, Z.; Zhu, Z.; Luo, G.; Zhao, D.; Ni, J. *Biochem. J.*, **1998**, *332*, 251.

1.34 (a) Das, M. C.; Ghosh, S. K.; Bharadwaj, P. K. *CrystEngComm*, **2010**, DOI:10.1039/b912264h; (b)Wallace, K. J.; Belcher, W. J.; Turner, D. R.; Syed, K. F.; Steed, J. W. *J. Am. Chem. Soc.*, **2003**, *125*, 9699; (c) Lakshminarayanan, P. S.; Ravikumar, I.; Suresh, E.; Ghosh, P. *Chem. Commun.*, **2007**, 5214.

1.35 (a) Bianchi, A.; Bowman-James, K.; Garcia Espana, E. *Supramolecular Chemistry of Anions, Eds,* Wiley-VCH, New York, **1997**; (b) Martinez-Manez, R.; Sancenon, F. *Chem. Rev.,* **2003**, *103***,** 4419; (c) Nagasawa, Y.; Oishi, A.; Itoh, T.; Yasuda, M.; Muramatsu, M.; Ishibashi, Y.; Ito, S.; Miyasaka, H. *J. Phys. Chem. C*, **2009**, *113*, 11868.

1.36 (a) Beer, P. D.; Gale, P. A. *Angew. Chem. Int. Ed.,* **2001**, 40, 486. (b) Schmidtchen, F. P.; Berger, M. *Chem. Rev.,* **1997**, *97*, 1609; (c) Atwood, J. L.; Holman, K. T.; Steed, J. W. *Chem. Commun.,* **1996**, 1401.

1.37 (a) Kang, J.; Kim, H. S.; Jang, D. O. *Tetrahedron Lett.,* **2005**, *4*, 6079; (b) Gunnlaugsson, T.; Davis, A. P.; O'Brien, J. E.; Glynn, M. O*rg. Lett.;* **2002**, *4*, 2449; (c) Kim, S. K.; Yoon, J.; *Chem. Commun.,***2002**, 770; (d) Vance, D. H.; Czarnik, A. W. *J. Am. Chem. Soc.,* **1994**, *116* 9397.

1.38 (a) Curiel, D.; Cowley, A. Beer, P. D. *Chem. Commun.;* **2005**, 236; (b) Kovalchuk, A.; Bricks, J. L.; Reck, G.; Rurack, K.; Schulz, B.; Szumna, A.; Weibhoff, H. *Chem. Commun.;* **2004**, 1946; (c) Klosterman, J. K.; Iwamura, M.; Tahara, T.; Fujita, M. *J. Am. Chem. Soc.*, **2009**, *131*, 9478; (d) Zeng, Y.; Zhang, G.; Zhang, D.; Zhu, D. *J. Org. Chem.*, **2009**, *74*, 4375.

1.39 (a) Zhang, X.; Guo, L.; Wu, F.-Y.; Jiang, Y.-B. *Org. Lett.*, **2003**, *5*, 2667; (b) Harpe, K. D. L.; Crespo-Hernandez, C. E.; Kohler, B. *J. Am. Chem. Soc.*, **2009**, *131*, 17557; (c) Shemesh, D.; Sobolewski, A. L.; Domcke , W. *J. Am. Chem. Soc.*, **2009**, *131*,1374.

1.40 (a) Beer, P. D. *Acc. Chem. Res.* **1998**, *31*, 71; (b) Henry, W.; Coates, C. G.; Brady, C.; Ronayne, K. L.; Matousek, P.; Towrie, M.; Botchway, S. W.; Parker, A. W.; Vos, J. G.; Browne, W. R.; McGarvey, J. J. *J. Phys. Chem. A*, **2008**, *112*, 10704.

1.41 (a) Wu, J.-S.; Zhou, J.-H.; Wang, P.-F.; Zhang, X.-H.; Wu, S.-K.; *Org. Lett.*; **2005**, *7*, 2133. (b) Nishizawa, S.; Kato, Y.; Teramae, N. *J. Am. Chem. Soc.;* **1999**, *121*, 9463; (c) Nishizawa, S.; Kaneda, H.; Uchida, T.; Teramae, N.; *J. Chem. Soc., Perkin Trans. 2,* **1998**, 2325.

1.42 (a) Fabbrizzi, L.; Marcotte, N.; Stomeo, F.; Taglietti, A. *Angew. Chem., Int. Ed.*; **2002**, *41*, 3811; (b) Wiskur, S. L.; Ait-Haddou, H.; Lavigne, J. J.; Anslyn, E. V. *Acc. Chem. Res.;* **2001**, *34*, 963; (c) Niikura, K.; Metzger, A.; Anslyn, E. V. *J. Am. Chem. Soc.;* **1998**, *120*, 8533.

1.43 (a) Antonisse, M. M. G.; Reinhoudt, D. N. *Electroanalysis,* **1999**, *11*, 1035; (b) Antonisse, M. M. G.; Reinhoudt, D. N. *Chem.Commun.,* **1998**, 443; (c) Wiskur, S. L.; Ait-Haddou, H.; Lavigne, J. J.; Anslyn, E. V. *Acc. Chem. Res.,* **2001**, *34*, 963;(d) Schmidtchen, F. P.; Berger, M. *Chem. Rev*., **1997**, *97*, 1609.

1.44 (a) Niikura, K.; Metzger, A.; Anslyn, E. V. *J. Am. Chem. Soc.,* **1998**, *120*, 8533; (b) Bazzicalupi, C.; Bencini, A.; Biagini, S.; Faggi, E.; Meini, S.; Giorgi, C.; Spepi, A.; Valtancoli, B.; *J. Org. Chem.*, **2009**, *74*, 7349; (c) Wang, X.; Sarycheva, O. V.; Koivisto, B. D.; McKie, A. H.; Hof, F. *Org. Lett.*, **2008**, *10*, 297.

1.45(a) Mecozzi, S.; West, A. P.; Dougherty, D. A. *J. Am. Chem. Soc.,* **1996**, *118*, 2307; (b) Thaher, B. A.; Koch, P.; Schattel, V.; Laufer, S. *J. Med. Chem.*, **2009**, *52*, 2613; (c) Beletskaya, I.; Tyurin, V. S.; Tsivadze, A. Y.; Guilard, R.; Stern, C. *Chem. Rev.*, **2009**, *109*, 1659.

1.46 (a) Reetz, M. T.; Niemeyer, C. M.; Harms, K. *Angew. Chem., Int. Ed. Engl*., **1991**, *30*, 1472; (b) Rich, R. L.; Myszka, D. G. *J. Mol. Recognit.,* **2008**, *21*, 355; (c)

1.47 (a) Morzherin, Y.; Rudkevich, D. M.; Verboom, W.; Reinhoudt, D. N. *J. Org. Chem*., **1993**, *58*, 7602. (b) Casnati, A.; Fochi, M.; Minari, P.; Pochini, A.; Reggiani, M.; Ungaro, R.; Reinhoudt, D. N. *Gazz. Chim. Ital*., **1996**, 99.

1.48 (a) Beer, P. D.; Hazlewood, C.; Hesek, D.; Hodacova, J.; Stokes, S. E. *J. Chem. Soc., Dalton. Trans*., **1993**, 1327; (b). Hansen, H. S.; Petersen, G.; Artmann, A.; Madsen, A. N. *Eur. J. Lipid Sci. Technol.,* **2006** , *108,* 877; (c) Alexander, Cameron.; Andersson, H. S.; Andersson, L. I.; Ansell, R. J.; Kirsch, N.; Nicholls, I. A.; O'Mahony, J.; Whitcombe, M. J. J. Mol. Recognit., **2006**, *19*, 106.

1.49 (a) Raposo, C.; Perez, N.; Almaraz, M.; Luisa Mussons, M.; Cruz Cabarello, M.; Moran, J. R. *Tetrahedron Lett*., **1995**, *36*, 3255; (b) Chen, K-H.; Liao, J-H.; Chan, H-Y.; Fang, J-M. *J. Org. Chem.*, **2009**, *74*, 895; (d) Bhosale, S. V.; Kalyankar, M. B.; Langford, S. J. *Org. Lett.*, **2009**, *11*, 5418.

1.50 (a) Custelcean, R.; Remy, P.; Bonnesen, P. V.; Jiang, D-E.;. Moyer, B. A. *Angew. Chem., Int. Ed. Engl*., **2008**, *47*, 186; (b) Cameron, B. R.; Loeb, S. J. *J. Chem. Soc., Chem. Commun.,* **1997**, 573; (c) Wyman, I. W.; Macartney, D. H. *J. Org. Chem.*, **2009**, *74*, 8031; (d) Ono, K.; Klosterman, J. K.; Yoshizawa, M.; Sekiguchi, K.; Tahara, T.; Fujita, M. *J. Am. Chem. Soc.*, **2009**, *131*, 12526; (e) Alemany, P.; Llunell, M.; Canadell, E. *Inorg. Chem.*, **2009**, *48*, 2919.

1.51 (a) Raposo, C.; Almaraz, M.; Martin, M.; Weinrich, V.; Mussons, M. L. ; Alcazar, V.; Caballero, M. C.; Moran, J. R.; *Chem. Lett.,* **1995**, *9*, 759; (b) Berrocal, M. J.; Cruz, A.; Badr, I. H. A.; Bachas, L. G.; *Anal. Chem.,* **2000**, *72*, 5295; (c) Jose, D. A.; Kumar, D. K.; Ganguly, B.; Das, A. *Inorg. Chem.* **2007**, *46*, 5817; (d) Custelcean, R.; Moyer, B. A. Hay, B. P.; *Chem. Commun*., **2005**, 5971.

1.52 (a) Yang, H.-B.; Wang, D -X.; Wang, Q -Q.; Wang, M-X. *J. Org. Chem.,* **2007**, *72*, 3757; (b) Hou, B-Y.; Wang, D -X.; Zheng, Q-Y.; Wang, M-X. *J. Org. Chem.,* **2007**, *72*, 5218; (c) Wang, Q-Q.; Wang, D –X.;

Zheng, Q -Y.; Wang, M-X.; *Org. Lett.,* **2007**, *9*, 2847; (d) Wang, D-X.; Zheng, Q-Y.; Wang, Q-Q.; Wang, M-X. *Angew. Chem., Int. Ed. Engl.,* **2008**, *47,* 7485.

1.53 (a) Werner, F.; Schneider, H. J. *Helv. Chim. Acta,* **2000**, *83*, 465; (b) Kakuchi, R.; Nagata, S.; Sakai, R.; Otsuka, I.; Nakade, H.; Satoh,T.; Kakuchi, T. *Chem. Eur. J.,* **2008**, *14*, 10259.

1.54 (a) Kakuchi, R.; Nagata, S.; Tago, Y.; Sakai, R.; Otsuka, I.; Satoh, T.; Kakuchi, T. *Macromolecules,* **2009**, *42*, 1476; (b) Kakuchi, R.; Kodama, T.; Shimada, R.; Tago, Y.; Sakai, R.; Satoh, T; and Kakuchi, T. *Macromolecules,* **2009**, *42*, 3892.

1.55 (a) Deetz, M. J.; Smith, B. D. *Tetrahedron Lett.,* **1998**, *39*, 6841; (b) Beer, P. D.; Cadman, J. *New. J. Chem.,* **1999**, *23*, 347.

1.56 Yang, W.; Yan, Y.; Fang, H.; Wang, B. *Chem. Commun.,* **2003**, 792; (b) Martınez-Manez, R.; Sancenon, F. *Chem. Rev.,* **2003**, *103*, 4419.

1.57 Vance, D. H.; Czarnik, A. W. *J. Am. Chem. Soc.,* **1994**, *116*, 9397.

1.58 (a) Hosseini, M. W.; Blacker, A. J.; Lehn, J.-M. *J. Chem. Soc., Chem. Commun.,* **1988**, 596; (b) Hosseini, M. W.; Blacker, A. J.; Lehn, J.-M. *J. Am. Chem. Soc.,* **1990**, *112*, 3896.

1.59 Atwood, J. L.; Barbour, L. J. Jerga, A. *Science*, **2002**, *296*, 2367.

1.60 Kawamichi, T.; Haneda, T.; Kawano, M.; Fujita, M. *Nature*, **2009**, *461*, 633.

1.61 Mal, P.; Breiner, B.; Rissanen, K.; Nitschke, J. R. *Science*, **2009**, *324*, 1697.

1.62 (a) Higashiguchi, K.; Matsuda, K.; Irie, M. *Angew. Chem., Int. Ed.,* **2003**, *42*, 3537; (b) Kume, S.; Nishihara, H. *Dalton Trans.,* **2008**, 3260; (c) Nishihara, H. *Coord. Chem. Re*V., **2005**, *249*, 1468; (d) Durr, H., Bouas-Laurent, H. *Photochromism- Molecules and Systems Eds.;* Elsevier: Amsterdam, **2003**.

1.63 (a) Tsuchiya, S. *J. Am. Chem. Soc.* **1999**, *121*, 48; (b) Akasaka, T.; Inoue, H.; Kuwabara, M.; Mutai, T.; Otsuki, J.; Araki, K. *Dalton Trans,* **2003**, 815; (c) Otsuki, J.; Suka, A.; Yamazaki, K.; Abe, H.; Araki, Y.; Itob, O. *Chem. Commun* **2004**, 1290; (d) Otsuki, J.; Akasaka, T.; Araki, K. *Coord. Chem. Rev.,* **2008**, *252*, 32.

1.64 (a) Higgins, S. *Chem. Br.,* **2003**, *39*, 26; (b) Jennifer, A.; Weller, M. T. *Chem.Commun,* **2006**, 1094.

1.65 (a) Munakata, M.; Han, J.; Nabei, A.; Kuroda-Sowa, T.; Maekawa, M.; Suenaga, Y.; Gunjima, N. *Inorg. Chim. Acta,* **2006**, *359*, 4281; (b) Han, J.; Maekawa, M.; Suenaga, Y.; Ebisu, H.; Nabei, A.; Kuroda-Sowa, T.; Munakata, M. *Inorg. Chem.,* **2007**, *46*, 3313.

1.66 (a) Nishihara, H. *Bull. Chem. Soc. Jpn.,* **2004**, *77*, 407; (b) Tamai, N.; Miyasaka, H. *Chem. Rev.,* **2000**, *100*, 1857; (c)Yagai, S.; Karatsu, T.; Kitamura, A. *Chem. Eur. J.,* **2005**, *11*, 4054; (d) Irie, M. *Chem.Rev.*, **2000**, *100*, 1683; (e) Ikeda, T.; Tsutsumi, O. *Science,* **1995**, *268*, 1873; (f) Kawata, S.; Kawata, Y. *Chem. Rev.,* **2000**, *100*, 1777.

1.67 (a) Pramanik, K.; Shivakumar, M.; Ghosh, P.; Chakravorty, A. *Inorg. Chem.,* 2000, **39**, 195; (b) Velders, A.H.; Keojiman, H.; Spek, A.L.; Haasnoot, J.G.; de Vos, D.; Reedijk, J. *Inorg. Chem.*, **2000**, *39*, 2966; (c) Byabartta, P.; Pal, S.; Misra, T.K.; Sinha, C.; Liao, F.-L.; Panneerselvam, K.; Lu, T.-H. *J. Coord. Chem.,* **2002**, *55*, 479.

1.68 (a) Ghosh, B.K.; Chakravorty, A. *Coord. Chem. Rev.*, **1989**, *95*, 239; (b) Wu, F.; Chamchoumis, C.M.; Thummel, R. P. *Inorg. Chem.*, 2000, 39, 584.

1.69 (a) Pramanik, K.; Shivakumar, M.; Ghosh, P.; Chakravorty, A. *Inorg. Chem.*. **2000**, *39*, 195; (b) Shivakumar, M.; Pramanik, K.; Bhattacharya, I.; Chakravorty, A. *Inorg. Chem.,* **2000**, *39*, 4332; (c) Shivakumar, M.; Pramanik, K.; Ghosh, P.; Chakravorty, A. *Chem. Commun.,* 1998, 2103.

1.70 (a) Otsuki, J.; Suwa, K.; Sarker, K. K.; Sinha, C. *J. Phys. Chem. A,* **2007**, *8*, 1403; (b) Sarker, K. K.; Chand, B. G.; Suwa, K.; Cheng, J.; Lu, T.-H.; Sinha, C. *Inorg. Chem.,* **2007**, *46*, 670; (c) Sarker, K. K.; Sardar, D.; Suwa, K.; Otsuki, J.; Sinha, C. *Inorg. Chem.,* **2007**, *46*, 8291.

1.71 (a) Placidi, M. P.; Villaraza, A. J. L.; Natrajan, L. S.; Sykes, D.; Kenwright, A. M.; Faulkner, S. *J. Am. Chem. Soc.,* **2009**, *131*, 9916; (b) Kennedy, A. R.; Hughes, M, P.; Monaghan, M. L.; Staunton, E.; Teat S. J.; Smith, W. E. . *J. Chem. Soc., Dalton Trans.,* **2001**, 2199; (c) Sarker, K. K.; Sardar, D.; Suwa, K.; Otsuki, J.; Sinha, C. *Inorg Chem*., **2007**, *46*, 8291;(d) Ray, U. S.; Ghosh, B. K.; Monfort, M.; Ribas, J.; Mostafa, G.; Lu, T.-H.; Sinha, C. *Eur. J. Inorg. Chem*. **2004**, 250; (e) Bhuina, P.; Ray, U. S.; Mostafa, G.; Ribas, J.; Sinha, C. *Inorg. Chim. Acta* **2006**, *359*, 4660.

1.72 (a) Sarker, K. K.; Chand, B. G.; Suwa, K.; Cheng, J.; Lu, T.-H.; Otsuki, J.; Sinha, C. *Inorg Chem*., **2007**, *46*, 670; (b) Chand, B.G.;. Ray, U.S.; Mostafa, G.; Cheng, J.; Lu, T.-H.; Sinha, C. *Inorg. Chim. Acta,* **2001**, *313*, 21.

1.73 Pecoraro, V.L.; *Manganese Redox Enzymes,* VCH Publishers, New York, **1992**.

1.74 (a) Ribas, J.; Escure, A.; Monfort, M.; Vicente, R.; Cortes, R.; Lezama, L.; Rojo, T.; *Coord. Chem. Rev.,* **1999**, *193-195*, 1027; (b) Ray, U.S.; Jasimuddin, S. K.; Ghosh, B. K.; Monfort, M.; Ribas, J.; Mostafa, G. Lu, T.-H.; Sinha, C. *Eur. J. Inorg. Chem.,***2004,** 250.

1.75 (a) Wang, Y.; Ouyang, X.-M.; Li, Y.-Z.; Sun, W.-Y. *Bull. Chem. Soc. Jpn.,* 2003, 76, 1403; (b) Zhu, H.-F.; Li, L.; Okamura, T.; Zhao, W.; Sun, W.-Y. ; Ueyama, N. *Bull. Chem. Soc. Jpn.,* **2003**, *76*, 761.

1.76 (a) Das, D.; Chand, B.G.; Sarker, K.K.; Dinda, J.; Sinha, C. *Polyhedron*, **2006**, *25*, 2333; (b) Mathur, T.; Ray, U.S.; Liou, J.-C.; Wu, J. S.; Lu, T.-H.; Sinha, C. *Polyhedron*, **2005**, *24*, 739.

1.77 (a) Kennedy, A. R.; Kirkhouse, J. B. A.; Whyte, L. *Inorg. Chem.,* **2006**, *45*, 2965; (b) Blake, A. J.; Champness, N. R.; Huberstey, P.; Li, W.-S.; Withersby, M. A.; Schroder, M. *Coord. Chem. Rev.*, **1999**, *183*, 117; (c) Strang, P. J.; Olenyuk, B. *Acc. Chem. Res.*, **1997**, *30*, 502; (b) Bock, H.; Lehn, J.-M.; Pauls, J.; Holl, S.; Krenzel, V. *Angew. chem., Int. Ed.*, **1999**, *38*, 952.

1.78 (a) Faulkner, S.; Perry, W. S.; Natrajan, L. S.; Sykes, D. *Dalton Trans.* **2009**, *3890*; (b) Gunnlaugsson, T.; Leonard, J. P. *Chem. Commun.* **2005**, 311; (c) Ho, I-T.; Lee, G-H.; Chung, W-S. *J. Org. Chem.* **2007**, *72*, 2434.

Chapter 2

MATERIALS AND METHODS

2 Experimental Sections

A comprehensive account of the materials used in synthesis and relevant particulars of the instruments/equipments that has been used for the synthesis and characterization of all compounds are described in this chapter.

2.1 Materials

All the chemicals and solvents used for the present work were for analytical grade quality and were used without purification unless otherwise specified. Triethanol amine, thionyl chloride, 1-naphthol, 2-naphthol, tris-(2-aminoethyl) amine (tren), 8-hydroxyquinoline, sodium metabisulfite, sodium nitride, imidazole, 1-napthyl amine, aniline, *p*-Me aniline, *p*-OMe aniline, *p*-Cl aniline, *p*-Br aniline, *p*-I aniline, different metal salts, different organic acids and esters were obtained from Aldrich (US) and used as received. Inorganic acids were obtained from Merck (India) and used as received. All the solvents used for spectroscopic studies were of spectroscopy grade and further purified (dried and distilled) by following standard procedure.[2.1]

2.2 Particulars of Instruments/Equipment used for the following physiochemical studies

pH Measurement

pH values of the reaction solutions were recorded with a Systronics Type 355 digital pH meter and also by using Merck pH indicator paper.

Electrical Conductance Measurement

Solution electrical conductance measurements were measured on a Systronics Type 304 direct digital reading conductivity meter. Solution strength was maintained at 10^{-3} M in appropriate solvents by using 0.01N KCl solution as calibrate.

Infrared Spectroscopy

Infrared spectra of the compounds were recorded as KBr pellets or as thin films using a Nicolet Impact- 410 Fourier Transform Infra Red Spectrophotometer, or on a Perkin-Elmer Spectrophotometer (spectrum one)

Electronic Absorption Spectroscopy

UV-visible spectra were recorded, by dissolving a calculated amount of the sample in appropriate solvents, on a Hitachi UV-visible U-2001 Spectrophotometer or on a Perkin Elmer Lambda 25 UV-Visible Spectrophotometer.

^{1}H and ^{13}C NMR Nuclear Magnetic Resonance Spectroscopy

^{1}H and ^{13}C NMR spectra were recorded on a Varian 400 MHz spectrometers using tetramethylsilane (TMS) as internal standard.

Thermal Studies

Thermogravimetry (TG) and Differential Scanning Calorimetry (DSC) were conducted on a Metallo-Toledo TGA/SDTA 851^{e} and 821^{e} instruments. Experiments were done using either aluminum or platinum crucibles. Pure N_2 gas was used as the flow gas.

Powder X- ray Diffraction (PXRD)

The powder XRD was recorded on BRUKER-D8 ADVANCE with CuK_{α} source (λ = 154 Å) on a glass surface of air dried sample.

Magnetic susceptibility

Solid-state magnetic susceptibility of the complexes at room temperature was recorded using Sherwood Scientific balance MSB-1.

Elemental analysis

Elemental analyses were carried out on a Perkin-Elmer 2400 automatic carbon, hydrogen and nitrogen analyzer.

Mass Spectrometry

HRMS spectra were recorded in WATERS LC-MS/MS system, Q-Tof Premier^{TM}.

Electrochemistry

Cyclic voltammetric measurements were carried out using a CH Instruments make CHI660C electrochemistry system. The cell contained a glassy carbon working electrode, a Pt wire auxiliary electrode and a saturated calomel electrode (SCE) as reference electrode. A salt bridge (containing supporting electrolyte, tetra-*n*-butyl ammonium perchlorate (TBAP) dissolved in dry MeCN) was used to connect the SCE with the

electrochemistry solution.[2.2] All experiments were carried out under a dinitrogen atmosphere at RT and were uncorrected for junction potentials. Under our experimental conditions, the $E_{1/2}$ values (in Volts) for the couple Fc^+/Fc were 0.45 in MeCN vs. SCE.

EPR Spectroscopy

X-Band EPR spectra were recorded with a Jeol JES-FA series spectrometer fitted with a quartz dewar for measurements at liquid nitrogen temperature. The spectra were calibrated with with an internal manganese marker.

Optical Microscopy

Optical micrograph images were taken in *Zeiss-Axio Cam-MRc* microscope fitted with the digital camera of air-dried samples on glass micro slides.

Steady state Fluorescence

The steady state fluorescence spectra were recorded on a Varian Cary-Bio spectro-fluorimeter and corrected for emission. Fluorescence quantum yield was determined in each case by comparing the corrected spectrum with that of naphthalene ($\Phi_F = 0.23$) [2.3] in ethanol by taking the area under the total emission using the following equation .[2.4]

$$\Phi_S = \Phi_R (F_S A_R / F_R A_S)(\eta_S / \eta_R)^2$$

where Φ_S and Φ_R are the radiative quantum yields of the sample and the reference, F_S and F_R are the area under the fluorescence spectra of the sample and the reference, A_S and A_R are the absorbance of the sample and the reference (at the excited wavelength), η_S and η_R are the refractive indices of the solvent used for the sample and the reference. The quantum yield of naphthalene was measured using quinine sulfate in 1N H_2SO_4 as reference at λ_{ex} of 350 nm ($\Phi_F = 0.54$). The quantum yield of naphthalene was measured using quinine sulfate in 1N H_2SO_4 as reference at λ_{ex} of 350 nm ($\Phi_F = 0.54$).

Time-resolved Fluorescence Spectroscopy

Time-resolved intensity decays of the proteins were measured using a Life Spec II spectrofluorimeter (Edinburgh instrument). The sample was excited by *Pico-quant* 290 nm laser source and the decay was measured through 50 ns time scale at a time resolution of 0.0122 ns/channel. The decay curves were analyzed by FAST software using discrete

exponential method, provided by Edinburgh instrument along with the fluorescence instrument. The generated curves for intensity decay were fitted in the functions:

$$I(t) = \sum_i \alpha_i \exp(\frac{-t}{\tau_i})$$

Where, τ_i is the initial intensity of the decay component *i*, having a lifetime α_i. The mean lifetime (τ_m) of BSA in different experimental condition was calculated following the equation[2.5]

$$\tau_m = \frac{\sum_i \alpha_i \tau_i}{\sum_i \alpha_i}$$

X-ray Crystallography

The intensity data were collected using a Bruker SMART APEX-II CCD diffractometer, equipped with a fine focus 1.75 kW sealed tube Mo K_α radiation (λ = 0.71073 Å) at 273(3) K, with increasing ω (width of 0.3° per frame) at a scan speed of 3 s/frame. The SMART software was used for data acquisition. Data integration and reduction were undertaken with SAINT and XPREP[2.6] software. Multi-scan empirical absorption corrections were applied to the data using the program SADABS.[2.7] Structures were solved by direct methods using SHELXS-97 and refined with full-matrix least squares on F^2 using SHELXL-97.[2.8] All non-hydrogen atoms were refined anisotropically. The hydrogen atoms were located from the difference Fourier maps and refined. Structural illustrations have been drawn with ORTEP-3 for Windows.[2.9]

References:

2.1. Armarego, W. L. F.; Perin, D. D. *Purification of Laboratory Chemicals*, Fourth addition, 1997.

2.2 Sawyer, D. T.; Roberts, J. L. *Jr, Experimental Electrochemistry for Chemists*, Wiley, New York, 1974.

2.3 Birks, J. B. *Photophysics of Aromatic Molecules*, Wiley-Interscience, New York, 1970.

2.4 Uchiyama, S.; Matsumura, Y.; de Silva. A. P.; Iwai, K. ; *Anal. Chem.*, **2003,** *75*, 5926.

2.5 Swaminathan, R.; Krishnamoorthy, G.; Periasamy, N. *Biophys J.*, 1**994**, *67*, 2013.

2.6 SMART, SAINT and XPREP, Siemens Analytical X-ray Instruments Inc., Madison, Wisconsin, USA, 1995.

2.7 Sheldrick, G. M., SADABS: software for Empirical Absorption Correction, University of Gottingen, Institute fur Anorganische Chemieder Universitat, Tammanstrasse 4, D-3400 Gottingen, Germany, 1999–2003.

2.8 Sheldrick, G. M.; SHELXS-97, University of Gottingen, Germany, 1**997**.

2.9 Farrugia, L. *J. Appl. Crystallogr.*, **1997**, *30*, 565.

Chapter 3

SUPRAMOLECULAR PHOTOCHEMISTRY OF NAPHTHALENE AND QUINOLINE BASED SYSTEMS

Importance of artificial receptors in chemistry and biology

Currently, selective recognition and sensing of cations and anions by artificial receptors have attracted a considerable research interest in terms of their potential applications in various areas, ranging from environmental monitoring, and industrial purposes to clinical diagnostics.[3.1] In order to develop an artificial receptor that is selective toward a specific analyte, multiple interactions between host and guest in a complementary fashion have to be considered. Several strategies can be followed in the design of artificial receptors with optimal selectivity toward a particular analyte. The receptor may contain a variety of functionalities, which must be organised to complement the size and shape of the analyte. The topology of the receptor is of importance in determining the overall receptor-ion interactions. The multipodal receptors constitute a special class of acyclic ionophores, which consist of multiarmed ligands with each arm bearing a functional group that can coordinate with the target ion. Multipodal receptors, which are hypothesised to be between cyclic and acyclic ligands with regards to preorganization, are believed to be able to complex an ion more effectively than analogous acyclic ones.[3.2] Therefore, this chapter is focused on multipodal-based molecules as receptors that provide multiple interaction sites toward given analytes, either cations,[3.3] anions[3.4] or neutral solvent molecules.[3.5] As a recognition motif, multipodal-based receptors have been reported to be used successfully as recognition components in ion-selective electrode membranes[3.6] and optical sensors.[3.7] The use of alkynes and aromatic spacing groups maintains the rigidity of the hosts and presents an easily accessible, preorganised three-dimensional space within their confines. The use of aromatic spacers also promotes their usefulness as hosts for aromatic guests by virtue of the substantial different non covalent interactions. In general, interactions to neutral guests are weaker than those to ions and the host needs to either self-assemble around the neutral guest or it must be highly preorganised. Generally, such preorganised hosts have permanent curvature to form an intrinsic cavity that persists in solution. This type of receptor is generically termed a *cavitand*. The inclusion of the guest within the cavity or cleft of the cavitand yields a *caviplex*. The molecular design allows the rational control of binding properties such as complex stability and selectivity. The selectivity of a multimodal receptor relates greatly to the rigidity of its arms and its cavity size.[3.8] Receptors or ligands that enforce multipodal topologies are known to have several advantages over monopodal receptors: (i) due to the enhanced chelating effects, multipodal ligands often bind to metal ions very strongly; and (ii) the bulkiness of multipodal ligands is highly tunable allowing for controlled reactivity to metal ions. Anion coordination and molecular recognition of anionic substrates by synthetic receptor

molecules have been much less studies than cation complexation, despite the important role anions play in chemistry and biology. Anions have a wide variety of geometries. They can be spherical (F^-, Cl^-, Br^-, I^-), linear (CN^-, SCN^-, N_3^-), trigonal planar (CO_3^{2-}, NO_3^-) tetrahedral ($H_2PO_4^-$, HSO_4^-, SO_4^{2-}, ClO_4^-), or octahedral $[Fe(CN)_6]_6^{4-}$, $Co(CN)_6^{3-}$. The difference in geometry between anions is an important factor to account for in the design of selective anion receptors, although it is not easy to synthesize receptor molecules with complementary binding sites in proper three dimensional arrangements. Due to these distinct benefits, the design and development of artificial receptor system represent an active area in supramoleculer chemistry. However, only limited number multipodal receptors have been reported in the literature.

Chapter-3 discusses molecular recognition of anion, cation and aromatic guest and solvent encapsulation by various multipodal ligands in solution and solid state. This chapter is sub-divided into three parts based on the type of ligands used for recognition.

In 1st part, we have reported a simple and novel tripodal fluorescent sensor, Tris-[2-(naphthalen-1-yloxy)-ethyl]-amine (**L_1**), Tris-[2-(naphthalen-2-yloxy)-ethyl]-amine (**L_2**). The binding of the hosts to a series of anions, cation and aromatic guest molecule were investigated by fluorescence, NMR and single crystal X-ray crystallography.

In 2nd part of the chapter 3, we have discussed about tripodal aminoquinoline based ligand Tris-[2-(naphthalen-2-yloxy)-ethyl]-amine (**L_3**), which have three chemically different types of nitrogen donating sites. This ligand is an example of selective phosphate ion sensor by multiple hydrogen-bonding interactions.

3rd part of the chapter 3, discussed about chiral *trans*-1,2-*bis*-(3-(naphthalen-1-yl)-thioureido cyclohexane (**L_4**) compound as a new host material with considerable structural adaptability over range of solvent. The solid state structural similarities and disimilarities and higher dimensional packing can be rationalized through multipoint solute-solvent non-covalent interactions in solid and solution phases. Solution phase photo-physical studies also carried out to emphasize the role of solvent polarity in non-covalent interactions.

Experimental Section

The Chemicals used were of reagent grade. The sources of the chemicals and solvents have all been recorded in Chapter 2. Details of all the equipment or instruments used for the physico-chemical studies have been summarized in Chapter 2.

PART - I

3.1. General synthesis of tripodal napthyl ether ligand (L_{1-2})

Tris-[2-(naphthalen-1-yloxy)-ethyl]-amine (**L_1**) and Tris-[2-(naphthalen-2-yloxy)-ethyl]-amine (**L_2**) has been synthesized following literature method (Figure 3.1.1).[3.1.1] To a solution of 1 and 2-naphthol (4.32g; 30 mmol) in 25 ml of dry *n*-Propanol crushed NaOH (1.6g; 40 mmol) was added. It was stirred for an hour at RT. Tris(2-chloroethyl)amine hydrochloride[3.1.2] (2.4g; 10 mmol) was then added to the above solution at RT. For completion of the reaction, the mixture was refluxed for 6 hours. The reaction mixture was poured into ice-cold water and kept over night at low temperature. The compound was collected by filtration under suction and washed with cold ethanol. The product obtained was pale yellow in color after re-crystallization from ethyl acetate: ethanol (1:3) mixture at room temperature.

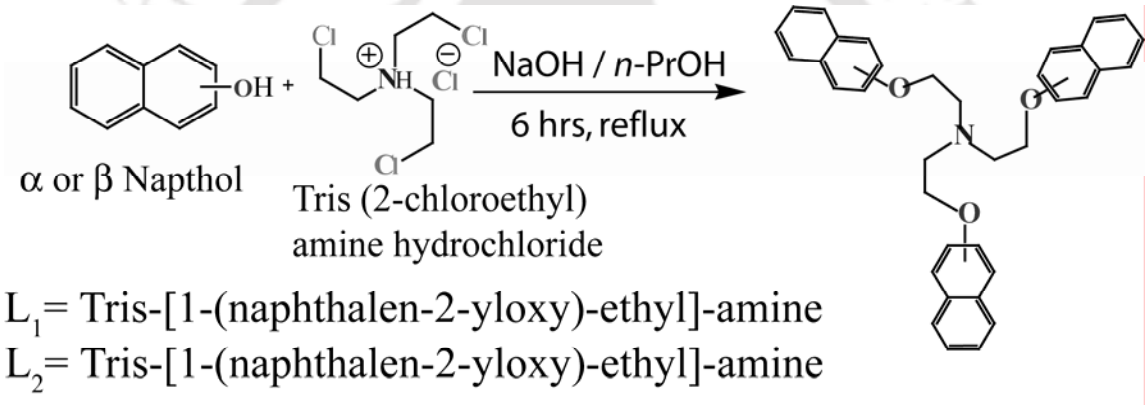

Figure 3.1.1. Synthetic procedure of tripodal napthyl ether ligands **L_1** and **L_2**.

L_1: Yield: 90%. M.pt.105 ^{0}C. ^{1}H NMR: (400MHz, $CDCl_3$, 250 C, TMS): δ 3.4 (6H, t, -CH_2N), 4.38 (6H, t, -CH_2O), 6.73 (3H, d, ArH), 7.37 (12H, m, ArH), 7.75 (3H, d, ArH), 8.2 (3H, d, ArH). ^{13}CNMR: (400MHz, $CDCl_3$, 25^{0}C, TMS): δ 67.329, 54.669, 154.31, 134.31, 127.27, 120.15, 104.56 (Figure 3.1.2). ESI-MS: M^+ = 528. Anal. Calcd $C_{36}H_{33}NO_3$: C, 81.95; H, 6.30; N, 2.65. Found: C, 81.99; H, 6.28; N, 2.67.

L_2: Yield: 92%. mp.132 ^{o}C, ^{1}H NMR (400MHz, $CDCl_3$, 25^{0}C, TMS): δ 3.2 (6H, t, NCH_2), 4.24 (6H, t, OCH_2), 7.09 (3H, s, Ar*H*), 7.11 (3H, s, Ar*H*), 7.29 (3H, t, Ar*H*), 7.38 (3H, t, Ar*H*), 7.65 (9H, m, Ar*H*), ^{13}C NMR (400MHz, $CDCl_3$, 25^{o}C, TMS): δ 54.48, 66.86, 106.60, 118.79, 123.47, 126.12, 126.59, 127.46, 128.81, 129.25, 134.33, 156.46 (Figure 3.1.3). ESI-MS: M^+ = 528. Anal. Calcd $C_{36}H_{33}NO_3$: C, 81.95; H, 6.30; N, 2.65. Found: C, 81.99; H, 6.28; N, 2.67.

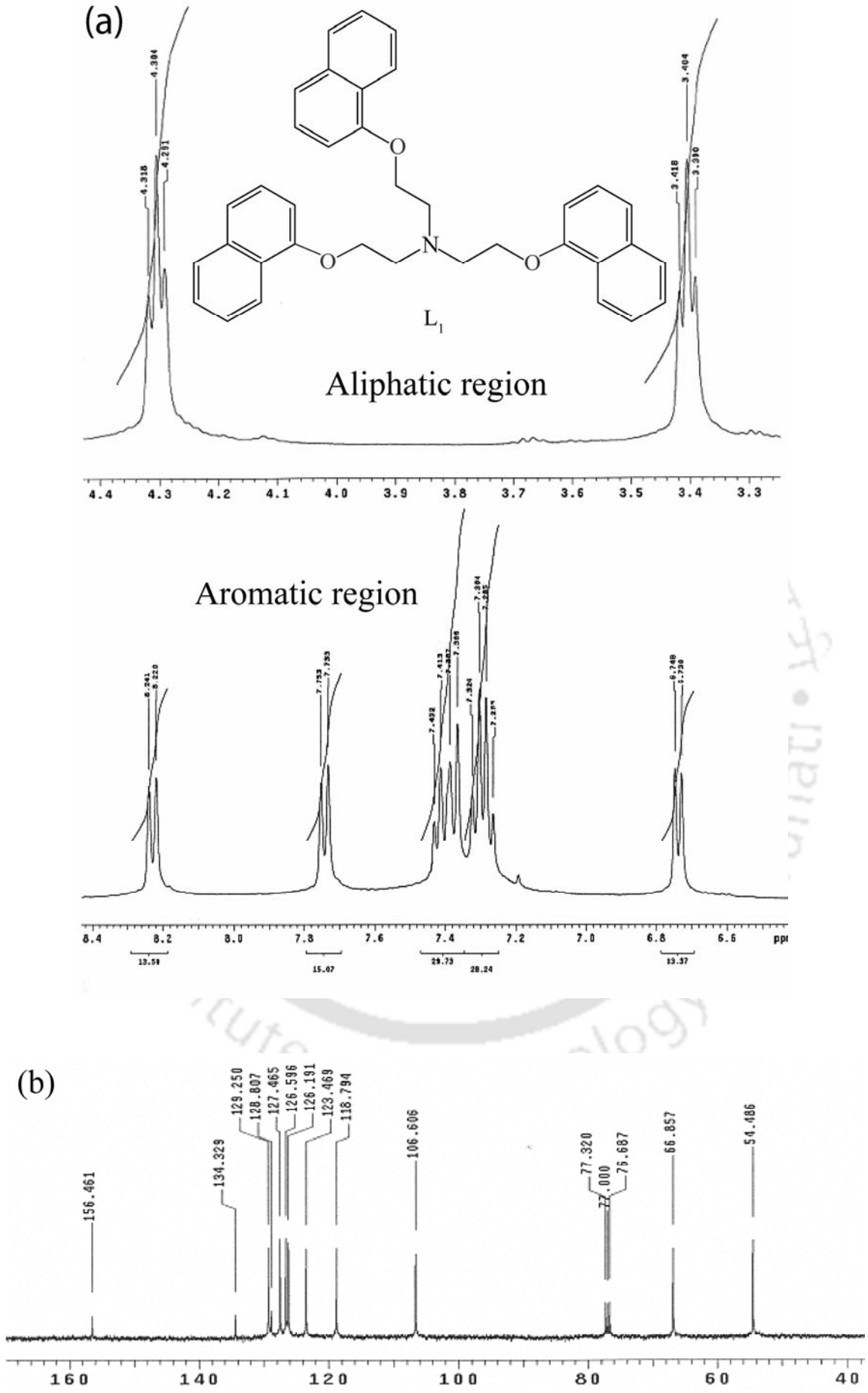

Figure 3.1.2. (a) ^{1}H NMR and (b) ^{13}C NMR spectra of $\mathbf{L_1}$ in $CDCl_3$.

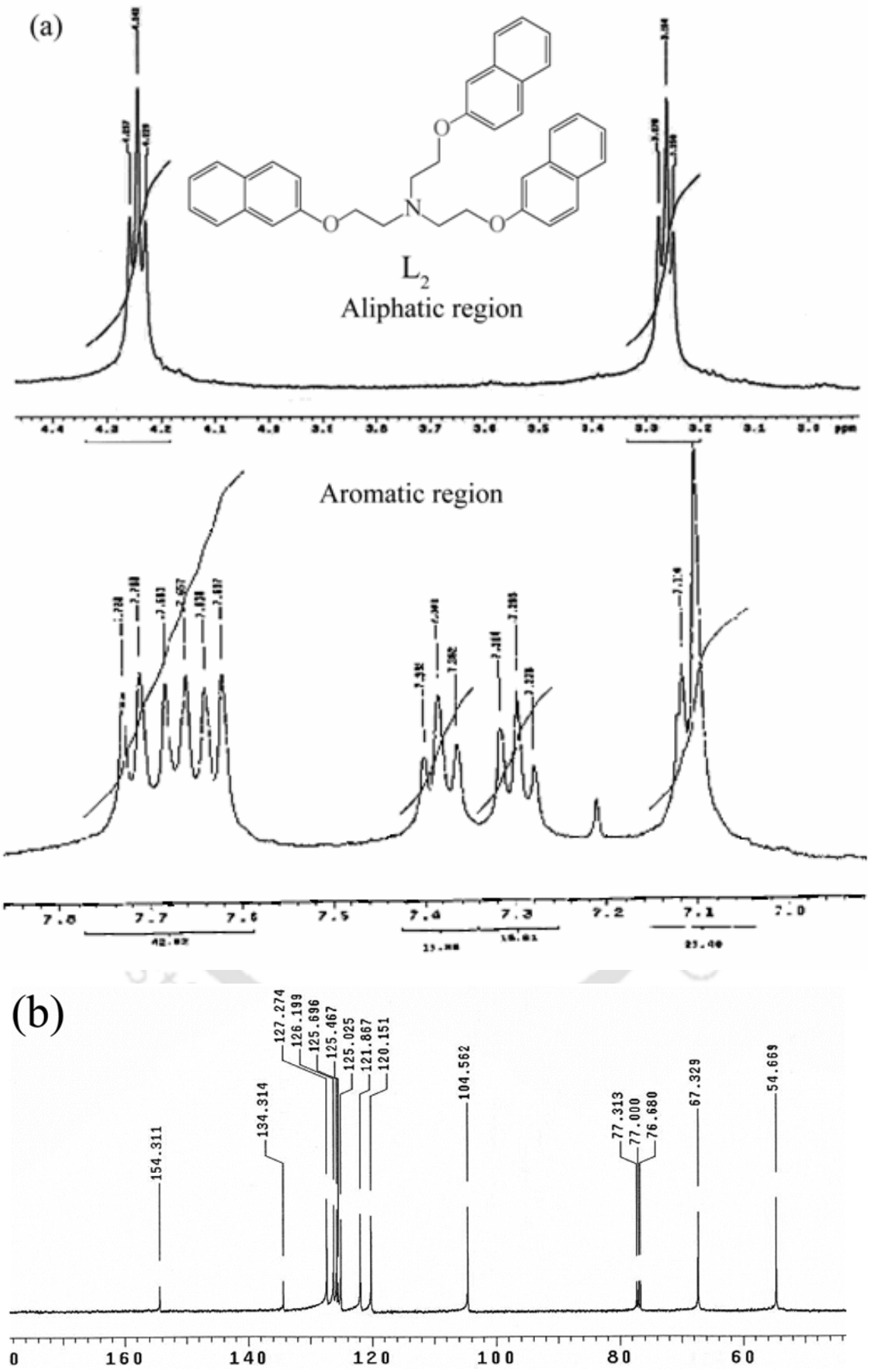

Figure 3.1.3. (a) ^{1}H NMR and (b) ^{13}C NMR spectra of **L_2** in $CDCl_3$.

3.1.1. Anion Recognition of Tripodal Napthyl Ether Ligand, L_1

Anion sensing has been of great interest in biological and environmental sciences for several decades. Various fluorescent sensors have been developed for sensitive and simple detections of anions. Therefore, the discovery and/or development of new simple and sensitive anion sensors are strongly desired. We have been focusing on the discovery of new supramolecular fluorescent sensor molecules. In this part of this chapter, we report the anion binding properties of the ligand **L_1.** Synthesize and characterizations of all salts (**1-5**) are described in appendix of this chapter.

3.1.1a. Crystal Structure Analysis

Some of our main concerns have been to ascertain the recognition of anion in the solid state and the consequences of weak hydrogen bonding in the intermolecular network structure. Accordingly, X-ray diffraction analyses of the four anionic complexes were done and supramolecular organization in the crystals determined and pertinent structural data are provided in Table in Appendix this chapter. The bridgehead tertiary nitrogen of the tripodal ligand **L_1** exists in monoprotonated form in presence of acid. The mono-protonated charge of the tripodal ligand is satisfied by external counter anions.

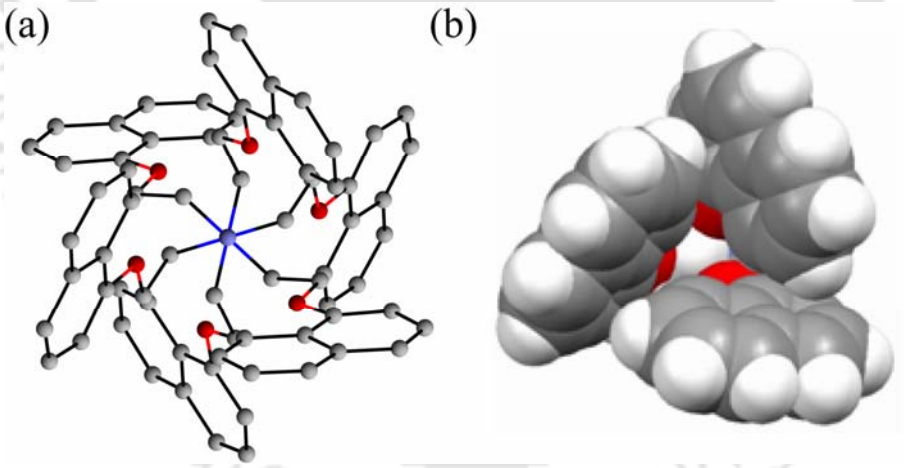

Figure 3.1.4. (a) C_3 axis of symmetry in **L_1** (b) space filling model of (hydrophobic pocket) ligand **L_1.**

The ligand has a C_3 axis of symmetry in the solid state (Figure 3.1.4a). Space-filling model of the ligand shows the presence of a cavity of average diameter of ~ 5 Å (Figure 3.1.2b). However, the cavity is exclusively hydrophobic in nature. Hence, in the solid state **L_1** cannot be an endo-receptor for hydrophilic anions. **L_1** encapsulate these anions in between space in the solid-state. Attempts were made to provide solid-state evidence for anion encapsulation by setting up a series of crystallization experiments of **L_1** with different anion. We have shown the crystal structure analyses of the following complexes: $[H\mathbf{L_1}^+][Br^-]$ **(1)**, $[H\mathbf{L_1}^+][Cl^-].C_2H_5OH$ **(2)**, $[H\mathbf{L_1}^+][NO_3^-]$ **(3)** and $[H\mathbf{L_1}^+][Pyromellitate^-$

].$CHCl_3$ **(4)** [HL_1^+][CF_3COO^-]H_2O **(5)**. We have crystallized L_1 in presence of CF_3COO^- also, but structural analysis of these crystals has met with limited success. The resolution of the structure was poor. CF_3COO^- unit is not behaved properly during refinement. However, ligand structure is properly solved. It appears that conformational freedom of the ligand in the crystal lattice is not so restricted thereby allowing different packing options. Thus, there is a significant degree of reciprocal intermolecular hydrogen bonding in the solid-state between molecules. Crystal structure analysis shows that L_1 acts as an exo-receptor for the anions. In the solid state, anions are present within a hydrophobic channel out side the ligand cavity (Figure 3.1.4b). Protonated bridgehead N atom is buried inside the hydrophobic region. Moreover, the proton attached to the apical nitrogen is in endo orientation. Therefore, it cannot form N–H····X type hydrogen bonding. All the C–N and C–O bond lengths in these salts are longer than the corresponding free L_1. This is because of the repulsion of the charged endo oriented N–H bond. The mean value of C–N–C bond angles in these salts are smaller than those in free L_1 (113.6(2)^o, which also indicates the repulsion.

The bromide complex **1** crystallizes in a highly symmetric cubic space group with one molecule in the asymmetric unit (Figure 3.1.5a). Ligand posses C_3 axis of symmetry in the solid state. Counter anion is outside the ligand cavity, which is true for all other complexes also. The ligand moieties are organized via intermolecular C–H····π interactions (see appendix). Ligand does not have any kind of strong or weak interactions with the bromide ion in the solid-state. It forms alternate up-down 3D network of dumbbell shape boxes (Figure 3.1.3b). Each naphthalene unit is parallel to the plane of the unit cell. Bromide ion is present in a triangular channel in the lattice formed by the self-assembly of the ligand (Figure 3.1.5b). When we replace the larger bromide ion with smaller chloride ion, the symmetry of the crystal is destroyed.

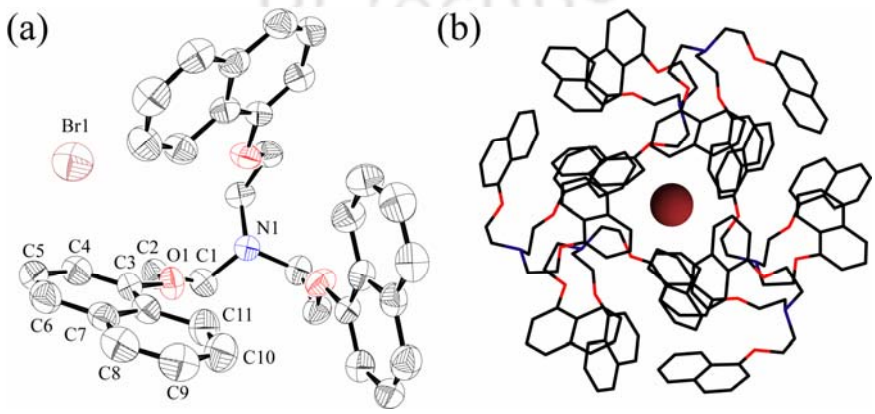

Figure 3.1.5. (a) ORTEP plot of complex **1**. Thermal ellipsoids set to 50% probability level, Hydrogen atoms are omitted for clarity and (b) Bromide recognition in the solid state

Chloride complex **2** crystallizes in triclinic space group. Asymmetric unit contains one C_2H_5OH molecule (Figure 3.1.6a). We have observed several other differences in the solid-state structure in comparison to the bromide complex **1**. The ligand moieties self-assembled via intermolecular C–H····π interactions. Unlike complex **1**, the ligand forms some addition weak hydrogen bond interactions. In complex **2**, ligand form intermolecular C–H····O interactions with oxygen atom of solvent molecule (see appendix). Several strong C–H····Cl^- interactions are also present in the chloride complexes.[3.1.3] Larger Br^- ion does not show this kind of interaction. All the chloride ions are lined up along crystallographic *a* axis. Ligands are organized as a bowl in alternated up and down manner in the solid-state. Chloride ion is situated in a rectangular channel formed by the self-assembled ligand in the crystal (Figure 3.1.6b). In the lattice, it is sandwiched between two naphthalene unit.

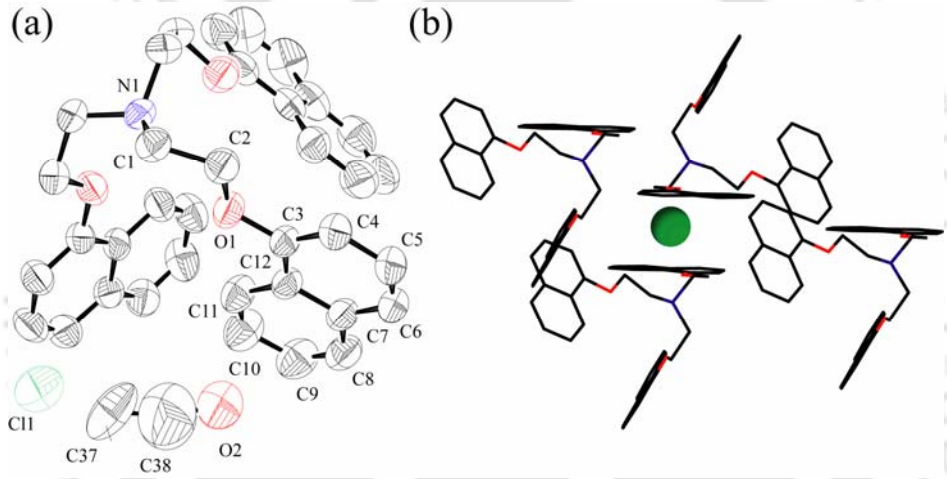

Figure 3.1.6. (a) ORTEP plot of complex **2**. Thermal ellipsoids set to 50% probability level and (b) Chloride recognition in the solid state.

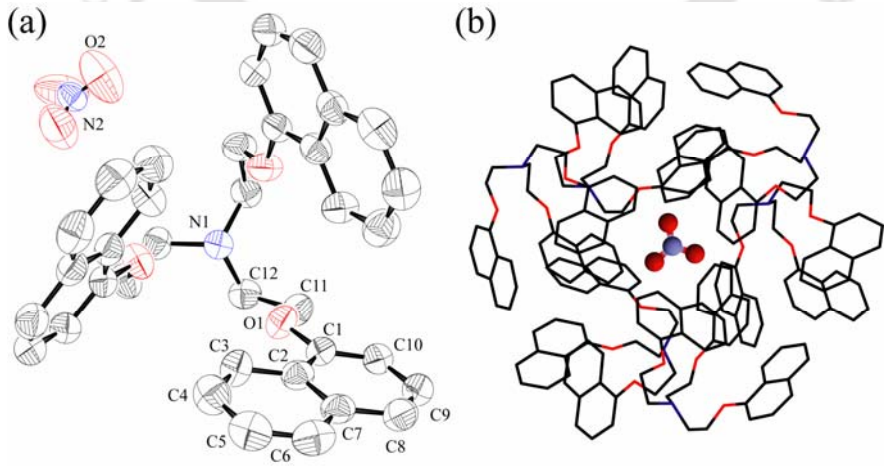

Figure 3.1.7. (a) ORTEP plot of complex **3**. Thermal ellipsoids set to 50% probability level; (b)) Nitrate recognition in the solid state.

Crystal structure of nitrate complex **3** is similar that of the bromide complex **1**. It also crystallizes in a highly symmetric cubic space group. Asymmetric unit contains one molecule (Figure 3.1.7a). Here ligand and anion has the similar 3D arrangement like complex **1**. The packing patterns of the bromide and nitrate complex are exactly same. However, in addition to the intermolecular C–H····π interactions ligand forms intermolecular C–H····O interactions with oxygen atom of anion (see appendix). Nitrate anion occupies the triangular hydrophobic void space in the crystal lattice, which is same as of bromide complex (Figure 3.1.7).

Ligand in presence of pyromellitic acid crystallizes in monoclinic space group. Asymmetric unit contains one $CHCl_3$ molecule (Figure 3.1.8a). Unlike CH_3OH molecule in **2**, $CHCl_3$ molecule does not form any type of weak interactions with the ligand or acid molecules.

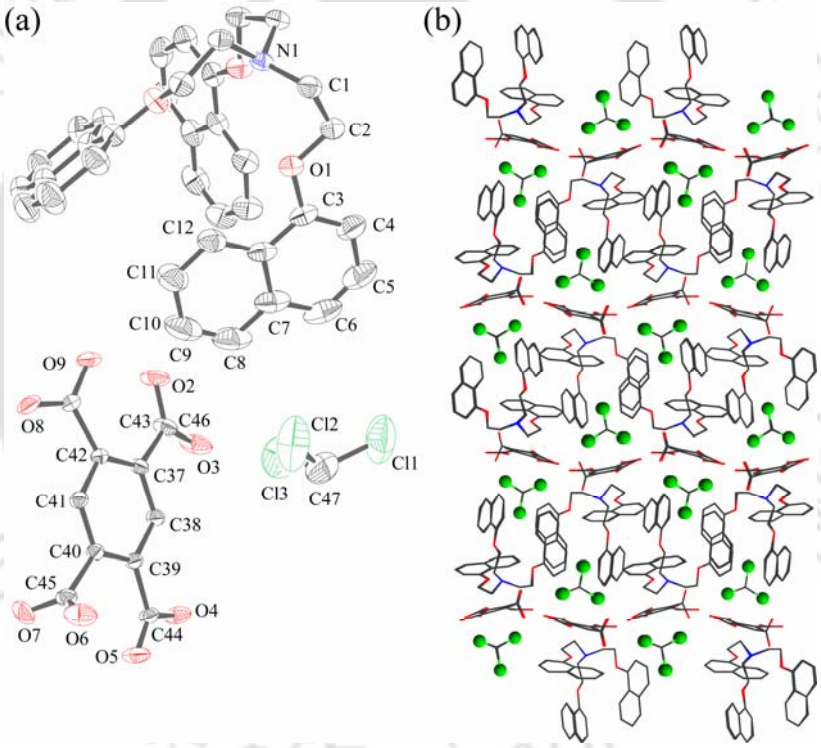

Figure 3.1.8. (a) ORTEP plot of complex **4**. Thermal ellipsoids set to 50% probability level; (b) flower mosaic network along the c axis.

All the pyromellitate ions are lined up along crystallographic *c* axis. Ligand and $CHCl_3$ molecules are arranged in-in alternate up-down manner in between two hydrogen bonded sheets. Each ligand is connected to the sheet via several C–H····O interactions. Geometry of the ligand does not allow two naphthalene units to come within the non-bonded distances in the solid-state. Hence, no π····π interactions are observed in the solid state within the ligand molecules. Electron deficient pyromellitic acid also does not show π····π interactions with electron rich ligand. Pyromellitic acid unit form a 2D hydrogen

bonded sheet along *ac* plane of the crystal. Another notable feature of the crystal structure of **4** is the formation of intra as well as intermolecular six membered intermolecular hydrogen bonding pattern along a axis (Figure 3.1.8b).

ORTEP plot of salt **5**, $[\mathbf{L_1}H]^+[CF_3COO]^-\bullet H_2O$ is shown in Figure 3.1.9a along with the atom numbering scheme. Complex contains one protonated and one neutral $\mathbf{L_1}$ in the asymmetric unit along with one water moiety is present there. The protonated form of ligand $\mathbf{L_1}$, there are two N–H····O hydrogen bonding interaction (N1–H····O4, 2.7460 Å and N2–H····O3, 2.809 Å. In the complex one water molecule is forms a strong H- bond with the trifluoro acetate ion via O-H····O interaction (O5-H····O7, 2.585 Å). The complex contains two C–H····π interactions are present there between aromatic π cloud of naphthalene moieties and aromatic and aliphatic C–H protons. The corresponding bond lengths are C18-H18····π, 3.721 Å, C18-H18····π, 3.556 Å, and C4-H4B····π, 3.972 Å respectively (see appendix). Overall coplex shows an arrey hydrophobic layer and hydrophilic layer to form a flower mosaic structure (Figure 3.1.9a).

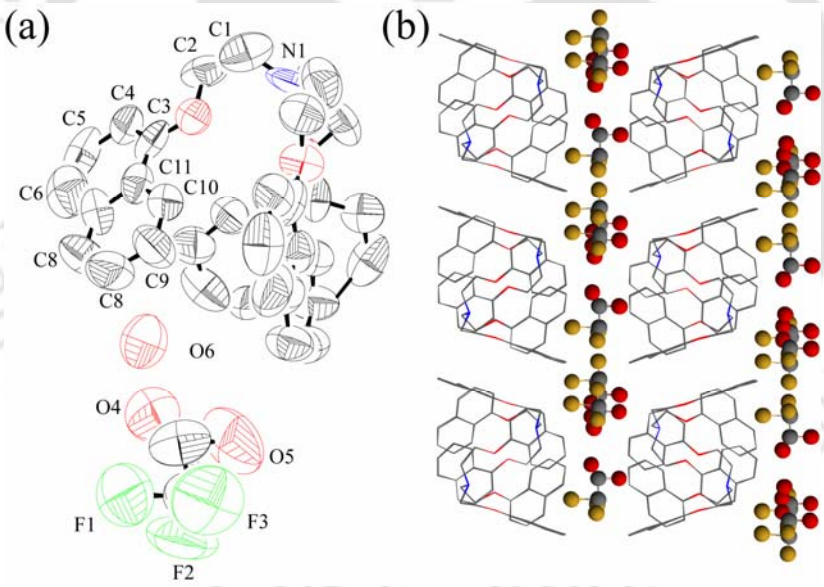

Figure 3.1.9. (a) ORTEP plot of complex 5. Thermal ellipsoids set to 50% probability level; (b) hydrophilic-hydrophilic layer by layer flower mosaic structure along *a* axis.

3.1.1b. Absorption spectroscopy

UV-visible absorption spectra of $\mathbf{L_1}$ in dry THF at 298 K shows the $^1L_a \leftarrow {}^1A$ transitions of the naphthalene unit in the region 250-300 nm with ε = 1905 $M^{-1}cm^{-1}$ and lower energy $^1L_b \leftarrow {}^1A$ transitions in the region 300-350 nm with ε = 932 $M^{-1}cm^{-1}$.[3.1.4] These transitions are found to be non-solvatochromic in nature. Changes in the UV-visible absorption spectra were monitored upon successive addition of anions to sensor $\mathbf{L_1}$. A very weak hypsochromic shift observed only when trifluoro acetic acid was added to $\mathbf{L_1}$ (Figure

3.1.10). All other sensor and inorganic anion combinations afforded almost no noticeable shift in the peak positions. These results suggest a different mode of binding of $\mathbf{L_1}$ to CF_3COO^-. During titration with pyromellitic acid we got an additional peak at 295 nm due to pyromellitic acid.

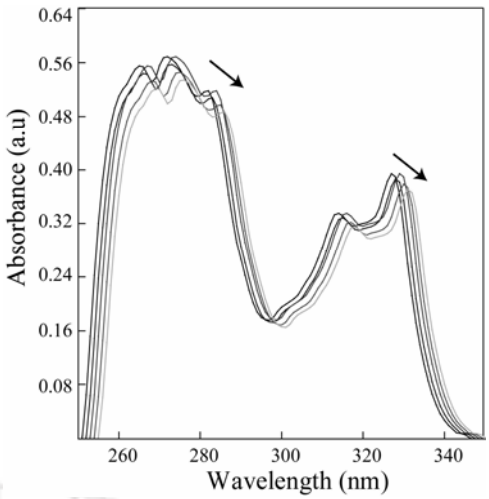

Figure 3.1.10. Changes in UV-visible absorption spectra upon addition of CF_3COO^- to a THF solution of $\mathbf{L_1}$ at 298 K.

3.1.1c. Fluorescence spectroscopy

The emission spectra of $\mathbf{L_1}$ in dry THF at 298 K shows a locally excited (LE) broad emission of naphthalene with emission maximum at 410 nm monitored (λ_{ex} = 330 nm) (Figure 3.1.11a). LE emission remains virtually unchanged with respect to solvent polarity. The excitation spectra monitoring λ_{max} of the emission band is identical with the absorption spectra of the free ligand in dry THF at 298 K. With increasing concentration of the ligand, the total intensity of fluorescence emission decreases significantly without the appearance of any broad band in the higher wavelength region. This suggests that self-quenching takes place without formation of any excimer at higher concentration.[3.1.5] Geometry of the ligand does not allow two naphthalene chromophores to come in contact with each other, which is similar to the reported observation.[3.1.4] The concentration of the ligand was maintained at 10^{-6} M throughout the study as the emission intensity is found to be maximum at this concentration. When THF solutions of acids were added gradually to THF solution of $\mathbf{L_1}$ the fluorescence was quenched to varying degrees (Figure 3.1.11b). The best results were observed for additions of nitric acid to $\mathbf{L_1}$, where 97% quenching was observed after 16 equiv of anion had been added (Figure 3.1.11a inset). Ligand $\mathbf{L_1}$ exhibits high selectivity toward nitrate anion over other anions present in solution. The linear Stern-Volmer response with nitrate as quencher is consistent with well-behaved fluorescence quenching systems.[3.1.6] The absence of the red shifted band in these systems excludes the possibility of an emission from a charge transfer state involving the protonated amine/ether oxygen and the naphthalene unit.[3.1.7] To demonstrate the selectivity of $\mathbf{L_1}$ toward nitrate, we have monitored the change in fluorescence quantum yields in the presence of different anions. Figure 3.1.11b clearly shows that $\mathbf{L_1}$ has a remarkably high selectivity toward nitrate anion in terms of change of fluorescence quantum yield. The

dissociation constant (K_d) of 4.8 μm (Figure 3.1.12a) was calculated from this fluorescence titration.[3.1.8] The spectral characteristics of **L_1** in the solid state are consistent with its solution phase behavior. In the solid state, **L_1** exhibits two broad absorption bands at 275 and 320 nm. It shows a broad emission band at 415 nm.

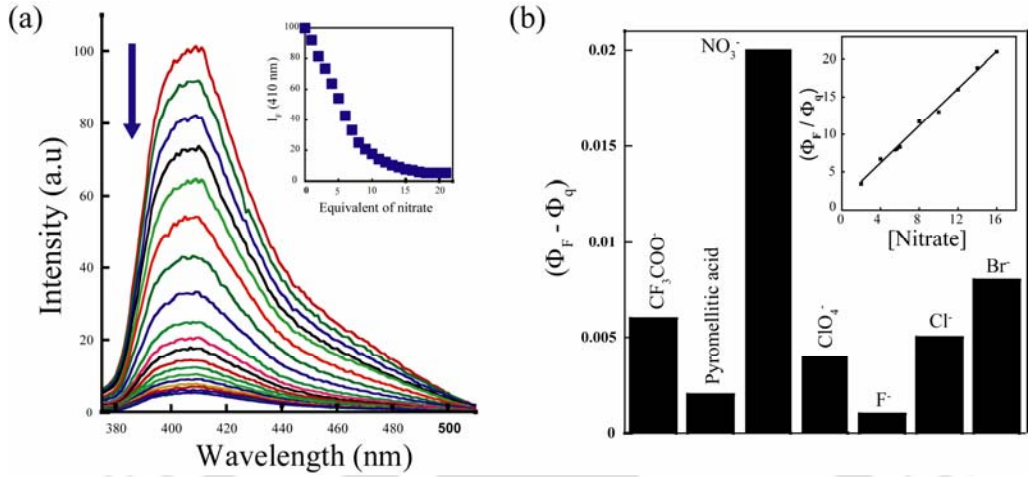

Figure 3.1.11. (a) Emission spectrum of **L_1** ($1x10^{-6}$ M in dry THF) during the titration with nitric acid from 0 to 20 equivalent; (b) Schematic representation showing the change of fluorescence quantum yield (Φ_F - Φ_q) of **L_1** upon addition of the anions. Φ_F and Φ_q are quantum yields of **L_1** in absence and presence of anion, respectively. Inset: Stern-Volmer plot for fluorescence quenching of **L_1** ($1x10^{-6}$ M) on gradual addition of nitrate ($1x10^{-6}$ M) in dry THF.

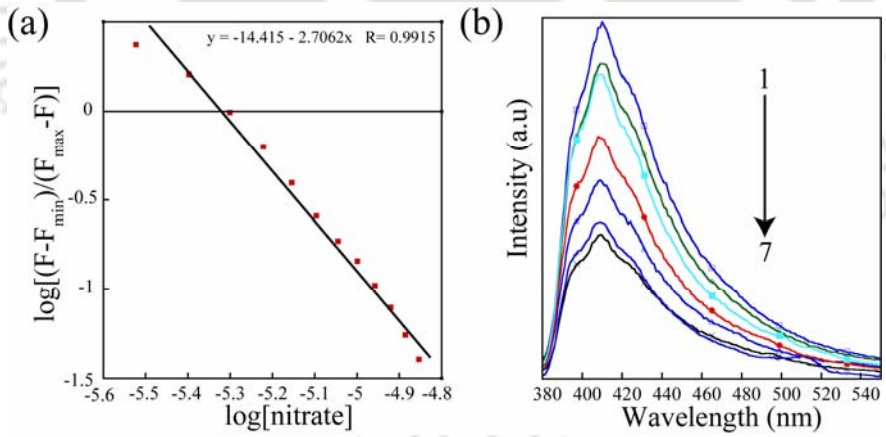

Figure 3.1.12. (a) Determination dissociation constant (K_d). The apparent K_d is at the X intercept, at a value of –5.32. The inverse log of this is 4.8μM; (b) Concentration dependent fluorescence spectra of **L_1**.

3.1.1d. Summary

The simple tripodal amine ligand Tris-[2-(naphthalen-1-yloxy)-ethyl]-amine (**L_1**) was screened for anion recognition. Four crystal structures confirmed the inorganic as well as organic anion recognition in the solid state. Solid-state structures are results of supramolecular self-assembly and 3D molecular network involves C–H····O and C–H····π bonding in the crystal lattice. In the solid state, it forms a strong C–H····Cl and C–H····O

type interactions with the anions. This anion recognition was also confirmed by steady state fluorescence spectroscopy. In complex **4**, $\mathbf{L_1}$ is confined between 2D hydrogen bonded sheet formed pyromellitic acid anion. $\mathbf{L_1}$ shows unusually high selectivity toward nitrate in solution resulting in both a dramatic color change and a concomitant quenching of luminescence. In conclusion, a simple tripodal naphthalene ether ligand $\mathbf{L_1}$ is reported as chromogenic anion sensor. It can selectively capture nitrate anion in solution. $\mathbf{L_1}$ form self-assembled structures in the solid state. In the solid-state different anions are encapsulated in the channel formed by the ligand. In the solid-state they are assembled via several week non-covalent interactions. The spectral features of the ligand as well as the anionic complexes are similar in solution phase and solid state. Anions quench the fluorescence intensity of the free $\mathbf{L_1}$. Therefore, there is substantial room for improvement of sensor performance, either fluorescence or optical, based on tripodal receptors. We look forward to witnessing and participating in the creative and innovative development of selective, sensitive, and accurate sensors for anions.

3.1.2. Aromatic guest inclusion by L_2

Aromatic guest sensing has been of great interest in biological and environmental sciences for several decades. Therefore, it is of high importance in the filed of photochemistry to discover and/or develop new simple and sensitive sensors for aromatic guest. Synthesis of these kinds of hosts should be simple enough to have a greater utility. We have been focusing on the discovery of new supramolecular fluorescent host molecules which can encapsulate various types of guest.[3.1.4] This part we have describe the simple electron rich tripodal naphthalene ether ligand Tris-[2-(naphthalen-2-yloxy)-ethyl]-amine ($\mathbf{L_2}$), which shows inclusion complex of the organic salt co-crystal of $\mathbf{L_2}$ with picric acid (Scheme 1).

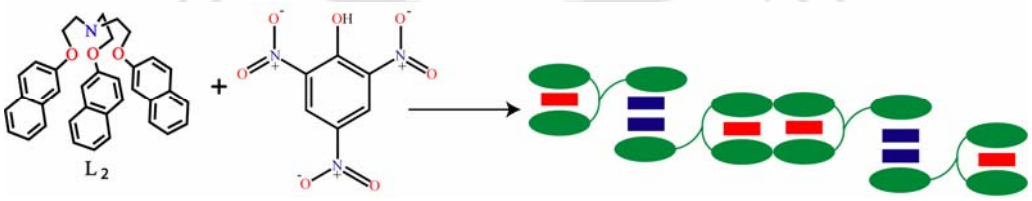

Scheme 3.1.1 Schematic representation of inclusion phenomenon in addition of picric acid with $\mathbf{L_2}$.

3.1.2a. Synthesis and characterization of complex $[(L_2H^+)(Pic)]\subset PicH]$,

To a magnetically stirred solution of $\mathbf{L_2}$ (0.53 g, 1 mmol) in $CHCl_3$ (20 mL), was added methanolic solution of picric acid (0.456 g, 2 mmol) in portions. With the constant stirring the five hours a whitish-yellow precipitate that formed was filtered, washed with dry ether, and dried under vacuum. Yield: 0.887 g, 90% based on $\mathbf{L_2}$. Single crystals suitable for X-

ray diffraction were obtained from slow evaporation of H_2O-C_2H_5OH (1:1) mixture solution of the compound at RT for fifteen days. Anal. Calcd (%) for $C_{38}H_{38}F_3NO_7$: C, 58.46; H, 3.98; N, 9.74. Found: C, 58.45; H,3.97; N, 9.77%.

3.1.2b. Crystal structure analysis

Some of our main concerns have been to ascertain the inclusion of aromatic guest in the solid-state and the consequences of weak intermolecular forces on the 3D network structure. Single crystal X-ray structural analysis confirmed the host-guest relationship between **L_2** and picric acid. Solid-state supramolecular organization in the crystals was discussed. X-ray quality red color crystals obtained from ethyl acetate and chloroform (1:2) mixture at low temperature. In the solid state, it forms an organic salt co-crystal. Each unit cell contains two symmetrically independent picric acid moieties (Figure 3.1.13a). One Picric acid is forming organic salt and another is forming inclusion complex with the protonated **L_1**. We have shown that picric acid form various organic salt co-crystal with different organic amines.[3.1.9] One of the naphthalene rings is located on top of the picric acid ring. Picric acid form strong π-π stacking interactions with the **L_2**.

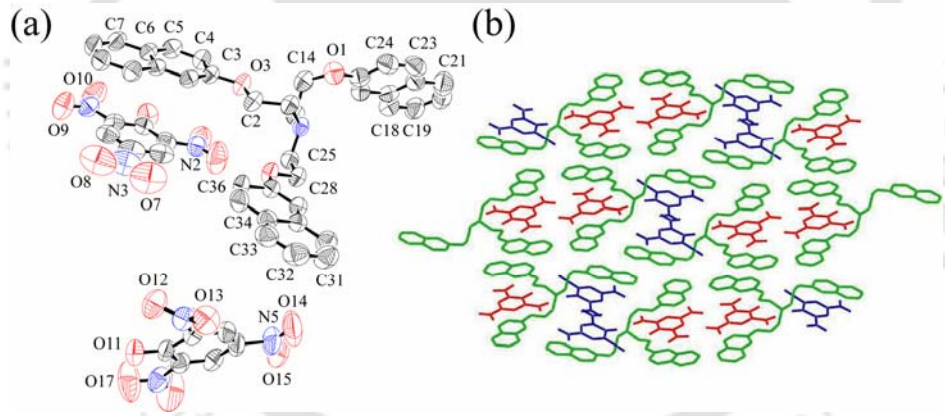

Figure 3.1.13. (a) ORTEP plot of [(L_2H+) (Pic−)]⊂PicH. H-atoms are omitted for clarity; (b) Packing of [(L_1H+) (Pic−)]⊂PicH along *a*-axis showing the π-stacking interaction scheme.

The aromatic ring of guest picric acid is sandwiched between two naphthalene rings of host molecule (Figure 3.1.13b) due to intermolecular π-π stacking interactions. In comparison to the similar ligand with 1-napthol unit **L_2** exists in more flatten conformation due to its special streochemical requirement. It does not form any cavity in the structure (see appendix). Therefore, bridgehead protonatd N atom is exposed enough to form strong hydrogen bond with the picrate anion, resulting the formation of organic salt co-crystal. Overall, solid state structure is stabilized by several weak C–H···π and C–H···O type interactions (see appendix). In the solid-state, **L_2** forms two different types of hydrophobic

void space, where picric acid is trapped in either end-on or side-on manner. Hence, there exist *aba* and *abba* type intermolecular π–π stacking interactions between **L_2** and picric acid (Figure 3.1.13b). All efforts to crystallize inclusion complexes between **L_2** and other electron deficient aromatic guest other than picric acid remain unsuccessful.

3.1.2c. Absorption spectroscopy

The UV-visible absorption spectra (Figure 3.1.14a) of **L_2** (10^{-5} M) was recorded in dry THF at 298 K. The absorption spectrum is found to be overlapping of two transitions in the 270–310 nm regions. The π→π* transitions of the naphthalene unit appear at 283 (ε = 29400 $M^{-1}cm^{-1}$) and 294 nm (ε = 33300 $M^{-1}cm^{-1}$).[3.1.4] The band at ~250 nm is assigned to the π–π interaction between the naphthalene units of the ligand.[3.1.10] In **L_2**, these transitions are found to be non-solvatochromic in nature. When **L_2** is titrated against different aromatic guest molecules, an absorption maximum corresponds to the guest absorption increases lineraly with simultaneous decrease in the absorbance corresponds to the host molecule. In dry THF, we are unable to detect any new peak at the higher wavelength due to the formation of host-guest complex in the solution. There is also no detectable shift in the peak positions of the π→π* transitions of the naphthalene unit upon guest addition.

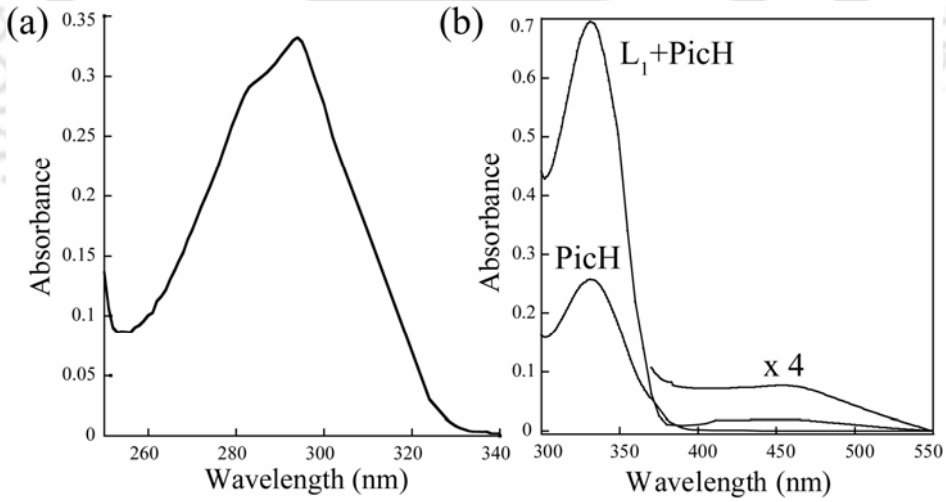

Figure 3.1.14. (a) UV-visible absorption spectra of **L_2** (10^{-5} M in dry THF) at 298 K; (b) Absorption spectra of Picric acid and mixture of **L_2** and picric acid in a mixed solvent of ethyl acetate and hexane (v/v 1:10).

Electron donor–acceptor complexes have been extensively studied in the widespread fields from biological to materials science.[3.1.11] The association behavior of the aromatic host-guest complexes and their absorption property are dependent on the ionization potential of the donor, the electron affinity of the acceptor, and environmental conditions. Formation of host-guest complex is a cumulative effect of various weak intermolecular interactions, which is much more prominent in the solid-state. In polar solvents, individual stronger

interaction of host and guest with the bulk solvent molecules outbreaks these weak interactions. Hence, in dry THF we have not observed any higher wavelength band in the absorption spectra due to the formation of host-guest complex. We have titrated **L_2** with picric acid in a mixed solvent of ethyl acetate and hexane (v/v 1:20) (Figure 3.1.14b). The absorption spectrum of the mixed solution has a broad absorption band at ~460 nm, which is not present in the pure compounds. The red shifted low intensity band is attributable to the formation of host-guest complex between aromatic moieties of electron rich **L_2** and electron-poor picric acid unit.[3.1.12]

3.1.2d. Fluorescence spectroscopy

The emission spectrum of **L_2** was recorded in dry THF at 298 K. Free **L_2** shows a locally excited structured monomer emission of naphthalene. The structured non-solvatochromic naphthalene emission of **L_2** was observed with (0,0) band centered at 323 nm (Figure 3.1.15a) along with vibrational structures at 338 and 352 nm when excited at 300 nm. The quantum yield of fluorescence monomer emission, Φ_F of the free ligand was found to be 0.19 (see appendix), which is comparable to that of naphthalene (Φ_F = 0.23).

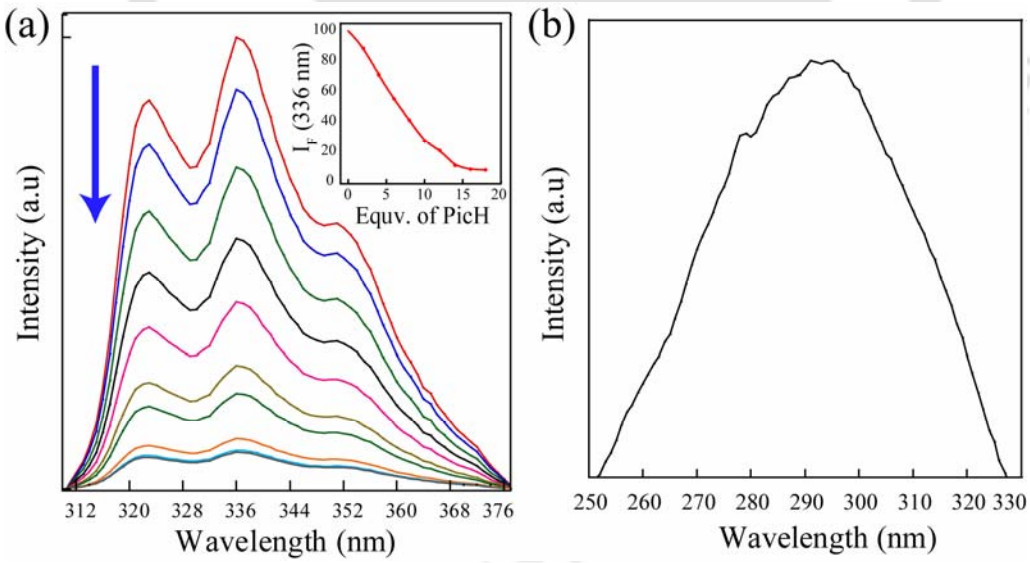

Figure 3.1.15. (a) Emission spectra of **L_2** (10^{-6} M in dry THF) during the titration with picric acid. Inset: Plot of the emission intensity (at 336 nm) of L_2 as a function of equivalent of picric acid added; (b) Excitation spectra of **L_2** (10^{-6} M in dry THF).

The excitation spectra monitoring the different bands of the structured emissions are the identical and match with the absorption spectra of the free ligand in dry THF at 298 K (Figure 3.1.15b). With increasing concentration of the ligand, the total intensity of fluorescence emission decreases significantly without the appearance of any broad band in the higher wavelength region. This suggests that self-quenching takes place without

formation of any excimer at higher concentration.[3.1.13] The concentration of the ligand was maintained at 10^{-6} M throughout the study as the emission intensity is found to be maximum at this concentration. When dry THF solutions of electron deficient aromatic guests were added to **L_2** the fluorescence intensity was quenched to varying degrees (Figure 3.1.15a and Figure 3.1.16). The best results were observed for additions of picric acid to **L_2**, where 98% quenching was observed (Figure 3.1.16). Fluorescence titration results revealed that maximum fluorescence quenching occurs when 16 equiv of picric acid had been added to **L_2**.

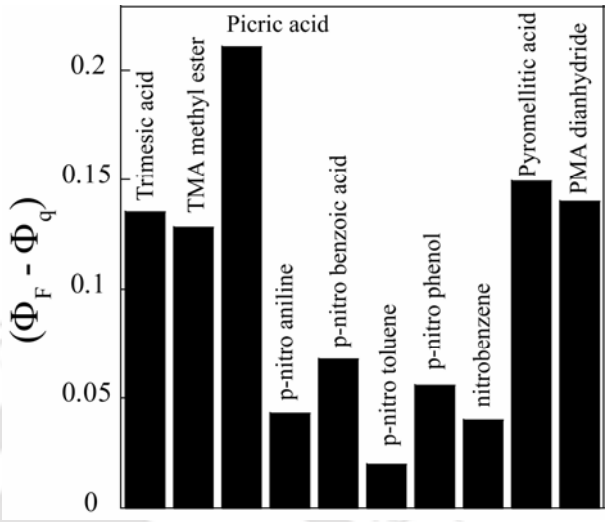

Figure 3.1.16. Schematic representation showing the change of fluorescence quantum yield ($\Phi_F - \Phi_q$) of **L_2** upon addition of the aromatic guest. Φ_F and Φ_q are quantum yields of **L_2** in absence and presence of guest, respectively.

Figure 3.1.14 clearly shows that **L_2** exhibits relatively higher selectivity toward picric acid over other electron deficient aromatic guests such as *p*-nitro aniline, *p*-nitro benzoic acid, *p*-nitro toluene, *p*-nitro phenol, nitrobenzene, trimesic acid, trimesic acid trimethyl ester, pyromellitic acid, pyromellitic dianhydride in terms of change of fluorescence quantum yield. In order to confirm the nature of molecular interactions between host and guest in solution we have chosen a guest containing different functional groups. We have observed that fluorescence quenching of the host molecules is a cumulative effect of both acid-base and aromatic interactions.

Figure 3.1.17 pictorially and schematically shown the quenching of fluorescence intensity of **L_2** in presence of electron deficient picric acid. Due to the stereochemical requirement, **L_2** adopts a flattened conformation and alone can not exhibit intra as well as intermolecular π–π interactions. Hence, it readily forms stable intermolecular π–π interactions with aromatic guest and form stable inclusion complex. The quenching of fluorescence is not a result of simple re-absorption of the guest molecules. The excitation spectra of host-guest complex resembles to the absorption spectra of the pure **L_2**. Upon gradual addition of picric acid to the THF solution of **L_2**, the intensity of the emission bands decreases. The linear Stern-Volmer response (Figure 3.1.18a) with picric acid as quencher is consistent with well-behaved fluorescence quenching systems.[3.1.14]

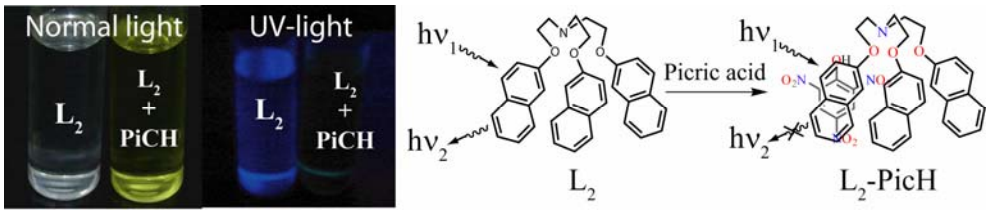

Figure 3.1.17. Pictorial representation of fluorescence quenching of L_2 and formation of inclusion complex in presence of picric acid.

The dissociation constant K_d[3.1.15] were estimated from the change in fluorescence quantum yield resulted from the titration data of **L_2** against picric acid solution. The linear fit of the data (Figure 3.1.18b) for picric acid inclusion complex was obtained by plotting $\log[(\Phi-\Phi_{min})/(\Phi_{max}-\Phi)]$ as a function of logarithm of picric acid concentration and the intercept of the linear regression determines K_d value of 5.6 μm in THF. This value indicates the formation of a stable inclusion complex and is in consistence with good correlation coefficients (> 0.99). Fluorescence quenching experiments results shows the stronger acids are relatively stronger quencher. We have also shown that electron deficient guest possessing no acidic group (*viz.* nitrobenzene, *p*-nitroaniline) can also quench the fluorescence. To test the effect of protonation of the bridgehead N atom on fluorescence quenching, we have titrated **L_2** with mineral acids (see appendix).

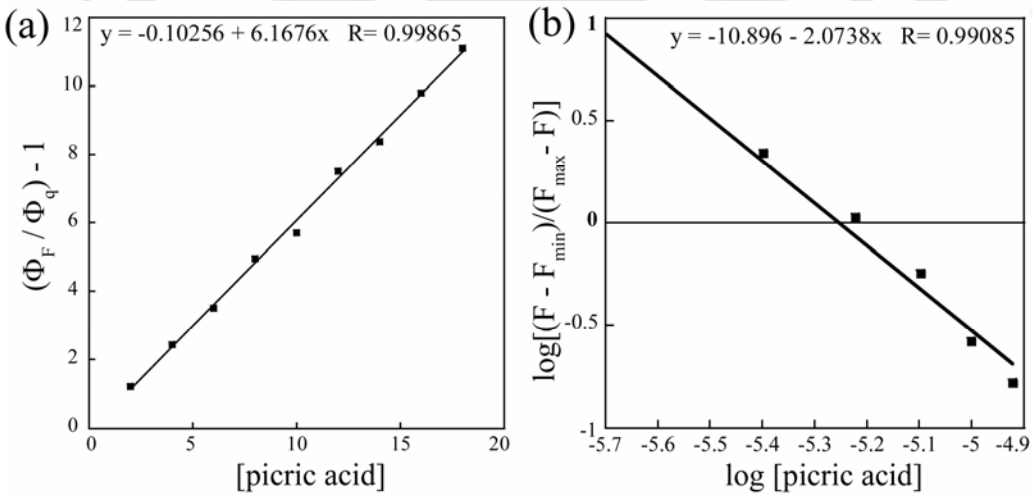

Figure 3.1.18. (a) Stern –Volmer plot with picric acid; (b) Linear regression plot for K_d determination obtained from the titration data of **L_2** with picric acid in THF.

Mineral acids have negligible effect on fluorescence quenching. Hence, the formation of organic salt along with the inclusion complex is responsible for the quenching of fluorescence. The spectral characteristics of **L_2** in the solid state are consistent with its solution phase behavior. In the solid state, **L_2** exhibits a broad absorption band in the 250–340 nm regions. It shows a broad emission band in 315–370 nm regions. All the detail

vibrational structures are lost in the solid-state. All the inclusion complexes in the solid-state also follow the similar trends. But these inclusion complexes show quenching in the fluorescence intensity in the solid-state. However, when these solid samples are dissolved in dry THF, on an average they reproduced the solution phase spectral behavior. In the crystals host-guest ratio is smaller than that of the solution, to have a similar extent of quenching.

3.1.2e. Summary

The simple tripodal ligand Tris-[2-(naphthalen-2-yloxy)-ethyl]-amine (**L_2**) act as a fluorescence signaling system for aromatic guest. It forms inclusion complexes with several electron deficient aromatic compounds. This inclusion phenomenon has been studied by steady state fluorescence spectroscopy and solid-state structural analysis. Electron rich **L_2** shows dramatic color change and a concomitant quenching of luminescence in solution as well as solid phase when titrated with several other electron deficient aromatic guest molecules. Rather high selectivity towards the picric acid was observed. L_2 simultaneously forms inclusion complex and organic salt co-crystal with the composition $[(L_2H^+)(Pic^-)]\subset$PicH (PicH= Picric acid) when crystallized in the presence of picric acid. In the solid state, it forms a strong π–π, C–H····π and C–H····O type interactions. In conclusion, we have presented the synthesis and characterization of a simple electron-rich tripodal fluorophore **L_2** for the first time. Electron rich **L_2** is an efficient fluorogenic host for inclusion of electron deficient aromatic molecules in solution. We have studied the formation of host-guest complexes with different electron deficient aromatic guest by steady state fluorescence spectroscopy and single crystal X-ray structural studies. We found that fluorescence quenching efficiency depends on the extent of electron deficiency in the aromatic guests coupled with their acidic nature. Guest molecules with protected acid groups with similar extent of electron deficiency can also quench the fluorescence. Electron rich **L_2** can from strong intermolecular π-stacking interaction with aromatic guest bearing a stronger electron-withdrawing group. So, we can suggest that fluorescence quenching of the host molecules is a cumulative effect of both acid-base and aromatic interactions in solution. We have also shown structurally the simultaneous formation of inclusion complex and organic salt co-crystal in the solid-state between Picric acid and **L_2**. In the solid-state, guest form mixed *aba* and *abba* type intermolecular π–π stacking interactions with **L_2**. Herein, the self-assembled structures exhibit a number of unusual weak non-covalent interactions in addition to conventional hydrogen bonding through supramolecular host-guest fluorescence signaling systems.

3.1.3. Metal ion recognition by L_2

This part describe the cation recognition of simple electron rich tripodal naphthalene ether ligand Tris-[2-(naphthalen-2-yloxy)-ethyl]-amine (**L_2**). Ag-complex forms an intermolecular sandwich complex via silver ion-induced self-assembly (Scheme 3.1.2).

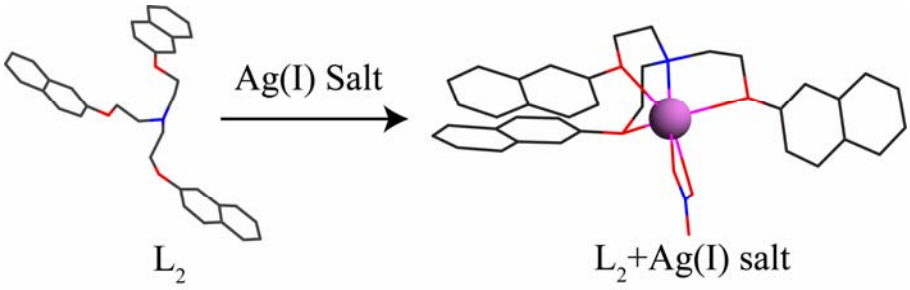

Scheme 3.1.2 Schematic representation of recognition phenomenon in addition of Ag(I) with **L_2**.

3.1.3a. Synthesis and characterization Ag(I) salt of L_2

To a magnetically stirred solution of **L_2** (0.53 g, 1 mmol) in $CHCl_3$ (20 mL), was added methanolic solution of Silver nitrate (0.168 g, 1 mmol) in portions. With the constant stirring the five hours a grayish-white precipitate that formed was filtered, washed with dry ether, and dried under vacuum. Yield: 0.626 g, 90% based on **L_2**. Single crystals suitable for X-ray diffraction were obtained from slow evaporation of H_2O-C_2H_5OH (1:1) mixture solution of the compound at RT for fifteen days. Anal. Calcd (%) for $C_{36}H_{33}Ag\ N_2\ O_6$: C, 62.05; H, 4.77; N, 4.02. Found: C, 62.07; H,4.75; N, 4.05%; IR (KBr disk) (cm^{-1}); ν(N=O), 1465 (s); ν(N-O), 1273 (m); ν(ONO), 989.

3.1.3b. Crystal structure analysis

The solid state structure of complex was determined by single-crystal X-ray diffraction. The neutral mononuclear Ag(I)-**L_2** complex in crystallized monoclinic P2(1)/c space group. ORTEP plot of Ag(I)-**L_2** complex is shown in Figure 3.1.17.a. In complex the Ag(I) is surrounded by tetra dentate **L_2** ligand and one NO_3 ion in distorted octahedral fashion. Ag(I) is connected with three ethereal oxygen on chelating ligand **L_2** (Ag1–O1=2.678Å, Ag1–O2=2.670Å, and Ag1–O3=2.725Å), one apical nitrogen (Ag1–N1=2.298Å) and two oxygen of bridging nitrate atom Ag1–O4=2.251Å, Ag1–O5=2.637Å respectively.[3.1.17] Naphthalene ring of one part of the ligand are forming C-H····π interactions (C25-H····π , 3.896 Å, C1-H····π , 3.415 Å C13-H····π , 3.598 Å) with the nearest C-H moiety of the other unit. Similarly there are another two non covalent interaction is observed between nitrate ion and C-H group of aromatic proton. The bond lengths are C36-H····O6, 3.329 Å and C36-H····N2, 3.511Å respectively (see appendix).

Overall intermolecular non covalent interactions results in the formation of 2D hydrophilic–hydrophobic channel network (Figure 3.1.19.b) and it also form a capsule network in the solid-state along *a* axis (Figure 3.1.19.c).

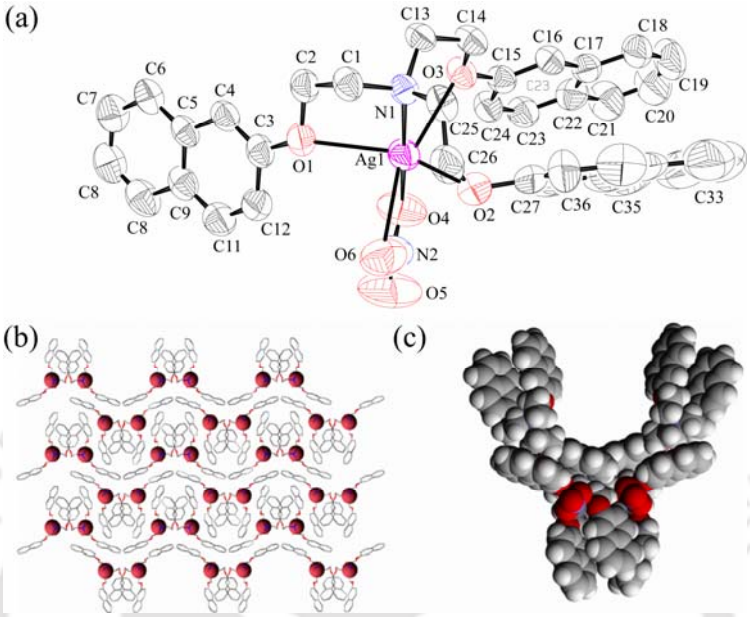

Figure 3.1.19. (a) ORTEP plot of complex $\mathbf{L_2}AgNO_3$. H-atoms are omitted for clarity; (b) 2D hydrophilic–hydrophobic channel network along the c axis; (c) Formation of capsule network along a axis.

3.1.3c. Absorption spectroscopy

The UV-visible absorption spectra (Figure 3.1.20) of $\mathbf{L_2}$ (10^{-5} M) was recorded in dry THF at 298 K. The absorption spectrum is found to be overlapping of two transitions in the 270–310 nm regions. The π→π* transitions of the naphthalene unit appear at 283 (ε = 29400 $M^{-1}cm^{-1}$) and 294 nm (ε = 33300 $M^{-1}cm^{-1}$).[3.1.4] The band at ~250 nm is assigned to the π–π interaction between the naphthalene units of the ligand.[3.1.10] When $\mathbf{L_2}$ is titrated against different metal salts, an absorption peak is decreases with increasing the concentration of metal salts. But in Ag(I) salts we have seen one additional peak is

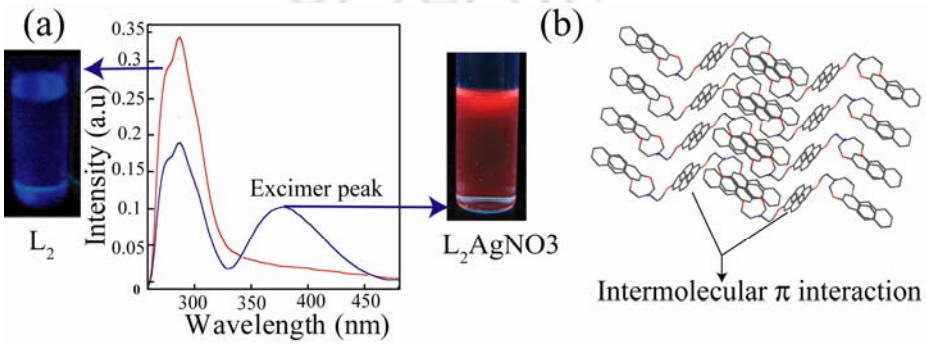

Figure 3.1.20. (a) UV-visible absorption spectra of L_2 and Ag complex at 298 K, $\mathbf{L_2}$ in UV light (left side) and $\mathbf{L_2}AgNO_3$ in UV light right side; (b) Intermolecular π interaction in solid state of Ag(I)-L_2 complex.

showing ~ 375 nm (Figure 3.1.20.a) which may be due to intermolecular π interaction of naphthalene moieties, which is reflected in solid state behavior of single crystal of the corresponding complex (Figure 3.1.20.b).[3.1.18] In addition in presence of UV light we have seen a blue color fluorescence solution of ligand **L_2** dry THF but in complex it shows red color fluorescence (Figure 3.1.20.a).

3.1.3d. Fluorescence spectroscopy

The emission spectrum of **L_2** was recorded in dry THF at 298 K. Free **L_2** shows a locally excited structured monomer emission of naphthalene. The structured non-solvatochromic naphthalene emission of **L_2** was observed with (0,0) band centered at 323 nm (Figure 3.1.21a) along with vibrational structures at 338 and 352 nm when excited at 300 nm. The fluorescence titration of ligand **L_2** with various metal ions was conducted to examine the selectivity.

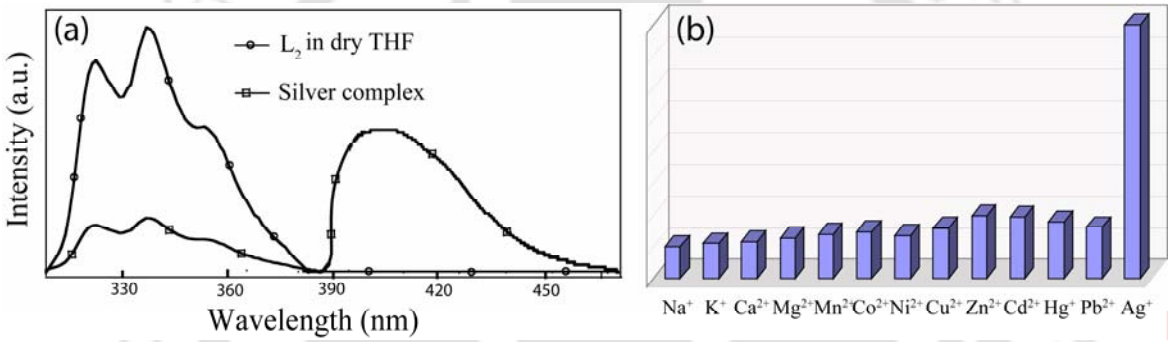

Figure 3.1.21. (a) Emission spectra of **L_2** and **L_2**-Ag complex in dry THF solvent; (b) Schematic representation showing the change of fluorescence quantum yield (Φ_F - Φ_q) of **L_2** upon addition of the different metal salts. Φ_F and Φ_q are quantum yields of L_2 in absence and presence of metal salts, respectively.

When **L_2** is titrated against different metal salts like Na^+, K^+, Ca^{2+} and Mg^{2+} etc there is no change in the spectral behavior. But transition metals, *e.g.* Mn^{2+}, Co^{2+}, Ni^{2+}, Cu^{2+} and Zn^{2+}, quenches the fluorescence, similar to heavy metal like Cd^{2+},Hg^{2+}, Pb^{2+}. But addition of Ag(I) results in the formation of an extra peak at higher wavelength (~ 420 nm) which is strongly support the preferred interaction in solution phase (Figure 3.1.21b).[3.1.19]

In the case of the solution-state study by ^{1}H NMR, when $AgNO_3$ was added to the DMSO-d_6 solution of **L_2**, the ^{1}H NMR spectrum shows a shift in the position of the NCH_2 proton from δ 3.41 ppm to the higher δ value of 3.64 ppm. This shift indicates the influence of the protonated apical nitrogen on the neighboring proton. Similar changes observed in the solution phase with other anions also (Figure 3.1.22.a and 3.1.22.b).

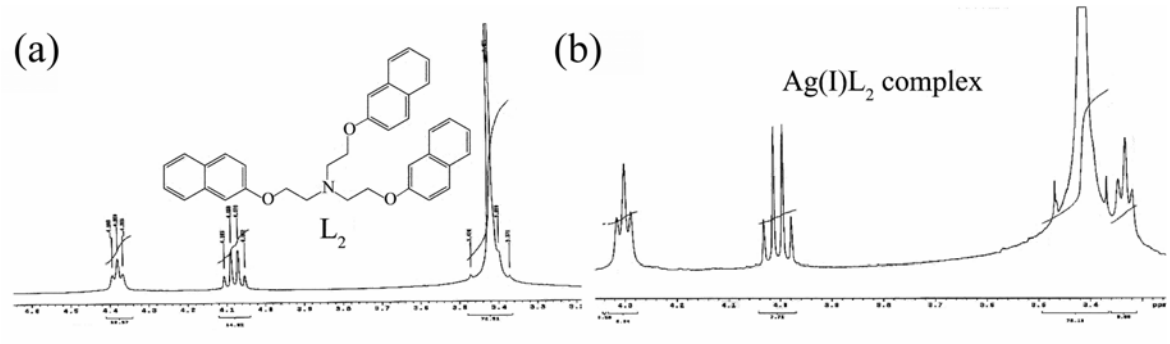

Figure 3.1.22. ^{1}H NMR spectra of (a) $\mathbf{L_2}$ and (b) Ag(I) complex of $\mathbf{L_2}$ in DMSO-d_6 (aliphatic region).

3.1.3e. Summary

The development and improvement of highly selective tripodal receptors or ionophores that allow measurements of analytes in complex real-life samples will remain a main issue in the development of chemosensors either in the fluorescence or the optical mode. The interest of many organic chemists in tripodal host compounds is expected to result in the development of many new interesting receptors, but where the low partitioning of ions and the limited solubility of several tripodal receptors might restrict their applicability. Here in. the effect of adding metal cations (Na^{1+}, K^{1+}, Ca^{2+}, Mg^{2+}, Cu^{2+}, Zn^{2+}, Cd^{2+}, Cu^{2+}, Hg^{2+}, Ag^{+}) on the fluorescence properties of a Tris-[2-(naphthalen-2-yloxy)-ethyl]-amine (L_2) bearing three end naphthalene fragments, We found that $\mathbf{L_2}$ behaves as the first molecular switch capable of quenching naphthalene excimer emission by the addition of all of Ag^+ metal cations in freshly prepared THF solvent. In summary, we have developed a new fluorescent sensor for AgI with remarkably high selectivity and sensitivity. Moreover, this molecule makes it possible to detect the Ag(I) cation potentially. We look forward to witnessing and participating in the creative and innovative development of selective, sensitive, and accurate sensors for cations and anions.

Reference:

3.1 (a) Diamond, D.; Nolan, K. Calixarenes: Designer ligands for chemical sensors. *Anal. Chem*., **2001**, *73*, 22A. (b) Ludwig, R.; Dzung, N. T. K. Calixarene based molecules for cation recognition. *Sensors,* **2002**, *2*, 397. (c) Beer, P. D.; Gale, P. A. Anion recognition and sensing: the state of the art and future perspectives. *Angew. Chem. Int. Ed. Engl.,* **2001**, *40*, 486. (d) Antonisse, M. M. G.; Reinhoudt, D. N. Potentiometric anion selective sensors. *Electroanalysis,* **1999**, *11*, 1035-1048.

3.2 (a) Berocal, M. J.; Cruz, A.; Badr, I. H. A.; Bachas, L. G. Tripodal ionophore with sulphate recognition properties for anion-selective electrode. *Anal. Chem*.,**2000**, *72*, 5295. (b) Antonisse, M. M. G.; Reinhoudt, D. N. Neutral anion receptors: design and application. *Chem. Commun.,* **1998**, 443.

3.3 Reinoso-Garcia, M. M.; Dijkman, A.; Verboom, W.; Reinhoudt, D. N.; Malinoswka, E.; Wojciechowska, D.; Pietrzak, M.; Selucky, P. *Eur. J. Org. Chem*., **2005**, 2131

3.4 Kim, S.-G.; Kim, K.-H.; Jung, J.; Shin, S. K.; Ahn, K. H. *J. Am. Chem. Soc*., **2002**, *124*, 591.

3.5 Cram, D. J.; Cram, J. M. *Container Molecules and their Guests*, The Royal Society of Chemistry,Cambridge, UK, 1994.

3.6 (a) Kim, Y.-K.; Ha, J.; Cha, G. S.; Ahn, K. H. *Bull. Korean Chem. Soc*., **2002**, *23*, 1420. (b) Sasaki, S.; Ozawa, S.; Citterio, D.; Iwasawa, N. *Anal. Sci*., **2001**, *17*, 1659.

3.7 (a) Schmuck, C.; Schwegmann, M. A. *Org. Biomol. Chem*., **2006**, *4*, 836-838. (b) Niikura, K.; Bisson, A. P.; Anslyn, E. V. *J. Chem. Soc., Perkin Trans., 2* **1999**, 1111. (c) Wiskur, S. L.; Ait-Haddou, H.; Lavigne, J. J.; Anslyn, E. V. *Acc. Chem. Res.,* **2001**, *34*, 963.

3.8 (a) Sato, K.; Arail, S.; Yamagishi, T. A. *Tetrahedron Lett*., **1999**, *40*, 5219. (b) Ballester, P.; Costa, A.; Deyii, P. M.; Vega, M; Morey, J. *Tetrahedron Lett*., **1999**, *40*, 171. (c) Fan, A. L.; Hong, H. K.; Valiyaveettil, S.; Vittal, J. J. *J. Supramol. Chem*., **2002**, *2*, 247.

3.1.1 Jiang, L.; Pan, Z.; Duan, C.; Luo, Q.; Liu, Y.; Huang, X.; Wu, Q. *J. Chem. Crystallogr.*, **1999**, *29* 943.

3.1.2 Ward, Jr. K. *J. Am. Chem. Soc.,* **1935**, *57*, 914.

3.1.3 (a) Moorthy, J. N.; Natarajan, R.; Mal, P.; Venugopalan, P. *J. Am. Chem. Soc.,* **2002**, *124*, 6530; (a) Thallapally, P. K.; Nangia, A. *CrystEngComm.,* **2001**, 1*27*, 1.

3.1.4 (a) Das, G.; Bharadwaj, P. K.; Basu Roy, M.; Ghosh, S. *Chem. Phys.,* **2002**, *145,* 277; (b) Das, G.; Bharadwaj, P. K.; Basu Roy, M.; Ghosh, S. *J. Photochem. Photobiol. A.,* **2000**, *135*, 7.

3.1.5 (a) Shon, R. S.; Cowan, D. O.; Schmiegel, W. W. *J. Phys. Chem.,* **1975**, *79*, 2087. (b) Parker, C.A.; Hatchard, C. G. *Trans. Faraday Soc.,* **1963**, *59*, 284.

3.1.6 Mojtaba, S.; Javad, C. M. *J. Photochem. Photobiol. A.,* **2003**, *155*, 69.

3.1.7 Chandross, E. A.; Thomas, H. T. *Chem. Phys. Lett.,* **1971**, *9,* 393.

3.1.8 Behanna, H. A.; Stupp, S. I. *Chem. Commun.,* **2005**, 4845.

3.1.9 Thakuria, H.; Borah, B. M.; Pramanik, A.; Das, G. *J. Chem. Crystallogr.,* **2007**, *37*, 807.

3.1.10 Sankaran, N. B.; Das, A.; Samanta, A. *Chem. Phys. Lett.,* **2002**, *351*, 61.

3.1.11 (a) Mulliken, R. S.; Person, W. B. *Molecular complexes: a lecture and reprint volume,* Wiley-Interscience, New York, **1969**; (b) Foster, R. *Organic Charge-Transfer Complexes,* Academic Press, London and New York, **1969**; (c) Slifkin, M. A. *Charge-Transfer Interactions of Biomolecules,* Academic Press, London and New York, **1971**.

3.1.12 (a) Allwood, B. L.; Spencer, N.; Zavaresh, H. S.; Stoddart, J. F.; Williams, D. J. *J. Chem. Soc. Chem. Commun.,* **1987**, 1064; (b) Philp, D.; Stoddart, J. F. *Angew. Chem., Int. Ed. Engl.,***1996**, *35*, 1154.

3.1.13 (a) Shao-Lin Shon, R.; Cowan, D. O.; Schmiegel, W. W. *J. Phys. Chem.,* **1975**, *79*, 2087; (b) Parker, C. A.; Hatchard, C. G. *Trans. Faraday Soc.* **1963**, *59*, 284.

3.1.14 Mojtaba, S.; Javad, C. M. *J. Photochem. Photobiol. A,* **2003**, *155*, 69.

3.1.15 Grynkiewicz, G.; Poenie, M.; Tsien, R. Y. *J. Biol. Chem.,* **1985**, *260*, 3440.

3.1.16 (a) Lee, A. W. M.; Chan, W. H.; Jiang, L. S.; Poon, K. W. *Chem. Commun*.,**1997**, 611; (b) Chan, W. H.; Yang, R. H.; Wang, K. M. *Anal. Chim. Acta,* **2002**, *460*, 123; (c) Zhang, H. K.; Chan, W. H.; Lee, A. W. M.; Wong, W. Y. *Tetrahedron Lett*., **2003**, *44*, 395.

3.1.17 (a) Graham, A.; Bowmaker, E.; Effendy, S.; Marfuah, B.; Skelton, W.; White, A. H. *Inorg. Chim. Acta.,* **2005**, *358*, 4371; (b) Yamada, S.; Ishida, T.; Nogami, T. *Dalton Trans*., **2004**, 898; (c) Liu, B.; Chen, W.; Jin, S. *Organometallics,* **2007**, *26,* 3660.

3.1.18 Yang, R-H.; Chan, W-H.; Lee, W. H. M.; Xia, P-F.; Zhang, H-K.; Li, K *J. Am. Chem. Soc.,* **2003**, *125*, 2884.

3.1.19 Shiraishi, Y.; Ishizumi, K.; Nishimura, G.; Hirai, T. *J. Phys. Chem. B,* **2007,** *111,* 8812.

PART - II

3.2 Tripodal Receptors for Multipoint anion recognition

In this part of the chapter we have described the synthesis of a new aminoquinoline based tripodal ligand (**L_3**) and its selective chemosensing properties toward phosphate anion (Scheme 3.2.1).

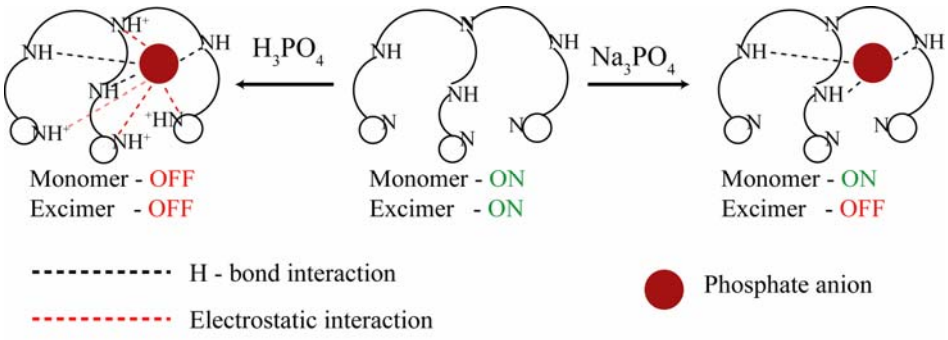

Scheme 3.2.1 Schematic representation of supramolecular host–guest complexes of **L_3** in the presence of phosphoric acid and its salt.

3.2.1. Synthesis of tris-(N-ethyl-8-aminequinoline) amine ligand (L_3)

A mixture of 8-hydroxyquinoline (1.45 g, 1 mmol), tris-(2-aminoethyl) amine (0.34 mL, 0.33 mmol), sodium metabisulfite (1.90 g, 1 mmol), and water (10 mL) was reflux for 10 days with continuous stirring. Upon cooling, the solution was made strongly alkaline (pH=12) by the addition of aqueous sodium hydroxide. The resulting mixture was cooled to rt and then filtered. The solid was extracted twice with dichloro methane (400 mL), and the dichloro methane extracts were combined, dried ($MgSO_4$), and the solvent was removed under reduced pressure. The solid obtained was triturated with hot ethanol (15 mL), filtered, and air-dried to give a yellow solid (2.43 g, 45%). It was crystallized from methanol/ water mixture by slow evaporation at room temperature.

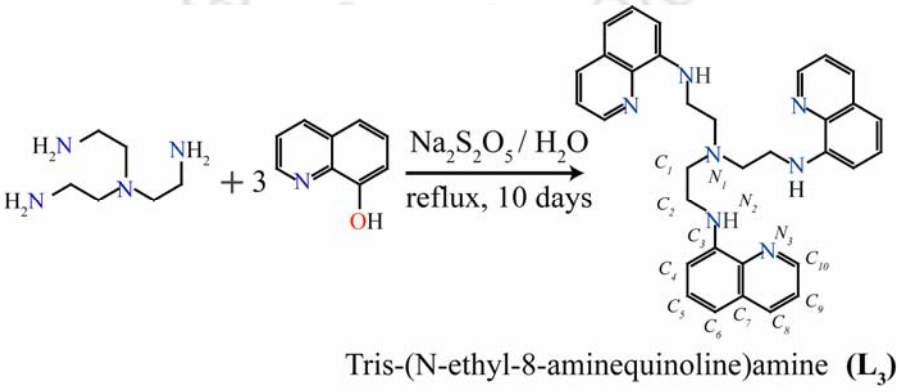

Figure 3.2.1. Synthetic procedure of tripodal napthyl ether ligands **L_3** .

L_3: Straw yellow solid, mp 126 ^oC, R_f=0.60 (EtOAC/hexane 15:85). IR (KBr) ν_{max}/cm^{-1} 3445, 2956, 2932, 2865, 1615, 1512, 1460, 1243, 1118 cm^{-1}. ^1H NMR ($CDCl_3$, 400 MHz): δH 8.53 (3H, dd, J_1=2.0 Hz, J_2=2.4 Hz, ArH), 7.99 (3H, dd, J_1=2.0 Hz, J_2=6.4 Hz, ArH), 7.27 (6H, m, ArH), 6.99 (3H, dd, J_1=0.8 Hz, J_2=7.2 Hz, ArH), 6.54 (3H, m, J_1=2.0 Hz, ArH), 3.43 (9H, q, J=6.0 Hz, NH–CH2), 3.04 (6H, t, J¼6.4 Hz, N–CH2); ^{13}C NMR (CDCl3; 100 MHz): δc 147.2, 144.7, 137.8, 136.1, 128.6, 128.0, 121.9, 113.4, 104.6 (ArC), 53.3, 41.4 (H2C). HRMS (ESI): m/z 527.2797 (M^+) Found: 527.2795. Elemental analysis: C, 75.10; H, 6.30; N, 18.59. Found: C, 75.15; H, 6.26; N, 18.60.

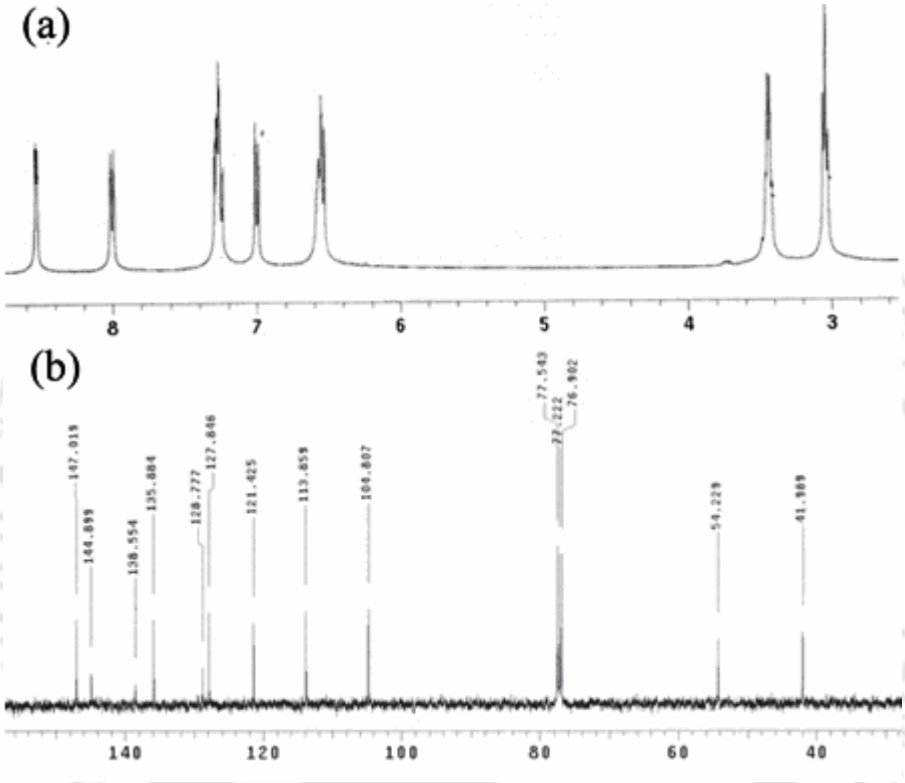

Figure 3.2.2. (a) ^1H NMR and (b) ^{13}C NMR spectra of **L_3** in $CDCl_3$**.**

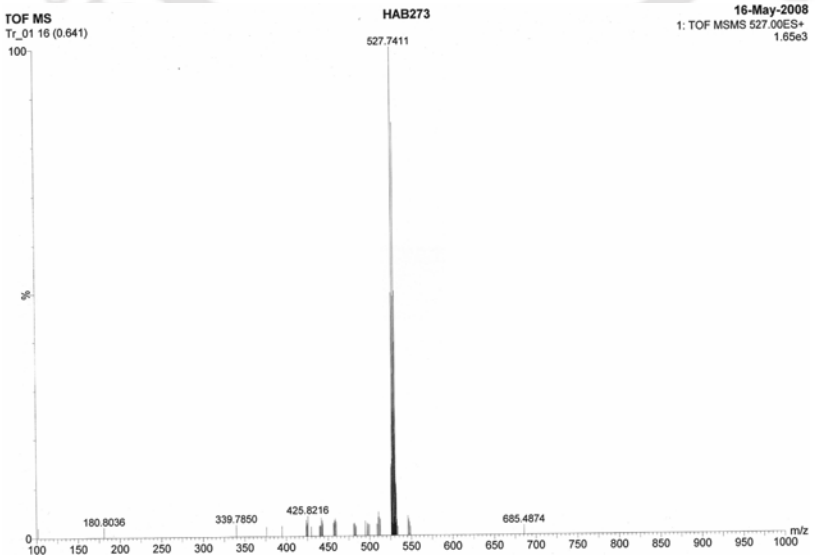

Figure 3.2.3. ESI-MS spectra of **L_3**.

3.2.2. Synthesis and characterization of phosphoric acid salt

L_3 (1 mmol) in 50% aqueous THF (20 mL) was added drop wise to a stirred alcoholic solution (20 mL) of H_3PO_4 (w1.1 mmol) at room temperature. The mixture was continued to stir for another 1 h at rt. This solution was evaporated to dryness under reduced pressure. A red solid powder was obtained. IR (KBr) ν_{max}/cm^{-1} 3460, 2965, 2941, 2881, 1631, 1534, 1478, 1213, 1257, 1156, 1135, 1077, 944, 879, 521. 1H NMR (DMSO-d_6; 400 MHz): δH 8.70 (3H, d, J_1=2.8 Hz, ArH), 8.24 (3H, d, J_1=6.8 Hz, ArH), 7.50 (3H, dd, J_1=4.0, 4.4 Hz, ArH), 7.26 (3H, t, J_1=8.0 Hz, ArH), 7.11 (3H, d, J_1=8.0 Hz, ArH), 6.70 (3H, d, J_1=7.6 Hz, ArH); 13C NMR (DMSO-d_6; 100 MHz): δc 147.22, 143.59, 137.35, 136.06, 128.72, 128.06, 122.18, 114.94, 105.72 (ArC), 52.38, 38.04 (H2C) MS ($^+$EI): m/z 625.2566 (M^+) Found: 625.2568. Elemental analysis: C, 66.33; H, 5.80; N, 15.67. Found: C, 66.35; H, 5.82; N, 15.65.

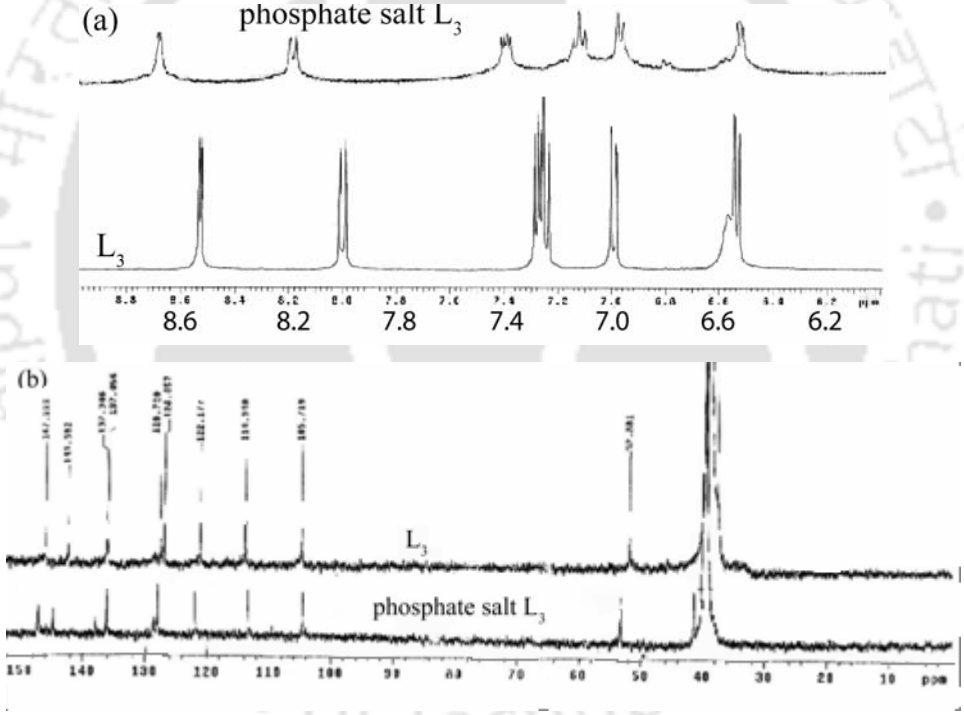

Figure 3.2.5. (a) ^{1}H NMR and (b) ^{13}C NMR spectrum of **L_3** and it's phosphate salt.

3.2.3. Crystal structure analysis

The neutral ligand **L_3** is crystallized monoclinic P2(1)/c space group. ORTEP plot of the ligand **L_3** is shown in Figure 3.2.6.a. Single crystal X-ray structure analysis shows that three arms are disposed in a non-parallel arrangement, which prevents the intramolecular π-stacking arrangement (Figure 3.2.6.a). However, all the aromatic quinoline moieties are disposed in the same side in the solid state. As a result it forms an open bowl shape cavity, (see appendix) which can accommodate spherical anions via N–H····X^- type hydrogen

bonding. Bridge head tertiary N atom is also present in endo-conformation, which can also enhance the anion binding in the semi-flattened cavity. In the solid state it forms several weak C–H····π interactions and results in the formation of brick-wall type 3D network (Figure 3.2.6.b).

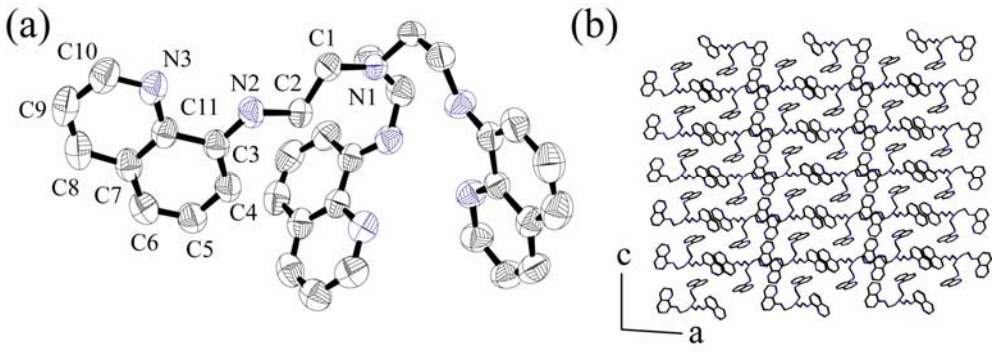

Figure 3.2.6. (a) ORTEP plot of complex L_2AgNO_3. H-atoms are omitted for clarity; (b) 2D hydrophilic–hydrophobic channel network along the c axis.

3.2.4. Absorption spectroscopy

The UV–vis spectrum of L_3 shows a high-intensity band in the UV region (256 nm, ε=47,427 M^{-1} cm^{-1}) and a relatively intense band at 366 nm (ε=9427 M^{-1} cm^{-1}) with a shoulder at 340 nm (ε=7639 $M^{-1}cm^{-1}$) in the near visible region (Figure 3.2.7). Peak in the UV region is corresponds to the n→π* transition while that of in the near visible region (340 nm and 366 nm) is most likely due to the π→π* transitions as seen in the other similar 8-aminoquinoline systems.[3.2.1,3.2.2] These bands are expected to shift upon protonation of amine/quinoline nitrogen atoms in the presence of different acid like HF, HCl, HBr, CH_3CO_2H, H_3PO_4, etc. In the presence of dilute H_3PO_4, peak corresponding to n→π* transition has shifted to longer wavelength (276 nm) while peak due to π→π* transition has shifted to shorter wavelength (325 nm). In addition, protonated ligand shows a broad band centered on 450 nm corresponds to intramolecular charge transfer (ICT) (Figure 3.2.7). Similar changes in the absorption spectra were observed in case of other acids. However, addition of salt of the corresponding anions shows no significant changes in the absorption spectrum.

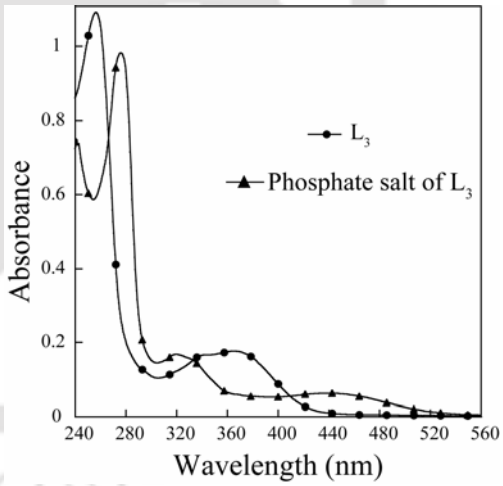

Figure 3.2.7. UV–vis spectra of **L_3** and in the presence of H_3PO_4 in THF.

3.2.5. Fluorescence spectroscopy

L_3 shows monomer emission at 310 nm when excitated at 270 nm. With gradual increase in concentration of **L_3** the peak corresponds to monomer decreases gradually with simultaneous increase of an additional red-shifted and non-structured emission band, centered at 475 nm. The peak at 475 nm is assigned to the excimer emission which is \characteristic to the similar quinoline based systems[3.2.3] (Figure 3.2.8). The excimer emission resulted from the intermolecular excimer formation, rather than intramolecular interaction, as indicated that dilute solution shows only the presence of monomer emission. The spectrum shows an isoemissive point at 410 nm. Anions are known to form strong N–H····X^- type of hydrogen bond with amine groups. However, anions do not interact with the aromatic ring or quilinoline nitrogen atoms of the ligand. Figure 3.2.9 shows the emission spectra of **L_3** with increasing concentrations of sodium phosphate (Na_3PO_4) in THF at 298 K. Addition of Na_3PO_4 leads to a decrease in the emission intensity of the excimer band only without showing isoemissive points (Figure 3.2.9a). Protonation of amine/quinoline nitrogen atoms prevents the intermolecular excimer formation due to charge repulsion. Moreover, it is already known that protonated pyridine moieties quench the fluorescence of known fluorophore.[3.2.4] Hence in the presence of acid, we have encountered the quenching of monomer as well as excimer fluorescence (Figure 3.2.9b). However, the degree of quenching of excimer emission is dependent on the nature of the anion, which is highly selective to phosphate ion (Figure 3.2.10a). The magnitude of the quenching efficiency (ϕ_Q) follows the order of $PO4^{3-}$ (0.98)>SO_4^{2-} (0.33)>CH_3COO^- (0.23)>Br^- (0.20)>Cl^- (0.13)>NO_3^- (0.08), which is a result of combine steric and electronic effect. Excitation spectrum of the **L_3** monitoring the peak at 475 nm resembles to the absorption spectra of the ligand (see appendix).

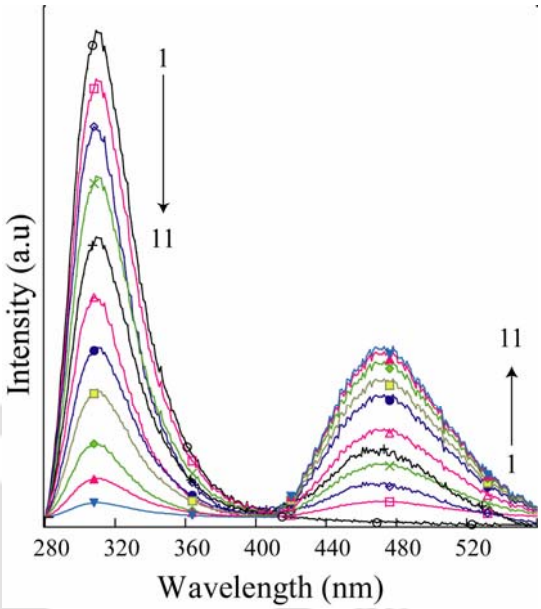

Figure 3.2.8. (a) Fluorescence spectra of **L_3** of different concentration in THF at 298 K. [**L_3**]: (1) 0.2, (2) 0.4, (3) 0.6, (4) 0.8, (5) 1.0, (6) 1.2, (7) 1.4, (8) 1.6, (9) 1.8, (10) 2.0, and (11) 2.2 μM.

.

Upon gradual addition of Na_3PO_4 to the THF solution of **L_3**, the intensity of the emission bands decreases. The dissociation constant[3.2.5] K_d was estimated from the change in fluorescence quantum yield resulted from the titration data of **L_3** against Na_3PO_4 solution. The linear fit of the data (see appendix) for Na_3PO_4 inclusion complex was obtained by plotting $\log[(\Phi-\Phi_{min})/(\Phi_{max}-\Phi)]$ as a function of logarithm of Na_3PO_4 concentration and the intercept of the linear regression determines K_d value of 6.76 mm in THF. This value indicates the formation of a stable inclusion complex and is in consistence with good correlation coefficients (>0.99). To demonstrate the selectivity of **L_3** toward phosphate, we have monitored the change in fluorescence quantum yields in the presence of different anions. Figure 3.2.10b clearly shows that **L_3** has a remarkably high selectivity toward phosphate anion in terms of change of fluorescence quantum yield. The linear Stern–Volmer response (Figure 3.2.10b inset) with Na_3PO_4 as quencher is consistent with well-behaved fluorescence quenching systems.[3.2.6]

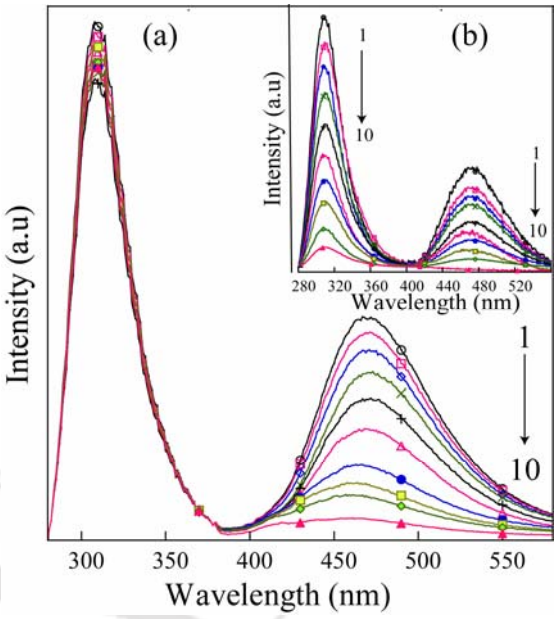

Figure 3.2.9. (a) Fluorescence spectra of **L_3** in the presence of Na_3PO_4 in THF at 298 K. [Na_3PO_4]: (1) 0.0, (2) 1.0, (3) 2.0, (4) 3.0, (5) 6.0, (6) 10.0, (7) 15.0, (8) 20.0, (9) 25.0, and (10) 30.0 μM; (b) Fluorescence spectra of **L_3** in the presence of H_3PO_4 in THF solution at 298 K. [H_3PO_4]: (1) 0.0, (2) 1.0, (3) 2.0, (4) 3.0, (5) 4.0, (6) 6.0, (7) 8.0, (8) 12.0, (9) 15.0, and (10) 20.0 μM.

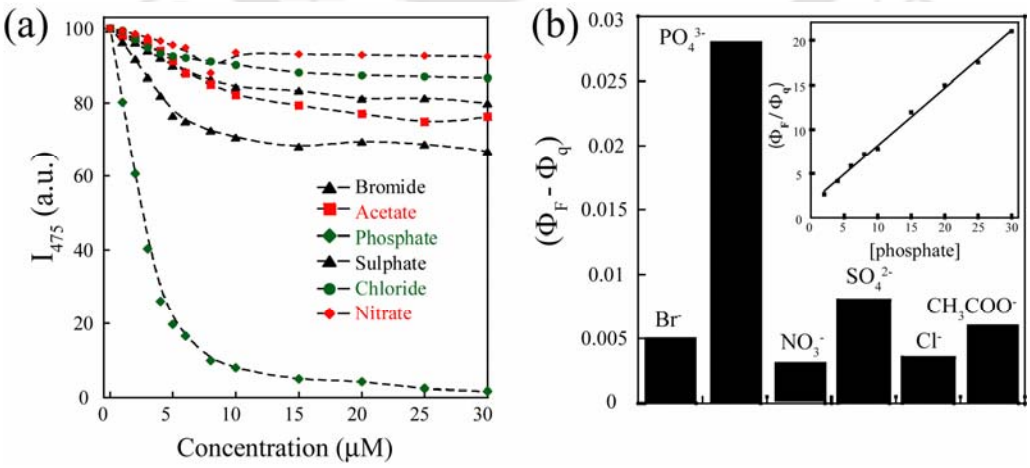

Figure 3.2.10. (a) Plot of the emission intensity (at 475 nm) of **L_3** as a function of concentration of anions; (b) Schematic representation showing the change of fluorescence quantum yield (ΦF-Φq) of **L_3** upon addition of the different acids. ΦF and Φq are quantum yields of **L_3** in absence and presence of guest, respectively. Inset: Stern–Volmer plot with sodium phosphate.

It is expected that N–H····PO_4^{3-} hydrogen bonding will takes place in solution. Two types of molecular interactions are possible in this mixture: (i) hydrogen bonding interactions between amine hydrogen and anion and (ii) electrostatic interaction of cationic protonated amine or quinoline group with anions. In the presence of H_3PO_4 both the interactions takes place in solution. Hence, addition of H_3PO_4 perturbs the monomer as well as excimer emission of ligand **L_3**. However, in the presence of Na_3PO_4, only electrostatic interaction is possible, which results in the selective perturbation of the excimer emission of **L_3** (Scheme 3.2.1). Interaction of the PO_4^{3-} with the **L_3** was further confirmed by ^{1}H NMR study (Figure 3.2.5.a and b). Broadening of the –NH signal in phosphate salt is observed compared to the pure **L_3**. On the other hand, selective large downfield shift (C8 $\Delta\delta$H=0.18, C6 $\Delta\delta$H=0.25, C4 $\Delta\delta$H=0.23, C7 $\Delta\delta$H=0.27, C5 $\Delta\delta$H=0.12, C3 $\Delta\delta$H=0.15) occurs in aromatic protons. Overall downfield shift has been confirmed to the formation of supramolecular host–guest complexes.

3.2.6. Summary

In conclusion, we have reported the design and synthesis of a new quinoline based tripodal fluorescent sensor. Ligand contains three different types of N-atoms with varying pKa values and hydrogen bond forming capabilities. An X-ray crystallographic study shows the 3D orientation of the aromatic ring on the same side resulting in the formation of bowl shape cavity for preferential binding of different type of anionic systems. This tripodal system is efficient phosphate sensor. The excimer emission has been used to confirm the selective recognition of phosphate ion. It combines three different types of N-donor with the elegant fluorescent signaling properties. Protonated form of phosphate is monomer as well as excimer quencher whereas unprotonated form is only excimer quencher. It shows the emission of intramolecular excimer in solution. This excimer emission is moderate and convenient for practical use to distinguish selectively phosphate ion from others anions present in the common biological systems. The excimers emission is also sensitive to the presence of acid in the solution.

Reference:

3.2.1 England, J.; Britovsek, G. J. P.; Rabadia, N.; White, A. J. P. *Inorg. Chem.,* **2007,** *46,* 3752.

3.2.2 Coakley, M. P. *Appl. Spectrosc.*, **1964**, *18*, 149.

3.2.3 Ghosh, K.; Adhikari, S. *Tetrahedron Lett.,* **2006**, *47*, 3577.

3.2.4 de Silva, A. P.; Gunaratne, H. Q. N.; McCoy, C. P. *Chem. Commun.,* **1996**, 2399.

3.2.5 Grynkiewicz, G.; Poenie, M.; Tsien, R. Y. *J. Biol. Chem.,* **1985**, *260*, 3440.

3.2.6 Mojtaba, S.; Javad, C. M. *J. Photochem. Photobiol. A.*, Chem., **2003**, *155*, 6.

PART - III

3.3 Multipoint solvent recognition within Napthyl based thiourea receptor

In this part of the thesis we have explored the solvent induced polymorphism of chiral *trans*-1,2-Bis-3-(naphthalen-1-yl)-thioureido cyclohexane (**L_4**) (Scheme 3.3.1).

The dipodal ligand **L_4** has been synthesized following literature procedure[3.3.1] using a mixture of 1-napthyl isothiocyanate (826 mL, 4.5 mmol) and *trans* cyclohexyl diamine (254 mg, 2.23 mmol) in dry $CHCl_3$ solvent under 15 hours starring condition (Figure 3.3.1). Then the mixture was allowed to cool to room temperature and was poured over hexane (25 mL), a white solid (0.917 g, 85%). Mp 139–142 ^{0}C; ^{1}H NMR (400 MHz, DMSO-d6): δ 9.67 (s, 2H, NH), 7.95 (δ, J=8.7 Hz, 2H), 7.90 (δ, J=7.5 Hz, 2H), 7.82 (δ, J=7.8 Hz, 2H), 7.65 (s, 2H, NH), 7.53 (m, 4H), 7.45 (m, 4H), 4.25 (m, 2H), 2.2 (m, 2H),1.65 (m, 2H), 1.25–1.21 (m, 4H); ^{13}C NMR (100 MHz, DMSO-d_6): δ 181.8,134.7,134.4, 130.1, 128.5, 126.9, 126.7, 126.6, 126.1, 125.4, 123.3, 57.9, 32.1, 25.5; EI-HRMS calcd for $C_{28}H_{28}N_4S_2$: 484.1755; found: 484.1757. We are unable to get single crystal of simple compound (**L_4**).

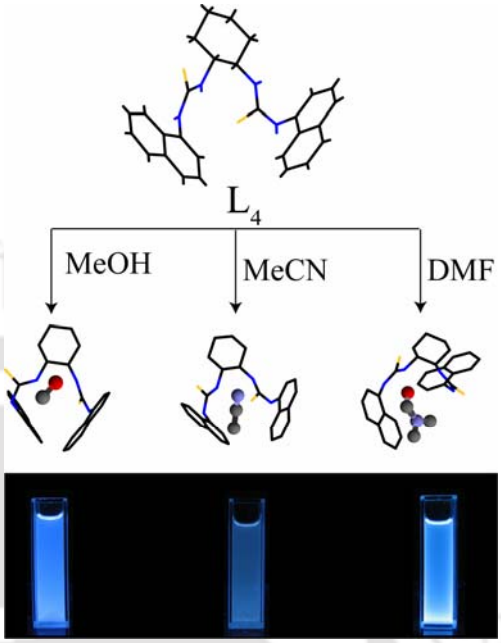

Scheme 3.3.1 Schematic representation of non-covalent interactions in solvated *trans*-1,2-Bis-(3-(naphthalen-1-yl) thioureido cyclohexane (**L_4**).

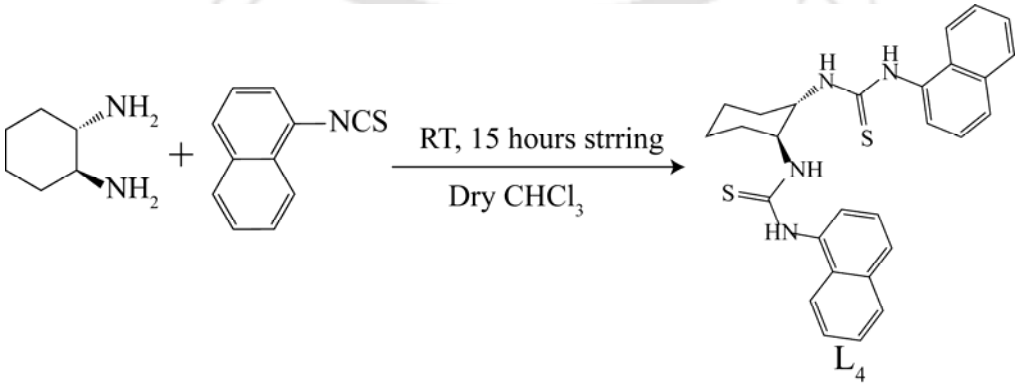

Figure 3.3.1. Synthetic procedure of dipodal dinapthyl bis thiourea ligands **L_4**.

3.3.1. Synthesis and characterization of different solvated *trans*-1,2-Bis-3-(naphthalen-1-yl)-thioureido cyclohexane (L_4) complexes

The compound was dissolved in methanol at 50 °C under agitation to get a saturated solution. Then, the solvent methanol was allowed to evaporate gradually by using a pierced film cover at 20 °C. Anal. Calcd (%) for $C_{29}H_{32}N_4OS_2$: C, 67.41; H, 6.24; N, 10.85 Found: C, 67.44; H, 6.22; N, 10.84%. Similarly the compound **L_4** was dissolved in MeCN at 50 °C under agitation to get a saturated solution. Single-crystals suitable for X-ray diffraction were obtained from slow evaporation after five days. Anal. Calcd (%) for $C_{30}H_{31}N_5S_2$: C, 68.54; H, 5.94; N, 13.33 Found: C, 68.56; H, 5.95; N, 13.35%. On the other hand **L** was dissolved in higher than the boiling point solvent like DMF at 120°C under agitation to get a saturated solution. Single-crystals suitable for X-ray diffraction were obtained from slow evaporation after fifteen days. Anal. Calcd (%) for $C_{31}H_{35}N_5OS_2$: C, 66.75; H, 6.33; N, 12.56 Found: C, 66.78; H, 6.34; N, 12.55%.

3.3.2. Crystal structure analysis

Solvent induced polymorph synthesis is facile for a host molecule with more flexibility or less rigidity. Urea/thiourea is well known building block for generating hydrogen bonded network in the solid-state.[3.3.2] Approaches involving crystallization of organic solvents with hydrogen bond donor and acceptor groups has been used to the formation of 1-, 2- and 3-D networks stabilized by several non covalent interactions. Since methanol solvent was found to be able to enter the crystal lattice via hydrogen bonding, therefore we have tried to crystallize **L_4** from MeOH. **L_4**•MeOH also crystallized in triclinic P-1 space group and asymmetric unit contain only one ligand and MeOH molecule (Figure 3.3.2a). Interestingly, compound **L_4** reorganizes in the solid-state to form a channel along *a* axis to accommodate solvent molecule (Figure 3.3.2b). Each of these channels is filled with discrete dimmer of MeOH molecules stacked in opposite orientation via C–H···O interactions (Figure 3.3.2c). Each dimmer is separated by 7.17 Å along *a* axis and 10.32 Å along *b* axis. The cavity dimension is 7.16 Å x 7.71 Å, which almost a square. MeOH molecule acts as a hydrogen bond acceptor as well as donor in the lattice. One of the NH attached to cyclohexyl unit form N-H···O type bonding with solvent. MeOH is also form O-H···S type hydrogen bond with neighboring thiourea unit. Adjacent thiourea unit form complementary N-H···S type hydrogen bond, which resulted in the formation of 1D hydrogen bonded chain along the diagonal of *bc* plane in the lattice. Two napthyl moieties in the pendant arm are oriented in the opposite direction with respect to the cyclohexyl unit. In crystal lattice neighbouring molecules are linked by thioamide···thioamide

hydrogen bonding forming a 1D chain along *c* axis (see appendix), which common to thiourea compound and its derivatives.[3.3.3, 3.3.4]

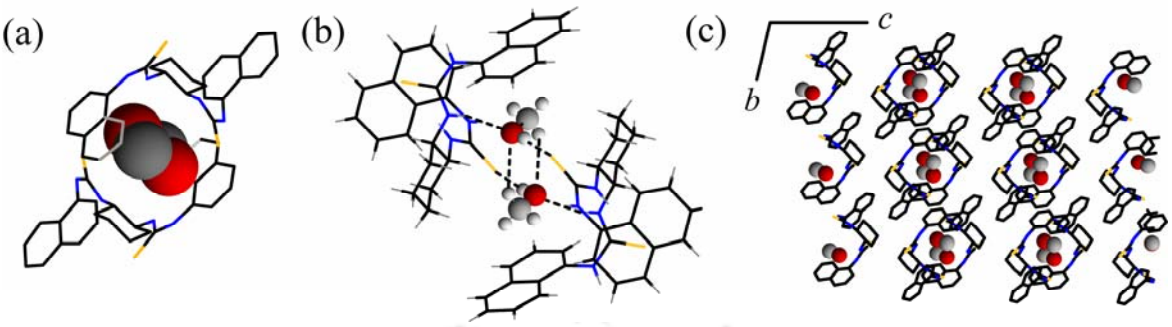

Figure 3.3.2. (a) Encapsulation of MeOH (b) Packing diagram highlighting the guest dimmer in the channel and (c) MeOH dimmer formation via C-H····O interaction.

Other supramolecular interaction like C-H····π, O-H····S type interactions are also present in the solid-state (see supporting information). Each thiourea unit has common *syn* and *anti* geometry. Both the *anti* conformation is having similar close to 180° dihedral angle. However, one of the *syn* N–H has dihedral angle very close to 0°, while other is little larger (6.87°). The dihedral angles of anti conformation are within the range. FT-IR spectrum of the crystal shows a broad band around 3300 cm^{-1}, which can be assigned to the O-H stretching vibrations of MeOH.

Similar observations have been found in acetonitrile solvated system as shown in Figure 3.3.3a. Similar to the MeOH solvate crystal, here also flexible compound **L_4** reorganizes to accommodate the solvent in the crystal lattice to accommodate the larger, linear MeCN unit in comparison to the previous crystal. 1D channel is running along *a* axis and each cavity along the channel contain a dimmer of solvent molecules, as observed in the case of

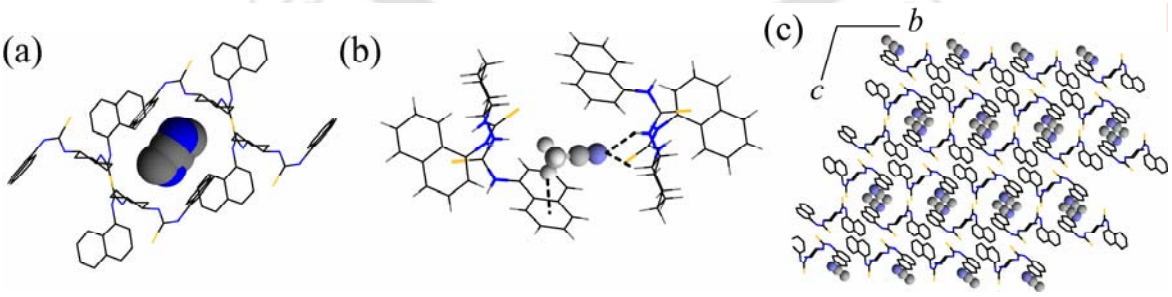

Figure 3.3.3. (a) Encapsulation of MeCN; (b) Perspective view highlighting the solvent dimmer in the cavities and (c) Non-covalent interaction associated with solvent in the lattice.

MeOH solvent (Figure 3.3.3b). It forms a rectangular cavity with dimension of 9.73 Å x 7.83 Å. The cavity size is larger than the MeOH solvate crystal to accommodate larger solvent, MeCN. Each of these solvent dimmer is separated by hydrophobic naphthalene

ring along c axis with a distance of 9.31 Å and along b axis they are separated by 12.95 Å by cyclohexyl unit. MeCN forms N-H····N, C-H····N and C-H····π type non- covalent interactions with the ligand (Figure 3.3.3c). However, in contrast to the MeOH crystal there is no such non-covalent interactions are observed between the solvent molecules. Similar to the previous two crystals only nitrogen atoms attached to the aromatic ring are involved in N–H····S hydrogen bonding interactions resulting in the formation of 1D chain. In the MeOH solvate crystal *syn* conformations more deviated than un-solvated crystal. FT-IR spectrum of the crystal shows the bands appearing at 2100 and 2356 cm^{-1}, which can be assigned to the C=N stretching frequencies of CH_3CN. In MeCN solvate crystal both the *syn* and *anti* N–H groups are within the normal range of dihedral angle (see appendix).

The switch from MeOH or MeCN to amide group containing solvent, DMF had a dramatic effect on the network structure (Figure 3.3.4a). Larger DMF molecule exists as a monomer in the crystal lattice, in contrast to the previous solvated crystal (Figure 3.3.5b). In the lattice it is included in a cylindrical cavity with a dimension of 9.58 Å x 7.96 Å. Along b axis the minimum distance between two DMF molecules is 8.38 Å and along c axis this distance is 8.61 Å. Similar to the previous crystals only nitrogen atoms attached to the aromatic ring (*syn* to C=S) are involved in N–H····S hydrogen bonding interactions resulting in the formation of 1D chain. In contrast to the previous all crystals, in DMF solvated crystal naphthalene unit forms C-H····S type bond with thiourea unit (see appendix). Each DMF molecule is stacked between two naphthalene rings in the solid-state and C=O group is pointed towards the thiourea unit (see appendix).

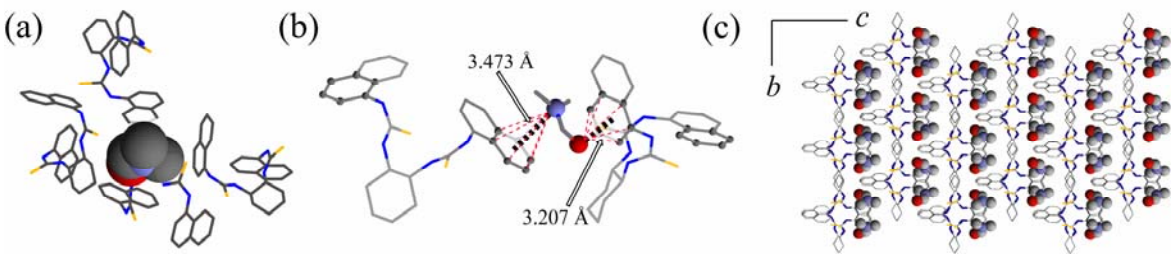

Figure 3.3.4. (a) ORTEP view of **L_4·DMF** with atom labelling scheme (hydrogen atoms are omitted for clarity); (b) Perspective views of **L_4·DMF** highlighting the guest molecules in the cavities and (c) Perspective views of the lone pair ···· π interaction in **L_4·DMF** via Olp····π and Nlp····π in DMF molecule.

This particular orientation of the DMF molecules helps in the formation of two rare type of non-covalent interactions viz. C=O····$\tilde{\pi}^{3.3.5}$ and lone pair (lp)····π $^{3.3.5,\ 3.3.6}$ (Figure 3.3.4c) interaction with the naphthalene unit in addition to the common N-H····O type hydrogen bonds (see appendix). FT-IR spectrum of crystal shows a lower C=O stretching frequency

at 1680 cm^{-1} than an unsubstituted C=O bond. Also, peaks at 1500, 1250, 1120 and 860 cm^{-1} are because of the partial double bond character, the rotation about the C-N bond. In this case, we have seen the more deformation of syn and anti conformation of the dihedral angle of S=C-N-H bonds than the previous systems. Comparisons of all the pseudopolymorph structures are presented in Figure 3.3.5. For easy comparison in the 3D conformation of the flexible ligand, all the solvent molecules are omitted and cyclohexyl unit is shown in the most stable chair conformation. Relative orientation of C=S groups in the pendent arms are largely differ in case of MeOH solvated system. However, relative orientation of the naphthalene units is similar in un-solvated ligand and MeCN solvated crystal. In other two solvated crystals these two aromatic rings are oriented in a different manner and large deviation is observed in DMF solvated crystal.

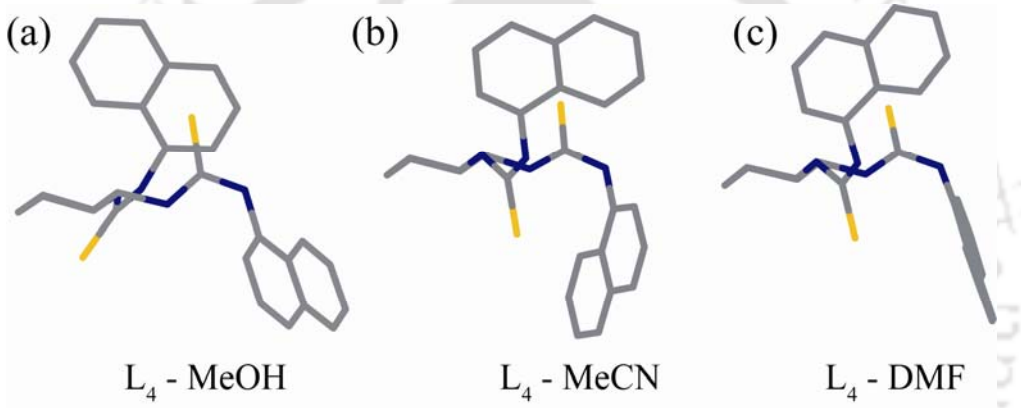

Figure 3.3.5. Comparison of conformation of ligand in different crystal form (solvent mocules are removed for clarity).

3.3.3. Crystal habit

Morphology of the crystal is another important manifestation for the quality of the final products besides the crystal structure. Regular-shaped crystals are generally more favourable over anomalistic ones in respect to the practical usability. Different crystallization parameters such as type of the solvent, the average levels of supersaturation and so on are important to obtain a desired crystal habit. Polarity of solvent is one of the most important properties that may affect the habit of the growing crystal.[3.3.7] Different solvent will have different types of non-covalent interactions in the crystal lattice with the receptor molecule, which will change the macroscopically crystal habit. Compound L is a polar molecule with active thiourea groups that can easily form intermolecular hydrogen bonds with solvent molecules, thus further affecting the habit of the crystals as shown in Figure 3.3.5. It shows rectangular habit when crystallized from MeOH, prismatic habit

when crystallized from MeCN and small sized crystals with a platelet-like habit from DMF. The relationship between the crystal structure and morphology and external crystallization conditions is complex. After heating the **L_4•MeOH** crystal at 130 ^oC for 2 hrs, crystalline nature got destroyed and resulted in the formation of powder bulk material (see appendix).

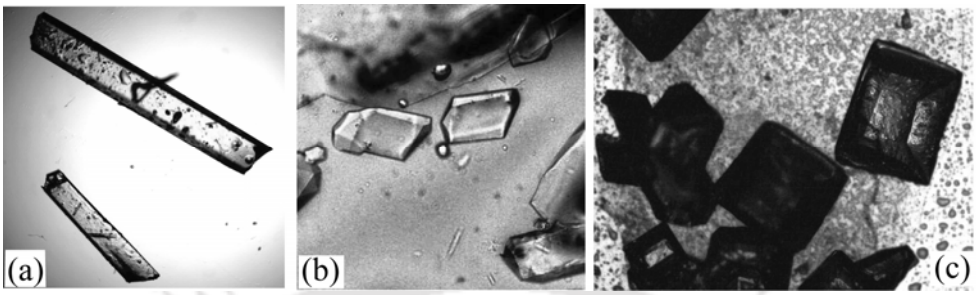

Figure 3.3.6. Optical micrograph of crystal (a**) L_4•MeOH,** (b) **L_4•MeCN** and (c) **L_4•DMF**.

3.3.4. Thermal analysis

The bis-thiourea compound (**L_4**) was crystallizes form different solvents. The DSC thermogram of the crystal without solvent was obviously different from the solvated systems as shown in Figure 3.3.7. In the simple ligand (**L_4**) one endothermic peak ~192 °C was observed. The peak around 192 ^oC was the melting peak of **L_4** with an onset temperature of 178 °C. The heat of melting was calculated to be 49.3 $kJ{\cdot}mol^{-1}$. However, in solvated systems two endothermic peaks were found on the DSC thermograms of the air dried samples. The peak at lower temperature, ~112 °C for **L_4•MeOH**, ~138 °C for **L_4•MeCN** and ~170 °C for **L_4•DMF**, was attributed to the desolvation process. These peaks are higher than the boiling point of the corresponding solvents, revealing that the solvents had intensive hydrogen bonding interaction with **L_4**. These observations are at par with the single crystal XRD studies also.

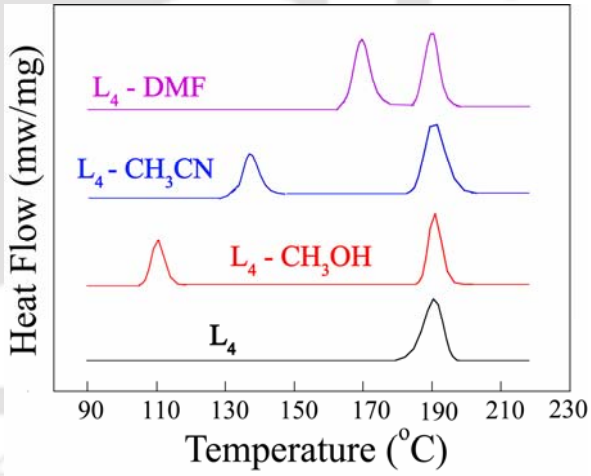

Figure 3.3.7. DSC thermograms of different solvated crystals.

3.3.5. Powder XRD analysis

The PXRD is an important tool to determine the crystalline nature in the bulk sample. As shown in Figure 3.3.8, the PXRD patterns of bis-thiourea compound (**L_4**) and solvated

crystals were completely different in the position and intensity of the diffraction peaks. These differences indicated different crystal structures of ligand **L_4** with the solvated crystals. Furthermore, these different PXRD patterns also implied that compound crystals might exhibit polymorphs or solvates. These differences in bulk crystalline properties are in agreement with the difference in their crystal structure.

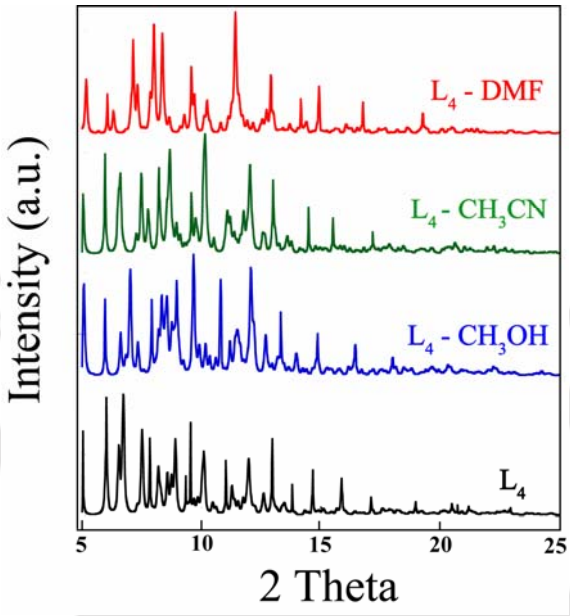

Figure 3.3.8. PXRD patterns of crystalline **L_4**, **L_4**•MeOH, **L_4**•MeCN and **L_4**•DMF.

3.3.6. Absorption spectroscopy

The ground state spectral properties of the bis-thiourea compound **L_4** was investigated by UV-vis spectrometer in MeOH at 25°C in a spectrometric cell of 1 cm path length from the range 250 to 500 nm. The UV-Vis spectrum of the ligand showed two absorption bands (Figure 3.3.9). The high intense band in the UV region (277 nm, ε =8900 M^{-1} cm^{-1}) may be assigned to the n→ π* transition and a relatively weak intense band at 320 nm (ε = 2675$M^{-1}cm^{-1}$) is due to π → π* transition.[3.3.8] These absorbance are all linear as a function of the concentration in methanol. However, it does not show sufficient solvatochromism.

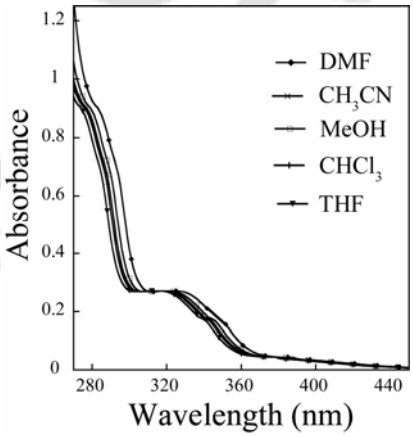

Figure 3.3.9 UV-visible spectra of the ligand **L_4** in different solvent.

In closer inspection we have noticed that, as the solvent polarity increases (or decreases), a hypsochromic (or bathochromic) shift of λ_{max} (~ 5 nm) is observed. A reasonable interpretation is that, upon excitation from the ground state to the electronic excited state,

electron density of the negative pole –C=S will be depressed due to the migration of electrons toward the positive pole (carbon atom of the thiourea group). Thus, the dipole moment of the molecule will be decreased after excitation. Therefore, as the solvent polarity increased, the energy depression of the ground state will be more than that of the excited state, and this causes a hypsochromic shift of the spectra.[3.3.9]

3.3.7. Fluorescence spectroscopy

There have been several experimental and theoretical studies on the solvatochromic behavior of thiourea derivatives.[3.3.10] The Bis thiourea compound (**L_4**) can form is stable adduct with solvent in solution too. The emission spectral character of compound (**L_4**) may be largely influenced by solvent polarities. To investigate the influence of solvent polarity on the excited state behaviour of the ligand, we have studied the steady state and lifetime emission spectra of **L_4** in solvents of different polarities. Steady state emission spectrum shows a monomer emission in between 387-410 nm when excitated at 320 nm with varying the solvent polarities (Figure 3.3.10a). With increasing the solvent polarity, a red shift has been observed in maximum emission wavelength. Moreover, enhancement of the solvent polarity causes a significant quenching the fluorescence spectra (Figure 3.3.10b). The quantum efficiency (Φ) of the ligand in different solvent follows the order of DMF (0.51)>CH_3CN (0.45)>MeOH (0.42)>$CHCl_3$ (0.37)>THF (0.27),[3.3.11] which may be attributed to the difference in the non-covalent interactions between solvents and the ligand **L_4** as supported by the crystal structure studies.

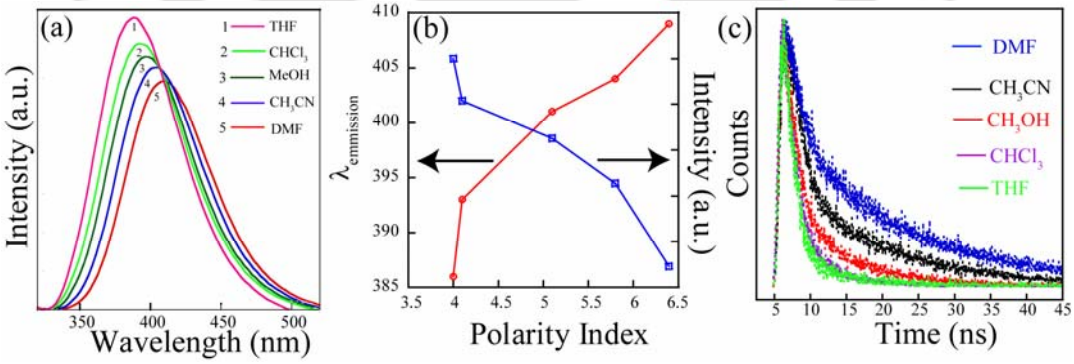

Figure 3.3.10 (a) Emission spectra of **L_4** in different solvents (λ_{ex} = 320 nm, 1.0 x 10^{-5} M, 298 K). (b) Plot of polarity index of different solvent versus fluorescence intensity and quantum yield of **L_4**; (c) Time-resolved fluorescence decay of **L_4** monitored at the corresponding emission maxima in different solvents.

A deeper understanding of the occurring phenomena in the excited state of the studied compounds demands the knowledge of its dynamic behavior in solution. Time-resolved fluorescence study was carried to investigate the effect of solvent polarity on emission

behavior of the ligand (Figure 3.3.10c). In all cases fluorescence decay was described by a linear combination of two exponential terms and positive pre-exponential factors (Table 3.3.1). It has been observed that both the lifetime (τ_1 and τ_2) value increases drastically with increasing the solvent polarity. Mean lifetime (τ_m) value spread over a range of 5.089 – 1.106 ns. It can be concluded the more polar solvent stabilize the excited as a result lifetime increases, which also supported by the solvent-ligand non-covalent interactions in the solid-state.

Table 3.3.1 Fluorescence lifetime parameters of $\mathbf{L_4}$ in different solvents**.**

Solvent	Polarity index	τ_1 (ns)	τ_2 (ns)	α_1	α_2	χ^2	τ_m ns)
DMF	6.4	0.27	6.70	0.0087	0.026	1.033	5.089
MeCN	5.8	0.36	5.07	0.0036	0.007	1.005	3.470
MeOH	5.1	0.24	2.88	0.0110	0.006	0.999	1.877
$CHCl_3$	4.1	0.11	1.44	0.0101	0.007	0.999	1.190
THF	4.0	0.12	1.73	0.0450	0.071	1.004	1.106

3.3.8. Summary

The flexible dithiourea compound shows pseudo polymorphism in the crystal lattice and it crystallized with varieties of solvent molecules. The crystal structure and morphology of the ligand are greatly influenced by the solvents used in the crystallization process. Flexible ligand reorganizes in the lattice to incorporate solvent molecules of different sizes. We observed the formation of N-H····S type of hydrogen bonds among the host molecules by syn N–H group in all cases. However, due to restricted disposition of the anti N–H group, it only forms weak interactions with the solvent molecules. In DMF solvate crystal we have encountered with lone pair (lp)····π interactions, which is uncommon non covalnet interaction in the literature. We have studied the solvent induced polymorphism in these crystals by optical microscopy, powder X–ray diffraction and thermal analysis. The ligand was appended with two naphthalene unit to check the solution phase non covalent interaction with different solvents using steady and time-resolved fluorescence spectroscopy. In steady state increase in the solvent polarity peak position is going 387-410 nm and more quenching takes place which is result to formation increases the nocovalent interactions. In time-resolved fluorescence spectra we have seen increase the solvent polarity increases the life time time of bis thiourea derivatives ($\mathbf{L_4}$) which is also supports the non covalent interaction with solvent molecules. Overall result is that, fluorescence quenching phenomenon revels the presence of various noncovalent interactions between the solvent and *bis*-thiourea derivative which have been observed in the solid-state. We are currently extending this result by preparing new thiourea based fluorescence receptors with novel structural and spectral properties.

References:

3.3.1 (a) Xie, H.; Yi, S.; Wu, S. *J. Chem. Soc., Perkin Trans. 2*, **1999**, 2751; (b) Costero, A. M.; Colera, M.; Gavina, P.; Gil, S.; Llaosa, U. *Tetrahedron,* **2008**, *64,* 7252.

3.3.2 Wang, W-H.; Xi, P-H.; Su, X-Y.; Lan, J-B.; Mao, Z-H.; You, J-S.; Xie, R-G. *Cryst. Growth Des.,* **2007**, *7*, 741.

3.3.3 Tobe, Y.; Sasaki, S.; Mizuno, M.; Hirose, K.; Naemura, K. *J. Org. Chem.,* **1998**, *63*, 7481.

3.3.4 Muthu, S.; Vittal, J. J.; *Cryst.Growth Des.,* **2004**, *4*, 1181.

3.3.5 Egli, M.; Sarkhel, S. *Acc. Chem. Res.,* **2007**, *40*, 197.

3.3.6 Mooibroek, T. J.; Gamez, P.; Reedijk, J.; *CrystEngComm.,* **2008**, *10*, 1501.

3.3.7 Srinivasan, K.; Sankaranarayanan, K.; Thangavelu, S. *J. Cryst. Growth,* **2000**, *212*, 246.

3.3.8 Kondo, S-I.; Sato, M. *Tetrahedron,* **2006**, *62*, 4844.

3.3.9 (a) Zhou, J. W.; Li, Y. T.; Tang, Y. W.; Song, X. Q. *J. Solution Chem.,* **1995**, *24,* 925; (b) Reichardt, C. *Solvents and Solvent Effect in Organic Chemistry,* 2nd Edition, VCH, Weinheim, **1988**.

3.3.10 (a) Brooker, L. G. S.; Keys, C. H.; Heseltine, D.W. *J. Am. Chem. Soc.,* **1951**, *73*, 5350; (b) C. Reichardt, *Chem. Rev.,* 1994, **94**, 2319.

3.3.11 (a) Nekipelovaand, T. D.; Shishkov, V. S.; *High Energy Chem.,* **2004**, *38,* 355; (b) Changa, C-C.; Chua, J-F.; Kuoa, H-H.; Kanga, C-C.; Lina, S-H.; Changa, T-C. *J. Lumin.,* **2006**, *119-120,* 84.

APPENDIX

3.1A. Synthesis and Characterization Salt 1, [$C_{36}H_{34}BrNO_3$]. To a magnetically stirred solution of L_1 (0.53 g, 1 mmol) in $CHCl_3$ (20 mL), was added methanolic solution of NH_4Br (0.095 g, 1 mmol) in portions. With the constant stirring the five hours a whitish-yellow precipitate that formed was filtered, washed with dry ether, and dried under vacuum. Yield: 0.563 g, 95% based on **L_1**. Single crystals suitable for X-ray diffraction were obtained from slow evaporation of C_2H_5OH-water (1:1) mixture solution of the compound at RT for seven days. Anal. Calcd (%) for $C_{36}H_{34}NO_3Br$: C, 71.14; H, 5.64; N, 2.30. Found: C, 71.19; H, 5.68; N, 2.32%.

3.2A Synthesis and Characterization Salt 2, [$C_{38}H_{40}ClNO_4$]. To a magnetically stirred solution of L_1 (0.53 g, 1 mmol) in $CHCl_3$ (20 mL), was added methanolic solution of NH_4Cl (0.055 g, 1 mmol) in portions. With the constant stirring the five hours a grayish precipitate that formed was filtered, washed with dry ether, and dried under vacuum. Yield: 0.534 g, 95% based on **L_1**. Single crystals suitable for X-ray diffraction were obtained from slow evaporation of C_2H_5OH-water (1:1) mixture solution of the compound at RT for seven days. Anal. Calcd (%) for $C_{38}H_{40}ClNO_4$: C, 74.84; H, 6.61; N, 2.29. Found: C, 74.85; H, 6.63; N, 2.28%.

3.3A. Synthesis and Characterization Salt 3, [$C_{36}H_{34}N_2O_6$]. To a magnetically stirred solution of L_1 (0.53 g, 1 mmol) in $CHCl_3$ (20 mL), was added methanolic solution of NH_4NO_3 (0.080 g, 1 mmol) in portions. With the constant stirring the five hours a whitish-yellow precipitate that formed was filtered, washed with dry ether, and dried under vacuum. Yield: 0.530 g, 90% based on **L_1**. Single crystals suitable for X-ray diffraction were obtained from slow evaporation of C_2H_5OH-water (1:1) mixture solution of the compound at RT for seven days. Anal. Calcd (%) for $C_{36}H_{34}N_2O_6$: C, 73.19; H, 5.80; N, 4.74. Found: C, 73.17; H, 583; N, 4.77%.

3.4A. Synthesis and Characterization Salt 4, [$C_{47}H_{40}Cl_3NO_{11}$]. To a magnetically stirred solution of **L_1** (0.53 g, 1 mmol) in $CHCl_3$ (20 mL), was added methanolic solution of pyrometallic acid (0.254 g, 1 mmol) in portions. With the constant stirring the five hours a whitish-yellow precipitate that formed was filtered, washed with dry ether, and dried under vacuum. Yield: 0.633 g, 85% based on **L_1**. Single crystals suitable for X-ray diffraction were obtained from slow evaporation of $CHCl_3$-C_2H_5OH (1:1) mixture solution of the compound at RT for seven days. Anal. Calcd (%) for $C_{47}H_{40}Cl_3NO_{11}$: C, 62.72; H, 4.48; N, 1.55. Found: C, 62.77; H,4.49; N, 1.53%.

3.5A. Synthesis and Characterization Salt 5, [$C_{38}H_{38}F_3NO_7$]. To a magnetically stirred solution of L_1 (0.53 g, 1 mmol) in $CHCl_3$ (20 mL), was added methanolic solution of trifluoro acetic acid (0.114 g, 1 mmol) in portions. With the constant stirring the five hours a whitish-yellow precipitate that formed was filtered, washed with dry ether, and dried under vacuum. Yield: 0.626 g, 95% based on **L_1**. Single crystals suitable for X-ray diffraction were obtained from slow evaporation of H_2O-C_2H_5OH (1:1) mixture solution of the compound at RT for seven days. Anal. Calcd (%) for $C_{38}H_{38}F_3NO_7$: C, 67.33; H, 5.65; N, 2.06. Found: C, 67.35; H,5.63; N, 2.03%.

Table 3.1A. Crystal Data and Structure Refinement for salt $\mathbf{L_1}$, Salt **1,** Salt **2,** Salt **3,** Salt **4,** and Salt **5.**

	Salt 1	Salt 2	Salt 3	Salt 4	Salt 5
Empirical formula	$C_{36}H_{34}BrNO_3$	$C_{38}H_{40}ClNO_4$	$C_{36}H_{34}N_2O_6$	$C_{47}H_{40}Cl_3NO_{11}$	$C_{78}H_{66}F_9N_2O_{13}$
Fw	608.55	610.16	590.6	901.15	1410.33
crystal system	Cubic	Triclinic	Cubic	Monoclinic	Hexagonal
space group	P2(1)3	P-1	P2(1)3	P2(1)/n	P6(3)
a, Å	14.3769(17)	11.526(3)	14.4685(5)	13.1145(6)	12.9469(4)
b, Å	14.3769(17)	11.805(3)	14.4685(5)	14.4685(5)	12.9469(4)
c, Å	14.3769(17)	14.313(6)	14.4685(5)	13.6777(7)	24.9484(12)
α, deg	90.00	112.108(10)	90.00	90.00	90.00
β, deg	90.00	108.979(10)	90.00	90.19(4)	90.00
γ, deg	90.00	96.360(7)	90.00	90.00	120.00
V, $Å^3$	2971.6(6)	1644.7(10)	3028.80(18)	4439.7(4)	3621.6(2)
Z	4	2	4	4	4
μ	1.420	0.150	0.088	0.271	0.088
F(000)	1264	596	1248	2255	1344
GOF(S)	0.829	1.058	1.002	1.071	0.957
R_{int}	0.093	0.0273	0.0650	0.0355	0.1164
final R indices	R1=0.0512	R1= 0.0603	R1= 0.0647	R1= 0.0556	R1= 0.0877
[I > 2σ(I)]	wR2= 0.1239	wR2= 0.2218	wR2= 0.0948	wR2= 0.0726	wR2= 0.1993
R indices (all data)	R1= 0.0930	R1= 0.0901	R1= 0.1658	R1= 0.1948	R1= 0.1186
	wR2= 0.1840	wR2= 0.2460	wR2= 0.1942	wR2= 0.2111	wR2= 0.2351

Table 3.2A. Selected Non-covalent interactions in complexes **1-5.**

Entry	D–H····A	H····A (Å)	D····A (Å)	∠D–H····A (°)
Complex **1**	C2-H2A····π	3.080	3.404	101.20
	C4-H4····π	3.572	4.443	157.02
	C9-H9····π	3.498	4.267	141.66
	C5-H5····O13	2.961	3.700	137.49
	C18-H18····O13	2.707	3.470	139.83
	C28-H28····O13	2.522	3.439	168.56
	C13-H13A····Cl1	2.731	3.529	139.92
	C13-H13B····Cl1	2.929	3.613	128.46

	C20-H20····Cl1	2.921	3.756	150.06
	C25-H25A····Cl1	2.823	3.594	137.01
	C37-H37A····Cl1	2.274	3.053	137.71
	C1-H1A····π	3.420	4.166	136.30
	C4-H4····π	3.572	4.443	157.02
	C9-H9····π	3.498	4.267	141.66
	C25-H25B····π	3.108	4.056	166.72
Complex **3**	C6-H6····O2	2.393	3.448	167.87
	C12-H12B····O2	2.547	3.380	145.50
	C11-H11B····π	3.227	3.461	92.39
	C10-H10····π	3.429	4.408	155.26
Complex **4**	C2-H2A····O10	2.614	3.266	124.83
	C13-H13A····O5	2.600	3.293	128.67
	C13-H13A····O7	2.572	3.432	147.85
	C25-H25A····O7	2.623	3.217	119.90
	C25-H25B····O11	2.592	3.244	124.74
	C28-H28····O4	2.468	3.377	165.91
	C32-H32····O7	2.654	3.239	121.43
	C18-H18····π	3.077	3.843	140.89
Complex **5**	N2-H····O1	2.502	2.809	121.03
	O5-H····O7	2.425	2.585	69.45
	C18-H18····π	2.489	3.721	156.23
	C4-H4B····π	3.338	3.972	127.37
	C18-H18····π	3.011	3.566	145.95

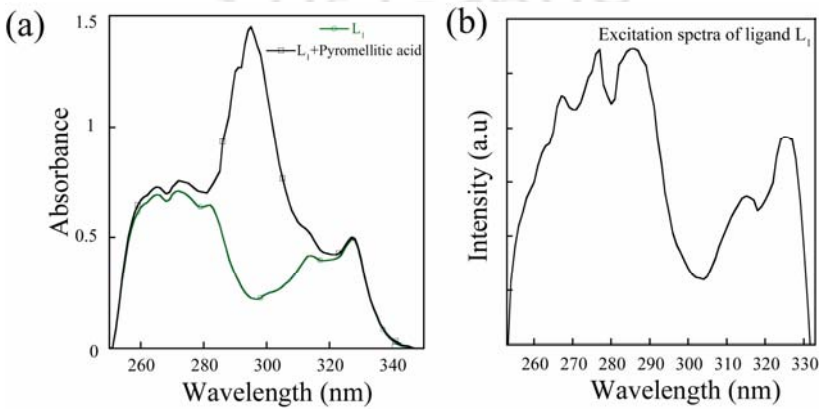

Figure 3.1A. (a) Absorption spectra of $\mathbf{L_1}$ in presence of pyromellitic acid; (b) Excitation spectra of $\mathbf{L_1}$ in THF solvent.

Table 3.3A. Fluorescence quantum yield of $\mathbf{L_1}$ with different anionic input.

Sr. No.	Anionic input	Φ_F	$\Phi_F - \Phi_q$
1	Nil	0.021	0.000
2	Br^-	0.013	0.008
3	Cl^-	0.016	0.005
4	F^-	0.020	0.001
5	NO_3^-	0.001	0.020
6	ClO_4^-	0.017	0.004
7	Pyromellitate	0.019	0.002
8	CF_3COO^-	0.015	0.006

Table 3.4A. Fluorescence quantum yield of $\mathbf{L_1}$ with different concentration of nitrate.

Sr. No.	$[NO_3^-]$ (M)	Φ_q	Φ_F/Φ_q
1	2×10^{-6}	0.0060	3.5000
2	4×10^{-6}	0.0031	6.7000
3	6×10^{-6}	0.0025	8.3000
4	8×10^{-6}	0.0018	11.700
5	10×10^{-6}	0.0016	13.000
6	12×10^{-6}	0.0013	16.000
7	14×10^{-6}	0.0011	18.900
8	16×10^{-6}	0.0010	21.000

Table 3.5A. Hydrogen bond distances and angels for $[(\mathbf{L_2}H^+)(Pic^-)]\subset PicH]$.

D–H····A	H····A (Å)	D····A (Å)	∠D–H····A (°)
C1-H1B····O4	2.465	3.413	165.63
C2-H2B····O10	2.563	3.251	127.95
C4-H4····O13	2.683	3.459	141.37
C13-H13B····O16	2.504	3.185	127.19
C13-H13B····O17	2.671	3.303	123.18
C25-H25A····O6	2.449	3.370	158.36
C25-H25B····O17	2.449	3.015	122.25
C26-H26B····O11	2.564	3.330	135.89
C28-H28····O15	2.432	3.340	165.52
C33-H33····O9	2.701	3.506	145.45
C1-H1A····π (Centroid[a])	3.408	3.855	141.62
C25-H25B····π (Centroid[b])	3.907	4.447	118.14
π (Centroid[c])····π (Centroid[d])		3.660	
π (Centroid[e])····π (Centroid[f])		3.615	

[a] Centroid of ring C6–C11, [b] Centroid of ring C18–C22, [c]Centroid of ring C16–C24, [d] Centroid of ring C43–C48, [e] Centroid of ring C27–C36, [f] Centroid of ring C37–C42.

Table 3.6A. Fluorescence quantum yield of $\mathbf{L_2}$ with different concentration of picric acid.

Sr. No.	[PicH] (μM)	Φ_q	Φ_F / Φ_q
1	2	0.10	2.210
2	4	0.067	3.430
3	6	0.051	4.500
4	8	0.039	5.950
5	10	0.034	6.700
6	12	0.027	8.510
7	14	0.025	9.380
8	16	0.021	10.80
9	18	0.019	12.11

Table 3.7A. Crystal Data and Structure Refinement for $[(\mathbf{L_2}H^+)(Pic^-)]\subset PicH]$, Complex $[\mathbf{L_2}AgNO_3]$ and $\mathbf{L_3}$.

Entry	Complex $[(\mathbf{L_2}H^+)(Pic)]\subset PicH]$	Complex $[\mathbf{L_2}AgNO_3]$	$\mathbf{L_3}$
Empirical formula	$C_{48}H_{39}N_7O_{17}$	$C_{36}H_{33}$ Ag N_2 O_6	C_{33} H_{33} N_7
Fw	985.86	697.51	527.66
crystal system	Triclinic	Monoclinic	Monoclinic
space group	P-1	P2(1)/c	P2(1)/c
a, Å	10.5087(3)	14.5290(3)	19.580(10)
b, Å	12.1588(4)	20.6889(4)	8.752(4)
c, Å	18.2172(6)	10.5802(2)	16.305(7)
α, deg	86.727(2)	90.00	90.00
β, deg	81.775(2)	92.3060(10)	92.72(3)
γ, deg	84.839(2)	90.00	90.00
V, Å^3	2292.08(13)	3177.72(11)	2791(2)
Z	2	4	4
μ	0.110	0.683	0.075
F(000)	1024	1432	1036
GOF(S)	0.829	1.038	0.955
R_{int}	0.0325	0.0734	0.0467
final R indices	R1=0.0532	R1= 0.0548	R1= 0.0521
$[I > 2\sigma(I)]$	wR2= 0.1847	wR2= 0.1600	wR2= 0.1277
R indices (all data)	R1= 0.0884	R1= 0.1002	R1= 0.0967
	wR2= 0.2377	wR2= 0.1796	wR2= 0.1741

Table 3.8A. Fluorescence quantum yield of $\mathbf{L_2}$ with different aromatic guests.

Sr. No.	Guest input	Φ_F	$\Phi_F - \Phi_q$
1	Nil	0.230	0.000
2	Trimesic acid	0.095	0.135
3	Trimesic acid Trimethyl ester	0.102	0.128
4	Picric acid	0.019	0.211
5	*p*-Nitro aniline	0.187	0.043
6	*p*-Nitro benzoic acid	0.162	0.068
7	*p*-Nitro toluene	0.210	0.020
8	*p*-Nitro phenol	0.174	0.056
9	Nitrobenzene	0.190	0.040
10	Pyromellitic acid	0.081	0.149
11	Pyromellitic dianhydride	0.090	0.140

Table 3.9A. Selected bond distances and angels for complex **Ag(I)-$\mathbf{L_2}$**.

Ag1 O4 2.251(4)	Ag1 N2 2.8341	Ag1 N1 2.298(3)
O4 Ag1 N1 174.22(14)	C13 N1 Ag1 110.4(2)	N2 O4 Ag1 105.9(4)
C25 N1 Ag1 111.5(3)	C1 N1 Ag1 108.5(2)	
C25-H••••π , 3.896̧ Å,	C1-H••••π , 3.415̧ Å	C13-H••••π , 3.598̧ Å
C36-H••••O6, 3̃.329̧ Å		C36-H••••N2, 3̃.511Å

Table 3.10A. Fluorescence quantum yield of $\mathbf{L_2}$ with different anionic input.

Sr. No.	Anionic input	Φ_F	$\Phi_F - \Phi_q$
1	Nil	0.021	0.000
2	Na^{1+}	0.015	0.005
3	K^{1+}	0.014	0.006
4	Ca^{2+}	0.013	0.005
5	Mg^{2+}	0.012	0.006
6	Mn^{2+}	0.011	0.007
7	Co^{2+}	0.010	0.008
8	Ni^{2+}	0.009	0.009
9	Cu^{2+}	0.007	0.010
10	Zn^{2+}	0.005	0.012
11	Cd^{2+}	0.006	0.011
12	Hg^{2+}	0.008	0.009
13	Pb^{2+}	0.007	0.008
14	Ag^{1+}	0.001	0.048

Table 3.11A. Fluorescence quantum yield of $\mathbf{L_2}$ with different concentration of silver nitrate.

Sr. No.	$[AgNO_3]$ (M)	Φ_q	Φ_F/Φ_q
1	2×10^{-6}	0.0080	2.6000
2	4×10^{-6}	0.0060	5.2000
3	6×10^{-6}	0.0040	7.8000
4	8×10^{-6}	0.0025	10.400
5	10×10^{-6}	0.0020	13.000
6	12×10^{-6}	0.0015	15.400
7	14×10^{-6}	0.0012	18.000
8	16×10^{-6}	0.0011	21.600

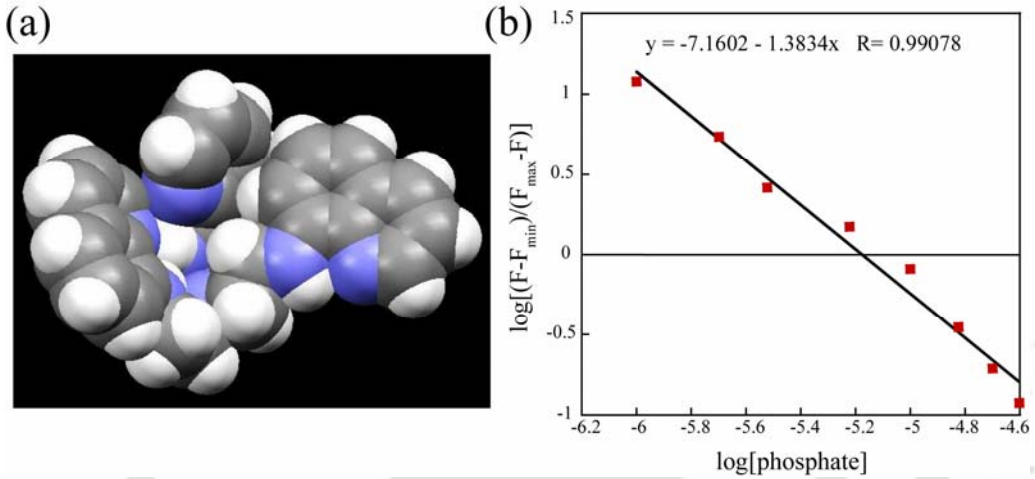

Figure 3.2A. (a) Formation of open bowl shape cavity in the solid-state; (b) Determination dissociation constant (K_d). The apparent K_d is at the X intercept, at a value of –5.17. The inverse log of this is 6.76 μM.

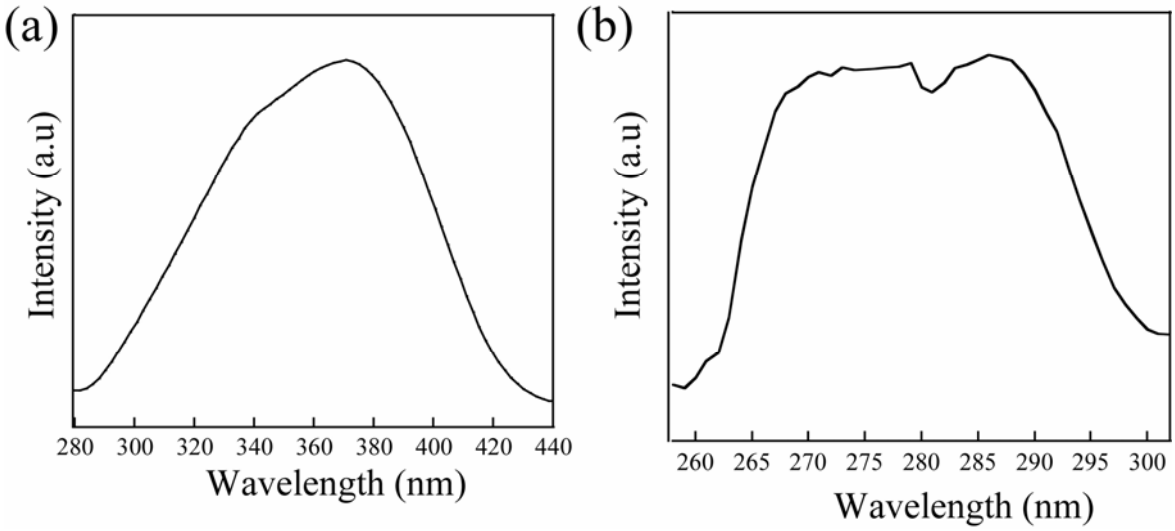

Figure 3.3A. (a) Excitation spectra of $\mathbf{L_3}$ monitored at 475 nm at 298 K; (b) Excitation spectra of $\mathbf{L_1}$ monitored at 310 nm 298 K.

Table 3.12A. Selected non-bonded distances in **L_3**.

C19–H19·····π^a 3.186 C13–H13A·····π^b 3.775 C23–H23A·····π^b 2.711

[a] Centroid of C7-C11; [b] Centroid of C18-C22; [c] Centroid of C7-C11;

Table 3.13A. Fluorescence quantum yield of **L_3** with different anionic input.

Sr. No.	Guest input	Φ_F	$\Phi_F - \Phi_q$
1	Nil	0.021	0.000
2	Nitrate	0.018	0.003
3	Chloride	0.017	0.004
4	Bromide	0.016	0.005
5	Acetate	0.015	0.006
6	Sulphate	0.013	0.008
7	Phosphate	0.001	0.028

Table 3.14A. Fluorescence quantum yield of **L_3** with different concentration of phosphate.

Sr. No.	$[PO_4^{3-}]$ (M)	Φ_q	Φ_F/Φ_q
1	2×10^{-6}	0.0080	2.6250
2	4×10^{-6}	0.0051	4.1390
3	6×10^{-6}	0.0036	5.8720
4	8×10^{-6}	0.0029	7.2210
5	10×10^{-6}	0.0027	7.8130
6	15×10^{-6}	0.0018	11.952
7	20×10^{-6}	0.0014	14.991
8	25×10^{-6}	0.0012	17.523
9	30×10^{-6}	0.0010	21.000

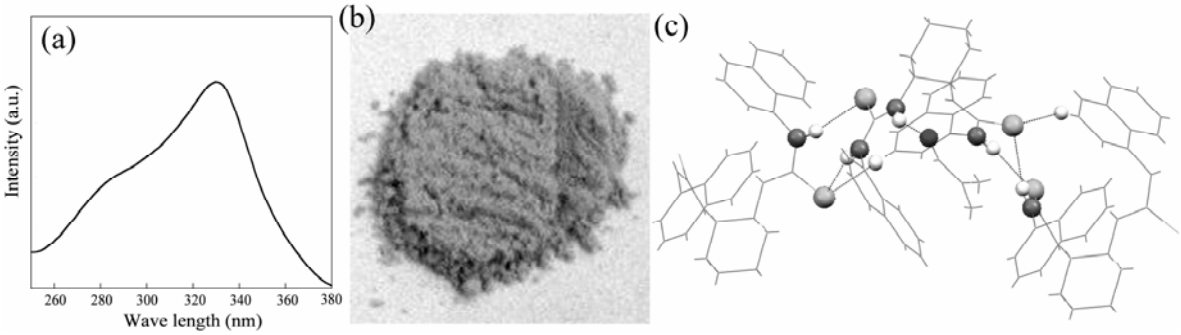

Figure 3.4A. (a) Excitation spectra of compound **L_4**;(b) Optical microscopy picture of heated **L_4**•MeOH crystal ;(c) Perspective views 2D sheet structure in **L_4**• DMF via N-H····S, N-H····O and C-H····S interactions.

Table 3.15 A. Crystal Data and Structure Refinement for **L_4.**CH_3OH, **L_4.**CH_3CN**,** and **L_4.** DMF**.**

	L_4.CH_3OH	**L_4.**CH_3CN	**L_4.** DMF
Empirical formula	$C_{29}H_{32}N_4OS_2$	$C_{30}H_{31}N_5S_2$	$C_{31}H_{35}N_5OS_2$
Fw	516.73	525.74	557.78
crystal system	Triclinic	Triclinic	Orthorhombic
space group	P-1	P-1	Pna2(1)
a, Å	10.9902(7)	10.9411(3)	14.333(2)
b, Å	11.1720(7)	11.3284(3)	10.7574(18)
c, Å	12.7825(9)	13.9479(7)	19.502(3)
α, deg	89.024(4)	111.849(3)	90.00
β, deg	75.506(4)	94.689(3)	90.00
γ, deg	65.624(5)	112.682(2)	90.00
V, $Å^3$	1377.43(16)	1428.36(9)	3006.9(8)
Z	2	2	4
μ	0.223	0.215	0.208
F(000)	548	532	1184
GOF(S)	1.023	1.039	0.971
R_{int}	0.0398	0.0418	0.1072
final R indices	R1=0.0531	R1= 0.0489	R1= 0.0424
[I > 2σ(I)]	wR2= 0.1349	wR2= 0.0557	wR2= 0.0662
R indices (all data)	R1= 0.0852	R1= 0.0864	R1= 0.0577
	wR2= 0.1526	wR2= 0.0623	wR2= 0.0903

Table 3.16A Non-covalent interactions in **L_4**•MeOH**,** **L_4**•**MeCN and **L_4**•**DMF.

D–H···A(Å)	H···A (Å)	D···A (Å)	D–H···A (◦)
L_4•MeOH			
N1–H····S1	2.618	3.336	141.62
N3–H····S2	2.602	3.457	173.31
N4–H····O1	2.144	2.890	144.84
O1–H····S1	2.570	3.372	166.11
C29–H····O1	2.704	3.375	166.11
C4–H····π_c	3.383	3.566	143.27

L_4•MeCN			
N3–H····N5	2.409	3.163	146.62
C16–H····N5	2.705	3.500	139.07
N1–H····S1	3.147	3.367	145.95
N4–H····S2	2.663	3.514	170.26
C4–H····π_c	2.562	3.328	140.00
C29–H····π_c	2.861	3.716	148.75
C8–H····π_c	3.062	3.894	149.80
C21–H····π_c	2.749	3.523	141.35
C20–H····π_c	3.109	3.883	141.83
L_4•DMF			
N2–H····O1	2.045	2.844	153.14
N1–H····S2	2.645	3.482	164.32
N2–H····O1	2.513	3.374	166.63
C21–H····S2	2.914	3.789	159.46
C29–H····S1	2.893	3.851	177.70
C22–H····π_c	3.499	4.248	139.25
π_c···· N5(lp)	3.669		
π_c····$\pi_{C=O}$	3.265		

Table 3.16A Quantum yield of Bis-thiourea compound (**L_4**) in different solvent.

Sr. No.	Solvent	Φ_F
1	THF	0.51
2	$CHCl_3$	0.45
3	MeOH	0.42
4	MeCN	0.37
5	DMF	0.27

Chapter 4

2-ARYL AZO IMIDAZOLE DYES – MOLECULAR RECOGNITION AND SELF-ASSEMBLY

4.1. Synthetic application of dyes and Scope of the work

Azo-dyes are widely used in analytical chemistry and dyestuff industry,[4.1] while textile mills predominantly use them, azo dyes can also be found in the food[4.2] pharmaceutical, paper and printing, leather, and cosmetics industries. We were interested in exploring derivatives of azo-chromophore with imidazole as the heterocyclic component belong to class of organic ligand that contain four nitrogen atoms coupled in conjugated system of π-bonds.[4.3] The presence of -N=N- group can lead to stabilize low valent metal oxidation state due to their π acidity and presence of low lying azo-centered π*-molecular orbitals.[4.4] Azo function is photochromic,[4.5] redox acive,[4.6] pH responsive[4.7] and their complexes act as a molecular switch.[4.8] The aryl azo containing imidazolium salts make different type of ionic liquids. Ionic liquids may serve as a new generation of solvents for organic reactions, and have received much attention.[4.9] Liquid crystals of imidazolium salts comprise an important component of this new solvent system.[4.10] The lyotropic properties of these neat ionic liquid crystals may provide an, alternative solvent system having a partially ordered environment.[4.11] These liquid crystals display excellent film forming properties which allows them to be studied as LB films.[4.12] Imidazolium salts are also known to be excellent precursors in the synthesis of metal–carbene complexes,[4.13] which are superior catalysts in many chemical reactions compared to metal–phosphine complexes.[4.14] The strong metal–carbene carbon bonds also make them good candidates in the design of organometallic materials.[4.15]

Supramolecular architectures assembled from various delicate noncovalent interactions such as hydrogen bonds, π···π stacking, C-H···π and electrostatic interactions, *etc*., have attracted intense interest in recent years because of their wide applications for catalysis, material and life sciences.[4.16, 4.17] Especially, the application of intermolecular hydrogen bonds is a well-known and efficient tool in the field of organic crystal designing because of its strength and directional properties.[4.18] Strong classical hydrogen bonds, such as O-H····N and O-H····O, are ideal to rationalize and systemize the relationship between hydrogen bond acceptor and donor molecules. Currently, H-bonding interactions have been widely used as one of the principal means to control such molecular assemblies during crystallization and thereby to engineer the structures of crystals.[4.19] Over the last several decades, although considerable effort has been devoted to the investigation of the relationships between component structure and resulting H-bonded crystal structure, it still remains difficult to predict how a particular molecule will pack in the crystal by such interactions.[4.20] Thus more studies are still required to further understand such systems. The hydrogen bond between different anions and heterocyclic nitrogen atoms has been

proved to be a useful and powerful organizing force and was utilized for the formation of supramolecules. Imidazole and its derivatives are ubiquitous in biological and biochemical structure and function and thus posses a special attention in the construction of some interesting salt and their dimensional frameworks in recent years.[4.21] On the other hand, the role of anions in the supramolecular chemistry is of great interest because of its application in ion pair recognition and especially to anion exchange.[4.22] Designing of receptors capable of anion binding by hydrogen bonds continues to be an area of active research. In contrast to many possible hydrogen bond donors, the imidazole ring does not contain a built-in hydrogen bond acceptor and this unique feature makes the imidazole moiety an attractive motif in anion recognition [4.23] It is also conceivable that great efforts have been directed to the development of organic molecular crystals containing a variety of imidazole architectures.[4.24]

Our interest lies in the design azo compounds containing heterocyclic system. We have used a ligand incorporating the phenylazo group in the imidazole heterocycle (Scheme 4.1) known as 2-(phenylazo)-imidazole (**L_5-L_{11}**). The unhindered ligand has two different N-donor metal coordination sites along with an efficient hydrogen bond donor site.

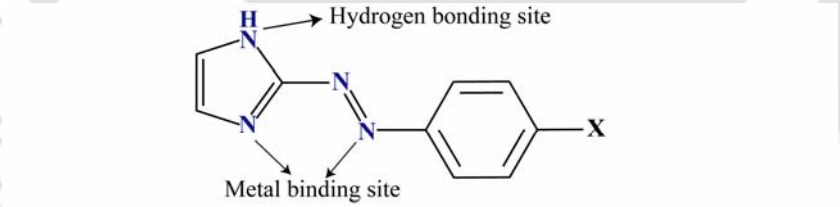

X = -H (L_5), -Me (L_6), -OMe (L_7), -Cl (L_8),-Br (L_9), -I (L_{10}) and -Ar =Nap (L_{11})

Scheme 4.1 2-aryl azo imidazole dyes (**L_5 – L_{11}**).

In the present thesis work, we chose to investigate a series of imiazole containing diazonium compounds [X = Br (**L_9**), X = I (**L_{10}**) and **L_{11}**] and their corresponding salts with different various anions (Scheme 1). We have focused on the aryl azo dye assisted recognition of anion/anion-water through molecular self-assembly. We have paid much attention on effect of counter anions like ClO_4^- (tetrahedral), NO_3^- (planner), and SCN^- (linear) upon the formation of supramolecular architectures with aryl azo imidazolium as a building blocks (Scheme 4.2). The main interest lies in the role of the topology of the anions upon formation of interesting supramolecular architectures. We have also investigated the solution phase interaction between aryl azo systems with different anion by monitoring their absorption and fluorescent spectral properties.

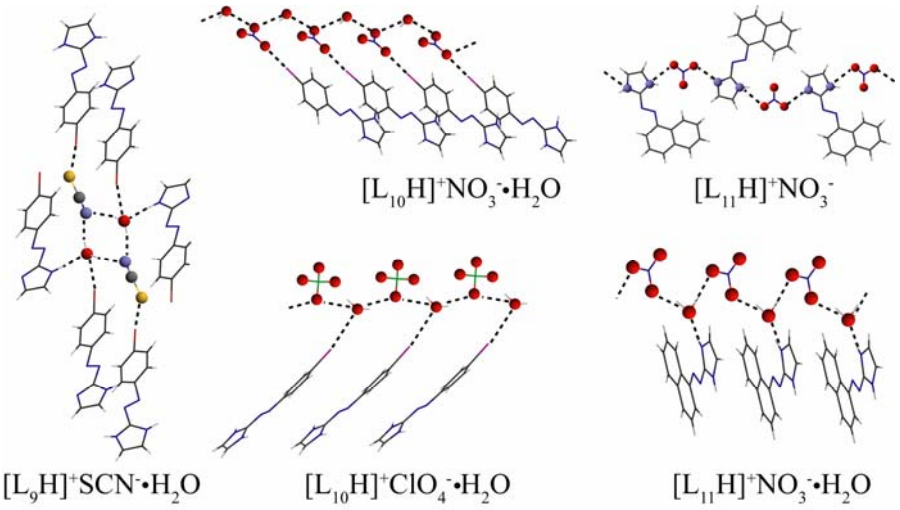

Scheme 4.2 Aryl azo imidazole dyes – Recognition of anion/anion-water through molecular assembly.

4.2. Experimental Section

The Chemicals used were of reagent grade. The sources of the chemicals and solvents have been mentioned in Chapter 2. Details of all the equipment used for the physico-chemical studies have been summarized in Chapter 2.

4.2.1. *p*-substituted 2-(phenylazo) imidazole ligands (**L_{5-11}**) were synthesized following literature method.[4.25]

4.2.2. Characterization of newly synthesized ligands **L_{10}**: The ligand **L_{10}** is synthesized newly. Dark purple solid, Yield, 95%, mp 202°C, Anal. Calc. for $C_9H_7N_4I$: C, 36.24; H, 2.36; N, 18.79. Found: C, 36.28; H, 2.32; N, 18.75%. ^{1}H-NMR ($CDCl_3$; 400 MHz): δH = 7.84 (2H d, J_1=9.6 Hz ArH), 7.64 (4H d, J_1=8.8 Hz ArH), 9.9 (1H s, N-H); (Figure 4.1a), ^{13}C NMR ($CDCl_3$; 400 MHz): δH = 152.3, 149.3, 140.3, 126.6, 122.5 and 104.8 (ArC); (Figure 4.1b), MS (+EI): *m*/z 298.96 (M^+), (Figure 4.2).

4.2.3. General synthesis of aryl azo imiazolium salts. To a magnetically stirred solution of the aryl azo lignad (1 mmol) in EtOH (20 mL), was added aqueous ammonium salt (1 mmol) in portions over a period of 1-2 hrs. Additional stirring for five hours a solid precipitate was formed which was then filtered, washed with ether, and dried under vacuum.

4.2.4. Synthesis and Characterization Salt 1, [$C_{19}H_{17}Br_2N_9OS$]. To a magnetically stirred solution of **L_9** (0.589.96 g, 2 mmol) in EtOH (20 mL), was added aqueous NH_4SCN (0.076, 1 mmol) in portions. With the constant stirring the five hours a greenish-yellow precipitate that formed was filtered, washed with EtOH, and dried under vacuum.

Greenish-yellow precipitate; Yield: 0.55 g, 95% based on **L_9**. Single crystals suitable for X-ray diffraction were obtained from slow evaporation of CH_3OH-water (1:1) mixture solution of the compound at RT for seven days. IR (KBr disk) (cm^{-1}); ν(SCN), 2190 (s), 2140, ν(O-H), 3590 (m), 3535 (m), ν(C=N), 1593 (m), ν(N=N), 1398 (m), ν(C=S), 685 (m). Anal. Calcd (%) for $C_{19}H_{17}Br_2N_9OS$: C, 39.51; H, 2.96; N, 21.84. Found: C, 39.53; H, 2.95; N, 21.86%.

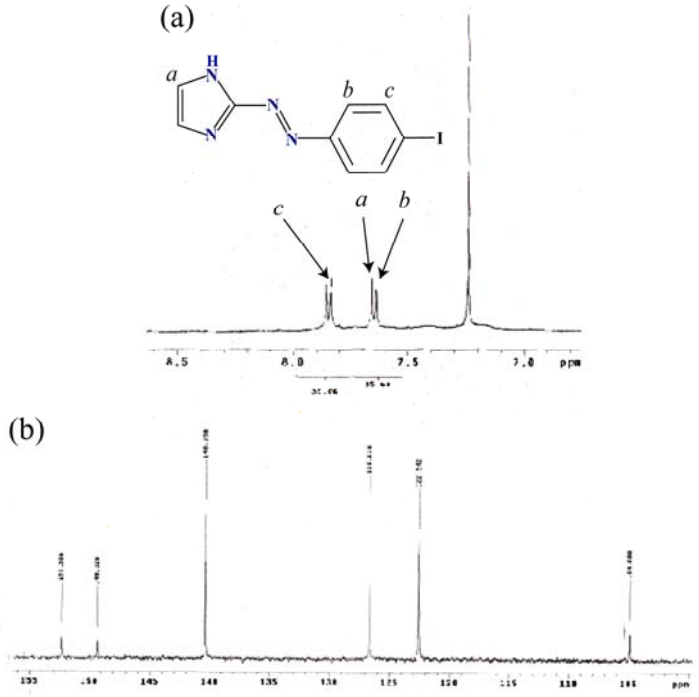

Figure 4.1. (a) ^{1}H NMR spectra of **L_{10}** in $CDCl_3$ and (b) ^{13}C NMR spectra of the ligand in $CDCl_3$.

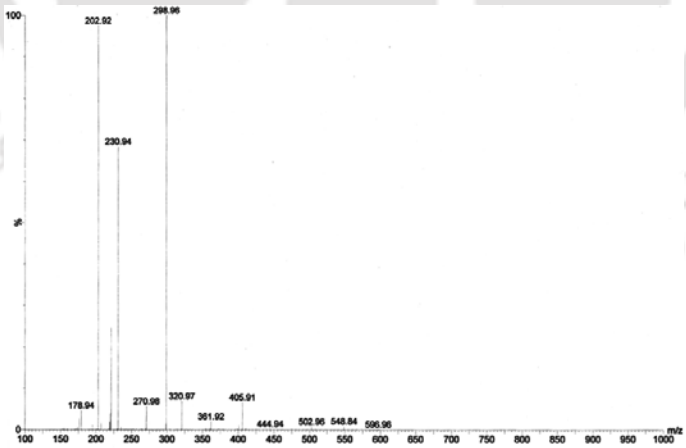

Figure 4.2. ESI-MS spectra of ligand **L_{10}**.

4.2.5. Synthesis and Characterization Salt 2, [$C_9H_{10}N_5O_4I$]. To a magnetically stirred solution of **L_{10}** (0.297 g, 1 mmol) in EtOH (20 mL), was added aqueous NH_4NO_3 (0.080, 1 mmol) in portions. With the constant stirring the three hours a pink-yellow precipitate that formed was filtered, washed with EtOH, and dried under vacuum. Reddish-yellow precipitate; Yield: 0.311 g, 85% based on **L_{10}**. Single-crystals suitable for X-ray

diffraction were obtained from slow evaporation of a CH_3OH-water (1:1) mixture solution of the compound at RT for ten days. Anal. Calcd (%) for $C_9H_{10}N_5O_4I$: C, 28.49; H, 2.65; N, 18.47. Found: C, 28.48; H, 2.66; N, 21.49%. IR (KBr disk) (cm^{-1}); ν(N=O), 1497 (s), ν(N-O), 1271 (m), ν(ONO), 992, ν(O-H), 3592 (m), 3531 (m), ν(C=N), 1600 (m), ν(N=N), 1406 (m).

4.2.6. Synthesis and Characterization Salt 3, [$C_9H_{10}N_4O_5ICl$]. To a magnetically stirred solution of **L_{10}** (0.297 g, 1 mmol) in EtOH (20 mL), was added aqueous NH_4ClO_4 (0.117, 1 mmol) in portions. With the constant stirring the three hours a crimson-red precipitate that formed was filtered, washed with EtOH, and dried under vacuum. **C**rimson-red precipitate; Yield: 0.37 g, 90% based on **L_{10}**. Single-crystals suitable for X-ray diffraction were obtained from slow evaporation of a CH_3OH-water (1:1) mixture solution of the compound at RT for fifteen days. Anal. Calcd (%) for $C_9H_{10}N_4O_5ICl$: C, 25.96; H, 2.42; N, 13.46. Found: C, 25.98; H, 2.44; N, 13.45%. IR (KBr disk) (cm^{-1}); ν(Cl-O), 1100 (m), 625(m), ν(O-H), 3588(m), 3537 (m) , ν(C=N), 1600 (m) ; ν((N=N), 1406 (m).

4.2.7. Synthesis and Characterization Salt 4, [$C_{13}H_{11}N_5O_3$]. To a magnetically stirred solution of **L_{11}** (0.186 g, 1 mmol) in EtOH (20 mL), was added aqueous NH_4NO_3 (0.080, 1 mmol) in portions. With the constant stirring the three hours a rosy-red precipitate that formed was filtered, washed with EtOH, and dried under vacuum. Rosy-red precipitate; Yield: 0.228 g, 80% based on **L_{11}**. Single-crystals suitable for X-ray diffraction were obtained from slow evaporation of a CH_3CN solution of the compound at RT for ten days. Anal. Calcd (%) for $C_{13}H_{11}N_5O_3$: C, 54.72; H, 3.88; N, 24.55. Found: C, 54.74; H, 3.87; N, 24.56%. IR (KBr disk) (cm^{-1}); ν(N=O), 1497 (s), ν(N-O), 1271 (m), ν(ONO), 992, ν(C=N), 1600 (m),ν(N=N), 1406 (m).

4.2.8. Synthesis and Characterization Salt 5, [$C_{20}H_{23}N_9O_4$]. To a magnetically stirred solution of **L_{11}** (0.372 g, 2 mmol) in EtOH (20 mL), was added aqueous NH_4NO_3 (0.080, 1 mmol) in portions. With the constant stirring the three hours a reddish-brown precipitate that formed was filtered, washed with EtOH, and dried under vacuum. Reddish-brown precipitate; Yield: 0.358 g, 85% based on the ligand **L_{11}**. Single-crystals suitable for X-ray diffraction were obtained from slow evaporation of a CH_3OH-water (1:1) mixture solution of the compound at RT for fifteen days. Anal. Calcd (%) for $C_{20}H_{23}N_9O_4$: C, 52.95; H, 5.11; N, 27.80. Found: C, 52.94; H, 5.13; N, 27.82%. IR (KBr disk) (cm^{-1}); ν(N=O), 1497

(s), ν(N-O), 1271 (m), ν(ONO), 992, ν(O-H), 3595 (m), 3539 (m), ν(C=N), 1600 (m), ν(N=N), 1406 (m).

4.3 Results and Discussion

4.3.1. Crystal Structure Studies

Shape of the anions of same charge as well as the presence of solvent molecules in the crystal can reorganize the packing of the host molecule and thereby facilitating, the inclusion of guest molecules.[4.26] Various types of strong as well as weak hydrogen bonds help the host molecules to reorient themselves in order to accommodate the solvent and guest and hence facilitate the formation of different types of supramolecular interactions.[4.27] The crystal structure analyses reveal that five salt crystals belong to the lower-symmetry monoclinic crystal systems (Table 4.1A). Salts **1**-**5** are all formed from aryl azo imidazole cations and inorganic anions with a variety of noncovalent interactions including hydrogen bonding, aryl stacking, and halogen bonding. These structures significantly differ, however, in packing modes of cation and anions in salts. Salt **1**,$[(\mathbf{L_9})_2H]^+[SCN]^-\bullet H_2O$ is crystallized in H_2O with thiocyanate (SCN^-**)** to yield a hydrated salt **1**, which has a 3D strong H-bonded supramolecular framework. ORTEP plot of salt **1** is shown in Figure 4.3a along with the atom numbering scheme. In the asymmetric unit one of the dye molecules is in protonated form. Protonated imidazolium cation subsequently forms salt co-crystal with linear thiocyanate (SCN^-) anion.

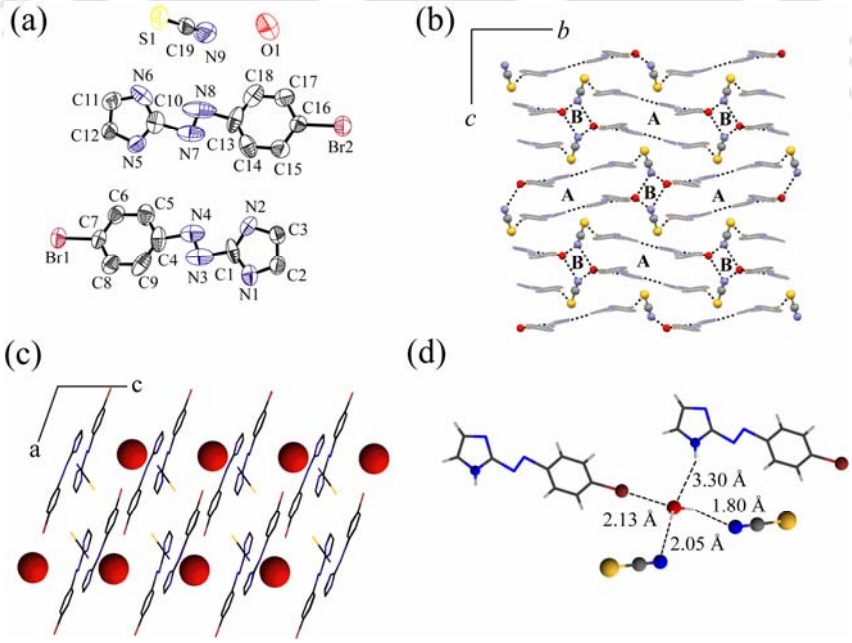

Figure 4.3. (a) (a) ORTEP plot (50% probability ellipsoids) of salt 1; (b) alternate parallelogram A and B when viewed along *a* axis and (c) linear water chain along *c* axis; (d) selected hydrogen bonding and halogen bonding pattern of salt 1.

Two of **L_9** are symmetrically non-equivalent and they are connected by a proton to form a homo-conjugated cationic system with a moderate, asymmetrical N–H····N hydrogen bond of the length of 2.77(3) Å. The dihedral angle between the planes of the ring is 6.0° and 0.89° respectively, for the protonated and unprotonated **L_9**. However, protonation of the ligand has little effect on the azo (N=N) system [**L_9**, -N=N- 1.128 Å, **L_9H^+**,-N=N- 1.101 Å]. Each water molecule is linked to the two adjacent SCN^- anions and one imidazole N via O–H····N and N–H····O hydrogen bonds (Figure 4.3b). Oxygen atom of water is also involved in halogen bond with neighboring Br1 of neutral **L_1**. The halogen bond Br1····O1 distance is 3.30 Å, which is very common halogen bond in biological process[4.27d] and this bond is shorter than the sum of van der Waals radii (1.85 Å for Br and 1.52 Å for O).[4.27a] The C7–Br1····O1 angle is 167.95°, implying the moderately strong halogen interaction. Thus, the O1 atom meets Br1 atom in line with the C–Br bond. Nitrogen end of the SCN^- anion forms strong O–H····N hydrogen bond with two neighboring water molecules (Figure 4.3b). However, sulfur end is engaged in the formation of halogen bond with neighboring Br2 of cationic **L_9**. In this case also, the halogen bond Br2····S1 distance is 3.535 Å, which is shorter than the sum of van der Waals radii (1.85 Å for Br and 1.80 Å for S). The C16–Br2····S1 angle is 165.1°, implying that the S1 atom meets Br2 atom in line with the C–Br bond.[4.28] Another interesting feature is the presence of weak N–H····π (N6-H6N····π, 2.6Å) interaction between protonated imidazole N-H with the π-cloud of the C=S bond of SCN^- anion. N–H bond forms edge-to-face π-stacking interaction and it is almost perpendicular to the C=S bond. Anion and water molecule forms water-thiocyanate-water-thiocyanate tetramer which is stabilized four halogen bonds and two N–H····O type hydrogen bonds. It forms a planar, zigzag arrangement of alternative parallelogram of type A and type B when viewed along *b* as well as *c* axis (Fig. 1b). All the water molecules are arranged linearly along *c* axis (Figure 4.3c). Distances between two water molecules along c and a axis are 8.21 Å and 10.20 Å respectively. The FT-IR spectra of salt **1** exhibit strong stretches at 2190, 2140 cm^{-1}, and 685 cm^{-1} which are in agreement with $\nu_{C=N}$ and $\nu_{C=S}$.[4.29] and there are two strong peak 3590 (m) and 3535 (m) which may be due to ν(O-H) of H_2O molecule present in the crystal system.

Figure 4.4a shows the ORTEP plot of salt **2**, $[L_{10}H]^+[NO_3]^-\bullet H_2O$ along with the atom numbering scheme. The dihedral angle between the planes of the ring is 2.36° respectively, which less compared to the protonated ligand **L_{10}**. Hence protonated **L_{10}** is more planar, which is also reflected in the increased azo bond length (-N=N- 1.264 Å). Offset face-to-face π packing occurs between two adjacent benzene ring and π cloud of

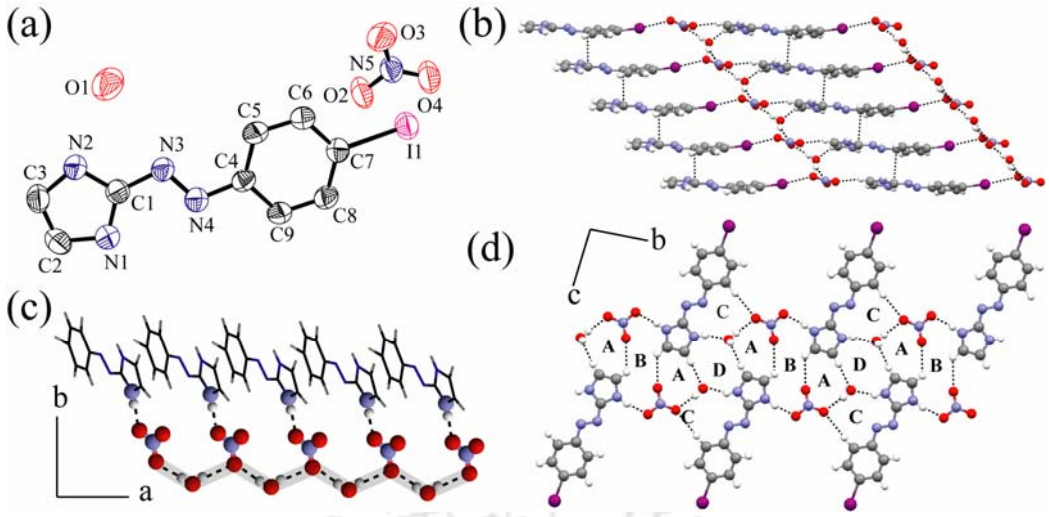

Figure 4.4. (a) ORTEP plot (50% probability ellipsoids) of salt 2; (b) staircase packing of alternate hydrophobic and hydrophilic layers along *a* axis; (c) water-nitrate-water 1D chain along *a* axis and (d) Repeat of hydrogen bonded ring ABA triad along *b* axis and CDC triad along *c* axis.

N=N bond 3.477 Å. It forms a staircase along a axis (Figure 4.4b). It forms an alternate hydrophobic and hydrophilic layer structure. Hydrophilic layer is consisting of planar NO_3^- anion and water molecule. Each hydrophobic layer is connected to the hydrophilic layer by C–H····O type weak hydrogen bonds and halogen bonds. Each planar NO_3^- anion is hydrogen bonded to two water molecules and one imidazole N2–H2N via O–H····O and N–H····O type hydrogen bonds. Similar to the salt 1, here also anion forms halogen bond with neighboring I atom. The halogen bond distance is 3.08 Å, which is much shorter than the sum of van der Waals radii (1.98 Å for I and 1.52 Å for O).[4.30] The C7–I1····O2 angle is 170.30°, implying the moderately strong halogen interaction. Thus, the O2 atom meets I1 atom in line with the C–I bond. However, solvent water does not form any kind of halogen bond like salt 1. Crystal water is forming two O–H····O hydrogen bonds and one N–H····O type hydrogen bond with NO_3^- anion and imidazole N1–H1N. Water and NO_3^- forms and 1D infinite zigzag chain along *a* axis (Figure 4.4c). Each O3 of anion is forming bifurcated hydrogen simultaneously to two water molecules. Overall non-covalent interactions in the solid-state results in the formation of four different type ring structures (Figure 4.4d). ABA triad ring is repeated along *b* axis where as CDC type triad is propagated along *c* axis. In salt **2** shows the strong sharp peak at 1497, 1271, 992 cm^{-1} which can be defined as the $\nu_{N=O}$ stretching frequency of the unidentate bonding of nitrate anion.[4.29]

But when we changed the planner NO_3^- anion to tetrahedral ClO_4^- anion spherical, there is a change in the overall packing and non-bonding interactions. ORTEP plot of salt **3**, $[\mathbf{L_{10}}H]^+[ClO_4]^-\bullet H_2O$ is shown in Figure 4.5a along with the atom numbering scheme. The dihedral angle between the plane through the ring is 1.41° with N=N distance 1.256Å

which is little shorter than previous one. To accommodate the larger ClO_4^- anion in the solid state in between the two ligands, there is no stacking interaction between the aromatic planes unlike the salt **2**.

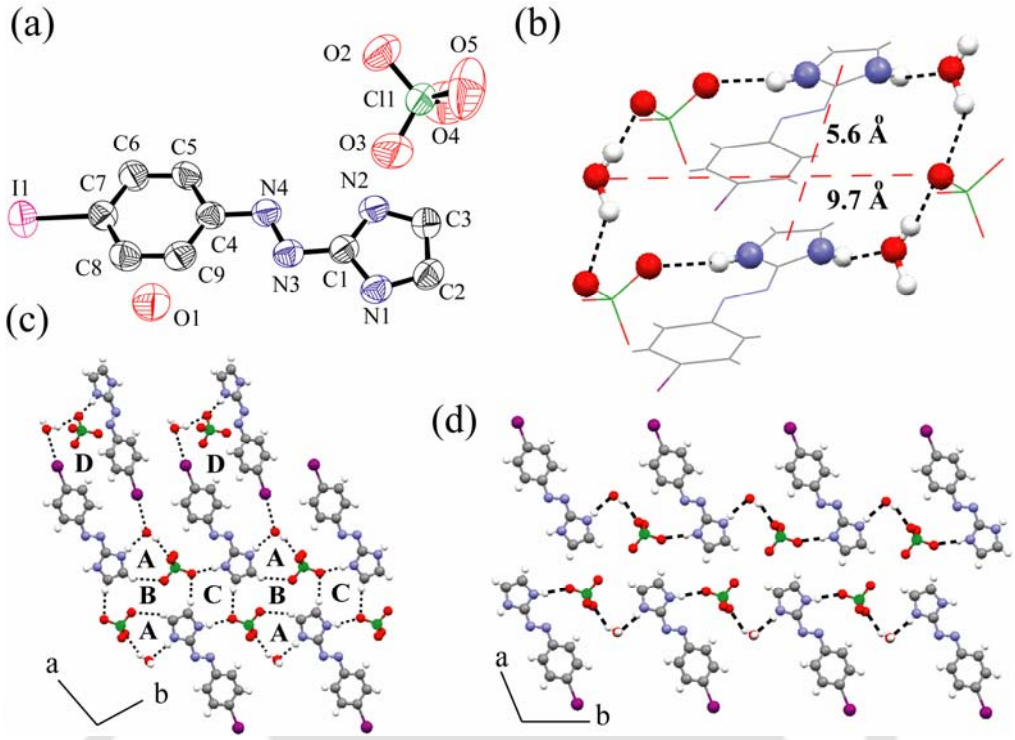

Figure 4.5 (a) ORTEP plot (50% probability ellipsoids) of salt 3; (b) the annulus structure of **3** formed via ionic hydrogen bonds; (c) repeat of hydrogen bonded ring DABA tetrad along *a* axis and BC diad along *b* axis and (d) water-ClO_4^--**L**H^+ one dimensional chain along *b* axis.

Moreover, four ligands form a kind of elliptical pocket to accommodate both the anion and crystal water molecule. Each water molecule forms two O–H••••O type hydrogen bond with two nearby ClO_4^- anions and one N–H••••O hydrogen bond with $\mathbf{L_{10}}H^+$ **(**Figure 4.4.A) similar to that of the salt 2. Similar to the salt **1**, here also water forms halogen bond with neighboring I atom. The halogen bond distance is 3.468 Å, which is little shorter than the sum of van der Waals radii (1.98 Å for I and 1.52 Å for O).[4.27] The C1–I1····O5 angle is 171.61°, implying the moderately strong halogen interaction. But unlike in salt **2** anion in salt 3 does not form any halogen bond. Anion forms O–H····O and N–H····O type hydrogen bond with water and imidazole N4–H4N. In salt **1** both anion and water forms halogen bonds, whereas in salt **2** only anion and in salt **3** only water forms halogen bonds. The existence of water molecule in the crystal lattice helps to form strong N–H••••O and O–H••••O hydrogen bonds in the salt **3** which is propitious to stabilize the annulus (Figure 4.5b). The annulus structure of **3** formed via ionic hydrogen bonds with the dimension of cavity was 9.7 Å X 5.6 Å. Combine effect of O–H••••O, N–H••••O and C–H••••O interactions in the solid state results in the formation of four different types of

ring structures (Figure 4.5c). Among them the ring D has the largest size. The DABA tetrad is repeated along *a* axis and the BC diad is repeated in the solid state along *b* axis. Along *b* axis water-ClO_4^--**L**H^+ forms an infinite 1D hydrogen bonded chain (Figure 4.5d). Then in the next part, we have studied the effect of increased hydrophobic nature of the ligand in the 3D solid state packing. Protonated naphthayl azo imidazole ligand $\mathbf{L_{11}}$ crystallize in presence of NO_3^- anion. ORTEP plot of salt **4**, $[\mathbf{L_{11}}H]^+[NO_3]^-$ is shown in Figure 4.6a along with the atom numbering scheme. Napthyl azo imidazole ligands are much more planar due to extended conjugation than the phenyl azo imidazole ligands.

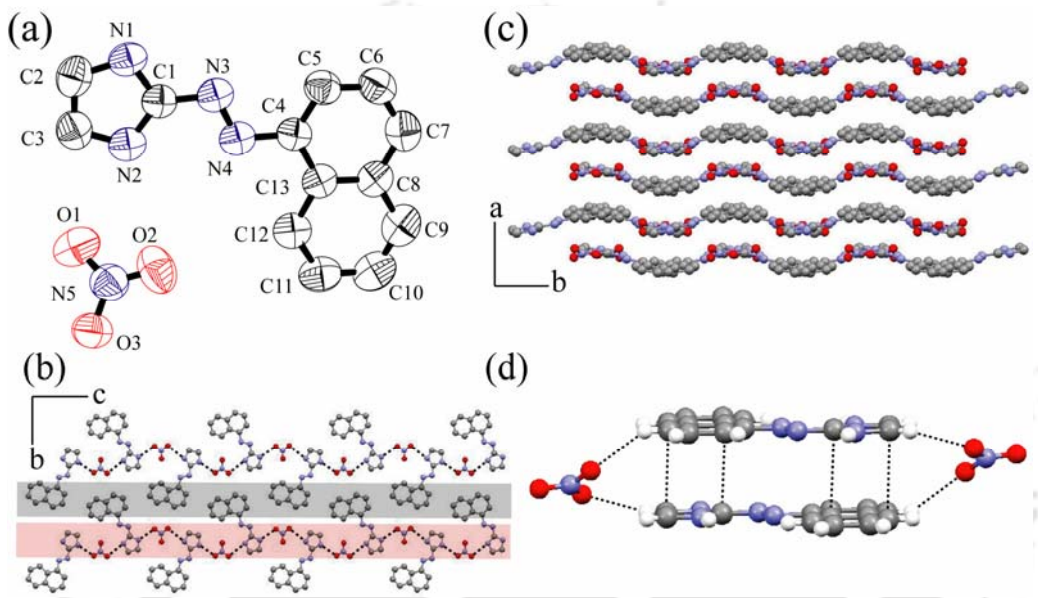

Figure 4.6 (a) ORTEP plot (50% probability ellipsoids) of salt 4; (b) zigzag H-bonded chain along *a* axis; (c) Wavy packing along *b* axis and (d) Stacking interaction in salt 4.

Hence, dihedral angle between the aromatic planes is 0.29° only. The N=N double bond character is decreased and bond distance is increased (1.259 Å) compared with the literature value.[4.31] In the crystal lattice each NO_3^- anion is forming three N–H••••O type intermolecular hydrogen bonding with imidazoles hydrogen present in the neighborhood. Cation and anion forms a 1D zigzag hydrogen bonded chain along *c* axis (Figure 4.6a) similar to the another nitrate salt **2**. In salt **2** all the ligands are oriented in the dame direction. However, in this case every other ligand is oriented in the same direction and contiguous ligands are disposed in the opposite direction. This is due to the inter-ligand steric repulsions of the bulky napthyl group in ligand $\mathbf{L_{11}}$. Several N–H••••O and C–H••••O interactions forms a wavy packing pattern along *b* axis (Figure 4.6c). Anti-parallel orientation of the ligand along *a* axis helps to form offset face-to-face π stacking interactions (3.416 Å) between napthyl and imidazole group (Figure 4.6d). Each of the π stacked dimmer is clipped and stabilized in the solid state in the both end *via* C–H••••O

interactions with the adjacent anions. The FT-IR spectra of salt **4** exhibit strong stretches at 1420, 1275, 980 cm^{-1} which are in agreement with NO_3^- moieties.[4.29]

Salt **5** is formed when crystallization of salt **4** is carried out in presence of water *i.e.* salt **5** is the hydrated form of salt **4**. ORTEP plot of salt **5**, $[\mathbf{L_{11}}H]^+[NO_3]^-\bullet H_2O$ is shown in Figure 4.7a. Similar to the salt **1**, it also contains one protonated and one neutral $\mathbf{L_{11}}$ in the asymmetric unit. In protonated species, the dihedral angle between the two least squares planes is only 2.31° whereas the unprotonated one is 4.75°. Both the ligands form homo-conjugate unit through N–H••••N bond. Protonated imidazole unit forms hydrogen bonds with water and neutral $\mathbf{L_{11}}$. On the other hand neutral $\mathbf{L_{11}}$ forms hydrogen bonds with anion and Protonated imidazole unit. Each anion is forming two O–H••••O bonds with the neighboring water molecules (Figure 4.4.A). Water is forming two O–H••••O bonds with anion and one two N–H••••O bond with imidazolium cation. All the bond non covalent interactions are given in appendix. Similar to the salt **2**, here also exists a 1D infinite water-nitrate hydrogen bonded chain along *a* axis (Figure 4.7b).

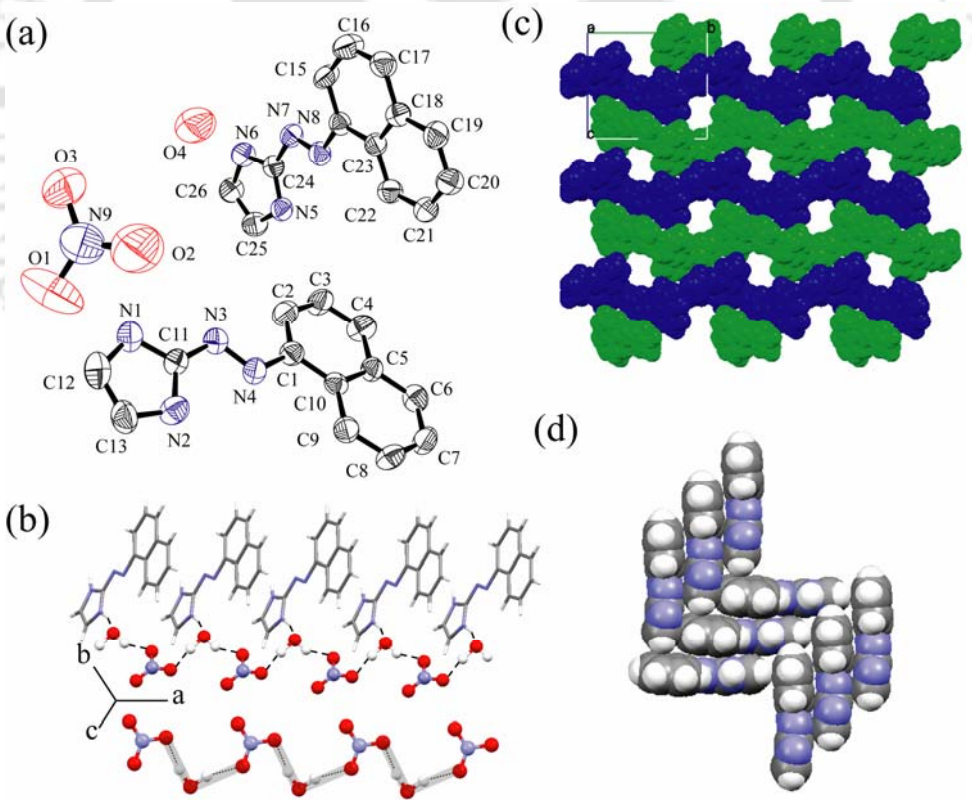

Figure 4.7 (a) ORTEP plot (50% probability ellipsoids) of salt 5; (b) 1D hydrogen bonded water-nitrate chain; (c) Alternate zigzag chain of two asymmetric $\mathbf{L_{11}}$ with a 1D channel along a axis and (d) π stacking interactions between $\mathbf{L_{11}}$

However, the pattern of bonding is different form the salt **2**. It forms an L-shape orientation of the 1D chain. The difference in network pattern is explained by the

difference in bonding of NO_3^- anion with the water molecules. In salt **2**, one O atom of the NO_3^- anion forms bridge between two water molecules. But in slat **5**, water molecules are bridged by O-N-O unit of the NO_3^- anion. Two symmetrically non-equivalent $\mathbf{L_{11}}$ ligands form zigzag chain along *b* axis (Figure 4.7c). The alternate chains stack along *c* axis. Along *a* axis it forms an rectangular 1D channel which is filled by the anion-water 1D infinite chain (Figure 4.4.A). Both the $\mathbf{L_{11}}$ units are perpendicular to each other. Neutral $\mathbf{L_{11}}$ is oriented in the perpendicular direction to each other in the adjacent layer. Each perpendicular neutral unit is connected *via* C-H····π interaction. Imidazole unit forms offset face-to-face π–π interaction with the napthyl moieties for both the $\mathbf{L_{11}}$ units (Figure 4.7a).[4.32] The FT-IR spectra of salt **5** exhibit strong stretches at 1420, 1275, 980 cm^{-1} which are in agreement with coordinated O-NO_2 moieties [4.29] and there are two extra peak present at 3595 (m) and 3539 (m) is due to ν(O-H) of water molecule present in the crystal system.

4.3.2. Powder X-ray diffraction (PXRD) Analysis

Powder X-ray diffraction (PXRD) pattern of salt **4** and **5** supports the crystalline nature of the bulk sample. Salt **5** contains a water of crystallization. Salt **5** was heated at 80°C for 2 hrs in vacuum and resulted crystalline solid was studied by PXRD.

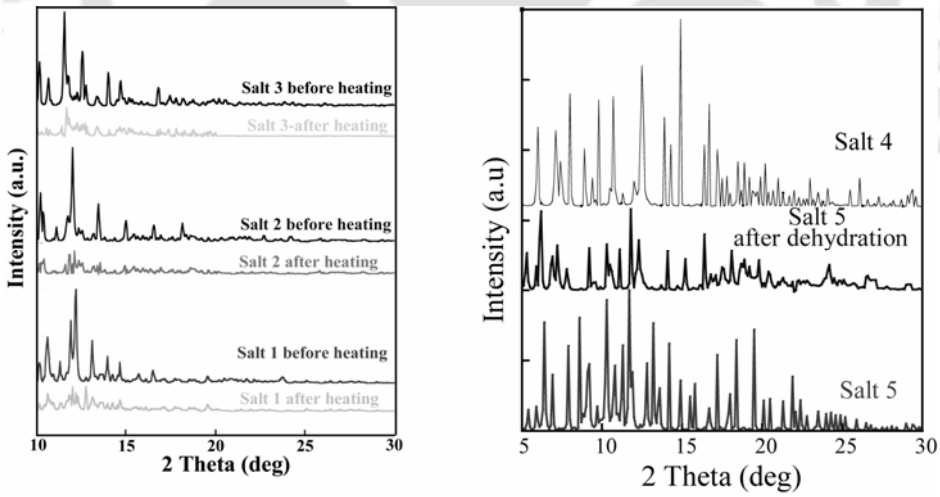

Figure 4.8 (a) PXRD patterns of crystalline salt 1, salt 2 and salt 3 before and after heating. (b) PXRD patterns of crystalline salt 4, salt 5 and salt 5 after removal of water

The PXRD pattern was closed to that of anhydrous salt **4** (Figure 4.8b). However, we are unable to maintain the single crystalline nature of the heated sample and thus not able to confirm the final structure by single crystal X-ray studies. However, FT-IR spectrum and PXRD pattern of is similar to that of salt **4**. Similarly, in the Salt **1**, Salt **2** and Salt **3** there

are also significant changes in the peak positions as well as intensities before and after water removal (Figure 4.8a).

4.3.3. Absorption spectroscopy

The UV-Vis absorption spectra of ligands were recorded in MeOH at 298 K. **L_9** and **L_{11}** shows a broad absorption band with maxima at 360 nm and 380 (Figure 4.9a). However napthyl chromophore in **L_{11}** shows the red shifted absorption band at 392 nm and 410 nm with $\varepsilon \sim 10^4\ M^{-1}cm^{-1}$ for both the peaks. These absorption bands corresponds to intra-ligand ($n–\pi^*/\pi–\pi^*$) transitions.[4.33] Addition of ammonium salts have negligible effect in the absorption spectra of **L_9** and **L_{10}**. However, the effect is more pronounced in case of **L_{11}**. In these ligands there are two sites for protonation *i.e.* azo and imidazole nitrogen. **L_{11}** has more electron density than **$L_{9\text{-}10}$**. In neutral and acid medium, absorption spectra of **$L_{9\text{-}10}$** does not change much, however, in basic medium (pH~10) a red shift occurred due to availability of electron density in imidazole N-H group.[4.34] The observed $\Delta\lambda$ value is ~33 nm (Figure 4.9a). On the other hand, batho-chromic shift is observed ($\Delta\lambda$ ~30 nm) in acidic pH (~3) in case of **L_3** (Figure 4.9b). The probable explanation for the contradictory nature of same type of ligands is due to electronic environment (depends on the basicity) of azo nitrogen and imidazole nitrogen.[4.35]

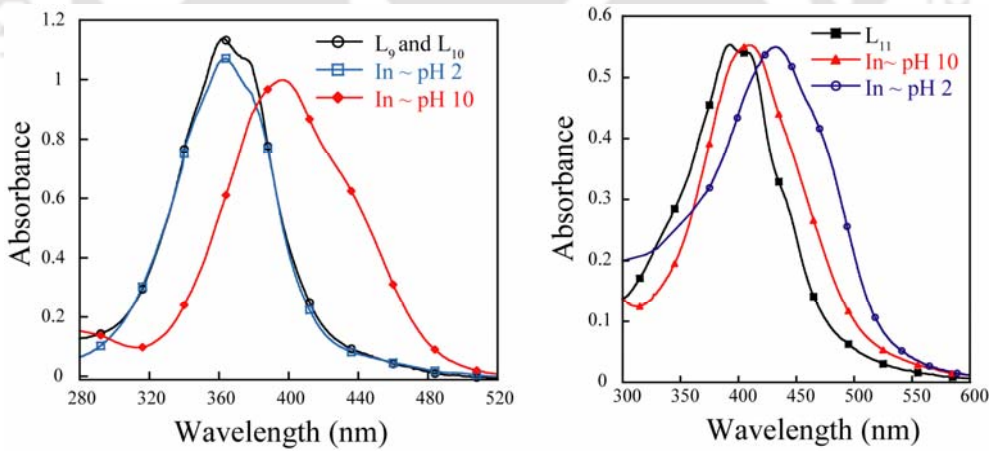

Figure 4.9 UV-Vis absorption spectra of (a) **L_9** and (b) **L_{11}** in presence of acidic and basic pH.

4.3.4. Fluorescence Spectroscopy

The studied *tran*-2-aryl azo naphthalene have small fluorescence quantum yield, which are scarcely affected by the solvent (Φ_F = 0.025). The fluorescence quantum yields depend weakly on the excitation wavelength, due to the presence in solution of conformational isomers with slightly different absorption spectra.[4.36] The emission spectra of **L_3** in hexane at 298 K shows a locally excited (LE) broad emission of naphthalene with emission at 425

nm and 450 nm (λ_{ex} = 400 nm) respectively. But in other solvent a very weak emission band is observed. Dual exponential fluorescence decays confirmed the presences two conformer's cis and *Trans* are interchanged in solution phase[4.37] (Figure 4.10a).

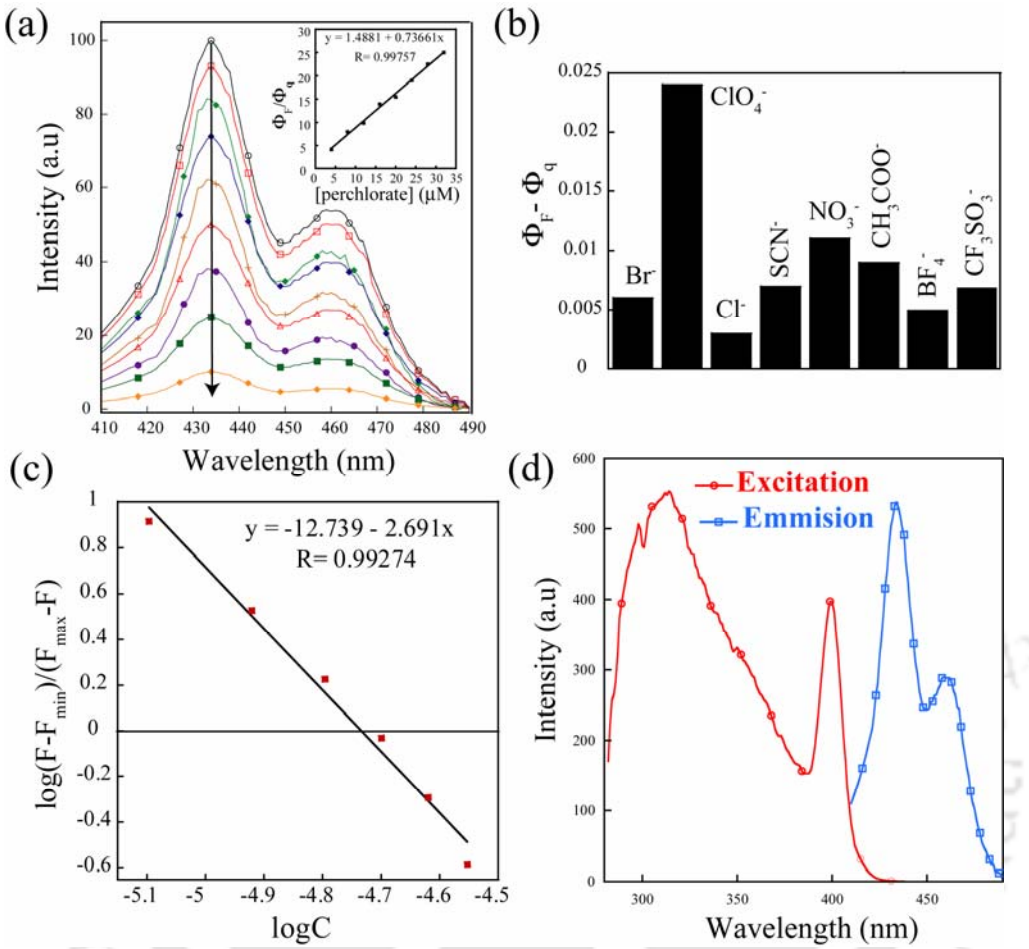

Figure 4.10 (a) Schematic representation showing the change of fluorescence quantum yield (ΦF-Φq) of $\mathbf{L_{11}}$ upon addition of the different acids. ΦF and Φq are quantum yields of $\mathbf{L_{11}}$ in absence and presence of guest, respectively. Inset: Stern–Volmer plot with Ammonium perchlorate; (c) Determination dissociation constant (K_d). The apparent K_d is at the X intercept, at a value of –4.73. The inverse log of this is 1.9 x 10^{-5} M; (d) Excitation and emission spectra of $\mathbf{L_{11}}$.

With increasing concentration of the ligand, the total intensity of fluorescence emission increases significantly without the formation of excimer. Upon gradual addition of different anions to the hexane solution of $\mathbf{L_3}$, the intensity of the emission bands decreases. The dissociation constant[4.38] K_d was estimated from the change in fluorescence quantum yield resulted from the titration data of $\mathbf{L_3}$ against NH_4ClO_4 solution. The linear fit of the data (Figure 4.10c) for NH_4ClO_4 inclusion complex was obtained by plotting $\log[(\Phi-\Phi_{min})/(\Phi_{max}-\Phi)]$ as a function of logarithm of NH_4ClO_4 concentration and the intercept of the linear regression determines K_d value of 1.9 x 10^{-5} M mm in hexane. This

value indicates the formation of a stable inclusion complex and is in consistence with good correlation coefficients (>0.99). To demonstrate the selectivity of **L_{11}** toward perchlorate, we have monitored the change in fluorescence quantum yields in the presence of different anions like nitrate, thiocyante, bromide, chloride, triflate, tetrafluoroborate and acetate. The magnitude of the quenching efficiency (Φ_Q)[4.39] follows the order of ClO_4^- (0.024) > NO_3^- (0.011) > $CF_3SO_3^-$ > (0.008) SCN^- (0.007) > Br^- (0.006) > BF_4^- (0.005) > Cl^- (0.003) (Table 4.3.A) which is a result of combine steric and electronic effect through non-covalent interactions. Figure 4.10b clearly shows that **L_{11}** has a remarkably high selectivity toward percholrate anion in terms of change of fluorescence quantum yield. The linear Stern–Volmer response of (Figure 4.10a, inset) ClO_4^- anion as quencher is consistent with well-behaved fluorescence quenching systems.

4.4. General discussion on the observed noncovalent interactions in the solid and spectroscopic behavior in solution phase

In continuation of the anion recognition and their spectroscopic studies with variety of host molecules,[4.39] herein we have shown aryl azo system containing imidazole moiety played crucial role in forming higher dimensional networks in presence of different anion. Imidazolium cation directed the anion assembly formation through strong hydrogen bonding interaction along with weaker noncovalent interactions. We have varied the shape of the anion to evaluate the effect of higher dimension ordering in the solid-state. In salt **1** we have seen the linear SCN^- anion is assembled via water to form H_2O-SCN^--H_2O-SCN^- unique tetrameric moieties, which is not the case in other non-linear anions. However, in salt **2**, planner NO_3^- ion is assembled through water molecule to form a 1D infinite zigzag chain formed by single oxygen atom bridge of nitrate. On the other hand, in case of salt **5**, the NO_3^- ion is assembled with water molecule to form a 1D infinite water-nitrate hydrogen bonded chain constituting two oxygen atom of nitrate ion bridged with two water molecules. In salt **4**, there is no water in the crystal lattice, which drastically changes the linear chain structure. In salt **4**, the napthyl azo imidazolium ion is stacked with nitrate ion to form a wave like structure. In the salt **3** contain spherical ClO_4^- ion is assembled with water to form a 1D zigzag chain network bearing oxygen atom of perchlorate bridged with two water molecules. In solution the UV-visible studies shows the bathochromic and hypsochromic shift with pH, which has been explained on the basis of electron density of aryl group (benzyl to napthyl) and the halogen substitution in the ligands. Fluorescence quenching studies also revel the presence of various noncovalent interactions[4.40] between the ions which has been observed in the solid-state.

4.5. Summary

To rationalize the influence of the non- covalent interactions of anion on the formation of supramolecular architectures with aryl-azo diazonium salts, we have shown that the size of the anions has marked influence upon the supramolecular assemblies. For the complexes with the different type of anions (linear, planner, spherical), one dimensional layered network with identical topologies has been found. As expected, the N atom of imidazole ring always acts as an excellent hydrogen-bonding acceptor by the formation of a strong O-H····N or ionic N-H···· O and O-H····O hydrogen bond due to the presence of water in the crystal systems. Additionally, this study shows that complex 1 and 5 is a good supramolecular building module that can produce bimolecular co crystals, and its modular nature makes it possible to select a comfortable configuration in the course of formation of self assembly hydrogen bond ($L\cdots LH^{+}$). Finally UV-Visible and fluorescence spectroscopy studies also confirmed the existence of weak supramolecular interaction. These results show that the types and ratios of cations and anions play significant roles in fabricating different solid-state structure.

References:

4.1 (a) Malcik, N.; Oktar, O.; Ozser, M. E.; Caglar, P.; Bushby, L.; Vaughan, A.; Kuswandi, B.; Narayanaswamy, R.; *Sensors Actuat.,* **1998,** *B53,* 211. (b) Malcik, N.; Tunoglu, N.; Caglar, P.; Wnek, G. E. *Sensors Actuat.* **1998**, *B53*, 204. (c) Kirkbright, G. F.; Narayanaswamy, R.; Welti, N. A. *Analyst,* **1984,** 15. (d) Ohzeki, K.; Sakuma, T.; Kambara, T. *Bull. Chem. Soc. Jpn.,* **1980**, *53.* 204.

4.2 (a) Weiss, B.; Williams, J. H.; Margen, Caan, B. B.; Citron, L. J.; Cox, C.; McKibben, J.; Ogar, D.; Schultz, S. *Science*, **1980**, *207*, 1487. (b) Swanson, J. M.; Kinsbourne, M. *Science*, 1980, **207**, 1487.

4.3 (a) Fei, Z.; Geldbach, T. J.; Scopelliti, R.; Dyson, P. J. *Inorg. Chem*., **2006**, *45*, 6331. (b) Yamamura, M.; Kano, N.; Kawashima, T. *Inorg. Chem*. **2006**, 45, 4697.

4.4 (a) Datta, D.; Chakravorty, A. *Inorg. Chem.*, **1983**, *22*, 1085. (b) Goswami, S.; Kharmawphlang, W.; Deb, A. K.; Peng, S-M. *Polyhedron*, **1996,** *15*, 3635.

4.5 (a) Rau, H.; Durr, H. I.; Bouas-Laurent, H. *Photochromism: molecules and systems.;* Amsterdam: Elsevier; 1990. (b) Tamai, N.; Miyasaka, H. *Chem. Rev.*, **2000**, *100*, 1857; (c) Yagai, S.; Karatsu, T.; Kitamura, A. *Chem.-Eur. J.,* **2005**, *11*, 4054.

4.6 (a) Glezer, V. In *The Chemistry of the Hydrazo, Azo and Azoxy Groups; Patai, S., Ed.;* Wiley & Sons: New York, 1997; p 729. (b) Oakes, J.; Wilkes, I. P.; Clark, R. J.; Gratton, P. L. *J. Chem. Soc., Perkin Trans. 2*, **1998**, 2569.

4.7 (a) Hartley, J. H.; James, T. D.; Ward, C. J. *J. Chem. Soc., Perkin Trans.1* **2000**, *19*, 3155. (b) DiCesare, N.; Lakowicz, J. R. *J. Phys. Chem. A,* **2001**, *105,* 6834.

4.8 (a) Renner, C.; Moroder, L. *ChemBioChem,* **2006**, *7*, 868; (b) Willner, I. *Acc. Chem. Res.*, **1997**, *30*, 347.

4.9 (a) Scott, J. L.; MacFarlane, D. R.; Raston, C. L.; Teoh, C. M. *Green Chem.,* **2000**, *2*, 123. (b) Wasserscheid, P.; Keim, W.; *Angew. Chem., Int. Ed.,* **2000**, *39*, 3772.

4.10 (a) Gordon, C. M.; Holbrey, J. D.; Kennedy, A. R.; Seddon, K. R. *J. Mater. Chem.,* **1998**, *8*, 2627. (b) Lee, K. M.; Lee, C. K.; Lin, I. J. B. *Chem. Commun.,* **1997**, 899, (c) Bowlas, C. J.; Bruce, D. W.; Seddon, K. R. *Chem. Commun.,* **1996**, 1625.

4.11 Lee, C. K.; Huang, H. W.; Lin, I. J. B. *Chem. Commun.,* **2000**, 1911.

4.12 (a) Carmichael, A. J.; Hardacre, C.; Holbrey, J. D.; Nieuwenhuyzen, M.; Seddon, K. R. *Mol. Phys.,* **2001**, *99*, 795. (b) Bardosova, M.; Hodge, P.; Korenova, A.; Nakanishi, F.; Tredgold, R. H. *Thin Solid Films,* **2001**, *397*, 8.

4.13 Bourissou, D.; Guerret, O.; Gabbaı, F. P.; Bertrand, G. *Chem. Rev.,* **2000**, *100*, 39.

4.14 (a) Cornils, B.; Herrmann, W. A. *Applied Homogeneous Catalysis with Organometallic Compounds*, Wiley, Chichester, **2000**, p. 725. (b) Louie, J.; Grubbs, R. H. *Chem. Commun.,* **2000**, 1479.

4.15 (a) Guerret, O.; Sole, S.; Gornitzka, H.; Teichert, M.; Trinquier, G.; Bertrand, G. *J. Am. Chem. Soc.,* **1997**, *119*, 6668. (b) Lee, C. K.; Lee, K. M.; Lin, I. J. B. *Organometallics,* **2002**, 10.

4.16 (a) MacGillivray, L. R.; Atwood, J. L. *Nature*, **1997,** *389*, 469. (b) Biradha, K.; Zaworotko, M. J. *J. Am. Chem. Soc.,* **1998**, *120*, 6431. (c) Childs, L. J.; Alcock, N. W.; Hannon, M.; *Angew. Chem., Int. Ed.,* **2001**, *40*, 1079.

4.17 (a) Honman, K. T.; Pivovar, A. M.; Swift, J. A.; Ward, M. D. *Acc. Chem. Res.,* **2001**, *34*, 107; (b) Wu, C. D.; Hu, A. G.; Zhang, L.; Lin, W. B. *J. Am. Chem. Soc.,* **2005**, *127*, 8940.

4.18 (a) AakerOy, C. B.; Seddon, K. R. *Chem. Soc. Rev.,* **1993**, *22*, 397, (b) Steed, J. W.; Atwood, J. L. *Supramolecular Chemistry,* John Wiley & Sons Ltd, Chichester, **2000**.

4.19 (a) Moulton, B.; Zaworotko, M. J. *Chem. Rev.,* **2001**, *101*, 1629. (b) Yaghi, O. M.; O'Keeffe, M.; Ockwig, N. W. Chae, H. K.; Eddaoudi, M.; Kim, J. *Nature*, **2003**, *423*, 705. (c) Kitagawa, S.; Kitaura, R.; Noro, S.-I. *Angew. Chem., Int. Ed.,* **2004**, *43*, 2334.

4.20 (a) Desiraju, G. R. *Acc. Chem. Res.,* **2002**, *35*, 565. (c) Dunitz, J. D. *Chem. Commun.,* **2003**, 545.

4.21 (a) Dobrzanska, L.; Lloyd, G. O.; Raubenheimer, H. G.; Barbour, L. J. J. *Am. Chem. Soc.,* **2005**, *127*, 13134. (b) Dobrzanska, L.; Lloyd, G. O.; Raubenheimer, H. G.; Barbour, L. J. *J. Am. Chem. Soc.,* **2006**, *128*, 698.

4.22 Awakeh, M.O.; Badia, A.; Brisse, F. Bu, X. H. *Inorg. Chem.,* **2006**, *45*, 1560.

4.23 Davis, A P. *Coordin. Chem. Rev.,* 2006, **250**, 2939.

4.24 (a) MacDonald, J. C.; Dorrestein, P. C.; Pilley, M. M. *Cryst. Growth Des.,* **2001**, *1*, 29. (b) Trivedi, D. R.; Ballabh, A.; Dastidar, P. *CrystEngComm,* **2003**, *5*, 358.

4.25 (a) Byabartta, P.; Pal, S.; Sinha, C.; Liao, F.-L.; Panneerselvam, K.; Lu, T.-H. *J. Coord. Chem.* **2002**, *55*. 479. (b) Chattopadhyay, P., Dolui, B. K., Sinha, C. *Indian J. Chem. Sect. A*, **1997**, *36*, 429.

4.26 Thallapally, P. K.; Lloyd, G. O.; Wirsig, T. B.; Bredenkamp, M. W.; Atwood, J. L.; Barbour, L. J. *Chem. Comm,* **2005**, 5272.

4.27 (a) Alfonso, I.; Bolte, M.; Bru, M.; Burguete, M. I.; Luis, S. V. *CrystEngComm,* **2009**, *11*, 735. (b) Ruiz, T. P.; Gomez, M. F.; Gonzalez, J. J. L.; Koziol, A. E. *Chem. Phys.,* **2006**, *320*, 164. (c) Lu, Y.; Shi, T.; Wang, Y.; Yang, H.; Yan, X.; Luo, X.; Jiang, H.; Zhu, W. *J. Med. Chem.* **2009,** *52,* 2854. *(d)* Auffinger, P.; Hays, F.A.**;** Westhof, E.; Ho, P. S. *Proc. Natl. Acad. Sci. U.S.A.,* **2004**,*101,* 16789.

4.28 Assmore, J.; Sutherland, G.; Whidden, T. K.; White, P. S.; Wong, C–M.; *Can. J. Chem.*;**1985**, *23*, 1209.

4.29 (a) Conley, R.T.; *Infrared Spectroscopy,* Allyn & Bacon, Boston, **1966**. (b) Nakamoto, K. *Infrared and Ramman Spectra of Inorganic and Coordination Compounds*, 5th ed.; John Wiley & Sons Inc.: New York, **1997**.

4.30 (*a*) Bondi, A.. *J. Phys. Chem.,* **1964**, *68*, 441. (b) Zhu, S. Z.; Xing, C. H.; Xu, W.; Jin, G. F.; Li, Z. T. *Cryst. Growth Des*., **2004**, *4,* 53. (c) Han, Z.; Gao, Y.; Zhai, X.; Peng, J.; Tian, A.; Zhao, Y.; Hu, C. *Cryst. Growth Des*., **2009**, *9*, 1225.

4.31 Banerjee, D.; Ray, U.S.; Wu, J. S.; Lu, T. H.; Sinha, C. *Polyhedron*, **2006**, *25*, 3077.

4.32 Wang, W-H.; Xi, P-H.; Su, X-Y.; Lan, J-B.; Mao, Z-H.; You, J-S.; Xie, R-G.; *Cryst. Growth Des*., **2007**, ***7,*** 741.

4.33 (a) D. Das, B.G. Chand, K. K. Sarker, J. Dinda and C. Sinha, *polyhedron*, 2006, **25,** 2333; (b) T. K. Misra, D. Das, C. Sinha, P. K. Ghosh and C. K. Pal, *Inorg. Chem.*,1998, **37**, 1672.

4.34 (a) Ibrahim, S. A.; Rageh, N. M.; Mohamad, A. A.; Ebead, Y. H. *J. Chem. Eng. Data,* **1999**, *44*, 451. (b) Esener, H.; Uyar, T. *Dyes Pigments,* **2007**, *7*, 109.

4.35 Mustroph, H.; Haessner. R.; Epperlein, J.; *J. Prakt. Chem.,* **1984**, *32,* 259.

4.36 Galiazzoa, G.; Bortolusb, P.; Gennaric, G. *J. Photochem. Photobiol. A., Chem.,* **1999**, *120,* 161.

4.37 Otsuki, J.; Suwa, K.; Sarker, K. K.; Sinha, C. *J. Phys. Chem. A.;* **2007,** *111,* 1403.

4.38 Grynkiewicz, G.; Poeniea, M.; Tsien, R. Y. *J. Biol. Chem.,* **1985**, *260*, 3440.

4.39 Das, G.; Bharadwaj, P. K.; Roy, M. B.; Ghosh, S.; *Chem. Phys.,* **2002**, 277, 145.

4.40 (a) Anzellotti, A. I.; Sabat, M.; Farrell, N. *Inorg. Chem.,* **2006**, *45*, 1638. (b) Acevedo, D. F.; Balach, J.; Rivarola, C. R.; Miras, M. C.; Barbero, C. A. *Faraday Discuss.,* **2006**, *131*, 235.

APPENDIX

Table 4.1 A. Crystal Data and Structure Refinement for salt **1**, **2, 3, 4** and **5.**

	Salt 1	**Salt 2**	**Salt 3**	**Salt 4**	**Salt 5**
CCDC No	736670	736671	736672	736673	736674
Empirical formula	$C_{19}H_{17}N_9OSBr_2$	$C_9H_{10}N_5O_4I$	$C_9H_{10}N_4O_5ClI$	$C_{13}H_{11}N_5O_3$	$C_{26}H_{23}N_9O_4$
Fw	579.30	379.12	416.56	285.27	525.53
crystal system	Monoclinic	Monoclinic	Monoclinic	Monoclinic	Monoclinic
space group	P2(1)/c	P2(1)/n	P2(1)/n	P2(1)/c	P2(1)
a, Å	12.1694(3)	4.88350(10)	5.60440(10)	6.8263(2)	5.6061(2)
b, Å	13.9841(4)	10.1720(3)	8.8412(2)	11.5549(3)	15.8135(6)
c, Å	14.3235(4)	27.4296(8)	29.3023(6)	17.0562(4)	14.0347(5)
α, deg	90	90	90	90	90
β, deg	105.557(2)	91.328(2)	95.3470(10)	96.7880(10)	97.281(2)
γ, deg	90	90	90	90	90
V, $Å^3$	2348.24(11)	1362.20(6)	1445.60(5)	1335.92(6)	1234.17(8)
Z	4	4	4	4	2
μ	3.572	2.372	2.426	0.107	0.102
F(000)	1152	764	1101	700	572
GOF(S)	1.055	1.050	1.028	1.004	0.973
R_{int}	0.0379	0.0402	0.0213	0.0251	0.0521
final R indices	R1=0.0452	R1= 0.0343	R1= 0.0356	R1= 0.0473	R1= 0.0519
[I > 2σ(I)]	wR2= 0.0918	wR2= 0.0675	wR2= 0.0963	wR2= 0.1172	wR2= 0.1135
R indices (all data)	R1= 0.0839	R1= 0.0752	R1= 0.0485	R1= 0.0898	R1= 0.0830
	wR2= 0.1100	wR2= 0.0495	wR2= 0.1054	wR2= 0.1473	wR2= 0.1445

Table 4.2 A. Selected Non-covalent interactions in salt **1-5**

D–H···A	H···A (Å)	D···A (Å)	D–H···A (◦)
		Salt 1	
C16–Br2····S1		3.535	165.06
C7–Br1····O1		3.301	167.95
C18–H18····N9	2.835(.005)	3.742 (7)	165.51 (33)
C14–H14····N7	2.483(.005)	2.636 (7)	88.96 (30)
N6–H6N····S1	2.652(.001)	3.483 (4)	162.84 (23)
C9–H9····N3	2.451(.004)	2.642 (7)	91.31 (33)
C3–H3····N7	2.953(.004)	3.514 (6)	120.18 (26)
N1–H1N····O1	1.839 (40)	2.696 (5)	173.88 (26
O1-H1O····N9	2.126 (70)	2.915 (6)	163.85 (95)
O1–H2O····N9	2.035 (45)	2.843 (6)	162.72 (61)
N5–H5N····N2	1.884 (3)	2.740 (5)	173.33 (26)
N6–H6N····N8	2.573 (5)	2.616 (7)	83.31 (32)
N5–H5N····N2	1.884 (3)	2.740 (5)	173.33 (26)
N6–H6N····π		. 3.55	
		Salt 2	
C2–I1····O2		3.079	170.30
C3–H3····O4	2.724 (36)	3.278 (5)	118.00 (61)
C2–H2····O1	2.467 (42)	3.340 (6)	153.95 (41)
C9–H9····O3	2.640 (32)	3.728 (5)	165.01 (33)
C5–H5····N3	2.490 (35)	2.751 (4)	94.51 (16)
N1–H1N····O1	1.851 (43)	2.656 (5)	160.35 (15)
O1–H1O····O3	1.942 (61)	2.753 (5)	175.95 (99)
O1–H2O····O3	2.109 (52)	2.806 (5)	150.51 (24)
N2–H2N····O2	1.807 (46)	2.705 (5)	173.41 (37)
N2–H2N····O4	2.634 (43)	3.188 (5)	120.54 (48)
O1–H2O····O2	2.779 (58)	3.405 (8)	139.87 (9)
N1–H1N····N4	2.500 (40)	2.684 (4)	93.43 (84)
π ····π_{azo}		3.532	
		Salt 3	
C9–H9····O3	2.648 (4)	3.512 (5)	154.77 (23)
C8–H8····O2	2.521 (4)	3.403 (6)	158.34 (26)
C4–H4····N3	2.453 (3)	2.703 (5)	95.34 (24)
C8–H8····O4	2.937 (4)	3.270 (6)	102.75 (26)
C3–H3····O1	2.834 (5)	3.758 (6)	172.97 (24)
C8–H8····O3	2.813 (4)	3.331 (6)	116.31 (26)
O5–H1O····O1	2.201 (10)	3.037 (6)	129.24 (98)
O5–H5O····O1	2.110 (63)	2.895 (6)	154.09 (69)
N4–H4N····O5	1.988 (45)	2.773 (4)	162.80 (48)
N5–H3N····O2	2.001 (41)	2.896 (5)	170.57 (75)
N5–H3N····N1	2.630 (40)	2.724 (5)	86.21 (48)
C1–I1····O5		3.468	170.61
		Salt 4	
C12–H12····O2	2.638 (2)	3.539 (3)	163.33 (15)
C7–H7····O1	2.528 (2)	3.329 (3)	144.53 (15)
C2–H2····O3	2.599 (2)	3.232 (3)	125.74 (15)
C3–H3····O1	2.783 (3)	3.420 (3)	126.60 (15)
C12–H12····N4	2.525 (2)	2.825 (3)	99.11 (13)
C5–H5····N3	2.427 (2)	2.703 (3)	96.97 (14)
C10–H10····O2	2.861 (2)	3.459 (3)	123.19 (15)
C7–H7····N1	2.528 (2)	3.329 (3)	144.53 (15)
N1–H1N····O3	1.845 (2)	2.703 (2)	174.72 (13)
N2–H2N····O1	2.364 (2)	2.913 (3)	165.98 (12)
N4–H4····N2	2.613 (2)	2.729 (3)	88.46 (13)
π ····π_{azo}		3.578	

Salt 5			
C4–H4····O3	3.564 (6)	2.658 (4)	164.67 (30)
N6–H6N····N1	1.815 (38)	2.685(.005)	177.74 (79)
N5–H5N····O4	1.754 (50)	2.818(.004)	160.93 (49)
O4–HOB····O2	1.778 (40)	2.841(.005)	170.10 (24)
O4–HOA····O3	1.947 (46)	2.923(.004)	158.89 (92)
N2–H2N····O1	2.340 (29)	3.166(.005)	169.47 (81)
N2–H2N····O2	2.472 (30)	3.078(.005)	130.17 (53)
N2–H2N····N4	2.647 (37)	2.726(.005)	86.40 (44)
N5–H5N····N8	2.553 (68)	2.687(.005)	84.81 (48)
O4–HOB····O3	2.346 (37)	3.139(.004)	129.41 (66)
O4–HOB····N9	2.422 (40)	3.450(.006)	159.82 (86)
N2–H2N····N2	2.797 (29)	3.567(.005)	154.12 (62)
O4–HOA····N9	2.854 (43)	3.864(.005)	170.24 (48)
C9–H9····O1	2.622 (4)	3.522 (7)	163.27 (29)
C22–H22····O4	2.695 (4)	3.607 (6)	167.03 (30)
C9–H9····N4	2.498 (3)	2.809 (5)	99.76 (26)
C2–H2····N3	2.430 (4)	2.704 (6)	96.89 (29)
C15–H15····N7	2.471 (4)	2.729 (6)	95.91 (29)
C22–H22····N8	2.506 (3)	2.814 (5)	99.54 (28)
C13–H13····O2	2.928 (5)	3.278 (6)	103.92 (29)
C4–H4····N9	2.898 (5)	3.712 (7)	147.02 (31)
C6–H6····O1	2.935 (5)	3.586 (7)	128.31 (30)
C4–H4····O3	2.658 (4)	3.564 (6)	164.67 (30)
C22–H22····O4	2.695 (4)	3.607 (6)	167.03 (30)
C25–H25····O3	2.827 (3)	3.313 (6)	113.83 (29)
C3–H3····O4	2.954 (4)	3.593 (6)	127.17 (30)
C19–H19····O4	2.868 (4)	3.564 (7)	132.58 (32)
C16–H16····O1	2.942 (5)	3.489 (7)	119.02 (35)
C16–H16····π		4.153	
π ····π_{azo}		3.4405	

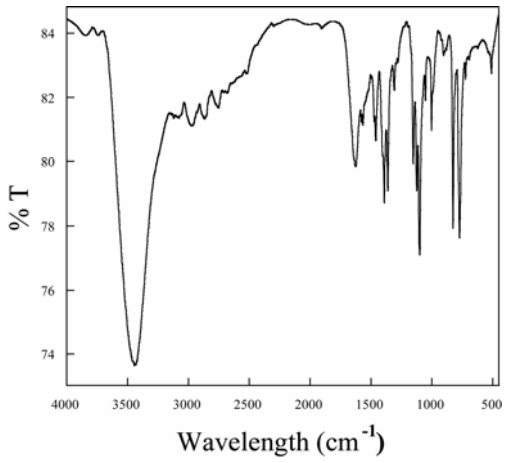

Figure 4.1.A. FT-IR spectra of **L_{10}.**

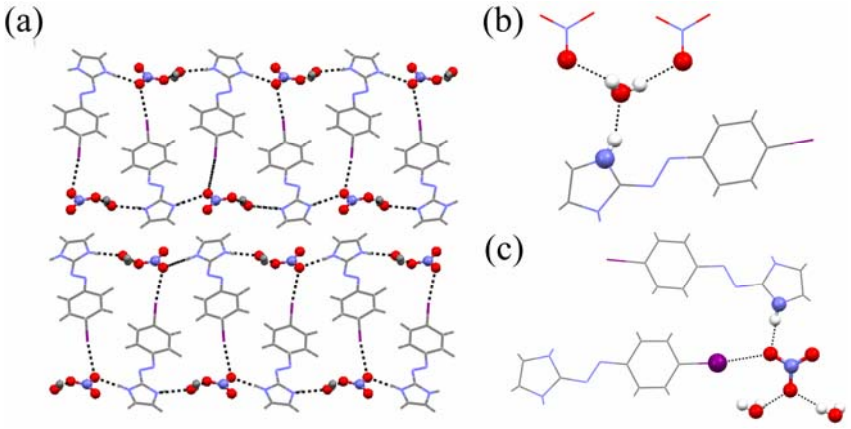

Figure 4.2.A. (a) Packing of salt **2** along *a* axis; (b) Hydrogen bonding pattern of crystal water and (c) NO_3^- anion in salt **2.**

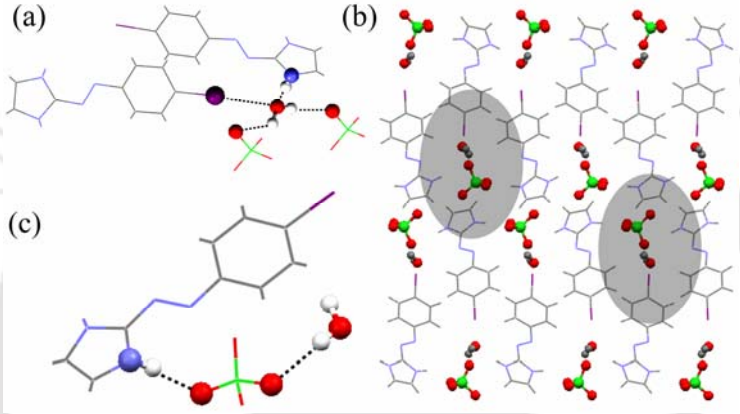

Figure 4.3.A. (a) Hydrogen bonding pattern of crystal water; (b) Elliptical pocket for anion and water in salt 3 along *a* axis and (c) $ClO4^-$ anion in salt **3.**

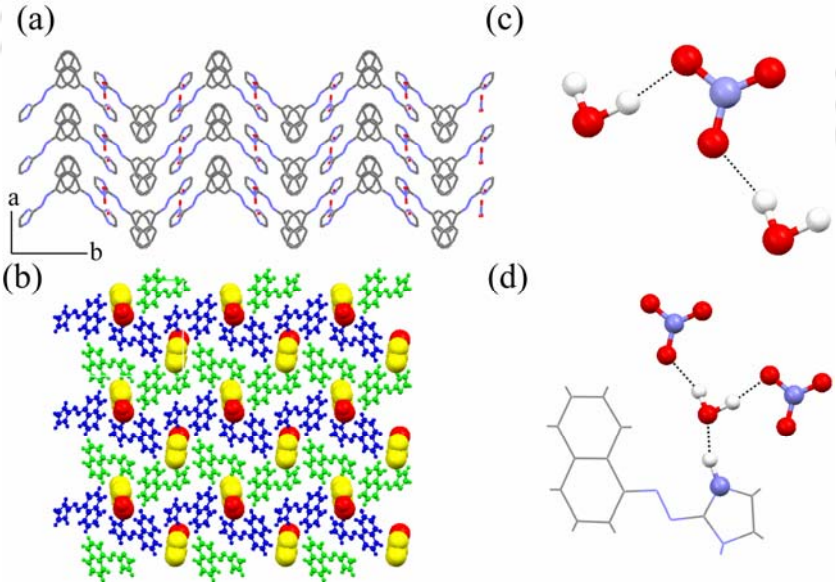

Figure 4.4.A. (a) Packing of salt **5** along *a* axis; (b) Packing of salt **5** along *c* axis; (c) Hydrogen bonding pattern of crystal water and (c) NO_3^- anion in salt **5.**

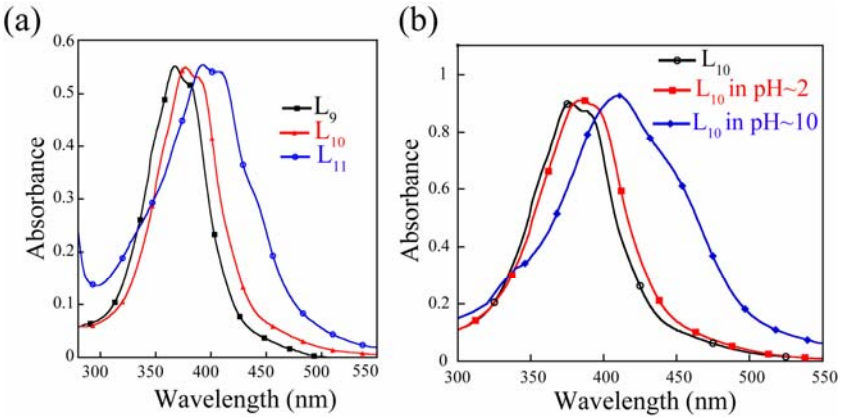

Figure 4.4.A. (a) UV-visible spectra of Ligands (**L_{9-11}**) and UV-visible spectra of **L_{10}** in high and low pH.

Table 4.3.A. Fluorescence quantum yield of **L_{11}** with different anionic input

Sr. No.	Anionic input	Φ_F	$\Phi_F - \Phi_q$
1	Nil	0.025	0.000
2	Br^-	0.019	0.006
3	Cl^-	0.022	0.003
4	SCN^-	0.018	0.007
5	NO_3^-	0.014	0.011
6	ClO_4^-	0.001	0.024
7	CH_3COO^-	0.016	0.009
8	$CF_3SO_3^-$	0.014	0.008
9	BF_4^-	0.020	0.005

Table 4.4.A. Fluorescence quantum yield of **L_{11}** with different concentration of ClO_4^-.

Sr. No.	$[ClO_4^-]$ (M)	Φ_q	Φ_F/Φ_q
1	4×10^{-6}	0.0060	3.5000
2	8×10^{-6}	0.0031	6.7000
3	12×10^{-6}	0.0025	8.3000
4	16×10^{-6}	0.0018	11.700
5	20×10^{-6}	0.0016	13.000
6	24×10^{-6}	0.0013	16.000
7	28×10^{-6}	0.0011	18.900
8	32×10^{-6}	0.0010	21.000

Chapter 5

2-ARYL AZO IMIDAZOLE DYES: COORDINATION CHEMISTRY

5.1 Importance of metal complexes of azo dyes and scope of the work

Azo-dyes with the heterocyclic diazo-component form coloured complexes with many metal ions in solution.[5.1] Great number of the spectrophotometric methods based on these reactions were developed and used in analytical chemistry. It has been known for many years that azo compounds are the most widely used class of dyes due to their versatile application in various fields such as the dyeing of textile fiber and coloring of different materials, and for plastics, biological-medical studies, and advanced applications in organic synthesis.[5.2] It is not surprising that these compounds have become a major environmental concern. Many of these dyes find their way into the environment via wastewater facilities. Because these compounds retain their color and structural integrity under exposure to sunlight, soil, bacteria and sweat, they also exhibit a high resistance to microbial degradation in wastewater treatment systems. They have often been used for micro determination of elements when adsorbed on ion exchange resins, either in ion-exchanger colorimetric methods or in the design of chemical optical sensors. Recently they have received much attention in the field of nonlinear optics, optical storage and other photoelectric applications.[5.3] Thermal analysis plays an important role in the study of the structure and stability of dyes.[5.4] The resistance to heat at elevated temperatures is one of the main properties required of dyes used in high temperature processes such as dyeing, printing and photocopying and in high technology areas such as lasers and electro optical devices.[5.5] Because of the good thermal stability of azo compounds, one of the most important applications of azo compounds is in the optical data storage. Secondly, transition metals as supramolecular building blocks structures of these compounds are of specific interest to the dye and pigment industries, as many of the materials' commercially significant properties (solubility, habit, stability and even colour) are dependent on or are influenced by their solid state structure.[5.6]

Correlating crystal structure to properties is fundamental to the pigment industry, where the colourant is typically used as a crystalline dispersion in the material to be coloured, but it is also of importance in the manufacturing process of both dyes and pigments, for which properties such as solubility and habit must be taken into account. Similarly, the pharmaceuticals industry has recognized the importance of structure–property relationships for some time,[5.7]as well as that elucidating the molecular–recognition properties of molecules is important as this provides insight into the binding behaviour of molecules of substrates. It can be argued that this is equally as relevant to dye–substrate interactions as it is to biological systems. Besides, recently, azo conjugated transition metal complexes have been shown to provide new opportunities towards redox, magnetic

and optical properties originating from the d-orbitals.[5.8] Interest in the transition metal coordination chemistry of the azoimine function (-N=N-C=N-) is rapidly expanding in several areas ranging from organometallic chemistry, metal assisted organic transformation, radical chemistry, stabilization of low valent metal oxidation state to DNA labelling and anticancer medicine. [5.9]

Nitrogen containing heteroaromatic systems have been among the most researched kinds of organic compounds primarily because of their importance[5.10] in pharmaceutical and chemical industries. In fact, a large majority of these compounds are medicinally important,[5.11] and their motifs are found in many natural products. Moreover, owning to the diversity of the coordination modes and high thermal stability, there has been a long-standing interest[5.12] in the coordination chemistry of aryl-azo imidazole ligands. Imidazole is a ubiquitous and essential group in biology, especially as a metal-coordinating site. The *trans*-isomer of this ligand forms stable complexes with several metal ions.[5.13]

We were interested in exploring derivatives of azo-chromophore with imidazole as the heterocyclic component belong to class of organic ligand that contain four nitrogen atoms coupled in conjugated system of π-bonds. We have been focusing on the synthesis, structural and thermal studies of metal complexes of mixed-donor azo dyes.[5.14] Earlier C. Sinha and his group have reported the *N*-substituted (*N*-Me, *N*-Et, *N*-Benz etc) azo-imdazole systems and their coordination assembly process of different metals like Ru(II), Os(II), Zn(II), Cd(II) and Hg(II) salts.[5.15] Herein we have explored the coordination chemistry as well as self-assembly of the azo-imdazole system (Scheme 5.1), we have used a ligand incorporating the electro donating (-Me, -OMe) and halogen (-Cl, -Br, -I) substitutions in *p*-position in phenylazo group in 2-phenylazo imidazole (**L_5**). The unhindered ligand has two different N-donor metal coordination sites along with an efficient hydrogen bond donor site. The complexes are $[Mn(\mathbf{L_5})_2(NCS)_2]$ - **1,** $[Ru(\mathbf{L_5})_2Cl_2]$ – **2,** $[Cu(\mathbf{L_5})_2Cl_2]$ – **3,** $[Cu(II)(\mathbf{L_6})_2(NCS)(SCN)]$ - **4**, $[Cu(II)(\mathbf{L_7})(H_2O)(NO_3)_2]$ - **5**, $[Zn(\mathbf{L_5})_2Cl_2](H_2O)$ – **6,** $[Zn(II)(\mathbf{L_6})_2(NCS)_2]$ - **7**, $[Zn(II)(\mathbf{L_7})(NCS)_2(H_2O)]H_2O$ - **8**, $[Zn(II)(\mathbf{L_9})_2(NCS)_2]EtOH$ - **9**, $[Zn(II)_2(\mathbf{L_{10}})_2(SCN)_4]H_2O$ - **10**, $[Cd(\mathbf{L_5})_2Cl_2](H_2O)$ – **11,** $[Cd(\mathbf{L_5})Cl_2]$ – **12,** $[Cd(II)(\mathbf{L_6})_2Cl_2]$ - **13**, $[Cd(II)(\mathbf{L_7})_2(NO_3)_2]$ - **14**, $[Cd(II)(\mathbf{L_8})_2(NO_3)_2]$ - **15**, $[Cd(II)_2(\mathbf{L_8})_2(SCN)_6]$ -**16**, $[Cd(II)(\mathbf{L_9})_2Cl_2]$ - **17**, $[Cd(II)(\mathbf{L_9})_2(NO_3)_2]$ -**18**, $[Cd(II)(\mathbf{L_{10}})_2(NO_3)_2]$ - **19**, $(H\mathbf{L_5})_2[Hg(II)(SCN)_4]$ – **20,** $(H\mathbf{L_9})_4[Hg(II)(SCN)_4]_2$ – **21.**

We have compared their molecular structure in controlling the higher dimensional supramolecular pattern formation of Mn(II), Ru(II), Cu(II), Zn(II), Cd(II) and Hg(II) salts. We have compared the observed solid-state packing considering the stereo-electronic effect of the substitution on the aniline ring in the aniline-imidazole dyes (Scheme 5.1).

We also have studied the influence of the counter anions on the solid-state packing. We have described the synthesis and characterization of the new ligand $\mathbf{L_5}$. We also studied their comparative absorption spectral behaviors, electrochemical analysis, EPR and thermal studies

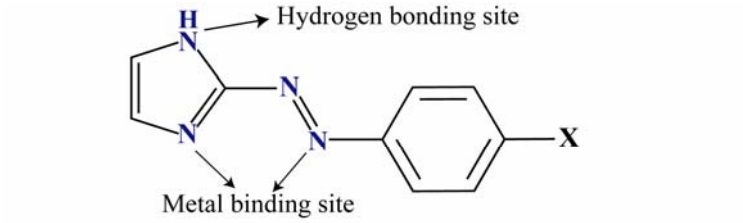

X = -H (L_5), -Me (L_6), -OMe (L_7), -Cl (L_8),-Br (L_9) and -I (L_{10})

Scheme 5.1 2-aryl azo imidazole dyes ($\mathbf{L_5}$ – $\mathbf{L_{10}}$).

5.2. Experimental Section

The Chemicals used were of reagent grade. The sources of the chemicals and solvents have all been recorded in Chapter 2. Synthesis and characterization of the complexes are described in detail in the Appendix of this chapter.

5.3. Results and Discussion

5.3.1. Comparative Crystal Structure Studies of L_5 and L_6

The crystal structure analysis of the ligand $\mathbf{L_5}$ shows that both imidazole and phenyl fragments are planar and the azo group is virtually coplanar with these groups. The dihedral angle between the two least squares planes is only 2.1°. The N=N bond length is 1.254(3) Å, which is smaller than similar system.[5.17] The bonding strength between azo-N(4) and phenyl [C(4)–N(4), 1.408(4) Å] is weaker than that of azo-N(3) and imidazole [C(1)–N(3), 1.373(4) Å]. This suggests that the extent of orbital overlap is more between azo and imidazole moieties than azo and phenyl moieties to form C–N σ-bond. The imidazole N(2)–H2A is intermolecularly hydrogen bonded with a second neighboring imidazole N(1) forming a 1D-chain along the diagonal of the *ac* plane. Phenyl ring of the molecule is arranged alternative direction about the 1D-chain (Figure 5.1a). Moderately intense stretching at 1445–1450 cm^{-1} are due to $\nu_{N=N}$, which shows a significant blue shift by 20–25 cm^{-1} in the complexes relative to the free ligand values.[5.18] In the present studies, we have compared the solid-state structure of the 2-(p-tolylazo) imidazole **($\mathbf{L_6}$)** with unsubstituted 2-(phenylazo) imidazole. In the solid state $\mathbf{L_5}$ contains two symmetrically independent molecules (Figure 5.1a). The substitution in *-p-* position with electron donating group (-CH_3) makes the ligand more planar than the unsubstituted one. Imidazole and phenyl ring are more planar and the azo group is virtually coplanar with these rings.

The dihedral angle between the two least-squares planes is only 1.75° compared to 2.1° in the unsubstituted ligand. The N=N bond length is 1.256(3) Å, which is similar to the previous one but smaller than a similar systems.[5.17] The bonds between azo-N and the phenyl as well as imidazole ring is longer than the unsubstitute system. However, the bond between imidazole ring and azo-N is stronger than the phenyl ring and azo-N, which has a similar trend with the known arylazo systems.[5.18] However, the N=N distance is almost same in both the ligands (1.254 vs. 1.256 in **L_6**). The imidazole N-H forms inter-molecular strong hydrogen bond with the imidazole N atom of the other asymmetric unit (N1····N6= 2.845 Å and N2····N5 = 2.856 Å). It forms a 1D hydrogen bonded chain along the bc plane. The phenyl ring of the molecule is arranged in an alternative direction about the 1D-chain (Figure 5.1b). Solid-state packing results in the formation of alternate hydrophilic and hydrophobic layers, as depicted in Figure 5.2b. The stretching frequency of the endocyclic νc=N bond of L6 appears at 1520 cm-1 and is red shifted by 40-80 cm^{-1} from that of unsubstituted ligand. The $\nu_{N=N}$ mode in the **L_2** appears at 1230-1260 cm^{-1} and is red shifted by 150- 170 cm^{-1} from that of unsubstituted ligand.[5.19,5.20]

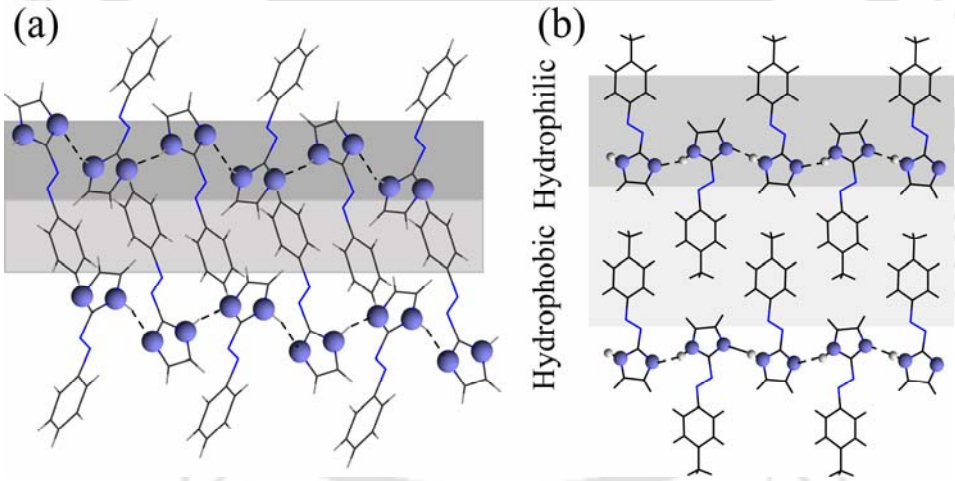

Figure 5.1. Perspective view 1D hydrogen bonded chain of (a) ligand **L_5** and (b) ligand **L_6**.

5.3.2. Comparative crystal structure studies of different the metal complexes

Formation of metal complex with the ligand involves the use of imidazole nitrogen, which was involved in the formation of hydrogen bonded network of ligand. Thus, in the complex 1D hydrogen bonded chain has been broken giving rise to less symmetrical higher dimensional structure. Figure 5.2a shows the molecular structure of the complex **1** [Mn(**L_5**)$_2$(NCS)$_2$] along with the atomic numbering scheme. The neutral monomeric complex consists of a central manganese atom surrounded by two **L_5** ligands and two unidentate NCS^- bonded through borderline N-atom to borderline Lewis acid Mn(II). The Mn atom is sitting at the center of inversion of a tetrahedron and one half of the molecule

is symmetrical with the other half. Azoimidazoles act as both bidentate chelators, N(azo) and N(imidazole),[5.21] as well as monodentate imidazole-N donor ligands.[5.22] Here, each ligand is acting as a unidentate ligand. Metal center forms stronger bond with thiocyanate-N (Mn1-N5=2.101) than imidazole-N (Mn1-N1=2.228). The complexes are non-electrolytes in nature. The N=N bond length is 1.266(2), which slightly greater than the free ligand (*vide supra*). The dihedral angle between the two least squares planes is only 1.74°. Hence, complex formation forced the ligand to become more planar compared to the free ligand. Along *c* axis complex form a flower mosaic structure (Figure 5.2b). The IR spectra of complex **1** exhibit a strong sharp stretch at 2090–2100 cm^{-1} along with a medium strong band at 770–775 cm^{-1} corresponding to $\nu_{C=N}$ and $\nu_{C=S}$ of a coordinated NCS group.[3.20] Mn(II) does not form any bond with azo-N, which has a little influence on the bond length and IR frequency of the –N=N- group. The magnetic moment, μ_{eff}, is ~ 5.2 BM at 300 K as expected for an isolated S = 5/2 (d^5) Mn(II) monomeric complexes.

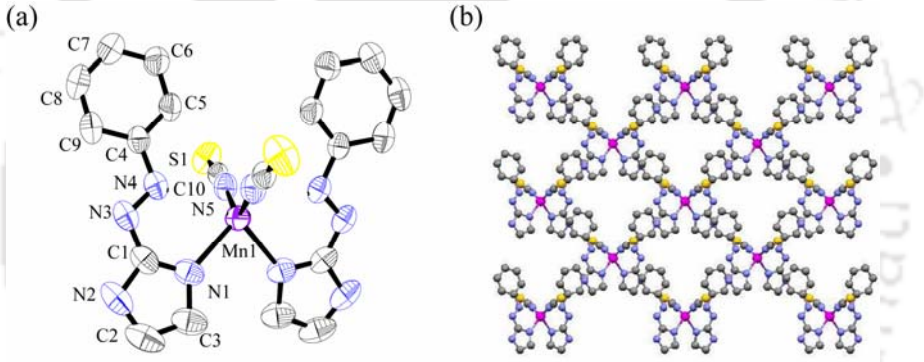

Figure 5.2. ORTEP plot of complex **1**. Thermal ellipsoids set to 50% probability level and (b) packing diagram of complex **1** along *c* axis.

View of the molecular structure of the complex **2** with atom numbering scheme is shown in Figure 5.3a. The distorted RuN_4Cl_2 octahedron coordination is generated by the coordination of two chloride ion and two bidentate chelated $\mathbf{L_5}$. The Ru atom is sitting at the center of inversion of an octahedron and one half of the molecule is symmetrical with the other half similar to the complex **1**. Both the chloride ions occupy the axial position. $\mathbf{L_5}$ is acting as a bidentate ligand. Hence the N=N bond length is largely elongated (1.297(3)) than free azo bond (vide supra). The increase in bond length is undoubtedly due to coordination of N(azo) to Ru which insists $d\pi(Ru) \rightarrow \pi^*(azo)$ back donation. Ru-N(azo) bond is slightly shorter than Ru-N(imidazole), which is indicative of metal–ligand π-interaction that is localized in the M-azo fragment.[3.23] In the solid-state each chloride ion form strong intermolecular hydrogen bonds with neighboring (imidazole)N-H and resulted

in the formation of 2D hexagon layer along *a* axis. In the solid-state it forms flower mosaic architecture (Figure 5.3b) along *c* axis.

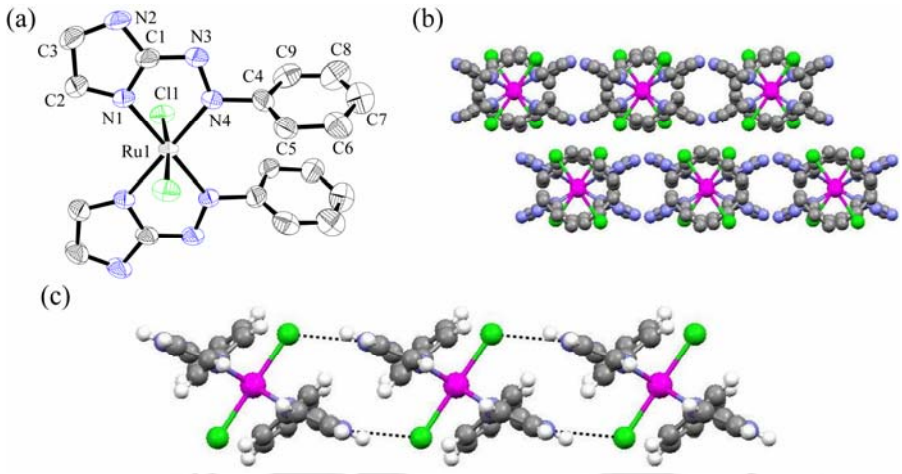

Figure 5.3. ORTEP plot of complex **2**. Thermal ellipsoids set to 50% probability level; (b) packing diagram of complex **2** along *c* axis and (c) Hydrogen bonded hexagon along *a* axis in complex **2**.

The asymmetric unit of the complex **3** contains a neutral monomeric [Cu($\mathbf{L_5}$)$_2$Cl$_2$] molecule (Figure 5.4a). The copper centre has a more nearly octahedral geometry. Cu-N bonds are much stronger than the Cu-Cl bonds. In the solid-state it forms several C–H····Cl, C–H····π weak interactions. The observed C–H····π interactions values are 3.480 Å

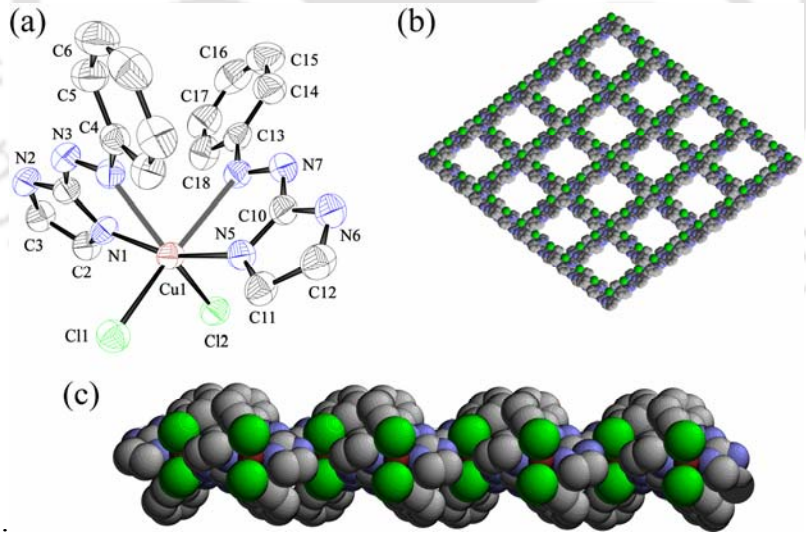

Figure 5.4. (a) ORTEP plot of complex **3**. Thermal ellipsoids set to 50% probability level; (b) Square grid network complex **3** along *a* axis and (c) Helical network of complex **3** along *b* axis.

for C2–H····π, 3.695 Å for C3–H····π, 3.571 Å for C12–H····π, and 3.706 Å C11–H····π respectively. Both chloride ion and the (imidazole)N-H of the complex form strong intermolecular hydrogen bonds extending through the structure. The observed N-H····Cl hydrogen bond distance are 3.112 Å (N2-H····Cl2) and 3.143 Å (N6-H····Cl6)

respectively.[5.24] Along *a* axis it forms a helical network (Figure 5.4c), with two chloride ions forming a square grid network along *b* axis (Figure 5.4b). The magnetic moment of the complex shows ~ 1.77 BM which can be assigned the existence of distorted octahedral Cu(II) mononuclear complex.

Complex **4** [Cu (II)($\mathbf{L_6}$)$_2$(NCS)(SCN)] along with the numbering scheme is shown in Figure 5.5a. It forms axially elongated neutral monomeric square pyramidal complex (τ = 0.05)[5.25] with two ambiedent SCN^- bonded to Cu(II). The anion SCN^- is bonded with Cu(II) in equatorial position with N donor (Cu – N = 1.998 Å) whereas in axial position with S donor (Cu – S = 2.559 Å). Normally in biological system Cu^{II}Pc (plastocyanin) contain Cu(II) bonded with S atom of costive thiolate or neutral methodize thioether,[5.26] but the complex of Cu(II) with thiocyanate (SCN^-) is very rare. One of the ligands bonded to the Cu(II) in bidentate manner in the equatorial plane. Cu(II) lies exactly on the equatorial plane formed by four coordinating atoms. Both the axial bonds are bent on the same direction with respect to the equatorial plane. Bite angle of the ligand in the equatorial plane is much smaller (~ 74^o) than other angles in the equatorial plane. In the solid-state it forms several C–H····N, C–H····S, C–H····π weak interactions. One of the imidazole N–H forms N–H····π interaction with π-bond of the C=N group in the equatorial NCS ion. It forms 3D hydrogen bonded flying wedge network architecture (Figure 5.5b). All the metal ions are line up along *b* axis. Analysis of the packing diagram of Complex **4** reveals that in each complex only one of the two imidazole N–H is forming strong conventional hydrogen bond (N–H····N = 2.717 Å) with the thiocyanate N of a neighboring molecule in the same layer. Moreover, there exist weak C–H····S and C–H····π interactions between neighboring molecules. Cumulative effects of these non-covalent interactions lead to the formation of 1D helical architecture along *b*-axis (Figure 5.5c). Along these chains two Cu(II) atoms are separated by 9.423 Å and the repeating period in the helical column is about 11.817 Å. In this system an inner channel runs parallel to the helical axis. The IR spectra of complex **4** exhibit a strong sharp stretch at 2090 and 2070 cm^{-1}, which corresponds to the $\nu_{C=N}$ of the SCN and NCS coordinating anion respectively.[5.19] The medium intense peak at 772 cm^{-1} corresponds $\nu_{C=S}$ stretching of the coordinated anion.[5.20] The magnetic moment, μ_{eff}, is ~ 1.78 BM at 300 K as expected for an isolated S = ½ (d^9) Cu(**II**) monomeric distorted square pyramidal complex.

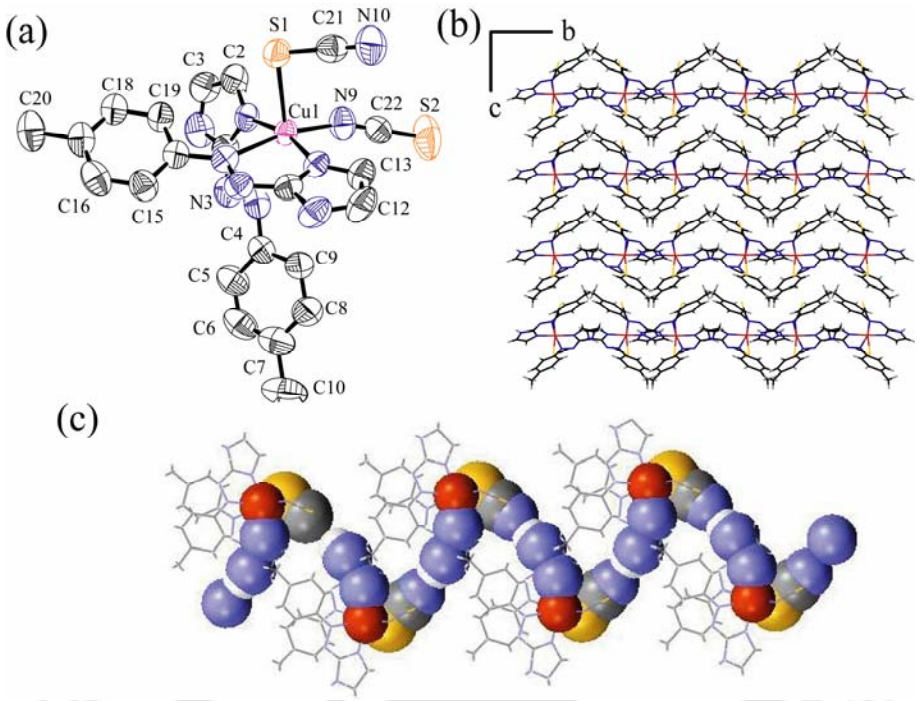

Figure 5.5. (a) ORTEP plot of complex 1. Thermal ellipsoids set to 50% probability level; (b) packing of complex **4** viewed along a axis and (c) view of intermolecular N–H····N interactions between adjacent molecules that lead to the formation of a 1D helical chain in complex 1 along b axis.

In absence of NH_4SCN, $\mathbf{L_7}$ forms a neutral monomeric complex [Cu(II)($\mathbf{L_7}$)(H_2O)(NO_3)$_2$] (5) when treated with Cu(NO_3)$_2$ (Figure 5.6a). The Cu(II) centre has distorted square pyramidal coordination geometry ($\tau = 0.05$).[5.25] Both the NO_3^- are monodentated in nature.

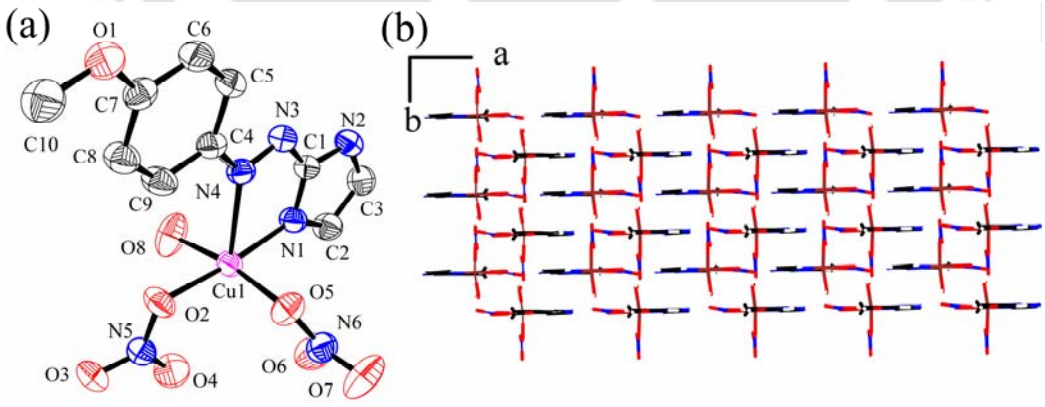

Figure 5.6. (a) ORTEP plot of complex **5**. Thermal ellipsoids set to 50% probability level and (b) packing of complex **5** viewed along *c* axis.

Cu(II) atom lies exactly on the square plane. Azo-N forms the axial bond (Cu–N4 = 2.3787). $\mathbf{L_7}$ act as bidentate chelating ligand. Equatorial bite angle is similar (~ 75^o) to that of the Cu(II) complex **5**. Imidazole-N forms strong hydrogen bond with nitrate-O atoms. Metal bound water forms strong O–H····O type hydrogen bond with neighboring nitrate-O atoms. Methoxy group is involved in C–H····O type hydrogen bond. Additionally π ••• π

interaction plays the crucial role for forming brick wall structure along ab plane (Figure 5.6b), in the solid-state. Complex **5** shows the strong sharp peak at 1497, 1271, 992 cm^{-1} which can be defined as the $\nu_{N=O}$ stretching frequency of the unidentate bonding of nitrate anion.[5.19] The magnetic moment of the complex shows ~ 1.89 BM which can be assigned the existence of square- pyramidal Cu(II) mononuclear complex.[5.27]

The molecular structure of Complex **6** is shown in Figure 5.7a. The structure shows a distorted tetrahedral structure with ZnN_2Cl_2 coordination. In the coordination zone two chloride groups and the two $\mathbf{L_5}$ act as monodentate imidazole-N donor ligands. The distortion from a regular tetrahedral geometry is reflected from the metric parameters: Zn–N(imidazole) (Zn1–N1=2.0341(14) and Zn1–N5=2.0134(15) Å) is shorter than Zn–Cl (Zn1–Cl1=2.2403(6) and Zn1–Cl2=2.3436(6) Å). The N=N distances is different for two bonded $\mathbf{L_5}$. The ligand with smaller N=N distance (N7-N8 = 1.248(2)) than free $\mathbf{L_5}$ in more planar (the dihedral angle between the two least squares planes is only 1.14°). On the other hand ligand unit having longer N=N distance (N7-N8 = 1.261(2)) are less planar (the dihedral angle between the two least squares planes is only 5.41°). Unlike complex 1, the tetrahedron is not a symmetric one. Here, both the chloride is directed in the opposite direction of the ligand. Imidazole unit is coordinated to the metal center from the opposite direction Asymmetric unit contains one water of crystallization. Packing along *a* axis shows the intermolecular hydrogen bonded network. One of the imidazole N-H form intermolecular hydrogen bond with chloride ion and another one form intermolecular hydrogen bond with water molecule. Water molecule form strong intermolecular hydrogen bond with chloride and imidazole N-H, which result in the formation of hydrogen bonded chain along *b* axis (Figure 5.7b). The FT-IR spectra of complex **6** exhibit strong stretches at 2190, 2140 cm^{-1}, and 685 cm^{-1} which are in agreement with $\nu_{C=N}$ and $\nu_{C=s}$ respectively.[5.19,5.20]

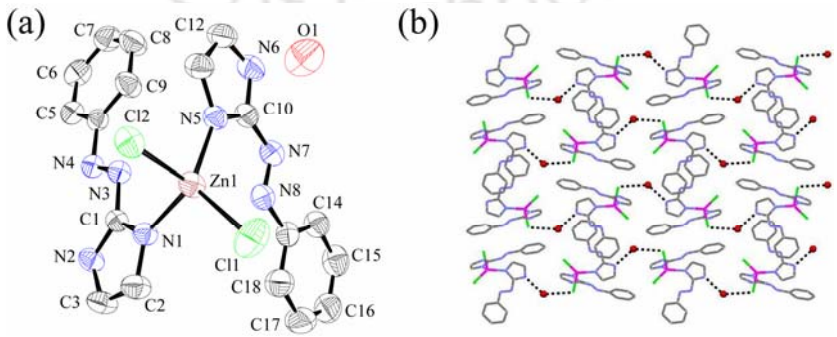

Figure 5.7. (a) ORTEP plot of complex **6**. Thermal ellipsoids set to 50% probability level and (b) formation of water assisted intramolecular H-bonded chain along b axis in complex 6.

In contrast to the Cu(II) complex **4** with ligand $\mathbf{L_6}$, Zn(II) forms completely different coordination geometry with the same ligand in same reaction condition. Zn(II) complex **7** forms mononuclear, neutral distorted tetrahedral complex (Figure 5.8a), which proved by the range of angles around Zn(II) center. Moreover, ambidentate thiocyante ion binds to the Zn(II) center only through N-atom, unlike to the complex **4**. Difference in coordinating behavior of the thiocyanate ion in complex **4** and **7** can be explained on the basis of HSAB principle. Both the ligands are unidentate and they are oriented in the cis orientation relative to the metal center. Ligands are oriented in the opposite direction to each other. Careful analysis of the crystal packing diagram reveals that both the imidazole-NH form N–H····S type hydrogen bond with neighboring same thiocyanate-S atom. However, other thiocyanate-S atom is involved in weak C–H····S type non-covalent interactions in the solid-state. Benzene ring of one ligand in the asymmetric unit is forming π-stacking interactions (π····π, 3.667Å) with the nearest imidazole ring of the same ligand. Other ligand in the asymmetric unit does not form this type of interactions as it is oriented perpendicularly with the neighboring similar ligand. It forms 3D honeycomb network structure along *bc* plane in the crystal (Figure 5.8b). The FT-IR spectra of complex **7** exhibit strong stretches at 2190, 2140 cm^{-1}, and 685 cm^{-1} which are in agreement with νC=N and νC=s respectively.[5.19,5.20]

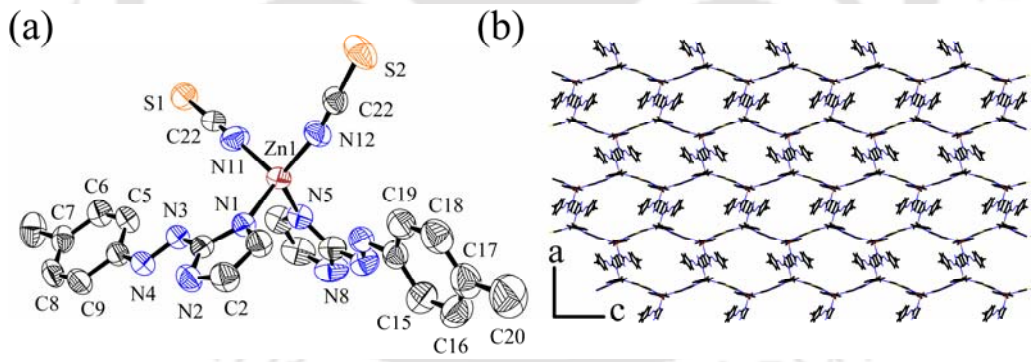

Figure 5.8. (a) ORTEP plot of complex 7. Thermal ellipsoids set to 50% probability level and (b) packing of complex **7** along *bc* plane.

In similar reaction condition but different crystallization condition, $\mathbf{L_7}$ forms Zn(II) complex with trigonal bipyramidal (TBP) geometry[5.28] (τ = 0.88). Zn(II) complex **8** is surrounded by two thiocyanate linkage, one bidentate ligand $\mathbf{L_7}$ and one water molecule (Figure 5.9a). Zn(II) atom lies exactly on the equatorial plane. Azo-N and water is in the axial position. Ligand is behaving as a bidentate ligand, in contrast to the Zn(II) complex **7**. The molecular packing shows a 1D coordination polymer running along the *c* axis. Distances between two nearest Zn(II) ions in the polymer chain is 6.673 Å. Ligand in the

adjacent 1D polymeric chain is directed in the opposite direction. Closest inter chain distance is 3.698 Å. Water of crystallization form one strong N–H····O hydrogen bond and three more weak hydrogen bonds. It forms a 1D water chain along *c* axis (Figure 5.9c). Metal bound water simultaneously forms weak hydrogen bonds with two adjacent S atoms of SCN ion and acting as bridge. It forms a ten member chair type hydrogen bonded ring (Figure 5.9b). The IR spectra of complex **1** exhibit a strong sharp stretch at 2182 and 2130 cm^{-1}, which corresponds to the $\nu_{C=N}$ bond and 680 cm^{-1} which corresponds to $\nu_{C=S}$ respectively.[5.19,5.20]

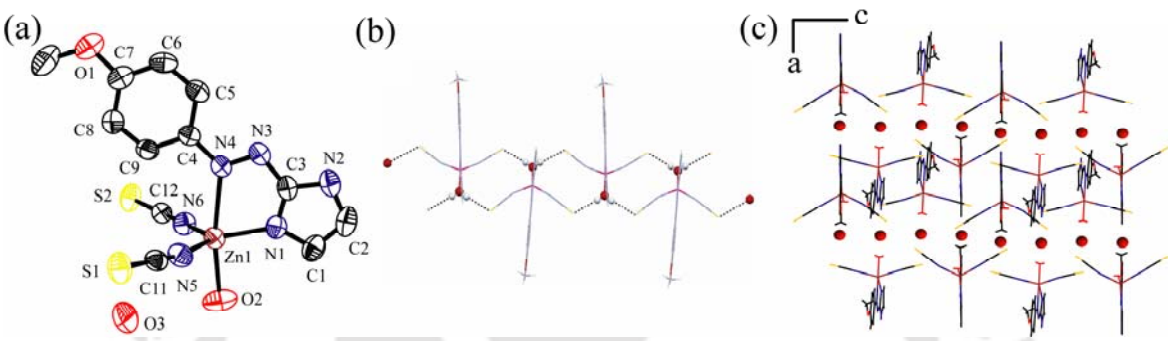

Figure 5.9. ORTEP plot of complex **8**. Thermal ellipsoids set to 50% probability level; (b) packing of complex **8** along *b* axis and (c) Water bridge ten member chair type hydrogen bonded architecture in complex **8**.

Similar to that the *p*- halo substituted ligand $\mathbf{L_9}$ also form mononuclear neutral distorted tetrahedral Zn(II) complex **9**. Metal is bonded to two unidentate $\mathbf{L_9}$ ligands and two thiocyanate moieties (Figure 5.10a). Asymmetric unit contains one EtOH solvent molecule. The structure of the complex **7** and **9** are similar, however due to the difference in electronic and structure property of the *para* substitutent coordination bond length and angles are different. Imidazole-N-Zn-N-imidazole bond angle in complex **9** is higher than complex **7** (112.67 vs. 104.23). Ligands are almost planner in both the complex. There is strong hydrogen bonding interaction between ethanol O-atom and imidazole N–H, while the other imidazole N–H forming weak N–H····S hydrogen bond.

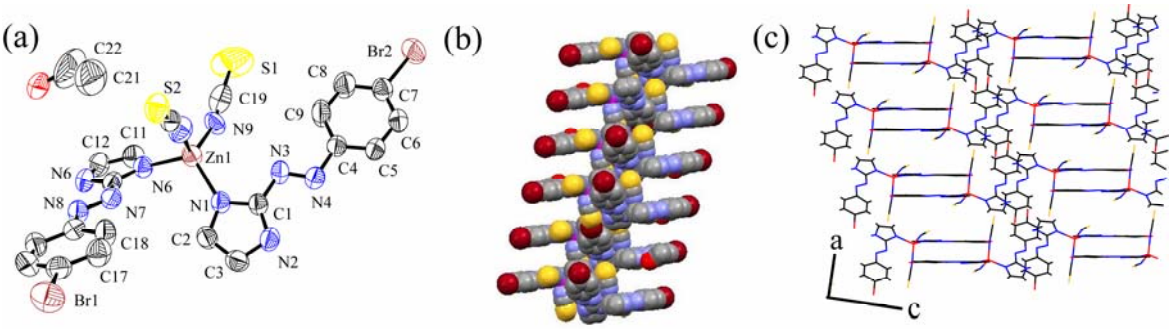

Figure 5.10. (a) ORTEP plot of complex **9** with out the solvent. Thermal ellipsoids set to 50% probability level; (b) stair case structure of complex **9** along *b* axis and (c) ladder like structure of complex **9**.

EtOH is forming weak interaction with SCN also. There is a weak non-bonded interaction between Br atom with the S1 (Br2····S1 = 3.464 Å).[5.29] In the solid-state it forms ladder like structure (Figure 5.10c). It forms stair case structure when viewed along *a* axis (Figure 5.10b). The FT-IR spectra of complex 5 exhibit strong stretches at 2186, 2133 cm^{-1} and 678 cm^{-1} which are in agreement with $\nu_{C=N}$ and $\nu_{C=s}$ respectively.[5.19,5.20]

The ligand **L_{10}** is also formed complex with Zn(II) ion. However, in contrast to the mononuclear complex formed by other ligand, it forms binuclear complex (Figure 5.11a). Neutral binuclear complex is formed by thiocyanate bridging. Each metal center is coordinated by three N-atoms, one from unidentate **L_{10}** and two from NCS ligands. Fourth coordination site is occupied by S-atom of bridging SCN ion which is very kind of coordination for Zinc(II) complex.[3.50] The coordination sphere around the central ion is distorted square-pyramidal (τ = 0.86) geometry. One water molecule is present in the crystal lattice. Water forms stronger hydrogen bonds with imidazole N–H, and weaker C–H····O, O–H····S hydrogen bonds. In the lattice C–H····I interactions are also present. The molecular packing shows that each binuclear motif forms 1D curvy layer along the diagonal of *bc* plane (Figure 5.11c). Water molecules are arranged linearly in between these layers. Bridging pseudo-halogen unit forms cyclic 8-membered chair form (Figure 5.11b). The Infrared spectra of this complexes exhibit strong stretches at 2190, 2140 and 685 cm^{-1} which corresponds to $\nu_{C=N}$ and $\nu_{C=S}$ stretching frequency respectively.[5.19,5.20]

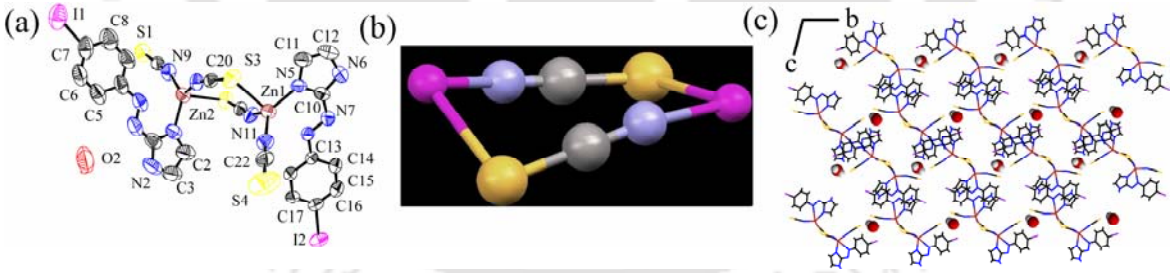

Figure 5.11. (a) ORTEP plot of complex **10**. Thermal ellipsoids set to 50% probability level, (b) View of the 8-membered $Zn_2(SCN)_2$ pseudo-halogen in a chair form and (c) packing diagram of complex **10** along *a* axis

The molecular structure of the non-ionic complex **11** is shown in Figure 5.12a. The Cd(II) salt is surrounded by two unidentate **L_5** and two chloride ion in a tetrahedral fashion. Metal ion is away form the center of inversion of the tetrahedron. Both the Cd-Cl bonds are largely elongated compared to the Cd-N bonds. Both the ligands are disposed in the opposite direction with respect to the Cd-N bond. Both the N=N bonds are similar to that of free ligand as azo-N is not involved in bonding with metal center. Asymmetric unit contain one water molecule. It forms stronger hydrogen bonds between (imidazole)N-H

and chloride ion. Chloride forms strong intermolecular hydrogen bonds with water and (imidazole) N-H. Overall intermolecular hydrogen bonding results in the formation of 3D square grid network (Figure 5.12c) and it is a infinite chain of $[Cd(\mathbf{L_5})_2Cl_2H_2O]_n$ In the solid-state water forms a linear wave along *a* axis.

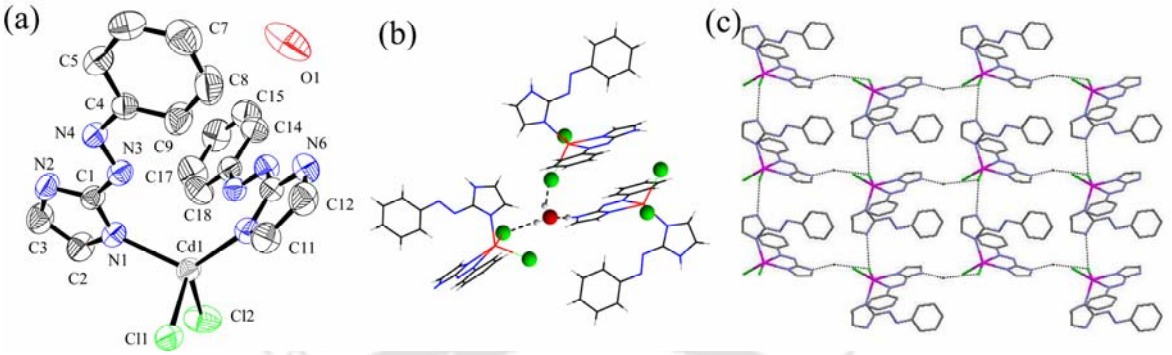

Figure 5.12. (a) ORTEP plot of complex **11**. Thermal ellipsoids set to 50% probability level; (b) Hydrogen bonding of water molecule in Complex 5 and (c) packing of complex **11** along *a* axis.

Cadmium permits a wide variety of geometries and coordination numbers for its d^{10} configuration. We have tried to exploit its coordination behavior by changing the solvent of crystallization. When crystallization was taken place in presence of dry ethanol we got mononuclear complex (**12**) with out any water of crystallization in contrast to the complex **11**. This solvent induced change in coordination behavior in the solid-state is attributed to factors such as crystal packing, hydrogen-bonding forces, relative Cd–Cl bond strength and ease of formation of the cadmium chloride framework.

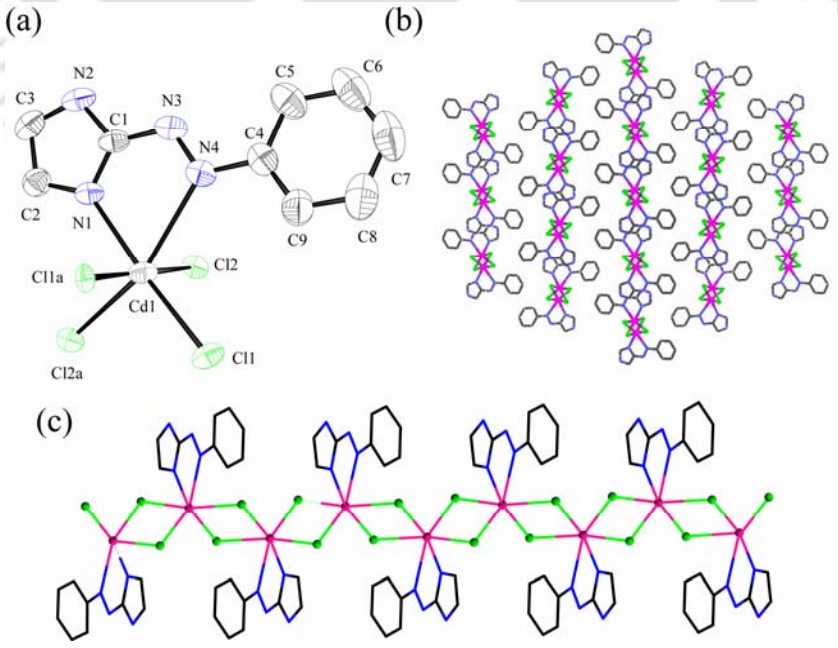

Figure 5.13. (a) ORTEP plot of complex **12** Thermal ellipsoids set to 50% probability level; (b) Flower mosaic packing of complex 12 along *a* axis and (c) packing of complex **12** along *a* axis.

Complex **12** crystallizes as infinite $CdCl_2$ chains in which cadmium atoms are doubly bridged by pairs of chloride atoms; ligand complete the pseudo-octahedral coordination of the cadmium atoms (Figure 5.13a) and link the $CdCl_2$ chains to form extended 3D layers. In both the complex Cd-N(imidazole) bond length is within the range of typical Cd-$N_{aromatic}$ bonding distances. The Cd-Cl bond lengths in both complexes are also within the range of typical values.[5.31] In complex **12**, one of the Cd–Cl bond lengths is relatively higher, where in complex **11** both are in the normal range. This increased in Cd–Cl bond length in **12** because of the increased electron density at the cadmium with donation of from softer electron rich azo-N. This has been suggested as the reason for similar systematic structural changes observed in a series of cadmium halide complexes with chelating nitrogen macrocyclic ligands.[5.32] The $CdCl_2$ chains propagate and stack along *a* axis. In contrast to the complex **11**, in complex **12** ligand is almost planar (∠C1-N3-N4-C4=179.83°). In complex **11** both *ortho* and *meta* C–H group form short contact with Cl atom while in **12** only one *ortho* C–H group form C–H···Cl type interactions. We observe N=N bond elongation (1.265(3) Å) compared to the free ligand, as azo-N participate in the coordination to the metal center. The complex forms flower mosaic packing along *a* axis (Figure 5.13b) and self-assembled ladder structure along *b* axis (Figure 5.13c).

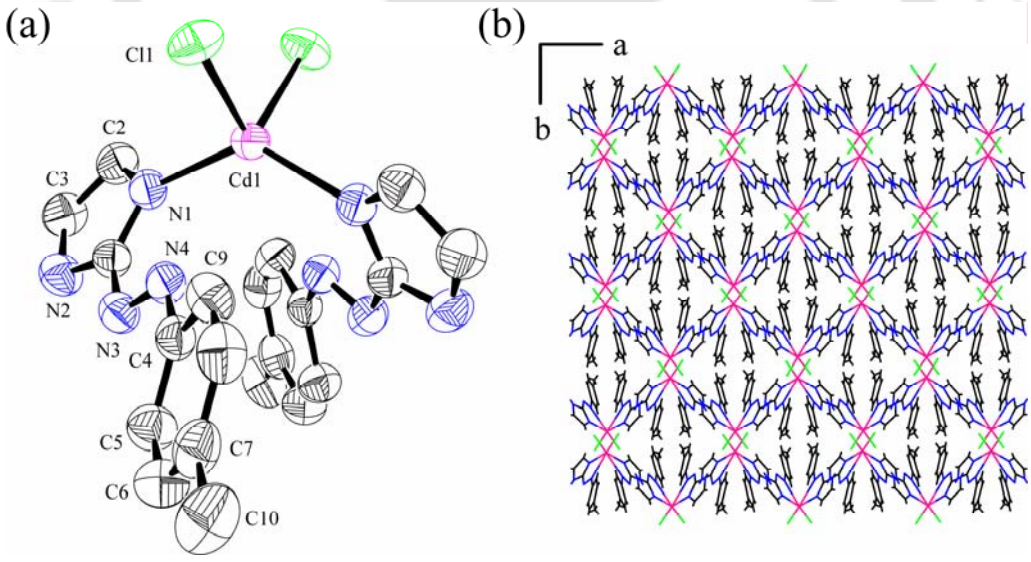

Figure 5.14. (a) ORTEP plot of complex **13**. Thermal ellipsoids set to 50% probability level and (b) packing of complex **13** along *a* axis.

In presence of $CdCl_2$ ligand $\mathbf{L_6}$ is forming neutral mononuclear complex **13** ((Figure 5.14a)). Cd(II) is surrounded by two unidentate $\mathbf{L_6}$ ligand and two Cl^- ion in distorted tetrahedral fashion. Both the ligand is disposed in the opposite direction with respect to the metal center. Imidazole-N-Cd-N-imidazole angle is 133.88°, which much higher than

tetrahedral angle. Torsion angle between two ring of the ligand is 4.86° *i.e.* ligand is less planar than the previous complex of $\mathbf{L_6}$. Each imidazole N–H for relatively strong hydrogen bond with neighboring coordinated chloride ion. This has a significant role in the formation of 3D network of rhombohedra, where each of them shared their corner with the adjacent one. *para* substitute Methyl group form weaker C–H···π interactions. This interaction helps to form 1D chain along *c* axis. Complex **13** forms flower mosaic architecture (Figure 5.14b), in the solid-state.

In presence of $Cd(NO_3)_2$ ligand $\mathbf{L_7}$ is forming neutral mononuclear complex **14** (Figure 5.15a). The molecular structure shows that Cd(II) ions adopt a distorted octahedral geometry. Metal center is surrounded by two unidentate ligands and two bidentate chelating nitrate groups. Both the ligands are in the same side of the metal ion. Imidazole N atoms form stronger bond than the oxygen atoms of the nitrate groups.[5.33] Each imidazole N–H for relatively strong hydrogen bond with the O-atom of the neighboring coordinated NO_3^- ion. The C–H moiety adjacent to the imidazole nitrogen forms C–H···O type hydrogen with O-atom of the neighboring coordinated NO_3^- ion. These combinations of interactions result in the formation of diamond shape 3D coordination polymer. The packing diagram reveals the self-assembly of the complex **14** in the formation of a flower mosaic architecture when viewed along *c* axis (Figure 5.15b). The FT-IR spectra of Cadmium nitrate complexes exhibit strong stretches at 1420, 1275, 980 cm^{-1} which are in agreement with coordinated O-NO_2 moieties. [5.19,5.20]

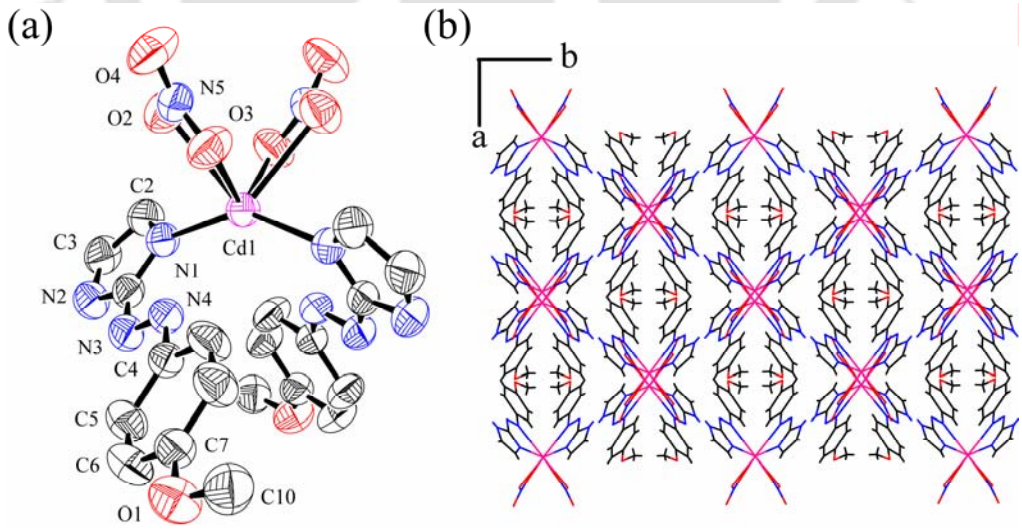

Figure 5.15. (a) ORTEP plot of complex **14**. Thermal ellipsoids set to 50% probability level and (b) packing of complex **14** along *a* axis.

Alcoholic solution of $\mathbf{L_8}$ in presence of $Cd(NO_3)_2$ form neutral mononuclear complex **15** (Figure 5.16a)), similar to the ligand $\mathbf{L_7}$. Complex **15** consists of a central cadmium atom

surrounded by two **L_8** ligands and two bidentate NO_3^- counter anions. Complex **14** and **15** are iso-structural. An intermolecular weak hydrogen bond is observed between imidazole N-H with the O-atom of the coordinated NO_3^- ions of the neighboring molecule and constitutes hydrogen bonded flower mosaic (Figure 5.16b) structure similar to that of complex **14**. However, complex **15** form bifurcated C–H···O type hydrogen bond with two adjacent O-atom of the NO_3^- ions resulted in the formation of four-member cycle.[5.34] The IR spectra of complex **15** are showing three characteristic peaks at 1415, 1280 and 990 cm^{-1} corresponds to NO_3^- ion.[5.19,5.20] The strong peaks at 1610 cm^{-1} and 1407 cm^{-1} corresponds to the $\nu_{C=N}$ and $\nu_{N=N}$ stretching frequencies in the complexes respectively.

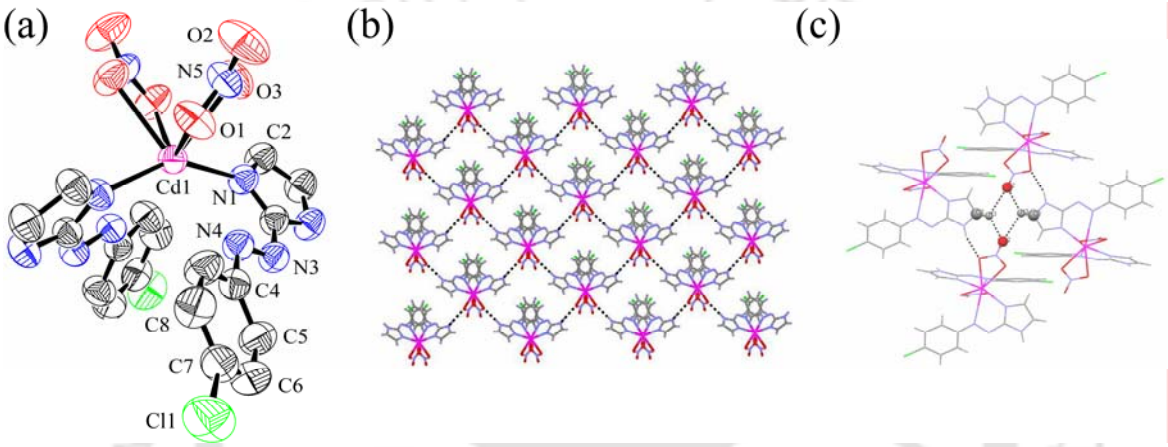

Figure 5.16. (a) ORTEP plot of complex **15**. Thermal ellipsoids set to 50% probability level; (b) packing of complex **15** along *a* axis and (c) bifurcated C–H···O type hydrogen bond in complex **15.**

During the synthesis of complex **15**, addition of two equivalent of NH_4SCN resulted in the formation of a binuclear complex **16** (Figure 5.17a). In the single crystal we observed that ligand is coordinated to the metal in bidentate fashion, unlike previous complex. Here we have shown that, the bond length of azo group (N_3=N_4) and associated angles does not change with the mode of binding to the metal ion. However, Cd-N1 bond distance increased by 0.06 Å with respect to the complex **15**. Bidentate NO_3^- in complex **15** is replaced by unidentate ambidentate SCN^-. Each cadmium (II) atom is in a slightly distorted octahedral arrangement. The dihedral angle between two least square planes is 5.41°. Interestingly, out of four SCN^- counter anions, two is coordinated through nitrogen and two through sulfur atoms. Two Cd atoms are doubly bridged by two SCN^- ions, similar to the Zn(II) complex **10**. However, here thiocyanate anion acts as a both terminal and bridge ligand. It is of much interest to observe that there is no strong hydrogen bonding interaction in the crystal structure. Thiocyanate anions are connected via metal knots in a face to face mode and edge to edge fashion to form 3D $[Cd(SCN)_2]_\infty$ coordination polymer of honey comb network (Figure 5.17c). Each Cd (II) ions from the

neighboring metallo-macrocycles are bridged by two thiocyanate groups in a μ2 end-to-end mode. Two anti-parallel thiocyanate ligands with two metal atoms form an 8-membered $[Cd_2(SCN)_2]$ parallelogram with edge lengths of 2.782 Å, (Cd1-S1) and 2.271 Å, (Cd1-N5) and angles of 79.83° (∠S1-Cd1-S2) and 96.97° (∠N5-Cd1-N6), respectively. The corresponding Cd-N-C bonds are almost linear (∠Cd1-N6-C11=164.99°, ∠Cd1-N5-C10=160.21°), whereas the Cd-S-C linkages are rather bent (∠Cd1-S2-C11=97.62°; ∠Cd1-S1-C10=103.30°). The Cd····Cd distance across the bridging thiocyanate anions is 5.776 Å. Bridged SCN^- form stronger Cd-S bond than the terminal SCN^- counter anion. Whereas terminal Cd-N bond is shorter in length compared to bridged Cd-N bond. However, in the solid-state they form several weak N–H····S and C–H····S type hydrogen bonding. Coordinated ligand is directed in the opposite direction in the adjacent metal center. Complex **16** form bifurcated N–H····S type hydrogen bond with two adjacent S-atom of the SCN^-.

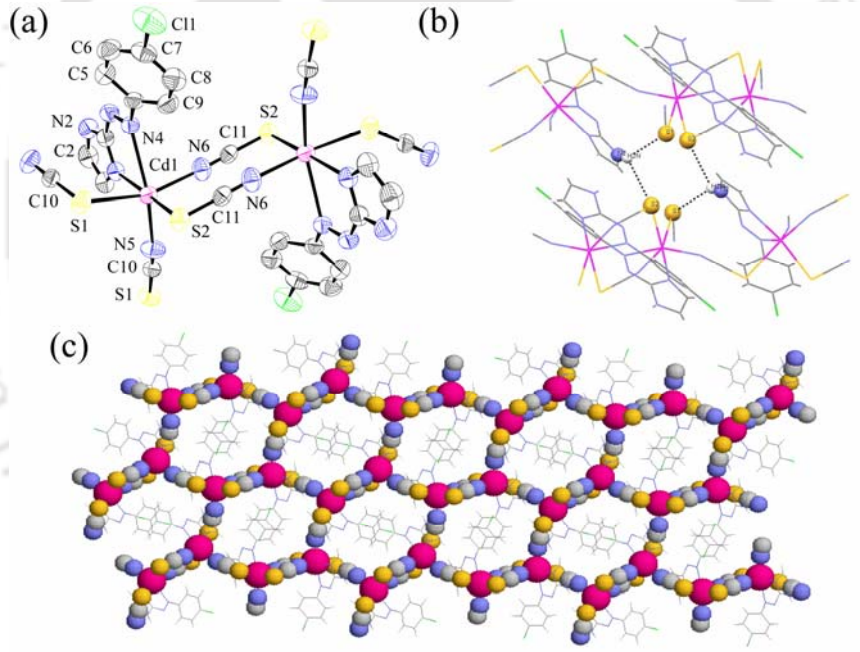

Figure 5.17. (a) ORTEP plot of complex **16**. Thermal ellipsoids set to 50% probability level (b) Bifurcated N–H····S type hydrogen bond and (c) Honey comb network structure of complex **16** along *a* axis.

In presence of $CdCl_2$, ligand $\mathbf{L_9}$ forming complex **17**, this is iso-structural with complex **13** (Figure 5.18a). Cd(II) is surrounded by two unidentate $\mathbf{L_9}$ ligand and two Cl^- ion in distorted tetrahedral fashion. Both the ligand is disposed in the opposite direction with respect to the metal center. Imidazole-N-Cd-N-imidazole angle is 133.40°, which much higher than tetrahedral angle. Bond length and bond angle around the metal center of these complexes are almost same. However, the dihedral angle between two least square planes of the ligands is 3.37°, which indicates that ligand is more planar the in the complex **13**.

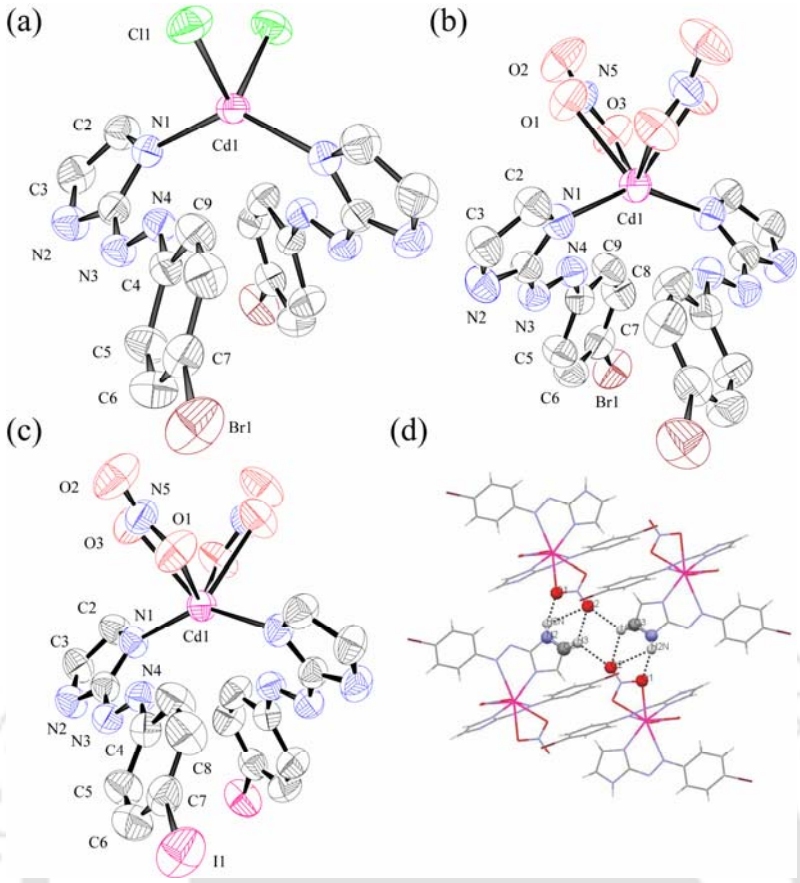

Figure 5.18. (a) ORTEP plot of complex **17**. Thermal ellipsoids set to 50% probability level; (b) ORTEP plot of complex **18;** (c) ORTEP plot of complex **19** and (d) Bifurcated C–H···O type hydrogen bond in complex **18.**

In this complex form C–H···Cl interaction is found, which is absent in the complex **13**. This can be attributed to the presence of electron withdrawing group Br adjacent to the C–H, which forms this weak hydrogen bond. In the solid-state similar flower mosaic architecture is formed. Br atom attached to benzene ring form weak interaction with the π-cloud of the neighboring imidazole ring in the solid-state (Br••••π = 3.567 Å).[5.35] Ligand $\mathbf{L_9}$ and $\mathbf{L_{10}}$ forms Cd(II) complex **18** and **19** respectively. These two complexes are iso-structural with complex **15** (Figure 5.18b, 5.18b). The Cadmium centre is in a distorted octahedral position surrounded by an N_2O_4 coordination sphere. All these complexes form similar weak N–H···O, C–H···O type interactions like complex **15**. Similar bifurcated C–H···O type hydrogen bond also formed with two adjacent O-atom of the NO_3^- ions resulted in the formation of four-member cycle. These weak hydrogen bond interactions have same bond length and angle associated with it in all these complexes. They have similar packing in the solid-state.

Cadmium and mercury are chemically similar[5.36] and we could apprehend structurally identical compounds of $\mathbf{L_5}$. However, $\mathbf{L_5}$ when treated with $HgCl_2$ in presence of NH_4SCN it forms a complex of the structure of $[\mathbf{L_5}]_2[Hg(SCN)_4]$ composition. As shown in Figure

5.19a, the structure of compound **20** consists of a simple ionic salt of two mono cationic ligand $\mathbf{L_5}$ and tetrathiocyanatomercurate dianions. SCN^- is an ambidentate ligand. It binds to soft/boarder line metal ions by the S-donor centre that makes the metal ions softer than its precursor. The symbiosis is the leading force for the formation of central dianion with out the coordination form the ligand. The tetrahedral coordination of Hg(II) of the anion is fulfilled by four monodentate SCN ligands. The sp^2 N atom of the imidazole ring in $\mathbf{L_5}$ is protonated. Each of the terminal N atoms of the SCN ligands forms strong hydrogen bonds with neighboring N–H of the $\mathbf{L_5}$. Tetrahedral anion takes a propeller shape and surrounded by cationic $\mathbf{L_5}$. Planar monocationic $\mathbf{L_5}$ stacks along *b* axis forming a 2D sheet structure. Each of the 2D layers is interconnected by the central complex anion forming a 3D chain along the diagonal of the *ac* plane (Figure 5.19b). The molar conductance (Λ_M) of complexes lies between 100 and 120 Ω^{-1} cm^2 mol^{-1} suggesting a 1:1 type electrolytic nature of the compounds.

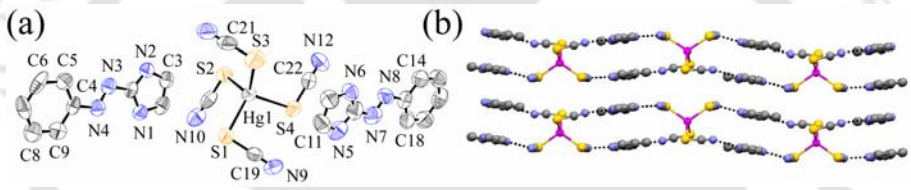

Figure 5.19. (a) ORTEP plot of complex **20**. Thermal ellipsoids set to 50% probability level and (b) packing of complex **20** along *a* axis.

In presence of NH_4SCN, ligand $\mathbf{L_9}$ does not coordinate to the softer Hg(II) ion when treated with $HgCl_2$. Hg(II) prefers to bind softer S-atom of thiocyanate and form a tetrahedral anionic complex (**14**) $[Hg(SCN)_4]^{2-}$.[5.37] Two $\mathbf{L_9}H^+$ is acting as counter cation in the crystal lattice (Figure 5.20a). Each of N-atom in the free end of the coordinated SCN group form several stronger N–H····N type hydrogen bond with the protonated imidazole N–H group. In the solid-state it also forms several week C–H····N, C–H····S and C–H····Br type interactions. It forms layer of cations and anions in the 3D network in the crystal lattice (Figure 5.20b). In a similar coordination environment Cd(II) forms polymeric interaction with SCN^-, whereas in case of higher homologue Hg(II) discrete monomer is forming. The limitation of Hg(II) may be due inclusion of lanthanide contraction and some relativistic effect of heavy metals.[5.36] The strong sharp single stretching at 2118 cm^{-1} is due to ν_{SCN} in the IR spectra of complex **21**. This band confirms the thiocyanato-S coordination with the mercury atom.[5.38] Moderately intense stretching at 1598 cm^{-1} is observed may be due to $\nu_{C=N}$ stretching frequency. The molar conductance (Λ_M) of

complexes lies between 100 and 120 Ω^{-1} cm^2 mol^{-1} suggesting a 2:1 type electrolytic nature of the compounds.

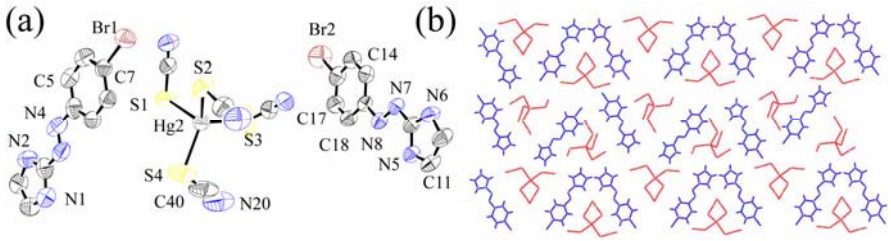

Figure 5.20. (a) ORTEP plot of complex **21**. Thermal ellipsoids set to 50% probability level and (b) packing of complex **21** along *a* axis.

5.3.3. Absorption Spectral Studies

The electronic absorption spectra of aniline-imidazole[5.39] dye show intense broad absorption band in the visible region at ca. 361 nm in MeOH. All the *para*-substituted ligands $\mathbf{L_{5\text{-}10}}$ shows Bathochromic shift with respect to the unsubstituted ligand (Figure 5.21a and 5.22a). Maximum red-shift is found in case of $\mathbf{L_7}$ (-OMe substituted) and minimum effect is observed for $\mathbf{L_6}$ (-Me substituted). The amount of shift is attributed to the electronic effect of the substituted group. These absorption bands in between 360 - 380 nm correspond to intra-ligand $n\rightarrow\pi^*$ as well as $\pi\rightarrow\pi^*$ electronic transition.[5.40] In addition; $\mathbf{L_7}$ shows a weak shoulder at 421 nm. In the Cu(II)-complex of $\mathbf{L_6}$ and $\mathbf{L_7}$, the absorption bands in the visible region are shifted to higher wavelengths relative to the ligands. Mn(II) complex (**1**) shows two weak MLCT and d–d transitions at > 400 nm along with ligand transition at 357 nm. This supports the distorted *Td*–Mn(II) coordination environment. Figure 5.20b shows the absorption spectra of $\mathbf{L_5}$ when titrated with Cu(II) (complex **3**) . Ligand absorption at 361 nm decreases with simultaneous appearance of a peak at 422 nm with an isosbestic point at 392 nm (Figure 5.21b). In the –Me substituted Cu(II) complex **4**, the observed $\Delta\lambda_{max}$ $(n\rightarrow\pi^*)$ is ~12 nm and $\Delta\lambda_{max}$ $(\pi\rightarrow\pi^*)$ is ~ 14 nm whereas in case of complex **5** the observed $\Delta\lambda_{max}$ $(n\rightarrow\pi^*)$ is ~30 nm and $\Delta\lambda_{max}$ $(\pi\rightarrow\pi^*)$ is ~ 26 nm (Figure 5.21c). Additionally, in the Cu(II) complex a third band is observed in the visible region ~ 434 nm for complex **4** and ~ 443 nm for complex **5**.[5.39] This higher wavelength band originates from the forbidden $\tilde{d}$-*d* transition of the metal center, which is generally weak in nature.[5.39] Alternatively in all the Cu(II) complexes, a weak spectral band is observed ~ 550–660 nm (ε = 825-850 $M^{-1}cm^{-1}$), which is generally exhibit for d_{xz}, d_{yz} $\rightarrow d_{x2\text{-}y2}$ transitions. This band can be assigned is typical of pentacoordinated Cu (II) complexes with square-pyramid geometry.[5.41]

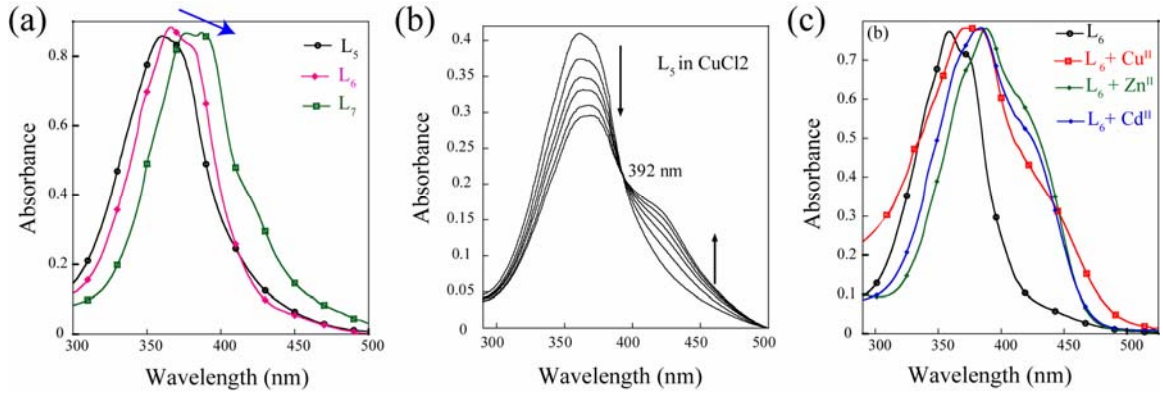

Figure 5.21. (a) Absorption spectra of **L_5**, **L_6** and **L_7** in MeOH (0.5 x 10^{-5} M) ; (b) Absorption spectra of **L_5** in presence Cu(II) salts and (c) Absorption spectra of **L_6** in presence of Cu^{II}, Zn^{II} and Cd^{II} metal salts (0.1 mM).

In presence of d^{10} system (Zn^{II}, Cd^{II}, Hg^{II}) bathochromic shift is observed, due to MLCT transition (Figure 5.22b). In addtition of Zn^{II}, Cd^{II} and Hg^{II} salts of **L_8**, **L_9** and **L_{10}**, the absorption bands in the visible region are shifted to higher wavelengths relative to the ligands. In the observed values the observed (in case of Zn Salts) $\Delta\lambda$max $n\rightarrow\pi^*$ is ~18 nm and $\Delta\lambda$max $\pi\rightarrow\pi^*$) is ~ 8 nm whereas in case of Cd and Hg Salts the observed $\Delta\lambda$max ($n\rightarrow\pi^*$) is ~17 nm and $\Delta\lambda$max $\pi\rightarrow\pi^*$ is ~ 18 nm respectively. A weak long wavelength transition at ~430 nm may be assigned to the $d^{10}\rightarrow\pi^*$(azoimine) transition. However, the ligands as well as the complexes do not exhibit any significant solvatochromism. Overall feature is that, effect of electron halogen substituents can change electron density of the ligand system as a result sharp change is observed in absorption behaviors.

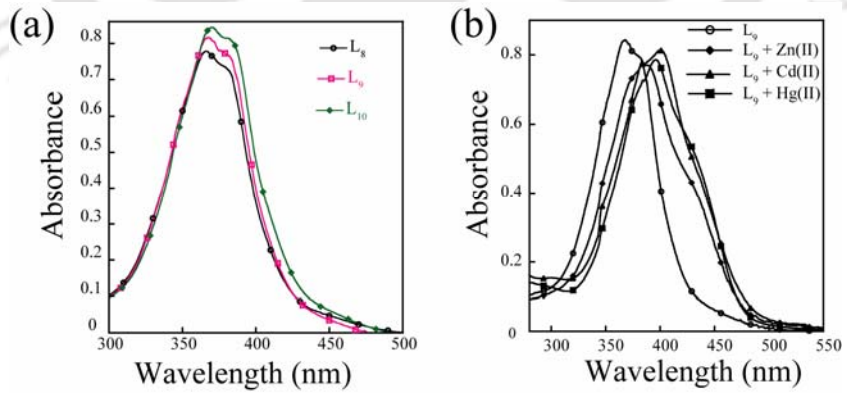

Figure 5.22. (a) Absorption spectra of **L_8**, **L_9** and **L_{10}** in MeOH (0.5X 10^{-5} M) and (b) Absorption spectra of **L_9** in presence of Cu^{II}, Zn^{II} and Cd^{II} salts (0.1 mM).

5.3.4. Electrochemistry

The electrochemical properties of the Cu(II) complexes were examined by cyclic voltametry at platinum working electrode in acetonitrile (0.1M TBAP) and the potentials

are reported with reference to SCE (at 50 mV s^{-1} scan rate). The voltammogram display metal based redox couple in the positive side and the ligand based redox couple in the negative side with respect to the SCE (Figure 5.23). Ligand oxidation peak $\mathbf{L_5}$ shows two oxidation responses in the negative potential may be attributed to the redox couple one irreversible peak in table 5.1 (*E*pa = -0.129 V) (Figure 5.23a).[5.42] But in the complex there is a one quasi-reversible couple peak is observed may be due to azo bond oxidation (*E*pa = -0.583 V, *E*pc = -0.677 V, Δ*E*p = 94 mV and $E_{½}$ = -0.63 V) (Figure 5.23c). The voltammogram of the Cu(II**)** complex **3** shows only a single reduction peak of Cu(II**)**/Cu(I**)** at 0.495 V (*E*pc) during the anodic potential scan, just after the reduction peak a cathodic peak is observed at 0.403 V (*E*pa). The separation between anodic and cathodic peak potentials value (ΔEp) of 92 mV indicates a quasi-reversible redox process assignable to the Cu(II**)**/Cu(I**)** couple and $E_{1/2}$ is equal to 0.449 V (Figure 5.23b). It is believed that this response arises from oxidation of the azoimine function. The role of the azoimine function in bringing about the high Cu(II)/Cu(I) potential is well established.[5.43]

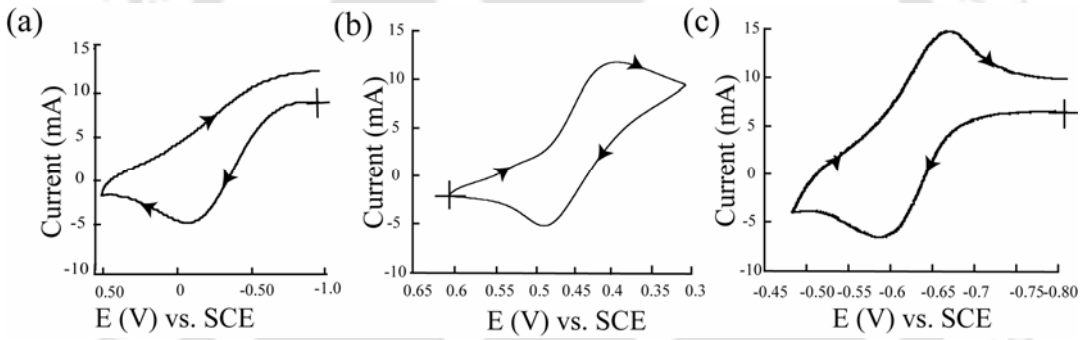

Figure 5.23. (a) Cyclic voltammogram of $\mathbf{L_5}$ in MeCN; (b) Reduction of Cu(II)/Cu (I) couple in complex **3**; (c) Oxidation of azo system in complex **3**.

Substitution of *para*-H with electron donating –Me/-OMe groups increase the overall electron density in the ligand frame, which in turn increases the oxidation potential of the ligand compared to the unsubstituted one. Similarly in –Me substituted ligand $\mathbf{L_6}$ oxidation peak remain similar without any significant changes (*E*pa = -0.133 V). In the complex **4** there is a one quasi-reversible couple peak is observed may be due to azo bond oxidation (*E*pa = -0.604V, *E*pc = -0.695 V, Δ*E*p = 91 mV and $E_{½}$ = -0.65 V) (Figure 5.24c) and Cu(II) complex **4** shows the quasi-reversible CV response (*E*pa = 0.414 V, *E*pc = 0.508 V, Δ*E*p = (94 mV and $E_{½}$ = 0.46 V) corresponds to the Cu(II)/Cu(I) redox process (Figure 5.23b). In case of $\mathbf{L_7}$ oxidation peak remain similar without any significant changes (*E*pa = -0.156 V). Similarly But in the complex **5** there is a one quasi-reversible couple peak is observed may be due to azo bond oxidation (*E*pa = - 0.613V, *E*pc = -0.705 V, Δ*E*p = 92 mV and $E_{½}$ = -0.66 V) (Figure 5.23f)and Cu(II) complex **5** shows the quasi-reversible CV

response (*E*pa = 0.441 V, *E*pc = 0.534 V, Δ*E*p = (93 mV and $E_{½}$ = 0.537 V) corresponds to the Cu(II)/Cu(I) redox process (Figure 5.24e).

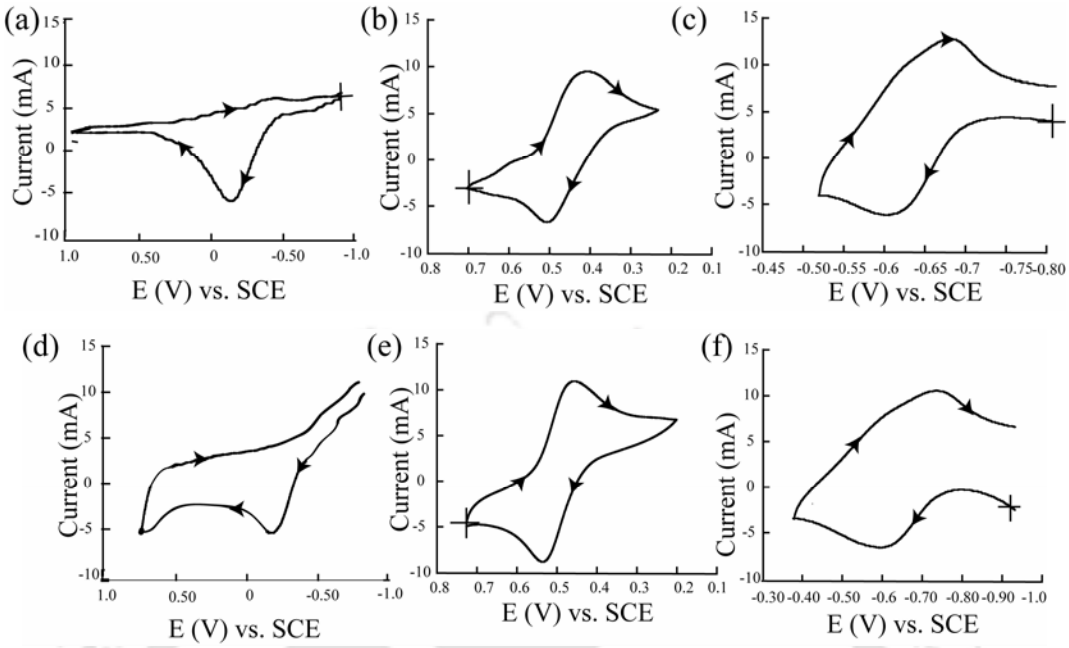

Figure 5.24. (a) Cyclic voltammogram of $\mathbf{L_6}$ in MeCN; (b) Reduction of Cu(II)/Cu (I) couple in complex **4**; (c) Oxidation of azo system in complex **4;** (d) Cyclic voltammogram of $\mathbf{L_7}$ in MeCN; (e) Reduction of Cu(II)/Cu (I) couple in complex **5**; (f) Oxidation of azo system in complex **5.**

Table 5.1 Cyclic voltametry data of $\mathbf{L_5}$, $\mathbf{L_6}$ and $\mathbf{L_7}$ and with their corresponding Cu^{II} salts.

Entry	Epc,V	Epa,V	ΔEp,mV	$E_{1/2}$,V
$\mathbf{L_5}$		-0.129		
$\mathbf{L_6}$		-0.133		
$\mathbf{L_7}$		-0.156		
$\mathbf{L_5}$-Cu(II) complex	0.403	0.495	92	0.449
	-0.677	-0.583	94	0.630
$\mathbf{L_6}$-Cu(II) complex	0.414	0.508	94	0.46
	-0.695	-0.604	91	0.65
$\mathbf{L_7}$-Cu(II) complex	0.441	0.534	93	0.537
	-0.705	-0.613	92	0.660

5.3.5. EPR spectral analysis

EPR spectra were recorded for both the Cu(II) complexes. In methanolic solution of complex **3**, only an isotropic spectrum containing four copper hyperfine lines is observed at 77K (Figure 5.25a). It contains an axial symmetry, with four hyperfine peaks in the parallel region derived from the coupling of the copper nucleus and the unpaired electron.[5.44] The results obtained are summarized as follows: $g_{\perp}$ = 2.204, g_{11} = 2.237 and A_{11}=180 G. The fact $g_{11} > g_{\perp}$ confirms an elongated octahedral stereochemistry with a $(d_{x^2-y^2})^1$ ground state in complex **3**. The X- band EPR spectrum of complex **4** in MeOH glass (77K) is displayed in the Figure 5.25b. The spectrum is a typical for monomeric Cu^{II}

complex in distorted square pyramidal geometry with ($g_{\perp}$ = 2.06, g_{11} = 2.43, A_{11}=175 G) with dx^2-y^2 ground state. Thus, the stronger effect of the axial S donor as compared with N donor is indicative of a slightly strong perturbation to Cu(II) center.[5.45] This may be attributed to a marked deviation of the axial Cu-S bond from the unique axis of the tetragonal square basal plane, as has been demonstrated for violet thiocyanate S-Cu(II) complex with a distorted square pyramidal structure. Also in solid-state, complex **4** exhibits a broad EPR signal around *g* = 2 with no visible hyperfine interaction at 300 K. Alternatively in the complex **5** we have shown that the monomeric Cu^{II} is surrounded by three O-donors and one N donor is in the basal plane and weak azo N donor is in the equatorial plane. Since the EPR spectrum of complex **5** in methanol glass at 77 K resembles monomeric Cu(II) EPR spectrum ($g_{\perp}$=2.05, g_{11}=2.20, A_{11}=182.3 G) appears in the solution (Figure 5.25c).[5.46]

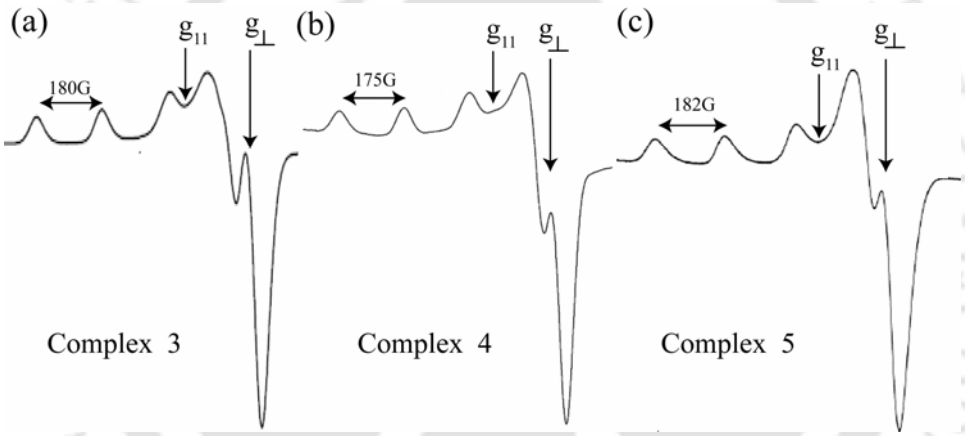

Figure 5.25. X-band EPR spectrum measured in methanol at 77 K of (a) Complex **3**; (b) Complex **4** and (b) Complex **5**.

5.3.6. Powder XRD analysis

PXRD patterns also confirm the crystalline nature of the complexes. PXRD patterns of complex **6** show significant changes in the peak positions as well as intensities before and after water removal (Figure 5.26a). After heating the crystal of **6** at 150 ^{o}C for 3 h in a muffle furnace, powder XRD was recorded. Loss of overall crystallinity after water removal confirms that the stability of solid-state framework due to formation of strong hydrogen bonding interactions involving crystal water molecule. Similar observation was made with complex **11** (Figure 5.26a). The PXRD of other complexes we have shown in the appendix of this chapter.

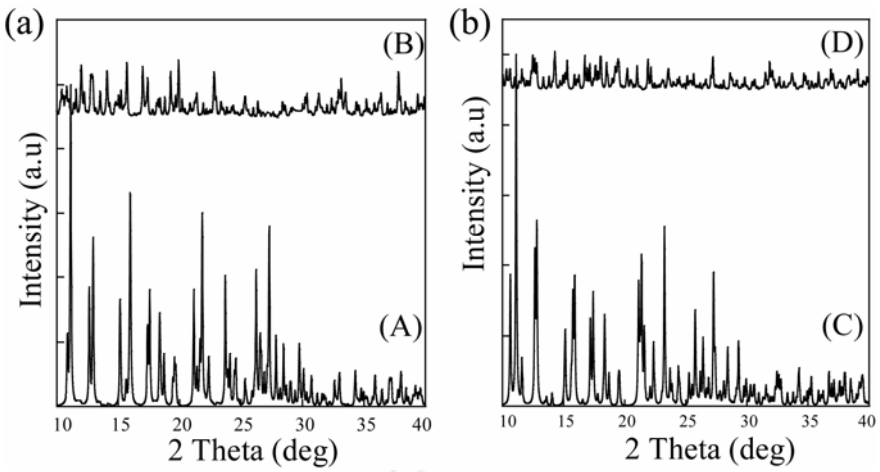

Figure 5.26. (a) PXRD pattern of the crystal of complex **6** (A) before; (B) after water removal and (b) PXRD pattern of the crystal of complex **11** (A) before; (B) after water removal.

5.3.7. Thermal Studies

The interaction between the complexes and the solvent molecules in the solid-state can be commented with the help of thermo gravimetric analysis of the corresponding complexes. Thermal characterizations of the products were accomplished by thermo gravimetric analysis (TGA). The onset temperature of weight loss and decomposition temperature were 160 and 190 °C respectively for the free ligand $\mathbf{L_5}$ (Figure 5.27a). Metal-azo dyes were more thermally more stable than that of the azo dye. All the complexes containing solvent molecules in their crystal structure (*viz.* complexes **6**, **8**, **9, 10** and **11**) decomposed thermally in a number of steps. However, other complexes show either single step or continuous weight loss in between 50 – 600 ^{o}C. The robustness of the solid-state framework is reflected in TGA. Both complex **6** and **11** decomposed thermally in a number of steps (Figure 5.27b). These complexes show successive thermal release of water of crystallization and the chloride followed by complete decomposition of the complex. The robustness of the solid-state framework is reflected in TGA.[5.47] TG analysis of complex **6** in N_2 atmosphere shows the release of one crystal water molecule (110–140 ^{o}C; Δm = 3.61% Calc.; 3.25% found) and two chloride ions (190–240 ^{o}C; Δm = 14.77% Calc.; 15.23% found) (Figure 5.28a, 5.28c), which is in good agreement with the X-ray crystal structure. Complete decomposition is achieved at ~ 310 ^{o}C. For complex **11**, dehydration occurs at littlie higher temperature range than that of **6**, (130–160 ^{o}C; Δm = 3.29% Calc.; 3.02% found) but the release of two chloride ion occurs at same temperature range at 200–240 ^{o}C (Δm = 13.45% Calc.; 13.16% found). Complete decomposition is achieved at ~ 300 ^{o}C. However, complex **12**, shows the release of four chloride ions in the broad temperature range of 200-250 ^{o}C (Δm = 39.94% Calc.; 39.21% found) followed by

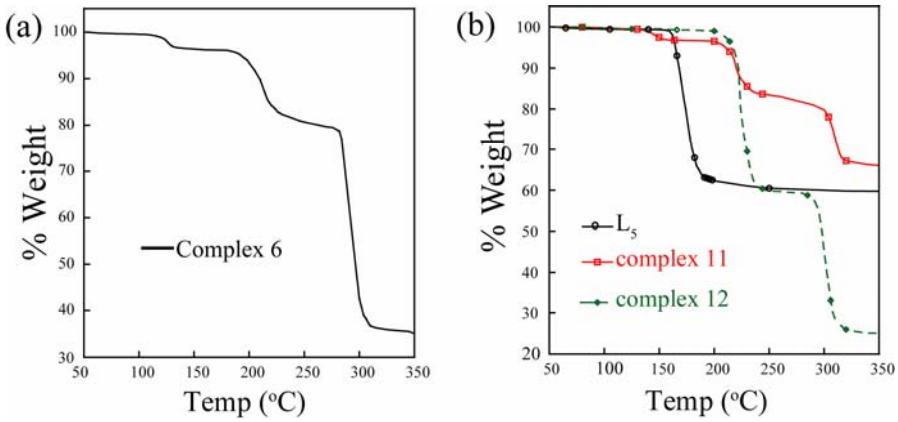

Figure 5.27. (a) TGA analysis of Complex **6;** (b) TGA analysis of ligand $\mathbf{L_5}$**,** Complex **11** and Complex **12**

complete decomposition at ~ 330°C. Similarly, the onset temperature of weight loss and decomposition temperature were 210 and 190 °C for $\mathbf{L_6}$, 160 and 200 °C for $\mathbf{L_7}$, 220 and 250 °C for $\mathbf{L_8}$, 240 and 270 °C for $\mathbf{L_9}$, 195 and 230 °C for $\mathbf{L_{10}}$ respectively. Complex **5** shows thermal release of metal bound water at ~ 150 °C (130-165 °C; Δm = 4.42 % Calc.; 4.18% found) followed by the complete decomposition in the temperature range 190 – 340 °C. Complex **8** shows successive thermal release of water of crystallization and metal bound water followed by complete decomposition of the complex (Figure 5.28b). TGA of complex **8** in N_2 atmosphere shows the release of one crystal water molecule (100-125 °C; Δm = 4.30% Calc.; 4.48% found) and one metal bound water molecule in relatively higher temperature range (190-220 °C; Δm = 4.50% Calc.; 4.76% found) and complete decomposition is achieved at ~ 310 °C which is in good agreement with the X-ray crystal structure. Similarly, in complex **9** releases one EtOH molecule at ~ 120 °C (90-130 °C; Δm = 6.34% Calc.; 6.78% found) and complete thermal decomposition occurs at in the temperature range 225 – 380 °C (Figure 5.28d), which is in good agreement with the X-ray crystal structure. Complex **10** shows thermal release of water of crystallization at ~ 140 °C (125-155 °C; Δm = 1.85% Calc.; 2.21% found) followed by the complete decomposition in the temperature range 225 – 390 °C which is also matching with the crystal structure analysis. TGA curves of the complexes are sharp and show good thermal capability. The thermal studies of other complexes we have shown in the appendix of this chapter. These data show that the Zn and Cd complexes would possibly be able to fabricate a small and sharp recording mark edge. Higher the decomposition temperature of complex, smaller is the thermal interference. The sharper the decomposition curve, the higher the sensitivity. On the basis of literature data, thermally stable compounds up to 250 °C are suitable for use as recording dyes[5.48], so according to the thermal stability of the azo-dye complexes we can conclude that these compounds are suitable for use as recording dyes.

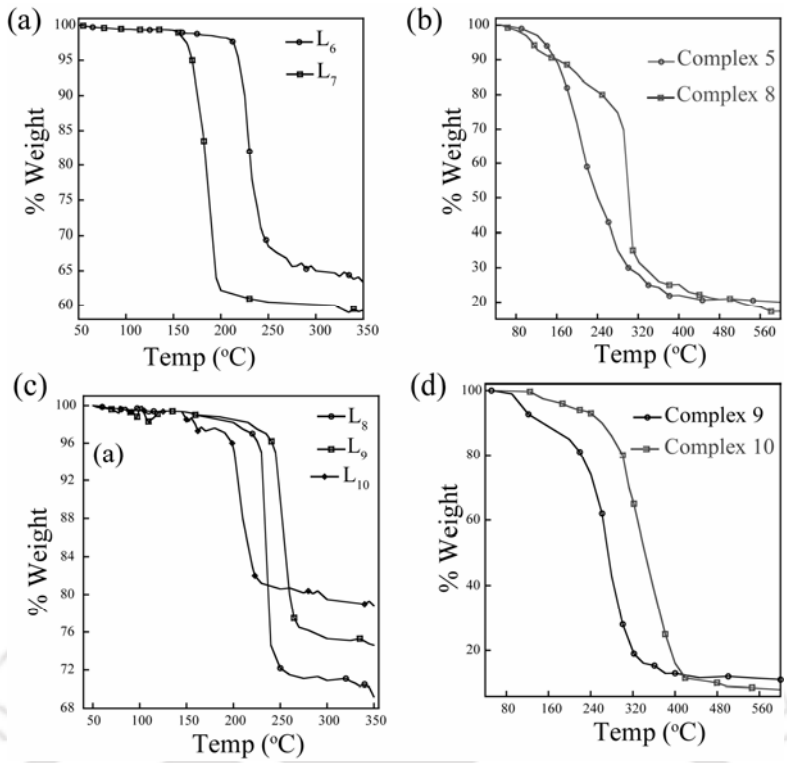

Figure 5.28. (a) TGA analysis of ligand $\mathbf{L_5}$ and $\mathbf{L_6}$**;** (b) TGA analysis of Complex **5** and Complex **8;** (c) TGA analysis of ligand $\mathbf{L_8}$, $\mathbf{L_9}$ and $\mathbf{L_{10}}$**;** (d) TGA analysis of Complex **9** and Complex **10**.

5.3.8. Summery

The work describes the synthesized and characterized a series of Mn(II), Ru(II), Cu(II) Zn(II), Cd(II) and Hg(II) twenty one metal complexes of un-substituted *p*-substituted 2-Phenylazo imidazole ligand. Simultaneous presence of hydrogen bonding site and metal coordination site of different chemical nature helps to form metal complexes with different metal ions and also helps them to self-assemble in the solid-state with different higher dimensional architecture.Counter anions and metal ions tune the coordination environment of complexes. Change in the coordination sphere has been reflected in their crystal structure and other physico-chemical properties Substitution in the *para* position with electron releasing group and the halogen group, which is away from coordination site have a strong influence in the self-assembly processes of the metal complexes in solid-state. Some interesting feature in that, Cu(II) shows a marked preference for the N end of this ambidentate ligand. However, CSD search shows that only ~6-7% of mononuclear Cu(II) complexes containing SCN- anion, contains Cu(II) center bonded through the S end. In complex **4**, we have both type of bonding at the same time. This can be rationalized by Pearson's hard–soft acid–base principle which requires matching hardness of two species for effective bonding. Bonding of SCN- through the S end to Cu(II) is not favored energetically. However, in complex **4**, inter-molecular H-bond between the N atom of the

thiocyanate and the N–H proton of the ligand L_6 of an adjacent molecule favored this type of bonding. Counter anion NO^{3-} shows both monodentate (complex **5**). The single crystals of the different complexes also showed formation of multifaceted networks in the resulting complexes. Solvent induced changes in the solid-state structure have been observed in the complexes **5, 6, 8, 9, 10** and **11**. Both the Cu(II) complexes **5** and **6** are having similar geometry but different coordination environment. In complex **4** two ligands are attached to metal center while in **5** only one ligand is coordinated to the Cu(II). More than 75% of the coordination sphere of **4** is hydrophobic while in **5** less than 25% surface is hydrophobic. It's reflected in their solid-state packing. Presence of electron donating group in ligand increase the electron density in the ring which in turn reduce the N=N bond strength in comparison to the unsubstituted ligand. C–H bond attached to OMe is more polarized in $\mathbf{L_7}$ than $\mathbf{L_6}$ where it is attached to -Me group. Moreover, presence of electronegative O atoms in the neighboring position in the solid-state helps to form C–H···O type hydrogen bond in complex **5**. On the other hand C–H bond of *para* -Me group form C–H···π type weak interaction with the imidazole ring in the solid-state. Presence of metal bonded as well as crystal water molecule in complex **8** with respect to the another Zn(II) complex **7**, resulted in the formation of more number of strong and weak hydrogen bonds in the solid-state. Coordination of the azo N decrease the electron density from N=N, which in turn decrease the azo bond strength. This is also change the planarity of the ligand which controls the solid-state packing. In complex **8** ligand is bidentate, as a result N=N bond is more elongated than similar complex **7**. The results of this study not only illustrate that the coordination modes of ligands and the nature of the neutral ligands play an important role in the construction of variety of coordination network. In complex **9**, one imidazole N–H is forming strong hydrogen bond with the O-atom of the solvent EtOH because of close proximity in the lattice. Other imidazole N–H is forming weak hydrogen bond with the S-atom of the free end of the bonded SCN in the neighboring molecule. Aryl azo imidazole ligand can act as unidentate or bidentate ligand, in which one of the azo N atoms is the second coordinating atom. Coordination of the azo N decrease the electron density from N=N, which in turn decrease the azo bond strength. This is also change the planarity of the ligand which controls the solid-state packing. The observed N–Cd–N bond angle is ~143^o in complex **13**, ~ 142^o in complex **18** and ~141^o in complex **19**. As electron withdrawing power decreases this angle decrease and ligand bonded to the metal center come closer to each other. The azo dye compleces shows cooddination polymeric complexes in complex **12** (chloro bridge one dimensional coordination polymer) and complex **16** (thiocyanato bridge two dimensional coordination polymer). The ambivalence nature of the SCN^-

counter anion plays crucial role in the formation of higher dimensional self-assembled coordination polymer in the solid-state. The bonding mode of thiocyanate with Zn(II) in complex **9** is dimeric and Cd(II) in complex 16 is polymeric respectively. In Zn(II) complex (complex **9)** this type of thiocyanate bridging is very rare in literature. This can be rationalized by Pearson's hard–soft acid–base principle which requires matching hardness of two species for effective bonding. Counter anion NO_3^- shows bidentate bridging (complex **5**, **14**, **15**, **18** and **19**) mode. The single crystals of the different complexes also showed formation of multifaceted networks in the resulting complexes. Thermal studies show that most of the metal-azo dyes had good thermal stability up to 300 °C, which is an important criterion to be a recording material for DVD-R. We are currently extending this result by preparing new imidazole containing aryl azo ligands of this type with different substituted organic functional groups. We anticipate this approach to be useful for the construction of a variety of new transition metal complexes and coordination polymers (including bimetallic polymeric compounds) with novel structures.

References:

5.1 (a) Savvin, S. B.; Dedkova, V. P.; Shvoeva, O. P. *Russ. Chem. Rev.,* **2000**, *69*, 187. (b) Lázaro, F.; Luque de Castro, M. D.; Valcárcel, M. *Anal. Chim. Acta,* **1988**, *214*, 217. (c) Morozko, S. A.; Ivanov, V. M. *Zh.Anal.Khim.,* **1995**, *50*, 629.

5.2 (a) Song, H.; Chen, K.; Wu, D.; Tian, H. *Dyes Pigments,* **2004**, *60*, 111. (b) Tanaka, K.; Matsuo, K.; Nakanishi, A.; Jo, M.; Shiota, H.; Yamaguchi, M.; Yoshino, S.; Kawaguchi, K. *Chem. Phar. Bull.,* **1984,** *8*, 3291. (c) Peters, A. T.; Chisowa, E. *Dyes Pigments,* **1993**, *22*, 223.

5.3 (a) Towns, A. D.; *Dyes Pigments,* **1999,** *42,* 3. (b) Holtslag, A. H. M.; Mccord, E. F.; Werumeus, B. G. H.; *Jpn. J. Appl. Phys*. **1992**, *31,* 484.

5.4 Masaund, M. S.; Khalil, E. A.; El-Sayed, E. S.; El-Enein, S. A. *J. Thermal Anal*., **1990**, *36*, 1033.

5.5 Egli, R.; *Color Chemistry: The Design and Synthesis of Organic Dyes and Pigments, ed*. A. T. Peters, H.S. Freeman, Elsevier, London, **1991**.

5.6 (a) Hao, Z.; Iqbal, A. *Chem. Soc. Rev.,* **1997**, *26*, 203. (b) Price, C. P.; Grzesiak, A. L.; Kampf, J. W.; Matzger, A. J. *Cryst. Growth Des.,* **2003**, *3*, 1021. (c) Vrcelj, R. M.; Shepherd, E. E. A.; Yoon, C.; Sherwood, J. N.; Kennedy, A. R. *Cryst. Growth Des.*, **2002**, *2*, 609.

5.7 Brittain, H. G.; *Polymorphism in Pharmaceutical Solids*, Dekker, New York, **1999**.

5.8 (a) Wang, S.; Shen, S.; Xu, H.; Gu, D.; Yin, J.; Tang, X. *Mater. Sci. Eng.,* **2000**, *B76*, 69. (b) Wu, S.; Qian, W.; Xia, Z.; Zou, Y.; Wang, S.; Shen, S.; Xu, H. *Chem. Phys. Lett.,* **2000**, *330*, 535.

5.9 (a) Ackermann, M. N.; Naylor, J. W.; Smith, E. J.; Mines, G. A.; Amin, N. S.; Kerns, M. L.; Woods, C. *Organometallics,* **1992**, *11*, 1919. (b) Shivakumar, M.; Pramanik, K.; Bhattacharyya, I.; Chakravorty, A. *Inorg. Chem.,* **2000**, *39*, 4332.(c) Santra, P.K.; Byabartta, P.; Chattopadhyay, S.; Falvello, L.R.; Sinha, C. *Eur. J. Inorg. Chem.,* **2002**, 1124.(d) Graham, D.; Brown, R.; Smith, W. E. *Chem. Commun.,* **2001**, 1002.

5.10 Butler, M. S. *J. Nat. Prod.* **2004**, *67*, 2141.

5.11 (a) Graves, D. E.; Velea, L. M. *Curr. Org. Chem*. **2000**, *4*, 915. (b) Bischoff, G.; Hoffmann, S.; Martínez, R.; Chacón-García, L. *Curr. Med. Chem*. **2002**, *9*, 321. (c) Martínez, R.; Chacón-García, L. *Curr.Med. Chem*. **2005**, *12*, 127.

5.12 (a) Krause, R. A.; Krause, K. *Inorg. Chem.* **1980**, *19*, 2600. (b) Goswami, S.; Mukherjee, R. N.; Chakravorty, A. *Inorg. Chem.* **1983**, *22*, 2825. (c) Velders, A. H.; Kooijman, H.; Spek, A. L.; Haasnoot, J. G.; de Vos, D.; Reedijk, J. *Inorg. Chem.* **2000**, *39*, 2996. (d) Panda, M.; Das, C.; Lee, G.-H.; Peng, S.-M.; Goswami, S. *Dalton Trans*. **2004**, 2655.

5.13 (a) Sarker, K. K.; Sardar, D.; Suwa, K.; Otsuki, J.; Sinha, C. *Inorg. Chem.* **2007**, *46*, 8291. (b) Ackermann, M. N.; Robinson, M. P.; Maher, I. A.; LeBlanc, E. B.; Raz, R. V. J. *Organomet. Chem.* **2003**, *682*, 248.

5.14 (a) Fei, Z.; Geldbach, T. J.; Scopelliti, R.; Dyson, P. J. *Inorg. Chem*. **2006**, *45* ,6331. (b) Yamamura, M.; Kano, N.; Kawashima, T. *Inorg. Chem*. **2006**, 45, 4697.

5.16 (a) Byabartta, P.; Pal, S.; Sinha, C.; Liao, F.-L.; Panneerselvam, K.; Lu, T.-H. *J. Coord. Chem.* **2002**, *55*. 479. (b) Misra, T. K.; Das, D.; Sinha, C.; Ghosh, P. K.; Pal, C. K. *Inorg. Chem*., **1998**, *37*, 1672.

5.17 Mathur, T.; Jasimuddin, S. K.; Milton, H.; Woollins, J. D.; Sinha, C.; *Inorg. Chim. Acta,* **2004**, *357,* 3503.

5.18 Misra, T. K.; Das, D.; Sinha, C. *Polyhedron,* **1997**, *16*, 4163.

5.19 Conley, R.T. *Infrared Spectroscopy,* Allyn & Bacon, Boston, **1966**.

5.20 Nakamoto, K. *Infrared and Ramman Spectra of Inorganic and Coordination Compounds*, 5th ed.; John Wiley & Sons Inc.: New York, **1997**.

5.21 Pal,S.; Das, D.; Sinha, C.; Kennard, C.H.L. *Inorg. Chim. Acta* **2001**, *21*, 313.

5.22 (a) Chand, B. G.; Ray, U. S.; Cheng, J.; Lu, T.-H.; Sinha, C. *Polyhedron* **2003**, *22*, 1213. (b) Chand, B. G.; Ray, U. S.; Mostafa, G.; Lu, T.-H.; Sinha, C.; *J. Coord. Chem*. **2004**, *57*, 627. (c) Banerjee, D.; Ray, U. S.; Chantrapromma, S.; Fun, H.-K.; Lin, J.-N.; Lu, T.-H.; Sinha, C. *Polyhedron* **2005**, *24*, 1071. (d) Mathur, T.; Ray, U. S.; Baruri, B. N.; Sinha, C. *J. Coord. Chem*. **2005**, *58*, 399.

5.23 (a) Anderson, C.; Beauchamp, A. L. *Inorg. Chem.,* **1995**, *34*, 6065. (b) Hatcidimitriou, A.; Gourdon, A.; Devillers, J.; Launacy, J. P.; Mena, E.; Amouyal, E. *Inorg. Chem.,* **1996**, *35*, 2215. (c) Keppler, B. K.; Wehe, D.; Endres, H.; Rupp, N. *Inorg. Chem.,* **1987**, *26*, 8440.

5.24 Sangeetha. N. R.; Pal, S.; Anson, C. E.; Powell, A. K.; Pal, S. *Inorg. Chem. Commun.* **2000**. *3*, 415.

5.25 Addision, A.W.; Rao, T. N.; Reedijk, J.; van Rijn., J. ; Verschoor, G. C. *J. Chem. Soc., Dalton Trans.* **1984**, 1349.

5.26 (a) Santra, B. K.; Reddy, P. A. N.; Nethaji, M.; Chakravarty. A. R. *Inorg. Chem*., **2002**, *41*, 1328. (b) Sen, S.; Mitra, S.; Hughes, D. L.; Rosair, G.; Desplanches, C. *Polyhedron,* **2007**, *26*, 1740.

5.27 (a) Earnshaw, *A. Introduction to Magnetochemistry;* Academic Press: London, **1968**. (b) Figgis, B. N.; Lewis, *J. Prog. Inorg. Chem*., **1964**, *6*, 37.

5.28 Bhattacharyya, P.; Parr, J.; Slawin, A. M. Z. *J. Chem. Soc., Dalton Trans.* **1998**, 3263.

5.29 (a) Hergue, N.; Leriche, P.; Blanchard, P.; Allain, M.; Gallego-Planas, N.; Frere, P.; Roncali, J. *New J. Chem*., **2008**, *32,* 932. (b) Xu, J.; Wang, W-L.; Lin, T.; Sun, Z.; Lai, Y-H. *Supramol. Chem.,* **2008**, *20*, 723.

5.30 (a) Xu, D.; Yu, W.-T.; Wang, X.-Q.; Yuan, D.-R.; Lu, M.-K.; Yang, P.; Guo, S.-Y.; Meng, F.-Q.; Jiang, M.-H. *Acta Cryst.,* **1999,** *C55*, 1203. (b) Adams, H.; Cummings, L. R.; Fenton, D. E.; McHugh, P. E. *Inorg. Chem. Commun.,* **2003**, *6*, 19.

5.31 Bailey, R. D.; Pennington, W. T.; *Polyhedron,* **1997**, *16*, 417.

5.32 Strasdeit, H.; Saak, W.; Pohl, S.; Driessen, W. L.; Reedijk, J. *lnorg. Chem.;* **1988**, *27*, 1557.

5.33 Das, D.; Chand, B.G.; Dinda, J.; Sinha, C. *Polyhedron,* **2007**, *26*, 555.

5.34 Menon, M.; Pramanik, A.; Chakravorty, A. *Inorg. Chem.,* **1994**, *33*, 403.

5.35 Noman, A.; Rahman, M. M.; Bishop, R.; Craig, D. C.; Scudder, M. L. *CrystEngComm.,* **2002,** *4*, 510.

5.36 Cotton, F.A.; Wilkinson, G.; Advanced Inorganic Chemistry, 5th ed., Wiley–Interscience, New York, **1999.**

5.37 Chand, B.G.; Ray, U.S.; Mostafa, G.; Cheng, J.; Lu, T-H.; Sinha, C. *Inorg. Chim. Acta,* **2005**, *358*, 1927.

5.38 Ribas, J.; Escuer, A.; Monfort, M.; Vicente, R.; Corte's, R.; Lezama, L.; Rojo, T. *Coord. Chem. Rev.,* **1999**, *1027*, 193.

5.39 Gup, R.; Giziroglu, E.; Kırkan, B. *Dyes Pigments* **2007**, *73*, 40.

5.40 Das, D.; Chand, B. G.; Sarker, K. K.; Dinda, J.; Sinha, C. *Polyhedron,* **2006**, *25*, 2333.

5.41 McLachlan, G. A.; Fallon, G. D.; Martin, R.E.; Spiccia, L.; *Inorg. Chem.* **1995**, *34*, 254

5.42 (a) Pal, S.; Mishra, T. K.; Chattopadhyay, P.; Sinha. C. *Proc. Indian Acad. Sci.* **1999**, *111*, 687. (b) Misra, T. K.; Das, V; Sinha, C. *Polyhedron,* **1997**, *16*, 4163.

5.43 (a) Datta, D.; Chakravorty, A. *Inorg. Chem.,***1983**, *22*, 1085. (b) Wilkinson, V. *Comprehensive Coordination Chemistry,* Vol. 5, Pergamon Press, Oxford, **1987**.

5.44 Zhu, S.; Lin, H.; Lin, C.; Kou, F.; Chen, Y. *Inorg. Chim. Acta,***1995**, *228*, 225.

5.45 Sakaguchi, U.; Addison, A. W. *J. Chem. Soc. Dalton Trans.* **1979**, 600.

5.46 Ali, M. A.; Mirza, A. H.; Fereday, R. J. Butcher, R. J.; Fuller, J. M.; Drew, S. C.; Gahan, L. R.; Hanson, G. R.; Moubaraki, B.; Murray, K. S. *Inorg. Chim. Acta,* **2005**, *358*, 3937.

5.47 (a) Pramanik, A.; Abbina, S.; Das, G.; *Polyhedron,* **2007**, *26,* 522. (b) Thakuria, H.; Borah, B. M.; Das, G. *Eur. J. Inorg. Chem.,* **2007**, *4,*524. (c) Thakuria, H.; Das, G. *Polyhedron,* **2007**, *26*, 149. (d) Pramanik, A.; Das, G. *J. Chem. Crystallogr.,* **2007**, *39*, 416.

5.48 Park, H.; Kim, E-R.; Kim, D, J.; Lee, H.; *Bull Chem Soc Jpn.,* **2002**, 75, 2067.

APPENDIX

5.1A. Synthesis and Characterization of complex (1), $[Mn(L_5)_2(SCN)_2]$. To a magnetically stirred solution of $\mathbf{L_5}$ (0.372 g, 2 mmol) in CH_3OH (20 mL), was added solid $CuCl_2$ (0.125 g, 1 mmol) in portions. Then the aqueous solution of NH_4SCN (0.152, 2 mmol) was added to this mixture. A greenish-yellow precipitate that formed was filtered, washed with ether, and dried under vacuum. Dark-brown, Yield: 0.489 g (95%). Single-crystals suitable for X-ray diffraction were obtained from slow evaporation of an EtOH: water (1:1) solution of the compound at RT. Anal. Calcd (%) for $C_{20}H_{16}N_{10}S_2Mn$: C, 46.60; H, 3.13; N, 10.66. Found: C, 46.67; H, 3.20; N, 10.51%. IR (KBr disk) (cm^{-1}); ν(NCS), 2090 (s); ν(SCN), 2070 (s); ν(C=N), 1595 (m) ; ν(N=N), 1401 (m); ν(C=S), 772 (m).

5.2A. Synthesis and Characterization of complex (2), $[Ru(L_5)_2Cl_2]$. To a solution of $\mathbf{L_5}$ (.372 g, 2 mmol) in CH_3OH (3 mL) solid $RuCl_2$ (0.25 g, 1 mmol) was added in portions, with constant stirring. Light green precipitate that formed immediately was collected by filtration, washed with ether (5 mL), and dried in vacuo. Dark green, Yield: 0.489 g (95%). X-ray quality crystals having the composition $C_{18}H_{16}Cl_2N_8Ru$ were grown by diffusion of EtOH: water (1:1) solution of the complex. Desolvation of crystals occurred, when they were kept without mother liquor. Anal. Calc. for $C_{18}H_{16}Cl_2N_8Ru$: C, 41.86; H, 3.12; N, 21.70. Found: C, 41.98; H, 3.02; N, 21.65%.; IR (KBr disk) (cm^{-1}); ν(C=N), 1598 (m) ; ν(N=N), 1399 (m).

5.3A. Synthesis and Characterization of complex (3), $[Cu(L_5)_2Cl_2]$. To a solution of $\mathbf{L_5}$ (.372 g, 2 mmol) in CH_3OH (3 mL) solid $CuCl_2$ (0.171 g, 1 mmol) was added in portions, with constant stirring. Light green precipitate that formed immediately was collected by filtration, washed with ether (5 mL), and dried in vacuo. Yellowish red, Yield: 0.453 g (95%). X-ray quality crystals having the composition $C_{18}H_{16}Cl_2N_8Cu$ were grown by diffusion of EtOH: water (1:1) solution of the complex. Desolvation of crystals occurred, when they were kept without mother liquor. Anal. Calcd (%) for $C_{18}H_{16}Cl_2N_8Cu$: C, 45.15; H, 3.36; N, 23.40 Found: C, 45.30; H, 3.24; N, 23..20%.; IR (KBr disk) (cm^{-1}); ν(C=N), 1605 (m) ; ν(N=N), 1401 (m).

5.4A. Synthesis and Characterization of complex (4), $[Cu(II)(L_6)_2(NCS)(SCN)]$. To a magnetically stirred solution of $\mathbf{L_6}$ (0.372 g, 2 mmol) in CH_3OH (20 mL), was added solid $CuCl_2$ (0.171 g, 1 mmol) in portions. Then the aqueous solution of NH_4SCN (0.152, 2 mmol) was added to this mixture. A greenish-yellow precipitate that formed was filtered, washed with ether, and dried under vacuum. Yield: 0.524 g (95%). Single-crystals suitable for X-ray diffraction were obtained from slow evaporation of an EtOH: water (1:1) solution of the compound at RT. Anal. Calcd (%) for $C_{22}H_{20}N_{10}S_2Cu$: C, 47.91; H, 3.66; N, 25.41. Found: C, 47.98; H, 3.60; N, 25.50%. IR (KBr disk) (cm^{-1}); ν(NCS), 2090 (s); ν(SCN), 2070 (s); ν(C=N), 1595 (m) ; ν(N=N), 1401 (m); ν(C=S), 772 (m).

5.5A. Synthesis and Characterization of complex (5), $[Cu(II)(L_7)(H_2O)(NO_3)_2]$. To a solution of $\mathbf{L_7}$ (0.20 g, 1 mmol) in CH_3OH (3 mL) solid $Cu(NO_3)_2$ (0.23 g, 1 mmol) was added in portions, with constant stirring. Light green precipitate that formed immediately was collected by filtration, washed with ether (5 mL), and dried in vacuo. Yield: 0.37 g (90%). X-ray quality crystals having the composition $[Cu(II)(L_2)(H_2O)(NO_3)_2]$ were grown by diffusion of EtOH: water (1:1) solution of the complex. Desolvation of crystals occurred, when they were kept without mother liquor. Anal. Calcd (%) for $C_{10}H_{12}N_6O_8Cu$: C, 29.48; H, 2.97; N, 20.64. Found: C, 29.51; H, 2.95; N, 20.65%.; IR (KBr disk) (cm^{-1}); ν(N=O), 1497 (s); ν(N-O), 1271 (m); ν(ONO), 992; ν(C=N), 1600 (m) ; ν(N=N), 1406 (m).

5.6A. Synthesis and Characterization of complex (6), $[Zn(L_5)_2Cl_2](H_2O)$. To a solution of $\mathbf{L_5}$ (.372 g, 2 mmol) in CH_3OH (3 mL) solid $ZnCl_2$ (0.136 g, 1 mmol) was added in portions, with constant stirring. Light

green precipitate that formed immediately was collected by filtration, washed with ether (5 mL), and dried in vacuo. Yellowish-red, Yield: 0.446 g (90%). X-ray quality crystals having the composition $C_{18}H_{18}Cl_2N_8OZn$ were grown by diffusion of EtOH: water (1:1) solution of the complex. Desolvation of crystals occurred, when they were kept without mother liquor. Anal. Calcd (%) for $C_{18}H_{18}Cl_2N_8OZn$: C, 43.35; H, 3.36; N, 22.46. Found: C, 43.25; H, 3.41; N, 22.53%.; IR (KBr disk) (cm^{-1}); ν(C=N), 1595 (m) , ν(N=N), 1402 (m); ν(O-H), 3550.

5.7A. Synthesis and Characterization of complex (7), [Zn(II)(L_6)$_2$(NCS)$_2$]. To a magnetically stirred solution of L_6 (0.37 g, 2 mmol) in CH_3OH (20 mL), was added solid $ZnCl_2$ (0.13 g, 1 mmol) in portions. Then the aqueous solution of NH_4SCN (0.15, 2 mmol) was added to this mixture. A yellowish-red precipitate that formed was filtered, washed with ether, and dried under vacuum. Yield: 0.47 g, 85% based on the ligand L_1. Slow evaporation of a EtOH-water (1:1) solution of the compound at RT produced single-crystals suitable for X-ray diffraction. Anal. Calcd (%) for $C_{22}H_{20}N_{10}S_2Zn$: C,47.82; H, 3.65; N, 25.36 Found: C, 47.91; H, 3.58; N, 25.45%.; IR (KBr disk) (cm^{-1}); ν(SCN), 2190 (s), 2140; ν(C=N), 1593 (m) ; ν(N=N), 1398 (m); ν(C=S), 685 (m).

5.8A. Synthesis and Characterization of complex (8), [Zn(L_7)(NCS)$_2$(H_2O)]H_2O. To a magnetically stirred solution of **L_7** (0.20 g, 1 mmol) in CH_3OH (20 mL), was added solid $ZnCl_2$ (0.13 g, 1 mmol) in portions. Then the aqueous solution of NH_4SCN (0.15, 2 mmol) was added to this mixture. A dark-yellow precipitate that formed was filtered, washed with ether, and dried under vacuum. Yield: 0.37 g, 90% based on the ligand **L_7**. Single-crystals suitable for X-ray diffraction were obtained from slow evaporation of EtOH: water (1:1) solution of the compound. Anal. Calcd (%) for $C_{12}H_{14}N_6O_3S_2Zn$: C, 34.45; H, 3.37; N, 20.10. Found: C, 34.55; H, 3.41; N, 20.02%.; IR (KBr disk) (cm^{-1}); ν(SCN), 2182 (s), 2130; ν(C=N), 1598 (m) ; ν(N=N), 1393 (m); ν(C=S), 680 (m).

5.9A. Synthesis and Characterization of complex (9), [Zn(L_9)$_2$(NCS)$_2$]EtOH. To a magnetically stirred solution of **L_9** (0.50 g, 2 mmol) in CH_3OH (20 mL), was added solid $ZnCl_2$ (0.13 g, 1 mmol) in portions. Then the aqueous solution of NH_4SCN (0.15, 2 mmol) was added to this mixture. A dark-yellow precipitate that formed was filtered, washed with ether, and dried under vacuum. Yield: 0.69 g, 95% based on the ligand **L_9**. Single-crystals suitable for X-ray diffraction were obtained from slow evaporation of an EtOH: water (1:1) solution of the compound. Anal. Calcd (%) for $C_{22}H_{20}Br_2N_{10}OS_2Zn$: C,36.37; H, 2.77; N, 19.29 Found: C, 36.35; H, 2.74; N, 19.28%.; IR (KBr disk) (cm^{-1}); ν(SCN), 2186 (s), 2133 (m); ν(C=N), 1603 (m) ; ν(N=N), 1401 (m); ν(C=S), 678 (m).

5.10A. Synthesis and Characterization of complex (10), [Zn$_2$(L_{10})$_2$(SCN)$_4$]H_2O. To a magnetically stirred solution of **L_{10}** (0.59 g, 2 mmol) in CH_3OH (20 mL), was added solid $ZnCl_2$ (0.27 g, 1 mmol) in portions. Then the aqueous solution of NH_4SCN (0.15, 2 mmol) was added to this mixture. A dark-yellow precipitate that formed was filtered, washed with ether, and dried under vacuum. Yield: 0.87 g, 90% based on the ligand **L_{10}**. Single-crystals suitable for X-ray diffraction were obtained from slow evaporation of a EtOH: water (1:1) solution of the compound. Anal. Calcd (%) for $C_{22}H_{16}I_2N_{12}OS_4Zn_2$: C, 27.11; H, 1.65; N, 17.25. Found: C, 27.13; H, 1.63; N, 17.27%.; IR (KBr disk) (cm^{-1}); ν(SCN), 2190 (s), 2140; ν(C=N), 1593 (m) ; ν(N=N), 1398 (m); ν(C=S), 685 (m).

5.11A. Synthesis and Characterization of complex (11), [Cd (L_5)$_2$Cl$_2$(H_2O)]. To a solution of **L_5** (.372 g, 2 mmol) in CH_3OH (3 mL) solid $CdCl_2$,H_2O (0.202 g, 1 mmol) was added in portions, with constant stirring. Light green precipitate that formed immediately was collected by filtration, washed with ether (5 mL), and

dried in vacuo. Pinkish-red, Yield: 0.354 g (65%). X-ray quality crystals having the composition $C_{18}H_{18}Cl_2N_8OCd$ were grown by diffusion of EtOH: water (1:1) solution of the complex. Desolvation of crystals occurred, when they were kept without mother liquor. Anal. Calcd (%) for $C_{18}H_{18}Cl_2N_8OCd$: C, 39.61; H, 3.32; N, 20.53. Found: C, 39.48; H, 63.43; N, 20.60%.; IR (KBr disk) (cm^{-1}); ν(C=N), 1595 (m) , ν(N=N), 1402 (m); ν(O-H), 3550.

5.12A. Synthesis and Characterization of complex (12), [CdL_5Cl_2]. To a solution of **L_5** (.186 g, 1 mmol) in CH_3OH (3 mL) solid $CdCl_2$ (0.182 g, 1 mmol) was added in portions, with constant stirring. Light green precipitate that formed immediately was collected by filtration, washed with ether (5 mL), and dried in vacuo. Light yellow, Yield: 0.267 g (75%). X-ray quality crystals having the composition $C_9H_8Cl_2N_4Cd$ were grown by diffusion of EtOH: water (1:1) solution of the complex. Desolvation of crystals occurred, when they were kept without mother liquor. Anal. Calc. for $C_9H_8Cl_2N_4Cd$: C, 30.40; H, 2.26; N, 15.75. Found: C, 30.52; H, 2.18; N, 15.82%.; IR (KBr disk) (cm^{-1}); ν(C=N), 1595 (m) ; ν(N=N), 1394 (m).

5.13A. Synthesis and Characterization of complex (13), [$Cd(L_6)_2Cl_2$]. To a solution of **L_6** (.37 g, 2 mmol) in CH_3OH (20 mL) solid $Cu(NO_3)_2$ (0.20 g, 1 mmol) was added in portions, with constant stirring. Light yellow precipitate that formed immediately was collected by filtration, washed with ether (20 mL), and dried in vacuo. Yield: 0.52 g, 90% based on the ligand **L_6**. Single-crystals suitable for X-ray diffraction were obtained from slow evaporation of a EtOH: water (1:1) solution of the compound. Anal. Calcd (%) for $C_{20}H_{22}Cl_2N_8Cd$: C, 43.01; H, 3.97; N, 20.07. Found: C, 43.11; H, 3.41; N, 20.01%.; IR (KBr disk) (cm^{-1}); ν(C=N), 1606 (m) ; ν(N=N), 1407 (m).

5.14A. Synthesis and Characterization of complex (14), [$Cd(L_7)_2(NO_3)_2$]. To a solution of **L_7** (.404 g, 2 mmol) in CH_3OH (20 mL) solid $Cd(NO_3)_2$ (0.30 g, 1 mmol) was added in portions, with constant stirring. Light yellow precipitate that formed immediately was collected by filtration, washed with ether (20 mL), and dried in vacuo. Yield: 0.52 g, 90% based on the ligand **L_7**. Single-crystals suitable for X-ray diffraction were obtained from slow evaporation of a EtOH: water (1:1) solution of the compound. Anal. Calcd (%) for $C_{20}H_{20}N_{10}O_8Cd$: C, 37.38; H, 3.13; N, 21.80. Found: C, 37.42; H, 3.15; N, 21.88%.; IR (KBr disk) (cm^{-1}); ν(N=O), 1420 (s); ν(N-O), 1275 (m); ν(ONO),980; ν(C=N), 1604 (m) ; ν(N=N), 1403 (m).

5.15A. Synthesis and Characterization of complex (15), [$Cd(L_8)_2(NO_3)_2$]. To a solution of **L_8** (.412 g, 2 mmol) in CH_3OH (20 mL) solid $Cd(NO_3)_2$ (0.30 g, 1 mmol) was added in portions, with constant stirring. Light yellow precipitate that formed immediately was collected by filtration, washed with ether (20 mL), and dried in vacuo. Yield: 0.51 g, 80% based on the ligand **L_8**. Single-crystals suitable for X-ray diffraction were obtained from slow evaporation of a EtOH: water (1:1) solution of the compound. Anal. Calcd (%) for $C_{18}H_{14}Cl_2N_{10}O_6Cd$: C, 33.23; H, 2.17; N, 21.54. Found: C, 33.29; H, 2.15; N, 21.51%.;IR (KBr disk) (cm^{-1}); ν(N=O), 1415 (s); ν(N-O), 1280 (m); ν(ONO),990; ν(C=N), 1610 (m) ; ν(N=N), 1407 (m).

5.16A. Synthesis and Characterization of complex (16), [$Cd_2(L_8)_2(SCN)_6$]. To a magnetically stirred solution of **L_8** (0.20 g, 1 mmol) in CH_3OH (20 mL), was added solid $Cd(NO_3)_2$ (0.30 g, 1 mmol) in portions. Then the aqueous solution of NH_4SCN (0.15, 2 mmol) was added to this mixture. A dark-yellow precipitate that formed was filtered, washed with ether, and dried under vacuum. Yield: 0.41 g, 95% based on the ligand **L_8**. Single-crystals suitable for X-ray diffraction were obtained from slow evaporation of a EtOH: water (1:1) solution of the compound. Anal. Calcd (%) for $C_{11}H_7ClN_6S_2Cd$: C, 30.28; H, 1.61; N, 19.27. Found: C, 30.25; H, 1.65; N, 19.25%.; IR (KBr disk) (cm^{-1}); ν(NCS), 2094 (s); ν(SCN), 2078 (s); ν(C=N), 1598 (m) ; ν(N=N), 1410 (m); ν(C=S), 775 (m).

5.17A. Synthesis and Characterization of complex (17), $[Cd(L_9)_2Cl_2]$. To a solution of $\mathbf{L_9}$ (0.50 g, 2 mmol) in CH_3OH (20 mL) solid $CdCl_2$ (0.20 g, 1 mmol) was added in portions, with constant stirring. Yellowish red precipitate that formed immediately was collected by filtration, washed with ether (20 mL), and dried in vacuo. Yield: 0.61 g, 90% based on the ligand $\mathbf{L_9}$. Single-crystals suitable for X-ray diffraction were obtained from slow evaporation of a EtOH: water (1:1) solution of the compound. Anal. Calcd (%) for $C_{18}H_{14}Br_2Cl_2N_8Cd$: C, 31.58; H, 2.06; N, 16.38. Found: C, 31.56; H, 2.08; N, 16.35%.; IR (KBr disk) (cm^{-1}); ν(C=N), 1602 (m) ; ν(N=N), 1401 (m).

5.18A. Synthesis and Characterization of complex (18), $[Cd(L_9)_2(NO_3)_2]$. To a solution of $\mathbf{L_9}$ (.504 g, 2 mmol) in CH_3OH (20 mL) solid $Cd(NO_3)_2$ (0.30 g, 1 mmol) was added in portions, with constant stirring. Yellowish red precipitate that formed immediately was collected by filtration, washed with ether (20 mL), and dried in vacuo. Yield: 0.63 g, 85% based on the ligand $\mathbf{L_9}$. Single-crystals suitable for X-ray diffraction were obtained from slow evaporation of a EtOH: water (1:1) solution of the compound. Anal. Calcd (%) for $C_{18}H_{14}Br_2N_{10}O_6Cd$: C, 29.27; H, 1.91; N, 18.97. Found: C, 29.28; H, 1.94; N, 18.95%.; IR (KBr disk) (cm^{-1}); ν(N=O), 1417 (s); ν(N-O), 1278 (m); ν(ONO),982; ν(C=N), 1600 (m) ; ν(N=N), 1401 (m).

5.19A. Synthesis and Characterization of complex (19), $[Cd(L_9)_2(NO_3)_2]$. To a solution of $\mathbf{L_9}$ (.59 g, 2 mmol) in CH_3OH (20 mL) solid $Cd(NO_3)_2$ (0.308 g, 1 mmol) was added in portions, with constant stirring. Yellowish red precipitate that formed immediately was collected by filtration, washed with ether (20 mL), and dried in vacuo. Yield: 0.66 g, 80% based on the ligand $\mathbf{L_9}$. Single-crystals suitable for X-ray diffraction were obtained from slow evaporation of a EtOH: water (1:1) solution of the compound. Anal. Calcd (%) for $C_{18}H_{14}I_2N_{10}O_6Cd$: C,25.90; H, 1.69; N, 16.79. Found: C, 25.88; H, 1.67; N, 17.78%.; IR (KBr disk) (cm^{-1}); ν(N=O), 1416 (s); ν(N-O), 1276 (m); ν(ONO),979; ν(C=N), 1603 (m) ; ν(N=N), 1402 (m).

5.20A. Synthesis and Characterization of complex (20), $[Hg(L_5H^+)_2(SCN)_4]$. To a magnetically stirred solution of $\mathbf{L_5}$ (0.372 g, 2 mmol) in CH_3OH (20 mL), was added solid $HgCl_2$ (0.271 g, 1 mmol) in portions. Then the aqueous solution of NH_4SCN (0.304, 4 mmol) was added to this mixture. A greenish-yellow precipitate that formed was filtered, washed with ether, and dried under vacuum. Dark-brown, Yield: 0.585 g (75%). Single-crystals suitable for X-ray diffraction were obtained from slow evaporation of an EtOH: water (1:1) solution of the compound at RT. Anal. Calcd (%) for $C_{22}H_{18}N_{12}S_4Hg$: C, 33.90; H, 2.32; N, 21.56. Found: C, 33.97; H, 2.40; N, 21.50%. IR (KBr disk) (cm^{-1}); ν(NCS), 2095 (s); ν(SCN), 2068 (s); ν(C=N), 1594 (m) ; ν(N=N), 1401 (m); ν(C=S), 770 (m).

5.21A. Synthesis and Characterization of complex (21), $(HL_9)_2[Hg(SCN)_4]_2$. To a magnetically stirred solution of $\mathbf{L_9}$ (0.50 g, 1 mmol) in CH_3OH was added solid $HgCl_2$ (0.27 g, 1 mmol) in portions. Then the aqueous solution of NH_4SCN (0.30, 4 mmol) was added to this mixture. A dark-yellow precipitate that formed was filtered, washed with ether, and dried under vacuum. Yield: 0.66 g, 70% based on the ligand $\mathbf{L_9}$. Single-crystals suitable for X-ray diffraction were obtained from slow evaporation of a EtOH: water (1:1) solution of the compound. Anal. Calcd (%) for $C_{22}H_{16}Br_2N_{12}S_4Hg$: C, 28.20; H, 1.72; N, 17.95. Found: C, 28.22; H, 1.74; N, 17.94%.; IR (KBr disk) (cm^{-1}); ν(SCN), 2190 (s), 2118;(C=N), 1598 (m) ; (N=N), 1399 (m); (C=S), 688 (m).

Table 5.1 A. Crystal Data and Structure Refinement for Complex **1- 5.**

	Complex **1**	Complex **2**	Complex **3**	Complex **4**	Complex **5**
Empirical formula	$C_{20}H_{16}N_{10}S_2Mn$	$C_{18}H_{16}Cl_2N_8Ru$	$C_{18}H_{16}Cl_2N_8Cu$	$C_{22}H_{20}CuN_{10}S_2$	$C_{10}H_{12}CuN_6O_8$
Fw	515.51	516.36	478.84	552.17	407.81
crystal system	Monoclinic	Orthorhombic	Monoclinic	Orthorhombic	Monoclinic
space group	C2/c	Pccn	P2(1)/n	Pca2(1)	P2(1)/c
a, Å	14.7423(4)	7.75010(10)	9.2659(4)	11.8175(3)	9.7920(1)
b, Å	11.6833(3)	11.9552(2)	18.1060(8)	12.7372(3)	6.9041(1)
c, Å	14.3886(4)	21.5104(3)	12.0298(5)	17.0007(4)	23.3863(3)
α, deg	90	90	90	90	90
β, deg	89.92	90	89.92	90	97.985(1)
γ, deg	90	90	90	90	90
V, $Å^3$	2018.22(15)	1993.02(5)	2018.22(15)	2558.98(11)	1565.70(3)
Z	4	4	4	4	4
μ	1.365	1.073	1.365	1.044	1.455
F(000)	965	1158	965	1156	694
GOF(S)	0.991	1.014	0.991	0.843	1.055
R_{int}	0.0255	0.0282	0.0255	0.0304	0.0181
final R indices [I > 2σ(I)]	R1= 0.0412 wR2= 0.1455	R1= 0.0304 wR2= 0.743	R1= 0.0412 wR2= 0.1455	R1= 0.0429 wR2= 0.1171	R1= 0.0260 wR2= 0.0712
R indices (all data)	R1= 0.0686 wR2= 0.1631	R1= 0.0491 wR2= 0.840	R1= 0.0686 wR2= 0.1631	R1= 0.843 wR2= 0.1432	R1=0.0320 wR2= 0.0744

Table 5.2 A. Crystal Data and Structure Refinement for Complex **6 - 10.**

	Complex **6**	Complex **7**	Complex **8**	Complex **9**	Complex **10**
Empirical formula	$C_{18}H_{18}C_{l2}N_8OZn$	$C_{22}H_{20}N_{10}S_2Zn$	$C_{12}H_{14}N_6O_3S_2Zn$	$C_{22}H_{20}Br_2N_{10}OS_2Zn$	$C_{22}H_{16}I_2N_{12}OS_4Zn_2$
Fw	498.69	554.01	419.82	729.81	977.33
crystal system	Monoclinic	Monoclinic	Monoclinic	Triclinic	Triclinic
space group	P2(1)/c	P2(1)/n	P2(1)/c	P-1	P-1
a, Å	8.1606(2)	11.0016(2)	10.2949(2)	8.0014(3)	8.2365(3)
b, Å	19.2921(5)	15.0798(2)	13.2491(2)	11.6256(4)	12.6506(5)
c, Å	14.0277(5)	15.5549(2)	13.1432(2)	17.0817(6)	16.5817(7)
α, deg	90	90	90	100.638(2	93.546(2)
β, deg	94.785(2)	92.6070(10)	91.698(1)	101.582(3)	92.767(2)
γ, deg	90	90	90	104.661(2)	101.740(2)
V, $Å^3$	2200.76(11)	2577.92(7)	1791.92(5)	1458.72(9)	1685.10(12)
Z	4	4	4	2	2
μ	1.388	1.146	1.631	3.756	3.546
F(000)	1088	1136	692	688	960
GOF(S)	1.024	1.010	0.979	1.018	1.018
R_{int}	0.0294	0.0230	0.0160	0.0291	0.0243
final R [I > 2σ(I)]	R1=0. 0.0309 wR2= 0.0730	R1=0.0332 wR2= 0.0720	R1= 0.0295 wR2=0.0630	R1= 0.0471 wR2= 0.1160	R1= 0.0605 wR2= 0.1690
R indices (all data)	R1= 0.0502 wR2= 0.0809	R1= 0.0563 wR2= 0.0808	R1= 0.0390 wR2=0.0674	R1= 0.1009 wR2= 0.1395	R1= 0.0972 wR2= 0.1956

Table 5.3 A. Crystal Data and Structure Refinement for Complex **11 - 15**.

	Complex **11**	Complex **12**	Complex **13**	Complex **14**	Complex **15**
Empirical formula	$C_{18}H_{18}Cl_2N_8OCd$	$C_9H_8Cl_2N_4Cd$	$C_{20}H_{22}CdCl_2N_8$	$C_{20}H_{20}CdN_{10}O_8$	$C_{18}H_{14}CdCl_2N_{10}O_6$
Fw	545.71	355.50	557.77	640.87	649.70
crystal system	Monoclinic	Monoclinic	Monoclinic	Triclinic	Monoclinic
space group	P2(1)/c	P2(1)/n	C2/c	C2/c	C2/c
a, Å	8.3278(2)	7.09440(10)	11.7834(14)	15.4614(3)	14.0672(3)
b, Å	19.3123(3)	20.1085(3)	12.9682(15)	10.9049(3)	12.2255(3)
c, Å	14.0265(3)	8.64560(10)	15.504(2)	16.3198(4)	15.6602(4)
α, deg	90	90	90	90	90
β, deg	94.4510(10)	95.3840(10)	101.697(8)	116.295(3)	111.1890(10)
γ, deg	90	90	90	90	90
V, $Å^3$	2249.06(8)	1227.92(3)	2320.0(5)	2466.88(12)	2511.14(10)
Z	4	4	4	4	4
μ	1.229	2.212	1.196	0.953	1.138
F(000)	1260	576	1120	1288	1288
GOF(S)	1.011	0.923	1.067	1.018	1.052
R_{int}	0.0205	0.0161	0.0359	0.0243	0.0256
final R	R1= 0.0283	R1= 0.0208	R1=0.0230	R1= 0.0242	R1=0.0311
I > 2σ(I)	wR2= .0636	wR2=0.0524	wR2= .0615	wR2= 0.0583	wR2= 0.0798
R indices (all data)	R1= 0.0410	R1= 0.0235	R1= 0.0253	R1= 0.0311	R1= 0.0373
	wR2= .0689	wR2=0.0539	wR2= 0.0629	wR2= 0.0615	wR2= 0.0838

Table 5.4 A. Crystal Data and Structure Refinement for Complex **16 - 21**.

	Complex **16**	Complex **17**	Complex **18**	Complex **19**	Complex **20**	Complex **21**
Empirical formula	$C_{11}H_7CdClN_6S_2$	$C_{18}H_{14}Br_2CdCl_2N_8$	$C1_8H_{14}Br_2CdN_{10}O_6$	$C_{18}H_{14}CdI_2N_{10}O_6$	$C_{22}H_{18}N_{12}S_4Hg$	$C_{22}H_{16}Br_2HgN_{12}S_4$
Fw	435.23	685.48	738.60	832.60	779.35	937.14
crystal system	Monoclinic	Monoclinic	Monoclinic	Monoclinic	Monoclinic	Triclinic
space group	P2(1)/n	C2/c	C2/c	C2/c	P2(1)/c	P-1
a, Å	10.2276(2)	12.2334(7)	13.9215(13)	13.9965(2)	20.4427(4)	11.5023(6)
b, Å	9.9873(2)	12.2602(7)	12.3270(13)	12.3668(2)	7.6319(2)	13.0468(7)
c, Å	15.2442(3)	15.8426(9)	15.8481(15)	16.3006(3)	19.6921(4)	24.1186(12)
α, deg	90	90	90	90	90	90.734(3)
β, deg	97.9800(10)	103.158(2)	110.220(8)	109.1580(10)	103.9830(10)	103.203(3)
γ, deg	90	90	90	90	90	112.881(3)
V, $Å^3$	1542.06(5)	2313.8(2)	2552.1(4)	2665.24(8)	2981.26(11)	3225.6(3)
Z	4	4	4	4	4	4
μ	1.865	4.655	1.455	3.193	5.479	7.579
F(000)	992	1320	1488	1548	1888	1784
GOF(S)	1.055	1.041	0.966	1.038	1.185	1.030
R_{int}	0.0164	0.0251	0.0273	0.0195	0.0316	0.0332
final R	R1= 0.0195	R1= 0.0340	R1= 0.0431	R1=0.0554	R1= 0.0383	R1= 0.0421
$I > 2\sigma(I)$	wR2= 0.0478	wR2= 0.0872	wR2= 0.0972	wR2= 0.1608	wR2= 0.0651	wR2=0.0888
R indices	R1= 0.0224	R1= 0.0396	R1= 0.0615	R1= 0.0641	R1= 0.0501	R1= 0.0900
(all data)	wR2= 0.0495	wR2= 0.0903	wR2= 0.1069	wR2= 0.1695	wR2= 0.0719	wR2=0.1031

Table 5.5 A. Selected bond length and bond angles in complexes **1-21**.

Complex **1**			
Mn1 N1 2.228(2)		Mn1 N5 2.101(2)	
N5 Mn1 N5a 130.10(11)	N5 Mn1 N1a 119.98(8)	N1 Mn1 N1a 89.65(11)	N5 Mn1 N1 95.66(7)
Complex **2**			
Ru1 N1 2.061(2)	Ru1 N4 2.000(2)	Ru1 Cl1 2.3881(9)	
N4 Ru1 N4a 104.70(14)	N1a Ru1 Cl1 90.54(8)	N4a Ru1 N1 178.70(9)	N4 Ru1 Cl1a 93.50(8)
N4 Ru1 N1a 178.70(9)	N1 Ru1 Cl1 85.61(8)	N1a Ru1 N1 102.76(13)	N4 Ru1 Cl1a 90.25(8)
N4a Ru1 N1a 76.28(10)	N1a Ru1 Cl1a 85.61(8)	N4 Ru1 Cl1 90.25(8)	N1 Ru1 Cl1a 90.54(8)
N4 Ru1 N1 76.28(10)	Cl1 Ru1 Cl1a 173.85(4)	N4a Ru1 Cl1 93.51(8)	
Complex **3**			
Cu1 N1 1.943(3)	Cu1 N4 2.535(2)	Cu1 N5 1.941(3)	
Cu1 N8 2.515(3)	Cu1 Cl1 2.4037(9)	Cu1 Cl2 2.4110(9)	
N5 Cu1 N1 161.17(12)	N1 Cu1 Cl2 96.79(7)	Cl1 Cu1 N8 166.23(7)	Cl1 Cu1 N4 88.67(6)
N5 Cu1 Cl1 95.27(7)	Cl1 Cu1 Cl2 100.62(3)	Cl2 Cu1 N8 86.55(6)	Cl2 Cu1 N4 165.72(6)
N1 Cu1 Cl1 94.99(8)	N5 Cu1 N8 72.06(10)	N5 Cu1 N4 93.09(9)	N8 Cu1 N4 86.72(8)
N5 Cu1 Cl2 96.80(7)	N1 Cu1 N8 95.82(10)	N1 Cu1 N4 71.40(9)	
Complex **4**			
Cu1 N5 1.966(3)	Cu1 N9 1.998(5)	Cu1 S1 2.5592(17)	
Cu1 N1 1.975(3)	Cu1 N8 2.357(4)		
N5Cu1N1163.81(15)	N5Cu1S196.84(14)	N9Cu1N8166.14(16)	N9Cu1S1100.85(16)
N5Cu1N993.38(17)	N5Cu1N874.31(15)	N1Cu1S1 94.48(13)	N8Cu1 S1 87.18(10)
N1Cu1 N9 95.82(16)	N1Cu1N894.78(14)		
Complex **5**			
Cu1 N1 1.9606(13)	Cu1 O8 1.9662(18)	Cu1 N4 2.3787(12)	
Cu1 O2 1.9659(12)	Cu1 O5 1.9884(13)		
N1Cu1 O2 173.89(5)	O2 Cu1 N4 99.03(5)	N3 N4 Cu1 110.90(10)	N1 Cu1 N4 75.13(5)
N1 Cu1 O8 92.85(8)	O8 Cu1 N4 98.53(8)	C4 N4 Cu1 133.88(10)	N6O5Cu1113.98(11)
O2 Cu1 O8 86.21(8)	C1 N1 Cu1 114.83(11)	O5 Cu1 N4 89.97(5)	N5O2Cu1113.50(11)
N1 Cu1 O5 93.32(6)	C2 N1 Cu1 139.03(11)	O8Cu1 O5 170.55(8)	O2 Cu1 O5 88.40(6)
Complex **6**			
Zn1 N1 2.0341(14)	Zn1 N5 2.0134(15)	Zn1 Cl1 2.2403(6)	Zn1 Cl2 2.3436(6)
N5 Zn1 N1 117.62(6)	N1 Zn1 Cl1 106.86(5)	N1 Zn1 Cl2 104.21(5)	
N5 Zn1 Cl1 122.10(5)	N5 Zn1 Cl2 97.50(5)	Cl1 Zn1 Cl2 105.80(2)	
Complex **7**			
Zn1 N2 1.9389(18)	Zn1 N1 1.9892(19)	Zn1 N8 2.0087(16)	Zn1 N3 2.0193(16)
N2Zn1 N1 104.21(8)	N1 Zn1 N8 97.63(8)	N1Zn1 N3 112.64(7)	
N2Zn1 N8 127.67(7)	N2 Zn1 N3 109.83(7)	N8Zn1 N3 104.23(7)	
Complex **8**			
Zn1 N5 1.9497(19)	Zn1 N1 1.9927(17)	Zn1 N4 2.3624(16)	Zn1 O2 2.149(2)
Zn1 N6 1.9601(18)			
N5 Zn1 N6117.12(8)	N6 Zn1 O2 90.85(9)	N6 Zn1 N4 92.35(7)	
N5 Zn1 N1119.14(8)	N1 Zn1 O2 96.67(9)	N1 Zn1 N4 73.59(7)	
N6 Zn1 N1122.79(8)	N5 Zn1 N4 94.94(7)	O2 Zn1 N4 169.92(8)	
N5 Zn1 O2 92.09(9)			
Complex **9**			
Zn1 N9 1.952(5)	Zn1 N1 2.003(3)	Zn1 N10 2.010(4)	Zn1 N5 2.013(3)
N9Zn1N1105.32(16)	N1Zn1 N5 112.65(14)	C10N5 Zn1 127.4(3)	
N9Zn1N10113.74(19)	N10Zn1N5101.23(15)	C11N5 Zn1 126.3(3)	
N1Zn1N10116.88(16)	C1 N1 Zn1 124.6(3)	C20N10Zn1153.9(6)	
N9Zn1 N5 106.79(16)	C2 N1 Zn1 129.0(3)	C19N9 Zn1 165.5(4)	

Complex **10**

Zn1 N9 1.933(5)	Zn1 N4 2.505(4)	Zn2N101.960(5)
Zn1 N11 1.960(5)	Zn1 S2 2.6098(18)	Zn2 N5 1.976(6)
Zn1 N1 1.979(5)	Zn2 N12 1.919(5)	Zn2S3 2.5787(18)
N9Zn1N11118.2(2)	N10Zn2N5116.1(2)	N10Zn2 S3 95.00(15)
N9Zn1 N1 119.7(2)	N12Zn2S3100.12(18)	N5 Zn2 S3 96.5(2)
N11Zn1N1118.1(2)	N1 Zn1 N4 71.72(17)	C21 S3 Zn2 93.6(2)
N9Zn1N489.56(19)	N9Zn1S298.53(17)	C20 S2Zn199.50(19)
N11Zn1N488.77(17)	C20 N10 Zn2157.6(5)	C1 N1 Zn1 118.9(4)
C11 N5 Zn2132.3(6)	C21 N11Zn1157.7(5)	C2 N1 Zn1 136.5(5)
C19N9Zn1174.2(6)	C10 N5 Zn2 121.3(6)	N3 N4 Zn1 110.5(3)
N11Zn1S294.85(14)	N4Zn1 S2 168.23(12)	C4 N4 Zn1 133.7(3)
N1 Zn1S2 96.75(15)	N12Zn2N10 117.9(3)	

Complex **11**

Cd1 N1 2.238(2)	Cd1 N5 2.214(2)	Cd1 Cl1 2.5441(7)	Cd1 Cl2 2.4291(8)
N5 Cd1 N1 120.98(8)	N1 Cd1 Cl2 103.77(6)		N1 Cd1 Cl1 103.03(6)
N5 Cd1 Cl2 128.46(6)	N5 Cd1 Cl1 90.58(6)		Cl2 Cd1 Cl1 103.74(3)

Complex **12**

Cd1 N1 2.2600(18)	Cd1 N4 2.6004(19)	Cd1 Cl1 2.5125(5)	Cd1 Cl2 2.6010(6)
N1 Cd1 Cl1 167.05(5)	N1 Cd1 Cl2 92.43(5)		Cl1 Cd1 N4 105.09(5)
N1 Cd1 N4 67.47(7)	N1 Cd1 Cl2 92.31(5)		N4 Cd1 Cl2 157.18(4)
Cl1 Cd1 Cl2 96.68(2)			

Complex **13**

Cd1 N1 2.2532(14)	Cd1 Cl1 2.4940(5)	
N1 Cd1 N1 133.85(7)	Cl1 Cd1 Cl1 104.90(3)	C8 N1 Cd1 121.34(11)
N1 Cd1 Cl1 98.39(4)	C8 N1 C10 105.53(15)	C10 N1 Cd1 132.92(12)
N1 Cd1 Cl1 109.38(4)		

Complex **14**

Cd1 N1 2.2240(14)	Cd1 O3 2.4238(18)	Cd1 O2 2.5489(16)
N1 Cd1 N1145.20(8)	N5 O2 Cd1 92.80(11)	C1 N1 Cd1121.54(13)
N1 Cd1 O3 83.43(6)	N5 O3 Cd1 98.72(13)	C2 N1 Cd1131.57(14)
N1 Cd1 O3115.33(6)	N1 Cd1 O2 79.16(5)	N1 Cd1 O2 131.18(6)
N1 Cd1 O3115.33(6)	O3 Cd1 O2 50.84(5)	O3 Cd1 O2 78.86(6)
N1 Cd1 O3 83.43(6)	O3 Cd1 O2 78.86(6)	O3 Cd1 O2 50.84(5)
O3 Cd1 O3116.76(8)	N1 Cd1 O2 79.16(5)	O2 Cd1 O2 76.30(8)
N1 Cd1 O2131.18(6)		

Complex **15**

Cd1 N1 2.210(2)	Cd1 O1 2.430(2)	Cd1 O3 2.5130(19)
N1Cd1N1142.94(11)	N1 Cd1 O3 82.24(7)	O1 Cd1 O3 79.33(8)
N1 Cd1 O1 82.62(7)	O1 Cd1 O3 51.32(7)	N5O1Cd197.48(17)
N1Cd1 O1 116.64(8)	N1 Cd1 O3 82.24(7)	N5O3Cd1 93.05(15)
N1Cd1 O1 116.64(8)	N1Cd1 O3 130.29(7)	C1 N1 C2 105.8(2)
N1Cd1O182.62(7)	O1 Cd1 O3 79.33(8)	C1N1Cd1122.08(17)
O1Cd1O1119.57(11)	O1 Cd1 O3 51.32(7)	C2N1Cd1132.03(17)
N1Cd1 O3 130.29(7)	O3Cd1 O3 72.81(11)	

Complex **16**

Cd1N12.2692(15)	Cd1N62.2938(18)	Cd1 S2 2.6482(5)
Cd1N52.2711(18)	Cd1N42.5934(15)	Cd1 S1 2.7820(5)
N1 Cd1 N5 90.76(7) .	N6 Cd1 S2 94.60(4)	C10S1Cd1103.29(6)
N1 Cd1 N6 91.51(6)	N4 Cd1 S2 105.77(4)	C1N1Cd1116.47(12)
N5 Cd1 N6 96.96(7)	N1 Cd1 S1 91.50(4)	C2N1Cd1137.61(15)
N1 Cd1 N4 67.06(5)	N5 Cd1 S1 104.90(5)	N3N4Cd1115.04(12)
N5 Cd1 N4 157.71(6)	N6 Cd1 S1 157.88(5)	C4N4Cd1128.89(11)
N6 Cd1 N4 82.07(6)	N4 Cd1 S1 78.97(4)	C11N6Cd1164.98(16)
N1 Cd1 S2 169.86(4)	S2Cd1 S1 79.827(15)	C10N5Cd1161.21(18)
N5 Cd1 S2 96.51(5)	C11 S2 Cd1 97.63(6)	

Complex **17**		
Cd1 N1 2.253(3)	Cd1 Cl1 2.4987(9)	
N1Cd1N1 133.37(13)	N1 Cd1 Cl1 12.99(7)	C1 N1 Cd1 121.5(2)
N1 Cd1 Cl1 95.68(7)	N1Cd1 Cl1 112.99(7)	C2 N1 Cd1 133.1(2)
Cl1Cd1 Cl1 103.59(5)	N1 Cd1 Cl1 95.68(7)	
Complex **18**		
Cd1 N1 2.210(3)	Cd1 O3 2.430(4)	Cd1 O1 2.502(3)
N1 Cd1 N142.28(19)	O3 Cd1 O1 80.61(14)	O3 Cd1 145.55(11)
N1 Cd1 O117.43(14)	O3 Cd1 O1 51.03(12)	O3 Cd1 N83.28(13)
N1 Cd1 O3 81.93(13)	N1 Cd1 O1 82.99(12)	O1 Cd1 100.83(12)
N1 Cd1 O3 81.93(13)	N1 Cd1O1129.72(12)	O1 Cd1 162.63(11)
N1 Cd1 O117.43(14)	O3 Cd1 O1 51.03(12)	C1 N1 Cd1 122.1(3)
O3 Cd1 O120.62(19)	O3 Cd1 O1 80.61(14)	C2 N1 Cd1 131.9(3)
N1 Cd1 O129.73(12)	O1 Cd1 O1 73.81(19)	N3 N4 Cd1 111.6(3)
N1 Cd1 O1 82.99(13)	N1 Cd1 N4 88.38(12)	C4 N4 Cd1 133.0(3)
N5 O3 Cd1 97.9(3)	N1 Cd1 N4 64.31(11)	N5 O1 Cd1 93.1(2)
Complex **19**		
Cd1 N1 2.219(5)	Cd1 O1 2.433(6)	Cd1 O3 2.513(5)
Cd1 N1 2.219(5)	Cd1 O3 2.513(5)	Cd1 N4 2.791(5)
Cd1 O1 2.433(6)		
N1Cd1N1141.6(3)	N5 O3 Cd1 93.4(4)	O1 Cd1 O3 82.5(2)
N1Cd1O181.24(19)	N5 O1 Cd1 98.0(4)	O1 Cd1 O3 50.74(17)
N1Cd1 O1 118.0(2)	N3 N4 Cd1 111.1(4)	O3 Cd1 O3 75.6(3)
N1Cd1 O1 118.0(2)	C4 N4 Cd1 133.1(4)	O1 Cd1 N4 83.38(19)
N1Cd1O181.23(19)	N1Cd1O3 129.17(17)	O1Cd1N4 144.47(16)
O1Cd1 O1 122.3(3)	N1 Cd1 O3 83.60(18)	O3Cd1N4 100.38(19)
N1Cd1N464.15(16)	N1 Cd1 N4 87.70(16)	O3Cd1N4 164.40(16)
O1Cd1O350.74(18)	N1 Cd1 O3 83.60(18)	C1 N1 Cd1 122.0(4)
O1 Cd1 O3 82.5(2)	N1Cd1O3 129.17(17)	C2 N1 Cd1 131.9(4)
Complex **20**		
Hg1 S1 2.5319(13)	Hg1 S4 2.5473(14) Hg1 S2 2.5480(14)	Hg1 S3 2.5021(14)
S3 Hg1 S1 112.18(6)	S1 Hg1 S4 106.06(5)	S1 Hg1 S2 112.19(5)
S3 Hg1 S4 110.21(5)	S3 Hg1 S2 109.03(5)	S4 Hg1 S2 107.00(5)
Complex **21**		
Hg1 S5 2.4854(16)	Hg1 S8 2.575(2)	Hg2 S2 2.4861(19)
Hg1 S7 2.526(2)	Br4 C34 1.897(6)	Hg2 S3 2.529(2)
Hg1 S6 2.539(2)	Hg2 S4 2.476(3)	Hg2 S1 2.6129(16)
S5Hg1 S7 115.71(6)	C43 S7 Hg1 98.0(2)	S3Hg2 S1 100.55(9)
S5Hg1 S6 117.99(8)	S4Hg2 S2 120.82(11)	C39 S3 Hg2 95.8(3)
S7Hg1 S6 104.44(8)	S4Hg2 S3 112.31(13)	C37 S1 Hg2 95.5(2)
S5Hg1 S8 106.58(7)	S2 Hg2 S3 111.89(8)	C41S5Hg1 100.8(2)
S7Hg1S8109.80(11)	S4 Hg2 S1 105.33(9)	C42 S6 Hg1 96.7(3)
S6Hg1 S8 101.28(9)	S2 Hg2 S1 103.09(6)	C44S8Hg1 101.9(2)
C40 S4 Hg2 99.3(4)	C38 S2 Hg2 100.8(3)	

Table 5.6A. Non-covalent interactions in complexes **1-21**.

D–H···A	H···A (Å)	D···A (Å)	D–H···A (◦)
Complex **1**			
N2–H2N····S1	2.691	3.380	138.11
π_c ····π_c		3.773	
C7-H7····π	2.754	3.560	140.28
Complex **2**			
C3–H2····Cl1	2.958	3.396	110.40
N2–H2N····Cl1	2.904	3.355	114.70
Complex **3**			
N2–H2N····Cl2	2.281	3.112	162.39
N6–H6N····Cl1	2.289	3.143	172.34
C2-H2····π	2.838	3.488	127.23
C3-H3····π	3.30	3.695	108.01
Complex **4**			
N6–H6N····N10	1.859	2.717	175.76
N2–H2N····π(C22-N9)	2.381	3.213	163.14
C3–H3····N10	2.680	3.393	134.10
C6–H6····S2	2.935	3.834	163.03
C20–H20A····S1	2.982	3.836	148.91
C12–H12····π^a	2.979	3.702	135.74
C20–H20B····π^b	3.155	4.102	169.32
Complex **5**			
N2–H3N····O3	2.258	2.978	149.54
N2–H3N····O4	2.484	3.229	154.89
O8–H8OA····O5	2.570	3.120	141.12
O8–H8OA····O7	2.123	2.759	159.11
O8–H8OB····O3	2.089	2.798	163.19
C2–H2····O1	2.574	3.485	170.46
C3–H3····O6	2.674	3.477	149.83
C10–H10C····O7	2.643	3.390	136.54
π^a····π^b			3.809
Complex **6**			
O1–H10····Cl2	2.209	3.214	165.17
N6–H6N····O2	1.922	2.766	166.54
C5–H5····Cl2	2.911	3.645	136.73
C8–H8····Cl1	2.831	3.679	152.11
π_c ····π_c		3.640	
Complex 7			
N4–H9····S1	2.800	3.478	142.06
N7–H22N····S1	2.616	3.390	148.93
C5–H5····S2	3.147	4.006	154.09
π^c····π^d			3.667
Complex **8**			
C2–H3····S2	2.969	3.800	162.26
N2–H50····O3	1.915	2.750	177.26
C10–H10A····O3	2.715	3.670	166.01
O2–H2OA····S1	2.485	3.849	173.99
O3–H3OA····S1	2.526	3.297	160.73
O2–H2OB····S2	2.493	3.262	173.50
O3–H3OB····O2	2.372	3.087	174.32
π^a····π^b		3.809	
Complex **9**			
N2–H2N····O1	1.916	2.762	167.12
N6–H6N····S1	2.444	3.265	159.71
O1–H1O····S2	2.732	3.402	140.83
Complex **10**			
C2–H2····I1	3.178	4.069	161.37
C3–H3····S3	2.918	3.795	157.73
N2–H2N····O1	1.844	2.686	166.15

N6–H6N····S4	2.467	3.302	164.35
C18–H18····O1	2.630	3.412	142.17
O1–H1O····S1	2.646	3.190	127.09
Complex **11**			
N6–H6N····O1	1.896	2.739	165.93
O1–H2O····Cl1	2.245	3.161	177.66
C8–H8····Cl2	2.815	3.691	157.40
C5–H5····Cl1	2.852	3.633	142.27
π_c ····π_c		3.770	
Complex **12**			
N2–H2····Cl1	2.726	3.474	146.28
N2–H2····Cl2	2.835	3.421	126.88
π_c ····π_c		3.909	
Complex **13**			
N2–H2N····Cl1	2.358	3.165	163.18
C10–H10A····π^a	3.415	4.280	151.02
Complex **14**			
N2–H2N····O2	2.201	2.962	147.56
C3–H3····O4	2.542	3.218	129.80
Complex **15**			
N2–H2N····O3	2.060	2.874	160.56
C3–H3····O2	2.497	3.049	118.22
C3–H3····O2	2.588	3.058	111.19
Complex **16**			
N2–H2N····S1	2.990	3.868	164.84
N2–H2N····S1	2.808	3.458	138.15
C3–H3····S1	2.915	3.476	127.93
Complex **17**			
N2–H2N····Cl1	2.387	3.159	149.56
C8–H8····Cl1	2.881	3.676	144.29
Complex **18**			
N2–H2N····O1	2.045	2.881	163.46
C3–H3····O2	2.517	3.043	116.12
C3–H3····O2	2.579	3.069	113.42
Complex **19**			
N2–H2A····O3	2.005	2.902	168.05
C3–H3····O2	2.558	3.052	113.59
C3–H3····O2	2.547	3.104	118.77
Complex **20**			
N2–H2····N9	1.989	2.824	164.06
N1–H1····N10	1.974	2.821	168.30
N5–H5····N11	2.028	2.865	164.32
N6–H6····N12	1.935	2.786	170.78
C3–H3····S2	2.981	3.772	143.74
C16–H16····S4	2.943	3.871	174.06
Complex **21**			
N1–H1N····N18	1.953	2.802	169.39
N2–H2N····N20	2.093	2.942	169.37
N5–H5N····N19	1.933	2.785	170.17
N6–H6N····N17	1.937	2.790	171.46
N9–H9N····N24	1.957	2.807	168.72
N10–H10N····N23	1.920	2.776	174.20
N13–H13N····N22	2.029	2.856	161.06
N14–H14N····N21	1.958	2.814	172.06
C6–H6····N19	2.704	3.521	147.17
C12–H12····N24	2.807	3.730	172.54
C11–H11···Br1	3.014	3.941	175.15
C14–H14····S2	2.860	3.736	157.32
C15–H15····N18	2.727	3.573	151.68
C17–H17···Br3	3.005	3.920	167.98
C21–H21····N17	2.804	3.678	156.79
C27–H27····S5	2.967	3.766	144.98

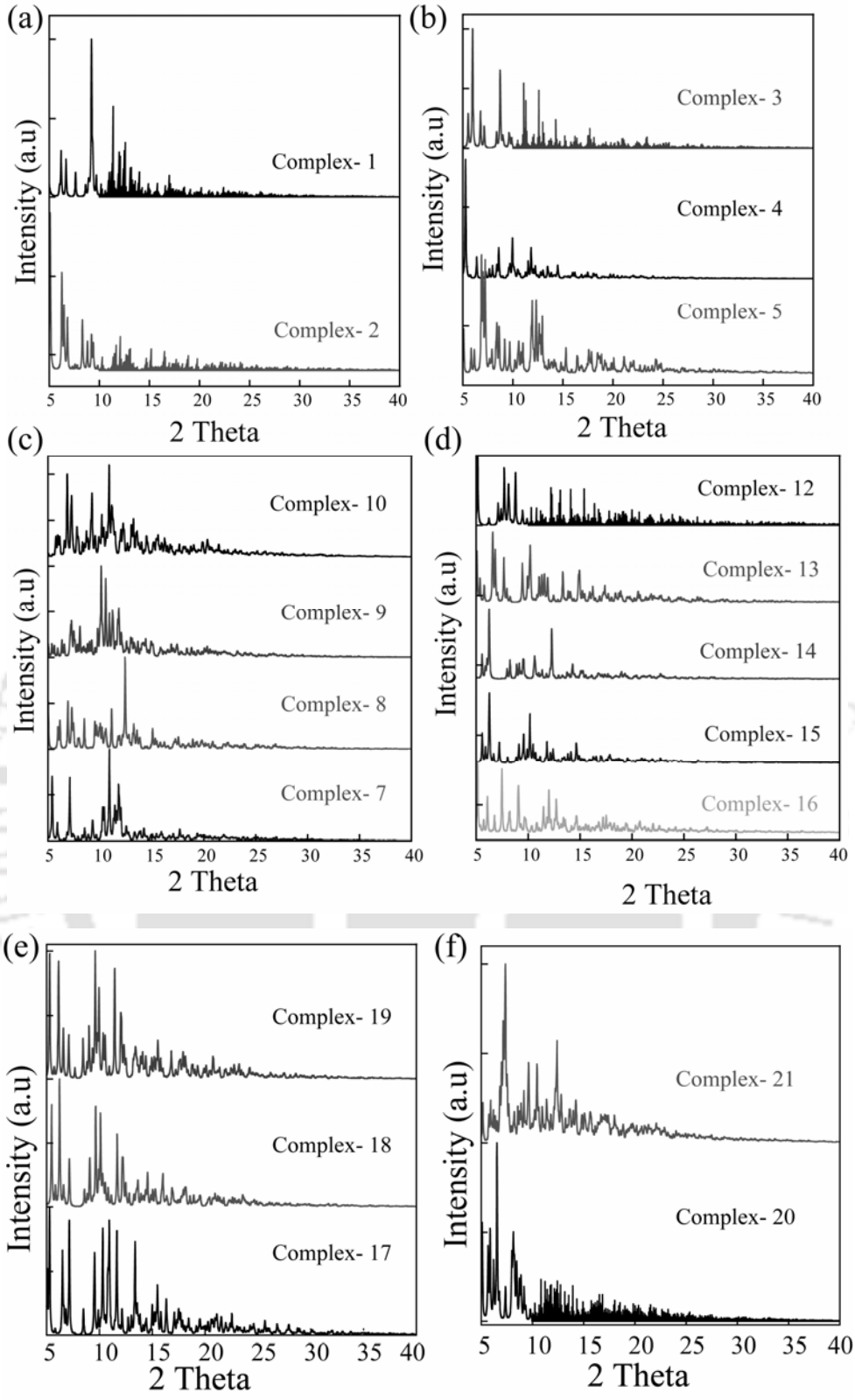

Figure 5.1.A. (a) PXRD pattern of crystalline complex **1** and **2**; (b) PXRD pattern of crystalline complex **3, 4** and **5**; (c) PXRD pattern of crystalline complex **7, 8, 9** and **10**; (d) PXRD pattern of crystalline complex **12, 13, 14, 15** and **16;** (e) PXRD pattern of crystalline complex **17, 18,** and **19;** (f) PXRD pattern of crystalline complex **20** and **21.**

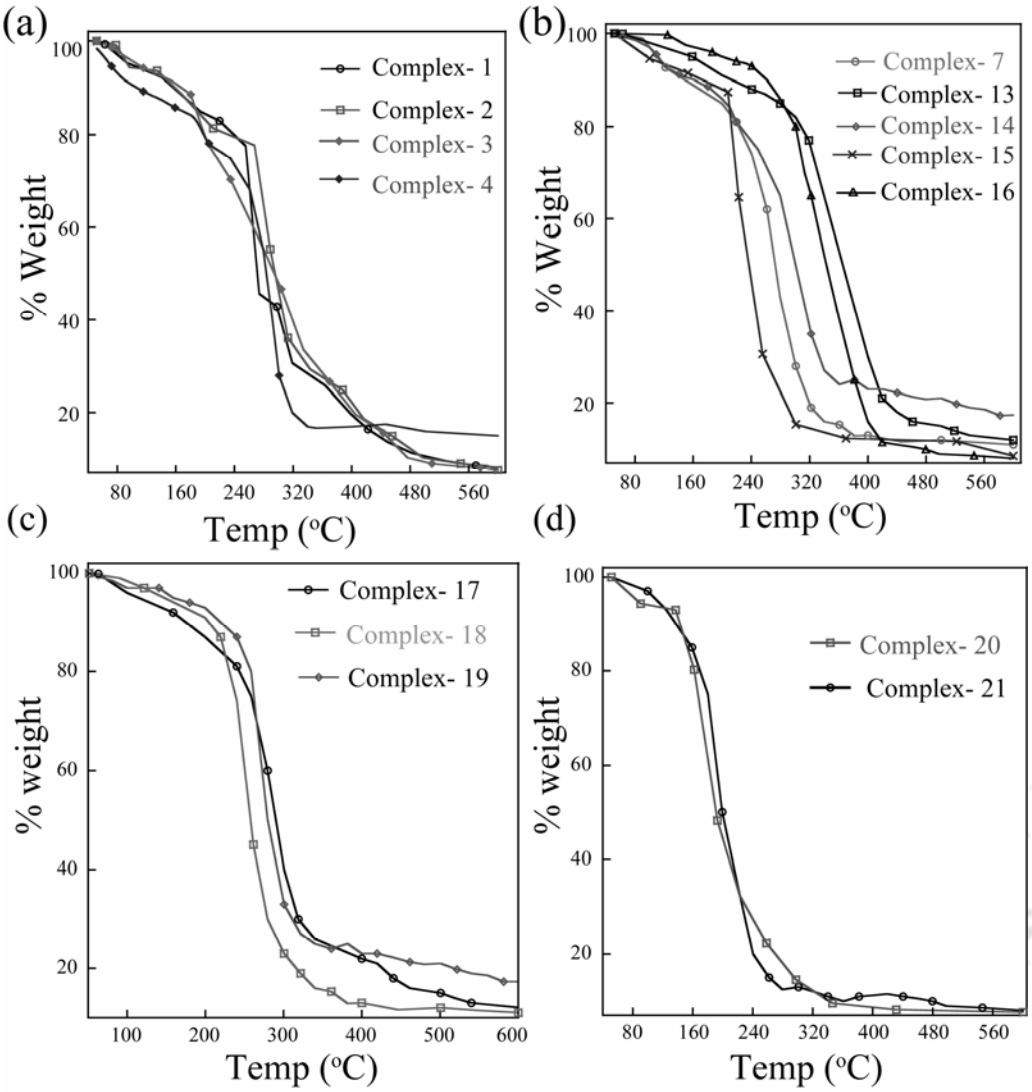

Figure 5.2.A. (a) TGA analysis of complex **1, 2, 3** and **4**; (b) TGA analysis of complex **7, 13, 14, 15** and **16**; (c) TGA analysis of complex **17, 18,** and **19**; (d) TGA analysis of complex **20** and **21.**

List of Publications

(1) "Precursory Ag- bipyridine 2D coordination polymer: A new and efficient route for the synthesis of Ag nanoparticles" **Avijit Pramanik**, Gopal Das, CrystEngComm, DOI: 10.1039/b908446k.

(2) "Aryl azo imidazoles assisted assembly of anion/anion-water through salt formation" **Avijit Pramanik**, Subhojit Majumdar, Gopal Das, CrystEngComm, DOI: 10.1039/b912454c.

(3) "An efficient phosphate sensor: tripodal quinoline excimer transduction" **Avijit Pramanik,** Gopal Das, Tetrahedron, 2009, 65(11), 2196-2200.

(4) "3D Solid-State Network from Hierarchical Supramolecular Self-Assembly of Transition Metal Complexes of Pyridine Based Ligand" **Avijit Pramanik,** Gopal Das, J Chem. Crystallogr., 2009, 39(6), 416-422.

(5) "Reduction of Coordinated Acetonitrile to Ethylamine in a Ruthenium Complex by p-Phenylenediamine or Hydroquinone" Amardeep Singh, **Avijit Pramanik**, Gopal Das, Biplab Mondal, Organometallics, 2008, 27(24), 6403–6404.

(6) "Molecular to Supramolecular Structure: Influence of Coordination Environment in Azo-dye Complexes" **Avijit Pramanik,** Gopal Das, Cryst. Growth & Design., 2008, 8(8), 3107–3113.

(7) "Aromatic guest inclusion by a tripodal ligand: Fluorescence and structural studies" **Avijit Pramanik,** Mouchumi Bhuyan, Gopal Das, J. Photoch. Photobio. A., 2008, 197(2-3), 149-155.

(8) "Tripodal naphthalene ether ligand: Solid-state anion recognition and fluorescence studies" **Avijit Pramanik,** Mouchumi Bhuyan, Rajib Choudhury, Gopal Das, J. Mol. Stur., 2008, 879(1-3), 88-95.

(9) "Molecular, supramolecular structure and catalytic activity of transition metal complexes of phenoxy acetic acid derivatives" **Avijit Pramanik,** Srinivas Abbina, Gopal Das, Polyhedron, 2007, 26(18), 5225-5234.

(10) "Solid State Synthesis and Hierarchical Supramolecular Self-assembly of Organic Salt Cocrystals" Harjyoti Thakuria, Ballav Moni Borah, **Avijit Pramanik**, Gopal Das, J. Chem. Crystallogr. 2007, 37, 807-816.

(11) "A one-pot synthesis and self assembled superstructure of an organic salt of 1,5-benzodiazepine derivative" Harjyoti Thakuria, **Avijit Pramanik,** Ballav Moni Borah, Gopal Das, Tetrahedron Lett. 2006, 47(18), 3135-3138.

(12) "Aryl azo imdazole assisted Self assembly of d^{10} metal (Zn^{11}, Cd^{11}, Hg^{11}) complexes: Influence of Halogen Substitution and Counter ions" **Avijit Pramanik**, Gopal Das (submitted).

(13) "Electron donating substituents and counter ion induced coordination assembles aryl azo imidazole complexes**" Avijit Pramanik**, Gopal Das (submitted).

(14) "Structural and Spectroscopic Aspects of Solvent Induced Conformational Analysis of Cycloxehane Dinapthyl Bis-thiourea System" **Avijit Pramanik**, Gopal Das (submitted).